SHORT-TERM COURSE

ON

SECONDARY STEELMAKING

Course Coordinators

Dr. D. MAZUMDAR

Dr. A. GHOSH

DEPARTMENT OF METALLURGICAL ENGINEERING

INDIAN INSTITUTE OF TECHNOLOGY KANPUR

DECEMBER, 1990

29 MAY 1992
LE RARY
Acc. No. 113508

ME-1990-D-MAZ-SHO

PREFACE

In recent years, there has been a growing trend for secondar processing of liquid steel after melting and refining in primar steelmaking units, such as EAF and LD. Popularly, known as 'Secondar Steelmaking' or 'Ladle Metallurgy', such secondary processing ma include deoxidation, vacuum and argon treatment, powder injectio composition and temperature adjustment etc. in ladles.

The growing demand for better quality steels and more stringer quality control, is the reason behind development of secondar steelmaking processes, since primary steelmaking alone was found to incapable of meeting such demand. Advent of continuous casting and it rapid growth as the dominant casting route are also inseparably link with development of secondary steelmaking.

In India, secondary steelmaking has so far been adopted only to limited extent. However it is going to come in a significant w during the decade of 1990 s.

Also the last two decades or so have witnessed scientif investigations and exploitation of scientific fundamentals on ever-increasing scale in the area of secondary steelmaking. As result, design, operation and control of these processes are no long art in technologically advanced countries.

With the above background in mind, it was decided to offer th short-term course. Broadly, the text is divided into three part Introduction, Scientific Fundamentals, and Secondary Steelmaki Processes. It has some informations on the processes. However t emphasis is on fundamentals and their application to processes. believe that as the Indian steel plants are moving towards large-sca adoption of secondary steelmaking, it is simultaneously necessary assimilate, collate and disseminate process fundamentals for succe of modernization program, and this is where academic institutes a expected to initiate efforts.

A short-term course can hope to succeed only through enthusiast participation from industry, R & D, Design organizations, a educational institutes. We wish to record our appreciation to vario participating organizations and the participants in this connection.

We wish to thank our colleagues, Dr.S.P. Mehrotra, Dr.N.K. Batr and Dr.S.C. Koria for agreeing to give some lectures in th course. Thanks are due to Shri B.D. Biswas for typing the manuscrip Shri S.K. Chaudhary for his assistance in processing of manuscrip and Shri A. Sharma and Shri D.P. Tripathy for miscellane assistance. It is not possible to mention individually many others w have also contributed to this endeavour.

Lastly we wish to thank our institute administration for the permission to conduct this course as well as for cooperation at stages.

D. Mazumdar **A. Ghosh**

TABLE OF CONTENTS

INTRODUCTION

CHAPTER 1 AN OVERVIEW OF SECONDARY STEELMAKING (A.GHOSH) 1

SCIENTIFIC FUNDAMENTALS

CHAPTER 2 THERMODYNAMICS (A.GHOSH) 9

CHAPTER 3 FLUID FLOW AND MIXING (S.P.MEHROTRA) 25

CHAPTER 4 MASS TRANSFER AND KINETICS (D.MAZUMDAR) 46

SECONDARY STEELMAKING PROCESSES

CHAPTER 5 FLUID FLOW AND MIXING IN LADLES (D.MAZUMDAR) 57

CHAPTER 6 ALLOYING OF STEEL (D.MAZUMDAR) 69

CHAPTER 7 DEOXIDATION AND CLEAN STEEL (A.GHOSH) 81

CHAPTER 8 DEGASSING AND DECARBURISING OF STEEL (N.K.BATRA) 120

CHAPTER 9 THERMODYNAMICS AND KINETICS OF DESULPHURIZATION REACTION (A.GHOSH) 143

CHAPTER 10 INJECTION METALLURGY (S.C.KORIA) 159

CHAPTER 11 PHYSICAL AND MATHEMATICAL MODELLING OF SECONDARY STEELMAKING PROCESSES (D.MAZUMDAR) 180

CHAPTER 12 MISCELLANEOUS TOPICS (A.GHOSH) 201

INTRODUCTION

CHAPTER 1

AN OVERVIEW OF SECONDARY STEELMAKING

A. GHOSH

1.1 INTRODUCTION

Prior to 1950 or so, after the steel was made in furnaces such as Open Hearth, converter or electric furnace, its treatment in ladles was limited in scope and consisted of deoxidation, carburization by addition of coke or ferrocoke as required, and some minor alloying. However stringent demands on steel quality and consistency in its physical properties require controls which are beyond the capability of the steelmaking furnaces. This is specially true for superior quality steel products in sophisticated applications. This requirement has led to development of various kinds of treatment of liquid steel in ladles besides deoxidation. These have witnessed massive growth and as a result have come to be variously known as `Secondary Steelmaking', `Ladle Metallurgy'. The author personally prefers the name `Secondary Processing of Liquid Steel', and he has used it elsewhere (1). Secondary steelmaking has become an integral feature of modern steel plants. Advent of continuous casting process, which requires more stringent quality control is an added reason for growth of secondary steelmaking. Steelmaking in furnaces, also redesignated now as `Primary Steelmaking', is therefore being employed more and more for speedy scrap melting and gross refining only, leaving further refining and control to secondary steelmaking.

Historically, Perrin process invented in 1933 is the forerunner of modern secondary steelmaking. Treatment of molten steel with synthetic slag was the approach. Vacuum degassing (VD) processes came in the decade of 1950-60. The initial objective was to lower hydrogen content of liquid steel in order to prevent cracks in large forging qualigty ingots. Later on, its objective also included lowering of nitrogen and oxygen contents. Purging with inert gas (Ar or N_2) in ladle using porous bricks or tuyeres (IGP) came later. Its primary objective was stirring with consequent homogenization of temperature and composition of melt. It offered the additional advantage of faster floating out of oxide particles. It was also found possible to lower carbon to a very low value in stainless steel by treatment of the melt with oxygen under vacuum or along with argon stream. This led to development of processes such as `Vacuum-Oxygen Decarburization (VOD)' and `Argon-Oxygen Decarburization (AOD)'.

Synthetic slag treatment and powder injection processes of molten steel in ladle were started in late 60 S and early 70 S with the objective of lowering sulphur content of steel to a low level demanded by many applications. This led to the development of what is known as `Injection Metallurgy (IM)'. Injection of powders of calcium bearing reagents, typically calcium silicide, was also found to prevent nozzle clogging by Al_2O_3 and lead to inclusion modification, which are of crucial importance in continuous casting as well as for better properties.

In traditional pitside practice without ladle metallurgical operations, the temperature drop of molten steel from furnace to mould is around 20-30°C. An additional temperature drop of 2-3°C per minute, i.e. about 20-40°C, occurs during secondary steelmaking. Continuous casting uses pouring through tundish causing some further drop of 10-20°C. Therefore provisions for heating and temperature adjustment during secondary steelmaking are very desirable. This has led to the development of special furnaces such as vacuum arc degasser (VAD), ladle furnace (LF), and ASEA-SKF ladle furnace. These are very versatile units capable of performing various operations.

Table 1.1 summarizes the features of various processes.

Table 1.1

Various Secondary Steelmaking Processes and their Capabilities (primarily from ref. 2)

Item	Processes						
	VD	VOD	IGP	IM	VAD	LF	ASEA-SKF
Desulphurization	minor	minor	minor	yes	yes	yes	yes
Deoxidation	yes	yes	yes	yes	yes	yes	yes
Decarburization	minor	yes	no	no	no	no	yes
Heating	no	yes*	no	no	yes	yes	yes
Alloying	minor	yes	minor	minor	yes	yes	yes
Degassing	yes	yes	no	no	yes	no	yes
Homogenization	yes	yes	yes	yes	yes	yes	yes
Achieving more cleanness	yes	yes	yes	yes	yes	yes	yes
Inclusion modification	no	no	minor	yes	yes	yes	yes

* Chemical heating only

1.2 TRENDS IN STEEL QUALITY DEMANDS

With passage of time customers are demanding better and better quality steels, which means

(a) less impurities,
(b) more cleanness (i.e. freedom from inclusions),
(c) more stringent quality control,
(d) microalloying to impart better properties, for plain carbon and low alloy steels.

The above demands, combined with other requirements such as :

(a) need for cost reduction in view of competetion from polymers etc.
(b) environmental pollution control,
and (c) sort of stagnant World steel market, pose enormous challenge to steelmaking community.

Changing demand on quality may be illustrated with the example of line pipe steel for North Sea gas (3).

Year	Maximum percent element in steel					
	C	S	P	H	N	O
1983	0.04-0.06	0.002	0.015	2×10^{-4}	0.01	-
1990		0.001	0.0015		0.0035	0.002
long term	S + O + P + N = 45 ppm					

Ramaswamy (4) has reviewed the subject, and has outlined some of the quality requirements of line pipe steel for sour gas applications, steels for off-shore platforms, bearing steels, steel for rod and wire industry, and for power plant rotors. Fig.1.1 shows the trends in residuals attained by Japanese Steel Works. Obviously such lowering of impurities have been attained through secondary steelmaking.

As shown in Table 1.1, all kinds of secondary steelmaking operations are capable of yielding steels with more cleanness. Inclusions are generally harmful to mechanical properties and corrosion resistance of steels. Choice of deoxidation practice combined with proper stirring is one of the measures to remove inclusions. However a more serious source of harmful inclusions (i.e. larger sizes) is erosion of refractory lining. Not only so, reaction of lining with melt is a source of impurity at such low impurity levels. Therefore, success of secondary steelmaking processes is intimately linked with development or use of newer refractory materials such as high alumina, zircon, magnesia, dolomite etc.

The cleanness consciousness has gone to such an extent that trials are going on for filtering of molten steel through ceramic filters to remove non-metallic inclusions. The technique is still in experimental stage.

Inclusion modification is one of the techniques to render inclusions less harmful to properties of steel. Injection of calcium into the melt is done for this purpose. Sometimes rare earths are also employed.

1.3 SCIENTIFIC FUNDAMENTALS

Application of scientific fundamentals is a contributing factor to such a progress of secondary steelmaking technology. This has been possible due to growth of applied sciences, including metallurgical sciences, and application of the same.

Ghosh (5,6) has reviewed the subject. Laws of thermodynamics had been well laid out by the turn of the last century. However application of the same to high temperature systems had to wait for lack of thermochemical data. Collection of such data started on a modest scale by the beginning of this century. The pace accelerated as years went by, and it began in a really massive scale after the Second World War. By about 1970, fairly reliable data were available on most of the systems and reactions of interest in pyrometallurgy.

Equilibrium calculations of processes call for experimental data on activity vs. composition relationships in liquids which may broadly be grouped into metallic solutions, SiO_2 based slag solution, etc. Most of these solutions are multicomponent. Development of metallurgical thermodynamics called for new techniques to handle them. Participation of renowned physical chemists besides metallurgists made these possible.

Kinetics is a late comer as compared to thermodynamics of pyrometallurgical reactions. Scientific investigations were started after 1950. However they picked up fast and for the last two decades it is being pursued vigorously. As a result, kinetics of pyrometallurgical reactions and processes is a subject in engineering science in its own right. Knowledge already available in chemical engineering has been instrumental in its development.

It had been recognized several decades back that lack of proper mixing in liquid bath adversely affects efficiency of steelmaking processes. A large number of investigations have been carried out, especially in the last two decades, on mixing. Again, mixing, mass transfer and phase dispersions depend on fluid flow in the bath. Such a flow is turbulent in steelmaking processes. Turbulence is a very complex phenomenon. Scientists and engineers in a variety of disciplines are trying to solve complex problems involving turbulent flow.

Experimental investigations on fluid flow and mixing at steelmaking temperatures are difficult. In this connection, water modelling (i.e. cold modelling or physical modelling) has contributed significantly to our understanding of these aspects. Here water typically simulates liquid metal. Transparent perspex or glass vessels allow flow visualization. Similarity criteria have been employed to various extents.

Quantitative approach in the area of fluid flow, mixing and mass transfer is based on fluid mechanics especially that related to turbulent flow. Such computations involve computer-oriented numerical methods. Considerable advances have been made in this direction so much so that these are being employed for interpretation of results, design and predictions.

1.4 PROCESS CONTROL

A variety of process control measures are to be adopted if desirable benefits are to be obtained from secondary steelmaking. It is neither possible nor necessary to list all these. Only some will be briefly mentioned below in view of their special significance.

1.4.1 Immersion Oxygen Sensor

Dissolved oxygen in molten steel is a key scientific as well as quality parameter in secondary steelmaking. Its measurement has been possible due to development of immersion oxygen sensor over the last two decades or so. It is actually an oxygen concentration cell with a solid electrolyte (typically ZrO_2 + MgO or ZrO_2 + CaO variety). The EMF of the cell allows estimation of dissolved oxygen content through thermodynamic relations. Since the signal is electrical and obtained within 15 secs. of immersion it is widely used to measure and control oxygen in molten steel. Through thermodynamic relations it allows us also to know soluble aluminium content of steel, which again is another valuable information steelmakers desire.

Immersion oxygen sensor has also been widely employed in a variety of scientific and technological investigations related to deoxidation reactions and behaviour of oxygen at different stages of steelmaking. The pioneering contribution of Kiukkola and Wagner (1956), who first set up such a cell for thermodynamic measurements in laboratory is to be recognized.

1.4.2 Some Other Process Control Measures

Gases such as oxygen and nitrogen are picked up from surrounding air during teeming, and pouring. It can significantly increase gas contents in liquid steel. Unless it is prevented most of the secondary steelmaking operations would not give any benefit. For continuous casting, use of either submerged nozzle or shrouding of nozzle by inert gas is the solution. For ingot casting this is difficult to practice. There management of teeming stream is the strategy.

For efficient deoxidation, synthetic slag treatment, and injection processes it is essential to prevent too much slag from primary steelmaking being carried over into ladles. All steelmakers know the associated difficulties if we do not desire lots of metal being left out untapped. Therefore considerable efforts are being made in technologically advanced countries on techniques of slag-free tapping.

In traditional ladles, refractory lined stoppers were employed for flow control during teeming through nozzle. A major development has been slide gate, which is superior as a flow control device.

Traditional method of addition of aluminium to liquid steel as ingots or shots makes efficiency of aluminium deoxidation poor as well as irreproducible leading to serious control problems. The technology of mechanised feeding of aluminium wire is a significant improvement in this connection. Now-a-day many plants have facilities of feeding wires consisting of Ca or CaSi powders clad in steel as well. This is an alternative to injection of these powders into melt by injection metallurgy techniques.

Fruehan (7) has reviewed some of these topics in concise fashion. Of course advances in instrumentation as well as use of computer have contributed significantly as in all other fields. Fig.1.2 shows the sketch of a ladle furnace which is the most versatile processing unit in secondary steelmaking. It has two covers, one fitted with arc heating electrodes and another for vacuum operation.

1.5 THE INDIAN SCENERIO

Srinivasan (2) has discussed it briefly. Alloy steelmakers in India are having secondary steelmaking facilities. However it is by and large lacking for conventional carbon steel grades. As a result, there is a major lag with respect to quality as well as yield when compared with technologically advanced countries. Installation of continuous casting facility in some shops has further aggravated the situation.

Therefore provision for secondary steelmaking facilities in all modernization programs is a must. This would require overcoming a traditional psychological barrier which is a belief that quality improvement means loss in productivity and yield.

Table 1.2 presents the technology plan for SAIL plants for secondary steelmaking.

Table 1.2

Secondary Refining in SAIL Plants
Technology Plan (2)

Proposed Technology	In Plants		
	Present Status	1990	1995
1. Ladle measurement of $\underline{O}$ and temp.	-	All plants	-
2. N_2/Ar purging	BSF, ASP limited extent	BSL, RSP	DSP, IISCO
3. Gas injection with top slag	-	BSP, BSL	-
4. LF/VAD	RSP, ASP	BSP, BSL	DSP IISCO
5. Powder injection	ASP	-	BSP, BSL DSP, IISCO
6. Al-wire injection	BSP	All plants	-
7. Ca-wire injection	-	BSP	Rest

REFERENCES

1. A. Ghosh, Principles of Secondary Processing and Casting of Liquid Steels, Oxford & IBH Publishers, New Delhi (in Press).
2. C.R. Srinivasan, in Proceedings of National Seminar on Secondary Steelmaking, Tata Steel and Ind. Inst. Metals, Jamshedpur (1989), p.15.
3. R. Scholey, Proc. 69th Steelmaking Conference, ISS-AIME, Washington D.C.(1986), p.V.
4. V. Ramaswamy, in ref. 2, p. 71.
5. A. Ghosh, in Frontiers in Applied Chemistry, A.K. Biswas ed., Narosa Pub. House, Delhi (1989), p. 53.
6. A. Ghosh, in Thermodynamics and Kinetics of Metallurgical Processes, M.M. Rao et al eds, Ind. Inst. Metals (1985), p. 161.
7. R.J. Fruehan, Ladle Metallurgy, ISS-AIME, Warrendale, PA, USA (1985).

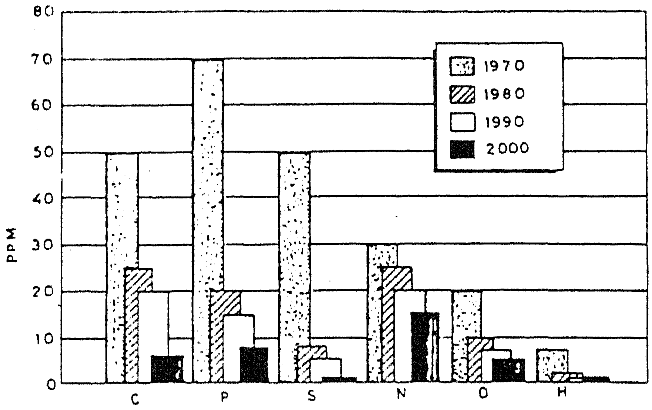

Fig. 1.1 : Minimum residual levels in steel in Japan

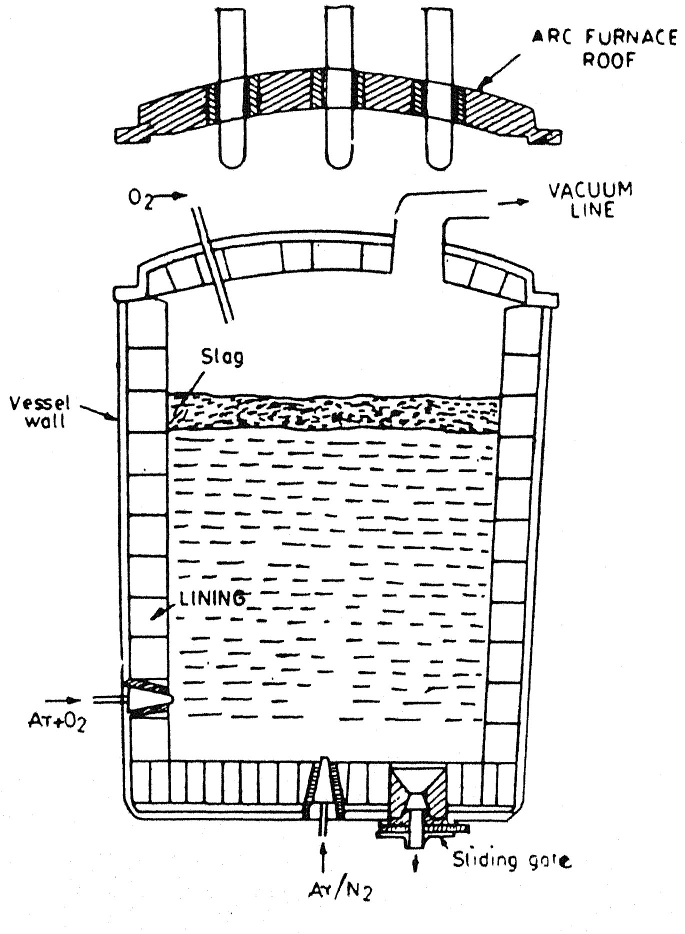
ARC FURNACE ROOF
O_2
VACUUM LINE
Slag
Vessel wall
LINING
Ar+O_2
Ar/N_2
Sliding gate

Fig. 1.2 : Sketch of a versatile ladle furnace.

SCIENTIFIC FUNDAMENTALS

CHAPTER 2

THERMODYNAMICS

A. GHOSH

Chemical thermodynamics is employed to predict whether a chemical reaction is feasible or not. It also allows quantitative calculation of the state of equilibrium of a system in terms of composition, pressure and temperature. Laws of thermodynamics are exact and, therefore, calculations based on them are, in principle, sound and reliable.

All reactions and processes tend towards thermodynamic equilibrium. If sufficient time is allowed then close attainment of equilibrium is possible. Steelmaking reactions and processes are very fast. As a result, some of these have been found to approach equilibrium closely within the short processing time. Examples of the same in secondary steelmaking shall be provided in subsequent chapters. Therefore, knowledge of thermodynamics should be fully exloited for understanding, control, design and development of metallurgical processes.

Thermodynamic equilibrium necessarily requires the attainment of mechanical, thermal and chemical equilibria. Mechanical interaction of a system with the surroundings is most commonly in the form of pressure. Therefore, in the absence of a field of force, **mechanical equilibrium** generally means pressure equilibrium i.e. uniform pressure all throughout the system. Similarly, **thermal equilibrium** implies uniformity of temperature, and **chemical equilibrium** in a broad sense means uniformity of **chemical potentials** for all species in the system. At chemical equilibrium, there is no tendency of further reaction.

It is possible that the system is at equilibrium with respect to some variables but not some others. It is known as partial equilibrium and thermodynamics is capable of handling this also. However, a precondition for handling any chemical equilibrium is establishment of mechanical and thermal equilibria.

2.1 CHEMICAL EQUILIBRIUM

Consider the following **isothermal** reaction which takes place at a temperature **T K**.

$$aA + bB = lL + mM \qquad \ldots 2.1$$

Here the capital letters are general symbols of chemical species and the small letters denote the number of moles of each. The word isothermal implies that the initial temperature at the begining of the reaction and the final temperature (when equilibrium is reached) are the same. It is not necessary that temperature remains unchanged all throughout during the progress of the reaction.

The free energy change for reaction represented by Eq.(2.1) may be expressed as

$$\Delta G = (l\bar{G}_L + m\bar{G}_M) - (a\bar{G}_A + b\bar{G}_B) \qquad \ldots 2.2$$

where $\bar{G}_i$ is the partial molar free energy of the species i. The horizontal bars on top of the letters indicate a general state in solution.

The **standard state** is the stablest state of the putre substance at the same temperature (T°K) and at one atmosphere pressure. The standard state could thus be a pure solid or liquid or ideal gas under one atmosphere pressure. The magnitude of a variable for any standard state is indicated by a superscript o.

It can be shown that

$$\bar{G}_i - G_i^o = RT \ln a_i \qquad \ldots 2.3$$

where G_i^o = free energy of species i at its standard state

a_i = activity of species i when its partial molar free energy is

$\bar{G}_i = f_i / f_i^o$

f_i is the **fugacity** of i at the state under consideration and f_i^o is the fugacity of i at its standard state. For ideal gases fugacity equals partial pressure.

By definition, activity, a_i is 1 when species i is at its standard state. If all the reactants and products are at their standard states, then

$$\Delta G^o = (l G_L^o + m\, G_M^o) - (a\, G_A^o + b\, G_B^o) \qquad \ldots 2.4$$

where ΔG^o is the standard free energy change of reaction represented by Eq.2.1 at temperature T°K. Combining Eqs. 2.2, 2.3 and 2.4,

$$\Delta G = \Delta G^o + RT \ln \frac{a_L^{\,l} \cdot a_M^{\,m}}{a_A^{\,a} \cdot a_B^{\,b}} \qquad \ldots 2.5$$

or $$\Delta G = \Delta G^o + RT \ln Q \qquad \ldots 2.6$$

where

$$Q = \frac{a_L^{\,l} \cdot a_M^{\,m}}{a_A^{\,a} \cdot a_B^{\,b}}$$

Q is called **activity quotient.**

The previous equation was derived assuming an isothermal condition i.e. the same temperature for reactants and products. It is further assumed that the reaction is **isobaric** i.e. the initial and final pressures are the same and also that thermodynamic equilibrium prevails. Then

$$(\Delta G)_{P,T} = 0 \qquad \ldots\ 2.7$$

combining Eqs. 2.6 and 2.7,

$$\Delta G^{\circ} = -\ RT\ \ln\ [Q]_{e} = -\ RT\ \ln\ K \qquad \ldots\ 2.8$$

where K is the value of the activity quotient at equilibrium. K is known as the **equilibrium constant.**

Eq.2.6 is the basis of predictions of feasibility of reactions. A reaction is spontaneous or feasible if ΔG is negative. It is impossible when ΔG is positive. Eq.2.8 is used to calculate the equilibrium condition or end-point of a reaction.

Thermodynamic predictions and calculations can be made if the following conditions are satisfied.

(i) The process should take place isothermally (i.e. the initial and final temperatures should be the same) and the temperature should be known.
(ii) The standard free energy change, ΔG°, should be available.
(iii) Activity versus composition relations for all species involved should be known.

Since changes in pressure as encountered in metallurgy do not affect thermodynamic properties significantly, the condition p that be constant, is not of importance.

2.2 ΔG° FOR OXIDE SYSTEMS

In secondary steelmaking, we primarily encounter formation or decomposition of inorganic oxides. Therefore, a brief write up is presented on free energies of oxide systems.

The standard free energies of formation reactions, representing formation of compounds from the elements, are now known for most of the inorganic compounds. These are called **standard free energies of formation** (ΔG°_{f}). While some data are accurate, others are not so and, therefore, constant efforts go on to gather more accurate data. A number of books carry compilations of such data. A few are listed.

1. J.F. Elliott and M. Gleiser, **Thermochemistry for steelmaking, Vol.1,** Addison-Wesley Publishing Co., Reading, Mass, USA (1960).
2. J.F. Elliott, M. Gleiser and V. Ramakrishna, **Thermochemistry for steelmaking, Vol.2,** Addison-Wesley Publishing Co., Reading, Mass, USA (1963).

3. O. Kubaschewski, E.Ll. Evans and C.B. Alcock, **Metallurgical Thermochemistry** (4th Ed), Pergamon Press, New York, (1967).

Consider the formation of an oxide from the elements.

i.e. $$\frac{2X}{Y} M + O_2(g) = \frac{2}{Y} M_xO_y \qquad \ldots\ 2.9$$

where M denotes metal.

Traditionally, all free energy data shown in the Ellingham diagram would be for a reaction such as Eq.2.9 where the formation reaction involves only one mole of oxygen. This would make it convenient to compare the data for different oxides.

If the metal, oxygen and oxide are in their standard states then the free energy change is

$$\Delta G^\circ = \Delta H^\circ - T\Delta S^\circ \qquad \ldots\ 2.10$$

where ΔH° and ΔS° are standard heat and standard entropy of formation respectively.

According to Kirchoff's law

$$\Delta H^\circ = \Delta H^\circ_1 + \int_{T_1}^{T} \Delta C^\circ_p \, dT \qquad \ldots\ 2.11$$

$$\Delta S^\circ = \Delta S^\circ_1 + \int_{T_1}^{T} \frac{\Delta C^\circ_p}{T} \, dT \qquad \ldots\ 2.12$$

where ΔH°_1 and ΔS°_1 are standard heat and standard entropy of formation at temperature T_1 and ΔC°_p is the difference of specific heats of products and reactants at standard states. The values of ΔC°_p are generally very small and, therefore, one may assume that ΔH° and ΔS° are essentially invariant with temperature. This allows us to express dependence of ΔG_f on temperature as :

$$\Delta G^\circ_f = C + D.T \qquad \ldots\ 2.13$$

where C and D are constants.

Table 2.1 provides values of C and D for oxides of importance in steelmaking in the steelmaking temperature range. Fig.2.1 presents the same graphically. ΔG° values are per gm.mole of O_2 for all of these. This normalization allows us to compare stabilities of oxides directly from the figure. For example Al_2O_3 is stabler than SiO_2 since the free energy of formation of the former is more negative as compared to that of the latter.

Quantitatively speaking, we are interested in the reaction :

$$4/3\ Al + SiO_2 = \frac{2}{3} Al_2O_3 + Si \qquad \text{... 2.14}$$

$$\Delta G^\circ \text{ (for reaction 2.14)} = \Delta G^\circ_f \ (2/3\ Al_2O_3) - \Delta G^\circ_f \ (SiO_2)$$

$$= \text{a negative quantity,}$$

and hence the reaction is feasible, if all reactants and products are at their respective standard states (i.e. pure substances), in accordance with free energy criteria.

However, if they are not pure (e.g. present as solution in molten iron or slag), then ΔG° does not provide correct guideline, and we have to find out ΔG or equilibrium compositions. These will require knowledge of activity as function of comosition.

2.3 ACTIVITY VS. COMPOSITION RELATIONSHIPS

Crudely speaking, activity is a measure of `free' concentration in a solution, i.e. concentration which is available for chemical reaction. Also, by definition, activity is dimensionless. In metallurgical processing, the gases behave as ideal and molecules are free. Hence activity of a component i in a gas mixture is equal to its concentration. Numerically, by convention, $a_i = p_i$, where p_i is partial pressure of i in atmosphere.

Composition of a solution can be altered significantly during processing only if mixing and mass transfer are rapid. Solid state diffusion is very slow. Hence during the short processing time, its composition does not change. For example, a particle of CaO will remain CaO as long as it does not dissolve in slag. It may get coated by another solid such as Ca_2SiO_4 or CaS during steel processing. Here solid CaO remains pure and its activity,by definition,is 1 since this is its standard state.

However liquid steel contains variable concentrations of impurities and alloying elements. Molten slag is also a solution of oxides with a variety of compositions. Hence activity versus composition relationships are required here for equilibrium calculations.

Table 2.1 : Variation of standard free energy of formation of some oxides with temperature at steelmaking temperatures

Reaction	$\Delta G^\circ_f = C + DT$ kilo joules per mol O_2	
	C	D
$4/3\ Al(l) + O_2\ (g) = 2/3\ Al_2O_3\ (s)$	- 1197	0.2574
$2C\ (s) + O_2\ (g) = 2CO\ (g)$	- 223.6	- 0.1754
$C\ (s) + O_2\ (g) = CO_2\ (g)$	- 394.4	$- 8.4 \times 10^{-4}$
$2Ca(g) + O_2\ (g) = 2CaO\ (s)$	- 1592	0.3904
$4/3Cr\ (s) + O_2\ (g) = 2/3Cr_2O_3\ (s)$	- 747.3	0.1733
$2Fe\ (s) + O_2\ (g) = 2FeO\ (s)$	- 519.6	0.1252
$2Fe\ (l) + O_2\ (g) = 2FeO\ (l)$	- 465.8	0.0907
$2Mn\ (l) + O_2\ (g) = 2MnO\ (s)$	- 798.9	0.165
$Si\ (l) + O_2\ (g) = SiO_2\ (s)$	- 953.4	0.2039

*FeO is actually non-stoichiometric compound Fe_xO, where $0.92<x<0.97$

2.3.1 Activities with conventional standard states

As already stated, a pure element or compound constitutes its conventional standard state. For example, pure Fe is conventional standard state for liquid steel, and $a_{Fe} = 1$ for pure iron. Similarly pure SiO_2 is the standard state for a slag containing silica.

In conventional standard state, an **ideal solution** obeys **Raoult's Law**, which states that

$$a_i = X_i \qquad \text{... 2.15}$$

where X_i is mole fraction solute i in the solution. For example, let liquid steel contain chromium and nickel. Then X_{Cr} is to be calculated from weight percentages as follows.

$$X_{Cr} = \frac{W_{Cr}/M_{Cr}}{W_{Cr}/M_{Cr} + W_{Ni}/M_{Ni} + W_{Fe}/M_{Fe}} \qquad \text{... 2.16}$$

where W denotes weight percent and M molecular mass.

Most real solutions do not obey Raoult's Law. They either exhibit positive or negative departures from Raoult's Law. For a binary solution (i.e. containing two species such as Fe+Ni or $CaO+SiO_2$), this is illustrated in Fig.2.2. For example, molten Fe-Mn, Fe-Ni, FeO-MnO solutions are ideal. Molten Fe-Si, $CaO-SiO_2$, $FeO-SiO_2$, $MnO-SiO_2$ etc. show negative departures. Liquid Fe-Cu exhibits positive departure.

Departures from Raoult's Law are quantified using a parameter, known as **Activity Coefficient** (γ), which is defined as :

$$\gamma_i = \frac{a_i}{X_i} \qquad \ldots\ 2.17$$

Activities in slag systems use conventional standard states as reference. However industrial slags are multicomponent systems. Hence presentation of activity versus composition diagrams is more complex and different from that of a binary solution.

Fig.2.3 shows values of activity of SiO_2 in $CaO-SiO_2 - Al_2O_3$ ternary system at 1600°C. These are in the form of isoactivity lines for SiO_2. Similarly, there would be diagrams presenting isoactivity lines for CaO and Al_2O_3. The liquid field is bounded by liquidus lines. In this diagram, Al_2O_3 has been written as $AlO_{1.5}$. This is because molecular mass of CaO, SiO_2 and $AlO_{1.5}$ are close, being equal to 56, 61 and 51 respectively. Therefore, the mole fraction scale is approximately the same as weight fraction scale. Slag activity data are available in several sources. But the most comprehensive is Slag Atlas, Verein Deutscher Eisenhuttenleute, published by Verlag Stahleisen mbH, Dusseldorf, 1981.

2.3.2 Activities with One Weight Percent Standard State

Liquid steel comes primarily in the category of dilute solution, where concentrations of solutes (carbon, oxygen etc.) are mostly below 1 weight percent or so except for alloy steels. Solutes in dilute solutions obey **Henry's Law**, which is stated as follows.

$$a_i = \gamma_i^{\circ} X_i \qquad \ldots\ 2.18$$

where γ_i° is a constant. Deviation from Henry's Law occurs when the solute concentration increases. The range differs depending on nature of solute.

Therefore activities of dissolved elements in liquid steel are expressed with reference to Henry's Law and not Raoult's Law. Since we are interested to find values directly in weight percent, composition scale is weight percent and not mole fraction. With these modifications, in a dilute solution of species i in liquid iron,

(i) if Henry's Law is obeyed by species i, then

$$h_i = W_i \qquad \ldots\ 2.19$$

(ii) if Henry's Law is not obeyed by species i, then

$$h_i = f_i W_i \quad , \text{ where } f_i \neq 1 \qquad \ldots 2.20$$

h_i is activity and f_i is activity coefficient in the so-called **1 weight percent standard state.** This is because at 1 wt.pct., h_i = 1, if Henry's Law is obeyed.

It is to be noted that the standard free energy change for reaction is not going to be the same if standard state is changed. For example, at 1600°C,

$$Si(l) + O_2(g) = SiO_2(s) \ ; \ \Delta G^\circ = -571.5 \text{ kJ mol}^{-1} \qquad \ldots 2.21$$

for pure liquid silicon as standard state.

$$[Si]_{wt.pct} + O_2(g) = SiO_2(s) \ ; \ \Delta G = -406.4 \text{ kJ mol}^{-1} \qquad \ldots 2.22$$

for 1 wt.pct. standard state of Si dissolved in liquid iron.

(Note : Si dissolved in liquid metal is denoted either as [Si] or $\underline{Si}$; SiO_2 dissolved in slag is indicated by (SiO_2))

2.3.3 : Solute-Solute Interactions in Dilute Multicomponent Solutions

It has been found that solutes in a multicomponent solution interact with one another and thus influence activities of other solutes. Fig.2.4 illustrates it for activity of carbon and oxygen in liquid iron at 1560°C. In Fe-C binary (i.e. without any other added element), $f_c = 1$, i.e. $\log f_c = 0$. In presence of a third element in liquid iron solution, f_c keeps changing systematically. It has been derived that, if in a dilute multicomponent solution, A is solvent (Fe in case of liquid steel) and B,C, ...i,j,... are solutes, then

$$\log f_i = e_i^B . W_B + e_i^C . W_C + e_i^i . W_i + e_i^j . W_j + \ldots\ldots \qquad \ldots 2.23$$

where e's are constants. e_i^j is called **Interaction Coefficient** describing influence of solute j on f_i. e_i^i is known as **self** interaction coefficient and has a non-zero value only if Fe-i binary deviates from Henry's Law.

Table 2.2 presents values of interaction coefficient for some common elements dissolved in liquid iron.

2.4 SOLVED EXAMPLES

Example 2.1 : Solid iron is in contact with a liquid FeO-CaO-SiO_2 slag, and gas containing CO and CO_2 at 1300°C. The activity of FeO in slag is 0.45 and p_{CO}/p_{CO_2} ratio in gas is 20/1. Predict whether it is possible to oxidize Fe. Also calculate equilibrium value of p_{CO}/p_{CO_2} ratio in gas.

Solution : We are to consider the following reaction :

$$Fe(s) + CO_2(g) = (FeO)_{slag} + CO(g) \quad \text{...Ex.2.1}$$

ΔG° for reaction Ex.2.1

$$= \Delta G_f^\circ [CO(g)] + \Delta G_f^\circ [FeO(s)] - \Delta G_f^\circ [CO_2(g)] \quad \text{...Ex.2.2}$$

Standard state for FeO is solid pure FeO, since its melting point is 1368°C.

With the help of Table 2.1,

$$\Delta G^\circ \text{ at } 1300^\circ C\ (1573K) = -249.8 - 161.3 + 395.7$$

$$= -15.38 \text{ kJ/mole} = -15.38 \times 10^3 \text{ J/mole}$$

(a) $\Delta G = \Delta G^\circ + RT \ln Q$ ... 2.6

$$= \Delta G^\circ + RT \ln \frac{p_{CO} \times (a_{FeO})}{[a_{Fe}] \times p_{CO_2}} \quad \text{...Ex.2.3}$$

As discussed earlier, solid would remain essentially pure in a limited time period and a_{Fe} may be taken as 1. Going through calculations,

$$\Delta G = +13.36 \text{ kJ/mole}$$

Since ΔG is positive, oxidation of Fe is not possible.

(b) At equilibrium, $\Delta G^\circ = -RT \ln K$ ... 2.8

$$\text{where } K = \frac{p_{CO} \times (a_{FeO})}{a_{Fe} \times p_{CO_2}} \text{ at equilibrium}$$

using value of ΔG°, p_{CO}/p_{CO_2} ratio at equilibrium with Fe and slag turns out to be 7.20.

(Note: R = 8.316 Joules/mol/K)

Example 2.2

Liquid steel is being degassed by argon purging in ladle at 1600°C. The gas bubbles coming out of the bath have 10 pct. CO, 5 pct. N_2, 5 pct. H_2. Assuming these to be at equilibrium with molten steel calculate hydrogen, nitrogen and oxygen concentrations in steel in parts per million (ppm). The steel contains 1 pct. carbon, 2 pct. manganese and 0.5 pct. silicon.

Solution :

(a) for hydrogen, the reaction may be written as :

$$[H]_{\text{ppm in steel}} = 1/2\ H_2(g) \qquad \text{...Ex.2.4}$$

for which $\log K = \frac{1905}{T} - 2.408$ ...Ex.2.5

(Note: Here standard state for [H] is 1 ppm)

Again, $K = \frac{p_{H_2}^{1/2}}{[h_H]}$, where h is in ppm ...Ex.2.6

Now, $p_{H_2} = 0.05$ atm and K at 1873K = 0.0407

So, h_H at equilibrium = 5.49 = f_H . ppmH

Again, $\log f_H = e_H^C \cdot W_C + e_H^{Mn} \cdot W_{Mn} + e_H^{Si} \cdot W_{Si}$ ...Ex.2.7

Assume interactions of dissolved H,N and O on f_H as negligible. This is justified in view of their very small concentrations.

From Table 2.2

$$\log f_H = 0.06 \times 1 - 0.0014 \times 2 + 0.027 \times 0.5$$

Putting in values, [ppm H] = 4.67.

(b) for nitrogen, the reaction may be written as :

$$[N]_{\text{wt. pct.}} = 1/2\ N_2(g) \qquad \text{...Ex.2.8}$$

for which, $\log K = \frac{187.9}{T} + 1.248$ ...Ex.2.9

Proceeding as for hydrogen, $[h_N] = 0.01$, in 1 wt. pct. standard state ...Ex.2.10

now, $h_N = f_N \cdot W_N$

and $\log f_N = e_N^C \cdot W_C + e_N^{Mn} \cdot W_{Mn} + e_N^{Si} \cdot W_{Si}$ ...Ex.2.11

Proceeding as for hydrogen,
Concentration of N = 0.0077 wt.pct. = 77 ppm.

(c) for oxygen, the reaction may be written as :

$$[C]_{\text{wt. pct.}} + [O]_{\text{wt. pct.}} = CO(g) \qquad \text{...Ex.2.12}$$

for which $\log K = \dfrac{1168}{T} + 2.07$ ...Ex.2.13

Again, $K = \dfrac{p_{CO}}{[h_C]\,[h_O]}$ ...Ex.2.14

$h_C = f_C \,.\, W_C = f_C \,.\, 1$

$$\log f_C = e_C^C \,.\, W_C + e_C^{Mn} \,.\, W_{Mn} + e_C^{Si} \,.\, W_{Si} \qquad \text{...Ex.2.15}$$

(as in previous cases, assume interactions of $\underline{H}$, $\underline{N}$, $\underline{O}$ on f_C as negligible).

Putting in values from Table 2.2, $f_C = 1.43$, and $h_C = 1.43$.

So, $h \;=\; \dfrac{p_{CO}}{K \,.\, h_C} = \dfrac{0.1}{494 \times 1.43} = 1.42 \times 10^{-4}$

Again, $W_O = h_O \,/\, f_O$,

$$\text{and } \log f_O = e_O^C \,.\, W_C + e_O^{Mn} \,.\, W_{Mn} + e_O^{Si} \,.\, W_{Si} \qquad \text{...Ex.2.16}$$

Putting in values (taking $e_O^C = + 0.075$)

Concentration of dissolved oxygen in steel

$$= 1.53 \times 10^{-4} \text{ wt.pct.} = 1.53 \text{ ppm.}$$

(Note : You are advised to carry out these calculations ignoring all interactions and see for yourself the difference.)

Table 2-2 : First order interaction coefficients in molten iron (e_i^j) at 1600°C[14]

j → ↓ i	Al	C	Cr	Mn	O	Si	Ti
Al	- 0.045	0.091	-	-	- 6.6	0.0056	-
C	0.043	0.14	- 0.024	- 0.012	- 0.34	0.08	-
Cr	-	- 0.12	- 0.0003	-	- 0.14	- 0.0043	0.059
H	0.013	0.06	- 0.0022	- 0.0014	- 0.19	0.027	- 0.019
Mn	-	- 0.07	-	-	- 0.083	0	-
N	- 0.028	0.13	- 0.047	- 0.02	0.05	0.047	- 0.53
O	- 3.9	- 0.45	- 0.04	- 0.021	- 0.20	- 0.131	- 0.6
Si	0.058	0.18	- 0.0003	0.002	- 0.23	0.11	-
Ti	-	-	0.055	-	- 1.8	-	0.013

$$e_C^O = 0.075 \times \frac{M_C}{M_O} + \frac{1}{\quad} \cdot \frac{M_O - M_C}{M_O} = 0.057$$

where M , M are atomic mass of oxygen and carbon respectively

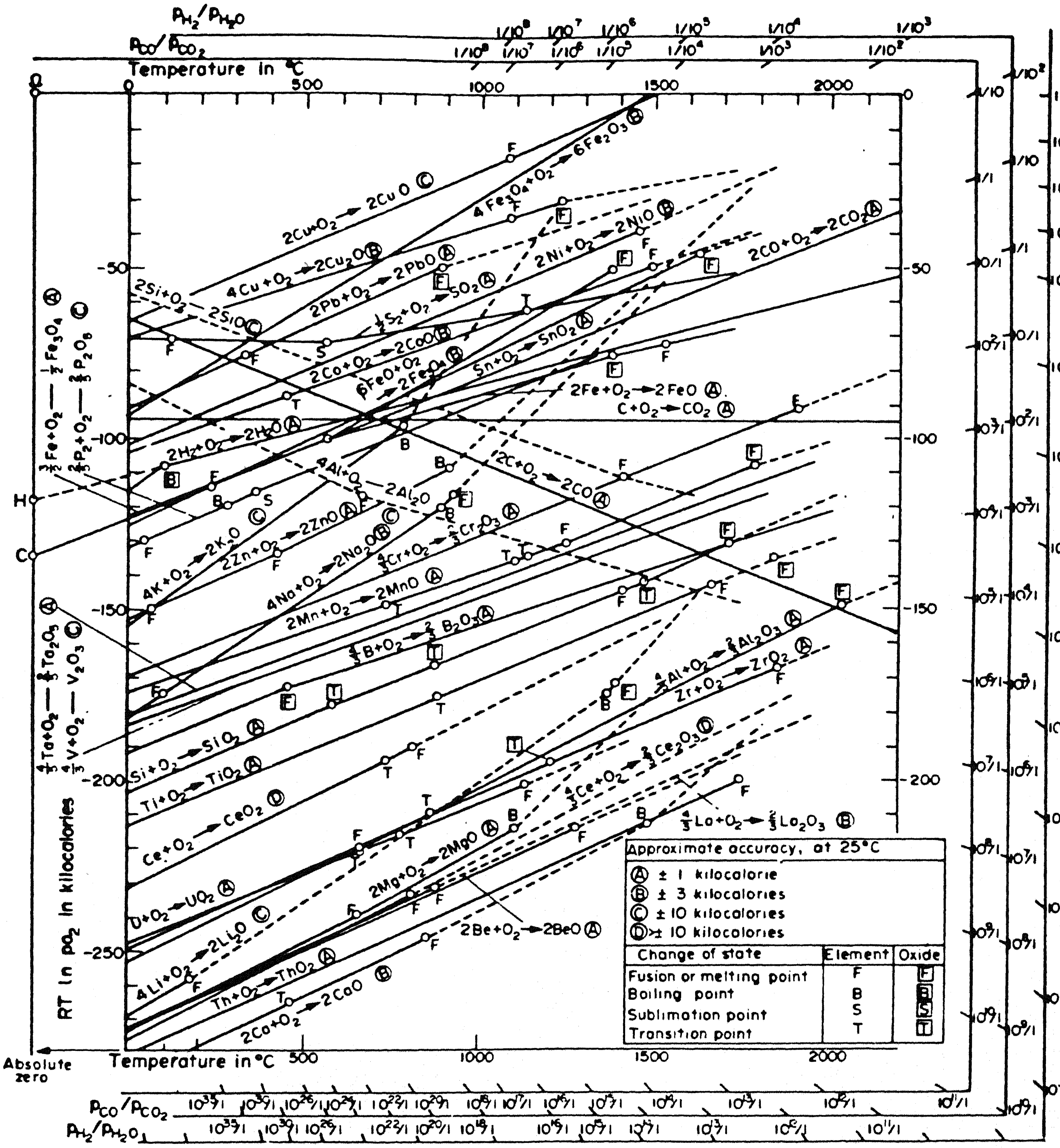

Fig. 2.1 : Standard free energy of formation of some oxides

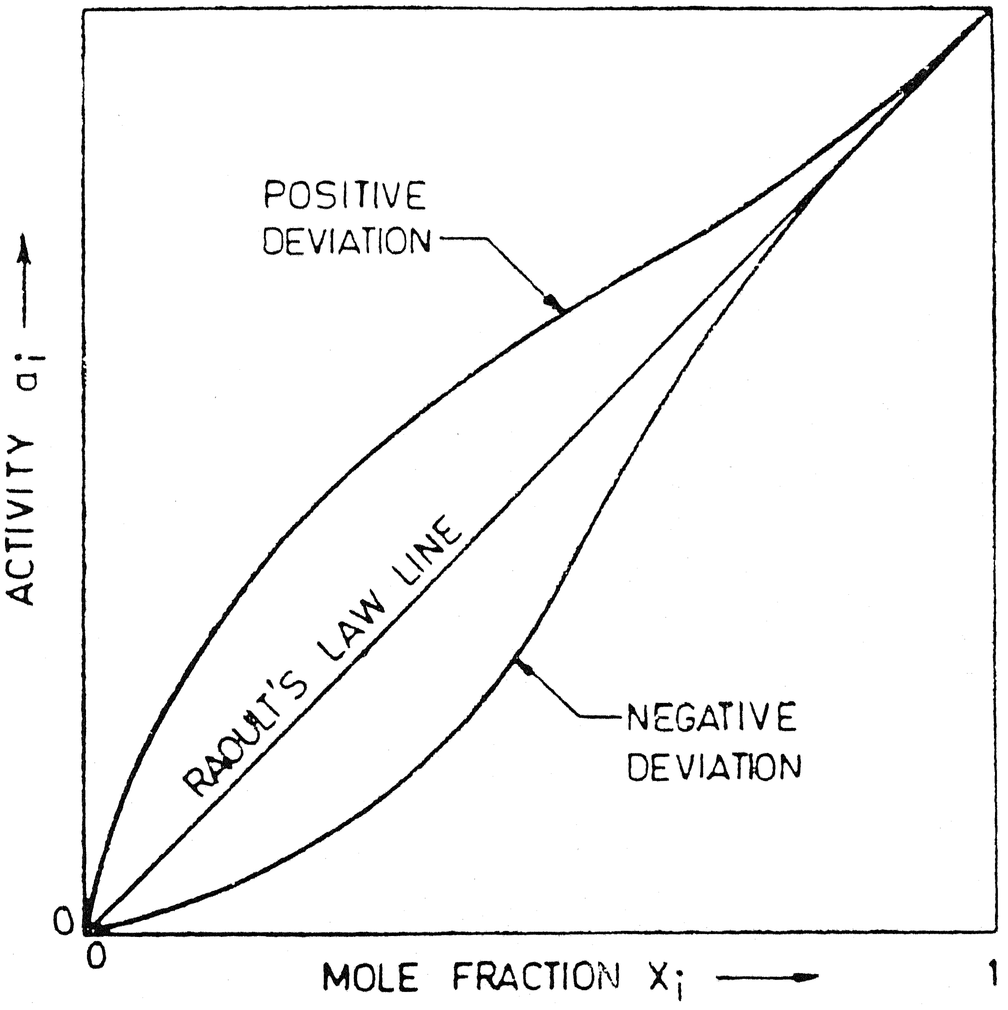

Fig. 2.2 : Raoult's law and real systems showing positive and negative deviations

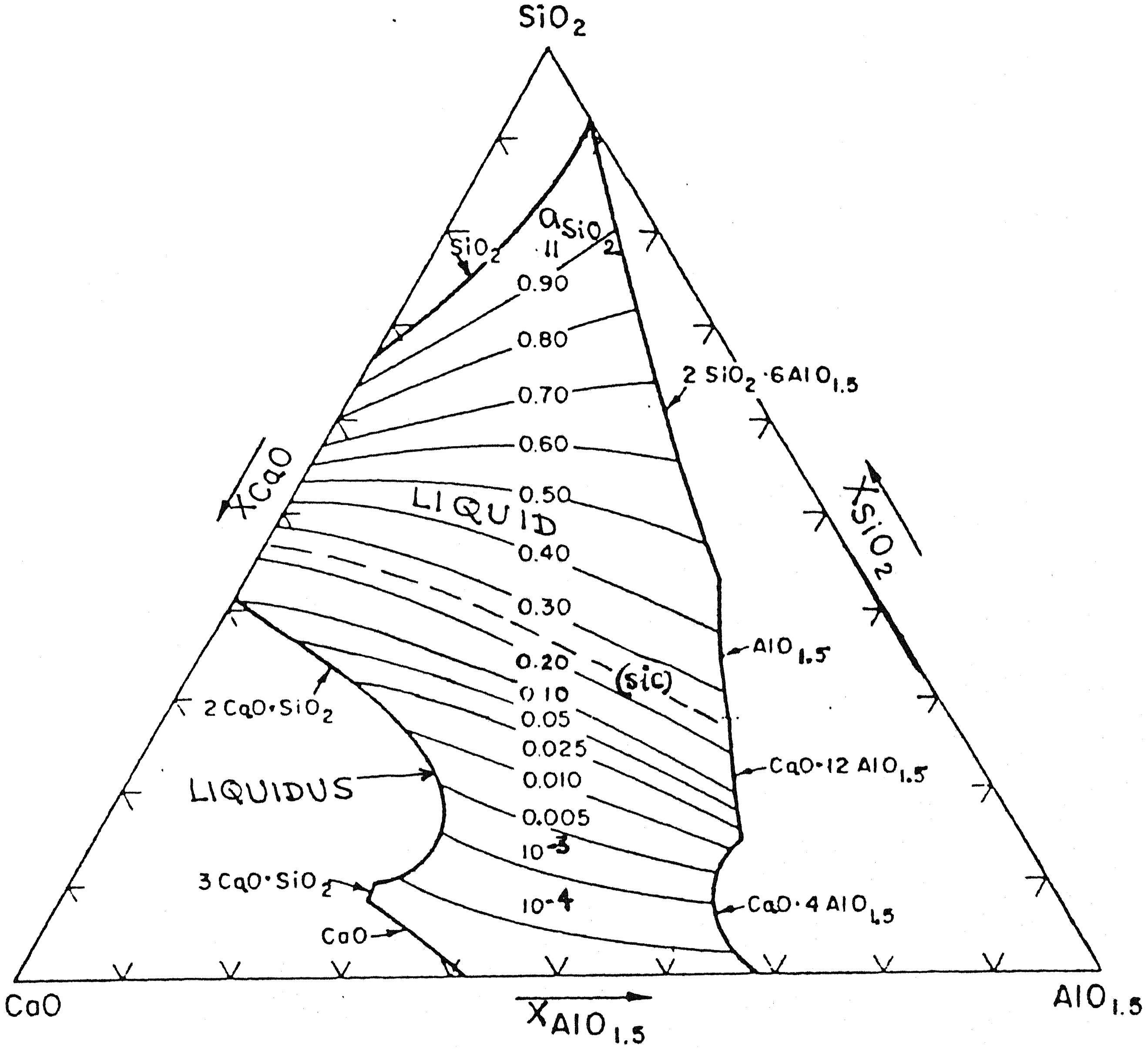

Fig. 2.3 : Activity of SiO_2 in SiO_2 - CaO - Al_2O_3 slag at 1600°C ; the liquid at various locations on liquidus is saturated with compounds as shown (R.H. Rein and J. Chipman, Trans. TMS - AIME, 233 (1965), 419)

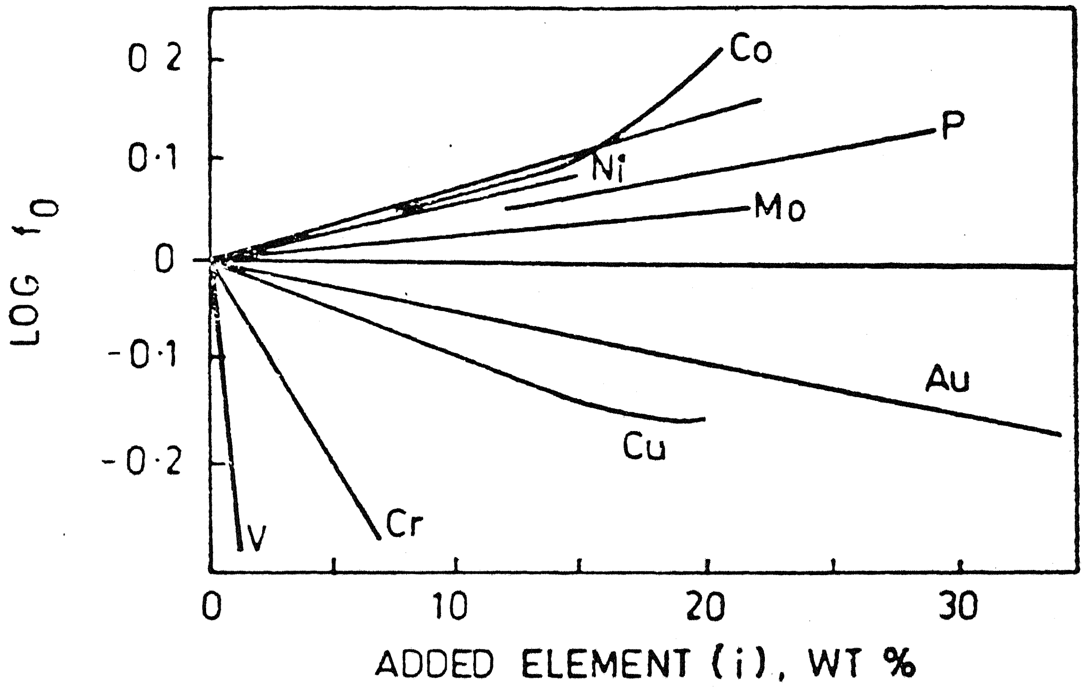

(a) Effect of a third element on Henrian activity co-efficient of oxygen in liquid iron at 1560 °C
[Source : T. P. Floridis and J. Chipman, Trans ASM vol. 29 (1941) 953]

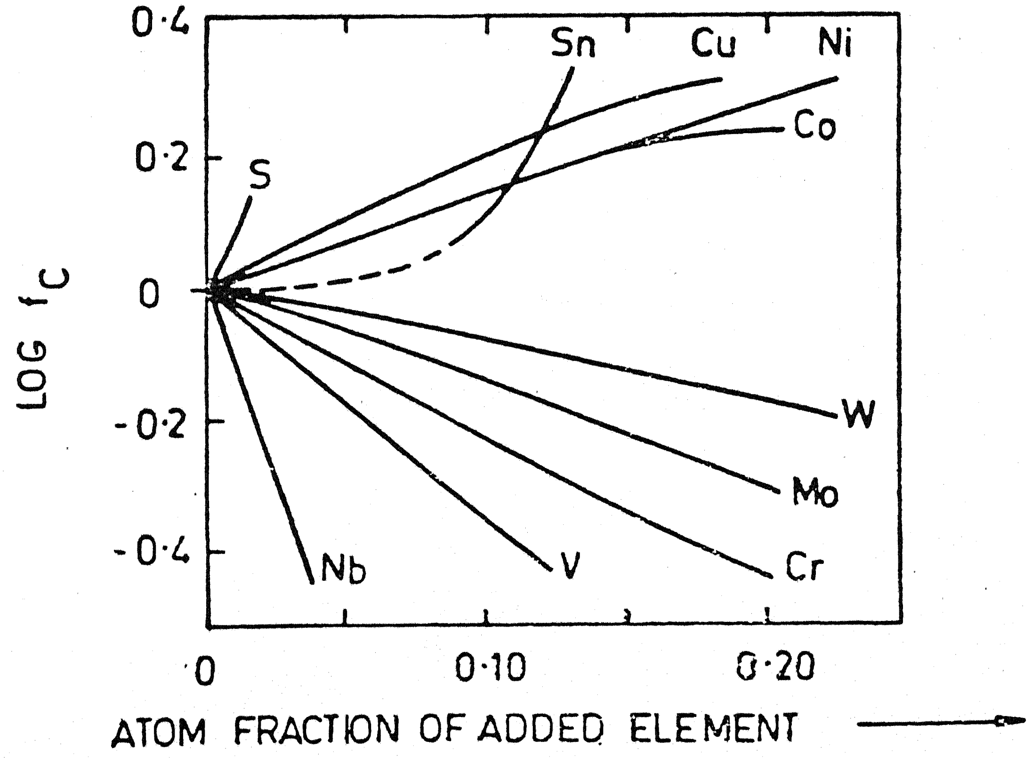

(b) Effect of a third element on Henrian activity co-efficient of carbon in liquid iron at 1560 °C
[Source : T. Fuwa and J. Chipman, Trans TMS, A I.M.E vol. 215 (1959) 708]

Fig. 2.4 Influence of alloying element in liquid iron on the activity co-efficient of a given solute

CHAPTER 3

FLUID FLOW AND MIXING

S.P. MEHROTRA

Mixing processes are prerequisites for homogeneity of temperature and concentrations. Both the distribution of the alloying elements and the exchange between metal, slag and gases are influenced by the fluid flows. Furthermore, the precipitation of new phases, for example during deoxidation, and desulfurization, are stimulated. Fluid flow and mixing are important for vacuum metallurgy too. Today's secondary steelmaking no longer deals with the treatment in the ladle alone but also with procedures in the specially developed metallurgical vessels such as ladle furnaces, vacuum installations, tundishes. A survey of the inducing of fluid flows and movements in melts is given in Fig. 3.1.

In this chapter a brief description of fundamentals of fluid flow and mixing is given.

3.1 SOME BASIC DEFINITIONS

3.1.1 Fluid

A fluid is a substance that deforms continuously under the action of a shear stress. The properties of an ideal fluid are :

(i) A fluid is considered to be a 'continuum' in which there can be no voids.
(ii) At rest the fluid cannot support shear stress.
(iii) Pressure imposed on a fluid at rest is transmitted undiminished to all other points in the fluid.

3.1.2 Stress

Consider a fluid element of arbitrary shape as shown in Fig. 3.2. Let us designate small area ΔA on the surface of this element and suppose that a force F is exerted by the surrounding fluid on this area ΔA. Force being on vectorial quantity can be resolved in two components F_n, and F_t We define

$$\text{Normal stress } \tau_n = \left(\frac{\Delta F_n}{\Delta A}\right)_{\Delta A \longrightarrow 0} \qquad \ldots 3.1$$

$$\text{Shear stress } \tau_t = \left(\frac{\Delta F_t}{\Delta A}\right)_{\Delta A \longrightarrow 0} \qquad \ldots 3.2$$

Fig. 3.3 shows stresses acting on a fluid element in the shape of a cube. The nine stress components are described by the stress tensor as

$$\tau = \begin{bmatrix} \tau_{xx} & \tau_{xy} & \tau_{xz} \\ \tau_{yx} & \tau_{yy} & \tau_{yz} \\ \tau_{zx} & \tau_{zy} & \tau_{zz} \end{bmatrix} \qquad \ldots 3.3$$

Stress tensor is symmetric, i.e.

$$\tau_{xy} = \tau_{yx} \;;\; \tau_{yz} = \tau_{zy} \;;\; \tau_{zx} = \tau_{xz} \qquad \ldots 3.4$$

3.1.3 Pressure Gradient

A particular case of surface forces acting on a fluid element is due to a pressure differential in the fluid. Pressure (P) is a scalar quantity. When shear stresses are absent, the net force on the fluid element is given by

$$F_P = - \nabla p \quad \text{or} \quad - \text{grad } p = - \left(\frac{\partial p}{\partial x} + \frac{\partial p}{\partial y} + \frac{\partial p}{\partial z} \right) \qquad \ldots 3.5$$

3.1.4 Viscosity

The viscosity of a fluid is a measure of its resistance to steady flow. In other words, then viscosity determines the stress of one fluid layer moving smoothly past an adjacent layer. The stress τ_{yx}, resisting the flow of one layer past another is proportional to the negative value of the velocity gradient, i.e.

$$\tau_{yx} = - \mu \frac{\partial v_x}{\partial y} \qquad \ldots 3.6$$

where v_x is the velocity of the fluid in the x direction (the flow direction), and y is distance measured perpendicular to the direction of flow. Proportionality constant μ is known as viscosity. Equation (3.6) is known as Newton's Law of Viscosity.

3.1.5 Newtonian Versus Non-Newtonian Fluids

All those fluids which satisfy Newton's relationship of viscosity are called Newtonian fluids. In such fluids the viscosity depends only on the temperature and pressure and is independent of the rate of shear stress and the time of shear. For fluids containing rather large molecules or dispersed particle or droplets, however, Eq. (3.6) does not apply. Such fluids are referred to as non-Newtonian fluids. For a Newtonian fluid, a plot of τ_{yx} versus $-(\partial v_x / \partial y)$ should give a straight line passing through the origin, and the slope of this line is viscosity. A non-Newtonian fluid would exhibit a non-linear behavior. (see Fig. 3.4)

3.2 FLUID FLOW CHARACTERIZATION

When the Reynolds number, defined as

$$Re = \frac{\rho \, v \, L}{\mu} \qquad \ldots 3.7$$

where v is velocity, ρ is density, μ is viscosity and L is the characteristic length, is small (for flow through conduits, the critical value is usually around 2000) the flow is laminar and when Re is large the flow is turbulent. There is an intermediate transitional regime between these limiting cases which is less well defined.

A laminar flow is microscopically time independent. Hence, on plotting the velocity at a particular location as a function of time, a horizontal straight line is obtained (see Fig. 3.5). In such a situation, transport of heat, mass and momentum takes place by molecular mechanism, with the transport coefficients such as viscosity, thermal conductivity and diffusivity being determined solely by chemical composition, temperature and pressure of the system. Under laminar flow the shear stress between adjacent fluid layers is given by Newton's law of viscosity (Eq. 3.6). The corresponding relationships between the heat and mass flux and the temperature and concentration gradients may be written as

$$q = - k \frac{dT}{dy} \qquad \ldots 3.8$$

and

$$N = - D \frac{dC}{dy} \qquad \ldots 3.9$$

The laminar flow is characterized by distinct streamlines with no cross mixing.

In contrast to a laminar flow, turbulent flow is a manifestation of flow instability and extensive mixing. In turbulent flow inertial (momentum) effects cause the velocity and density, ρ, of the flowing fluid to assume great importance. In this kind of flow, velocity at a particular point in the fluid is not steady but varies, fluctuating with time as, shown in Fig. 3.6.

In turbulent flow, the instantaneous velocity in the x direction is given by

$$v_x = \bar{v}_x \pm v'_x \qquad \ldots 3.10$$

where $\bar{v}_x$ is the time-averaged velocity at any point in the flowing fluid and v'_x is the fluctuation velocity. The fluctuation velocities are sometimes positive, sometimes negative and the time average of them is zero i.e. $\overline{v'_x} = 0$. It is convenient to express the amplitude of the fluctuation velocities in the x direction as $\overline{(v'_x)^2}$, which is the mean of the squares of the fluctuation velocities, this being necessarily positive. One can take the square root of this mean of squares to get a root mean square fluctuation velocity, denoted by $\tilde{v}_x$. Thus

$$\tilde{v}_x = [\,\overline{(v'_x)^2}\,]^{1/2} \qquad \ldots 3.11$$

The fluctuation velocity $\tilde{v}_x$ is a measure of the intensity of the turbulence in the x direction. Similarly, intensities of turbulence in y and z directions are also defined. For fluid flow through a pipe, turbulent intensity may have values of the order of 0.02 to 0.1. Systems where the intensity of turbulence is the same in all the direction are called isotropic.

The velocity fluctuations in a fluid can be measured with sophisticated instruments such as a 'Laser Velocimeter' or 'Hot Film Anemometer'. Figures 3.7 and 3.8 show sketches of these instruments.

The quantities $\rho\overline{v'_x v'_y}$, $\rho\overline{v'_z v'_x}$ have the dimensions of stress and are called Reynold stresses and designate the momentum transfer in the system due to the turbulent fluctuations. Fig. 3.9 is a plot of both the total shear stress and the shear stress contributed by the Reynolds stress for flow in a wind tunnel. It is seen that the Reynolds stresses contribute the dominant mechanism of momentum transfer everywhere except in the vicinity of the wall where the viscous transfer of momentum is important.

An essential feature of turbulent flow is the existence of fluid elements where rapid and local circulating flow occurs. These elements, which are formed and destroyed continually, are termed eddies. Figure 3.10 shows the turbulence eddies in a pipe as viewed by an observer moving at the mean flow rate (from left to right). Near the wall, the strong velocity gradient within the fluid tears the fluid into small eddies. Some of these migrate toward the centre, where larger eddies are also to be found. The large eddies which have dimensions typically one-tenth to one-third of the vessel characteristic length, are called the macroscale. These eddies contain turbulent kinetic energy which is associated with the fluctuating velocity components. The small eddies which may have dimensions of typically a hundred micron or so, are called the microscale of turbulence. It is in these eddies that the turbulent kinetic energy is being dissipated.

The presence of the eddies and the turbulence fluctuations brings about very effective mixing, because mass (and also heat and momentum) can be readily transported by the eddies from one part of the fluid to the other. Under turbulent conditions we can still write formally the following expressions for the shear stress, heat flux and mass flux :

$$\tau_{yx} = -\mu_{eff}\frac{dv_x}{dy} \qquad \ldots 3.12$$

$$q = -k_{eff}\frac{dT}{dy} \qquad \ldots 3.13$$

$$N = -D_{eff}\frac{dC}{dy} \qquad \ldots 3.14$$

but here the transport coefficients, that is, the effective viscosity, thermal conductivity and diffusivity, are no longer molecular properties but are functions of the flow system itself. Indeed, each is a sum of molecular and turbulent components. In general, the turbulent transport coefficients may be some hundred or several thousand times larger than the corresponding laminar values.

3.3 ANALYSIS OF FLUID FLOW

Quantitative analysis of fluid flow in a system primarily involves solution of equation of changes (conservation equations). Equations more relevant to fluid flow are :

(i) equation of continuity (conservation of mass)
(ii) equation of motion (conservation of momentum)

These conservation equations can be expressed in words as

$$\begin{bmatrix}\text{rate of transport in}\\ \text{through system}\\ \text{surface}\end{bmatrix} - \begin{bmatrix}\text{rate of transport out}\\ \text{through system}\\ \text{surface}\end{bmatrix} + \begin{bmatrix}\text{rate of generation}\\ \text{in control volume}\\ \end{bmatrix}$$

$$- \begin{bmatrix}\text{rate of consumption}\\ \text{in control volume}\end{bmatrix} = \begin{bmatrix}\text{rate of accumulation}\\ \text{in system volume}\end{bmatrix} \qquad \ldots 3.15$$

3.3.1 Equation of Continuity

Consider a stationary rectangular volume $\Delta x\ \Delta y\ \Delta z$ (Fig. 3.11) through which the fluid is flowing with velocity having components v_x, v_y, v_z. In a laminar flow transport of a component, say A, is by molecular diffusion and by bulk flow

Transport by molecular diffusion (three dimensions) :

$$x : \quad \overset{\text{In}}{\left[j_x^A (\Delta y\ \Delta z)\ \Delta t \right]_x} - \overset{\text{Out}}{\left[j_x^A (\Delta y\ \Delta z)\ \Delta t \right]_{x+\Delta x}} =$$

$$\left[j_x^A (\Delta y\ \Delta z)\ \Delta t \right]_x - \left[\left[j_x^A (\Delta y\ \Delta z)\ \Delta t \right]_x + \frac{\partial j_x^A}{\partial x} (\Delta y\ \Delta z\ \Delta x)\ \Delta t \right]$$

$$= - \frac{\partial j_x^A}{\partial x} (\Delta x\ \Delta y\ \Delta z)\ \Delta t$$

$$y : \quad \left[j_y^A (\Delta x\ \Delta z)\ \Delta t \right]_y - \left[j_y^A (\Delta x\ \Delta z)\ \Delta t \right]_{y+\Delta y}$$

$$= - \frac{\partial j_y^A}{\partial y} (\Delta x\ \Delta y\ \Delta z)\ \Delta t$$

$$z : \quad \left[j_z^A (\Delta x\ \Delta y)\ \Delta t \right]_z - \left[j_z^A (\Delta x\ \Delta y)\ \Delta t \right]_{z+\Delta z}$$

$$= - \frac{\partial j_z^A}{\partial z} (\Delta x \ \Delta y \ \Delta z) \ \Delta t \qquad \ldots 3.16$$

Transport by bulk flow (three dimensions) :

$$x : \quad \overset{\text{In}}{\left[v_x \rho_A (\Delta y \ \Delta z) \Delta t \right]_x} - \overset{\text{Out}}{\left[v_x \rho_A (\Delta y \ \Delta z) \ \Delta t \right]_{x+\Delta x}}$$

$$= - \frac{\partial (v_x \rho_A)}{\partial x} (\Delta x \ \Delta y \ \Delta z) \ \Delta t$$

$$y : \quad \left[v_y \rho_A (\Delta x \ \Delta z) \Delta t \right]_y - \left[v_y \rho_A (\Delta x \ \Delta z) \Delta t \right]_{y+\Delta y}$$

$$= - \frac{\partial (v_y \rho_A)}{\partial y} (\Delta x \ \Delta y \ \Delta z) \ \Delta t$$

$$z : \quad \left[v_z \rho (\Delta x \ \Delta y) \Delta t \right]_z - \left[v_z \rho_A (\Delta x \ \Delta y) \Delta t \right]_{z+\Delta z}$$

$$= - \frac{\partial (v_z \rho_A)}{\partial z} (\Delta x \ \Delta y \ \Delta z) \ \Delta t \qquad \ldots 3.17$$

Accumulation :

$$\left[\rho_A (\Delta x \ \Delta y \ \Delta z) \right]_{t+\Delta t} - \left[\rho_A (\Delta x \ \Delta y \ \Delta z) \right]_t$$

$$= \frac{\partial \rho_A}{\partial t} (\Delta x \ \Delta y \ \Delta z) \qquad \ldots 3.18$$

Generation :

$$r_A (\Delta x \ \Delta y \ \Delta z) \ \Delta t \qquad \ldots 3.19$$

where

ρ_A – mass density of component A

j_i^A – mass flux of component A by diffusion in i direction

r_A – rate of production (depletion) of A by chemical reaction

Substituting the Eqs.(3.16) to (3.19) in Eq. (3.15), dividing by $(\Delta x\ \Delta y\ \Delta z)\ \Delta t$ and then taking the limit $\Delta x, \Delta y, \Delta z$ and Δt simultaneously approaching zero, we get

$$\frac{\partial \rho_A}{\partial t} + \frac{\partial(\rho_A v_x)}{\partial x} + \frac{\partial(\rho_A v_y)}{\partial y} + \frac{\partial(\rho_A v_z)}{\partial z} = - \frac{\partial j_x^A}{\partial x} - \frac{\partial j_y^A}{\partial y} - \frac{\partial j_z^A}{\partial z} \quad \ldots 3.20$$

In the vector notation this equation can be rewritten as

$$\frac{\partial \rho_A}{\partial t} + \nabla(\rho_A v) = - \nabla\ j^A + r_A \quad \ldots 3.21$$

A similar equation can be written for component B in a binary system

$$\frac{\partial \rho_B}{\partial t} + \nabla(\rho_B v) = - \nabla\ j^B + r_B \quad \ldots 3.22$$

Addition of Eqns. (3.21) gives the equation of continuity on a total basis

$$\frac{\partial \rho'}{\partial t} + (\nabla . \rho v) = 0 \quad \ldots 3.23$$

Note that by definition $\rho_A + \rho_B = \rho$ and $r_A + r_B = 0$ because of conservation of matter in a chemical reaction. The term $(\nabla . \rho v)$ is called the 'divergence' of ρv, sometime also written as div ρv. Note that the vector ρv is the mass flux and its divergence has a simple significance; it is the net rate of mass efflux per unit volume. Equation (3.23) simply states that the rate of increase of density within a small control volume fixed in space is equal to the net rate of mass efflux to the control volume divided by its volume.

A very important special form of the equation of continuity is that for a fluid of constant density (incompressible fluid) for which:

$$(\nabla . v) = 0 \quad \ldots 3.24$$

For turbulent flows, the velocity components are given by the sum of the time smoothed and fluctuating quantities, i.e.

$$v_x = (\bar{v}_x + v'_x)\ ;\ v_y = (\bar{v}_y + v'_y)\ ;\ v_z = (\bar{v}_z + v'_z) \quad \ldots 3.25$$

Substituting Eq.(3.25) into Eq.(3.24) and time smoothing each term, i.e. applying the operator

$$\frac{1}{to}\int_{o}^{to} (v)\ dt$$

the fluctuating component will disappear. Thus we have

$$\frac{\partial \bar{v}_x}{\partial x} + \frac{\partial \bar{v}_y}{\partial y} + \frac{\partial \bar{v}_z}{\partial z} = 0 \qquad \text{or} \qquad (\nabla .\ \bar{v}) = 0 \qquad \ldots 3.26$$

3.3.2 Equation of Motion (Conservation of Momentum)

For a control volume Δx Δy Δz we can write a momentum balance in the following manner :

$$\begin{bmatrix}\text{rate of momentum}\\ \text{in}\end{bmatrix} - \begin{bmatrix}\text{rate of momentum}\\ \text{out}\end{bmatrix} + \begin{bmatrix}\text{sum of forces acting}\\ \text{on the system}\end{bmatrix}$$

$$= [\text{rate of momentum accumulation}] \qquad \ldots 3.27$$

It should be pointed out that unlike mass or energy, momentum is a vector. Thus Eq.(3.27) will represent a vector equation in each of the three coordinate directions x,y and z. For simplicity we consider only x component of Eq.(3.27).

Momentum may be transferred due to bulk motion of the fluid, i.e. convective transfer and due to the components of the stress tensor (molecular transfer).

The rate of transfer of x component of momentum through the six surfaces by convection

$$\qquad\qquad \text{In} \qquad\qquad\qquad\qquad\qquad \text{Out}$$

$$x : \quad \Big[\rho\, v_x v_x\Big]_x \Delta y\ \Delta z \ - \ \Big[\rho\, v_x v_x\Big]_{x+\Delta x} \Delta y\ \Delta z$$

$$= - \frac{\partial}{\partial x}(\rho\, v_x v_x)\ \Delta x\ \Delta y\ \Delta z$$

$$y : \quad \Big[\rho\, v_y v_x\Big]_y \Delta x\ \Delta z \ - \ \Big[\rho\, v_y v_x\Big]_{y+\Delta y} \Delta x\ \Delta z$$

$$= - \frac{\partial}{\partial y}(\rho\, v_y v_x)\ \Delta x\ \Delta y\ \Delta z$$

$$z : \quad \Big[\rho\, v_z v_x\Big]_z \Delta x\ \Delta y \ - \ \Big[\rho\, v_z v_x\Big]_{z+\Delta z} \Delta x\ \Delta y$$

$$= - \frac{\partial}{\partial z} (\rho \, v_z v_x) \, \Delta x \, \Delta y \, \Delta z \qquad \ldots 3.28$$

The rate of momentum transfer by molecular transport across the six surfaces

$$x : \quad [\tau_{xx}]_x \, \Delta y \, \Delta z - [\tau_{xx}]_{x+\Delta x} \, \Delta y \, \Delta z$$

$$= - \frac{\partial \tau_{xx}}{\partial x} \Delta x \, \Delta y \, \Delta z$$

$$y : \quad [\tau_{yx}]_y \, \Delta x \, \Delta z - [\tau_{yx}]_{y+\Delta y} \, \Delta x \, \Delta z$$

$$= - \frac{\partial \tau_{yx}}{\partial y} \Delta x \, \Delta y \, \Delta z$$

$$z : \quad [\tau_{zx}]_z \, \Delta x \, \Delta y - [\tau_{zx}]_{z+\Delta z} \, \Delta x \, \Delta y$$

$$= - \frac{\partial \tau_{zx}}{\partial z} \Delta x \, \Delta y \, \Delta z \qquad \ldots 3.29$$

In most cases the only important forces are those arising from the fluid pressure P and the gravitational force per unit mass g. Thus the resultant force in x direction will be

$$(p|_x - p|_{x+\Delta x}) \, \Delta y \, \Delta z + \rho \, g_x \, \Delta x \, \Delta y \, \Delta z \qquad \ldots 3.30$$

Finally the rate of accumulation of x momentum within the control volume is

$$\left(\frac{\partial \rho v_x}{\partial t}\right) \Delta x \, \Delta y \, \Delta z \qquad \ldots 3.31$$

Substituting foregoing expressions in Eq.(3.27) and dividing the resulting equation by $\Delta x \, \Delta y \, \Delta z$ and taking limits as Δx, Δy and Δz approach zero, we obtain x component of the equation of motion

$$\frac{\partial \rho v_x}{\partial t} = - \left(\frac{\partial}{\partial x} \rho \, v_x v_x + \frac{\partial}{\partial y} \rho \, v_y \, v_x + \frac{\partial}{\partial z} \rho \, v_z \, v_x \right)$$

$$- \left(\frac{\partial}{\partial x} \tau_{xx} - \frac{\partial}{\partial y} \tau_{yx} - \frac{\partial}{\partial z} \tau_{zx} \right) - \frac{\partial p}{\partial x} + \rho g_x \qquad \ldots 3.32$$

For Newtonian fluid with constant density and viscosity, the above is reduced to

$$\underbrace{\rho \frac{\partial v_x}{\partial t}}_{\text{Accumulation}} + \underbrace{\rho \left(v_x \frac{\partial v_x}{\partial x} + v_y \frac{\partial v_x}{\partial y} + v_z \frac{\partial v_x}{\partial z} \right)}_{\text{Transport by bulk flow}}$$

$$= \underbrace{- \frac{\partial p}{\partial x}}_{\substack{\text{Transport due}\\ \text{to pressure}\\ \text{forces}}} + \underbrace{\left(\frac{\partial}{\partial x} \tau_{xx} + \frac{\partial}{\partial y} \tau_{yx} + \frac{\partial}{\partial z} \tau_{zx} \right)}_{\text{Transport due to viscous forces}} + \underbrace{\rho g_x}_{\substack{\text{Transport due}\\ \text{to body force}\\ \text{(gravity)}}} \qquad ...3.33$$

The y and z components of the equation of motion may be similarly written. Adding up the three components of momentum and writing the resulting equation in the vector form we get

$$\frac{\partial}{\partial t} \rho v = - [\nabla . \rho v v] - \nabla p - [\nabla . \tau] + \rho g \qquad ...3.34$$

Using the concept of 'substantial derivative' and the equation of continuity, above equation for an incompressible fluid with constant viscosity be rewritten as

$$\rho \frac{Dv}{Dt} = - \nabla p + \mu \nabla^2 v + \rho g \qquad ...3.35$$

where $$\frac{D}{Dt} = \frac{\partial}{\partial t} + v_x \frac{\partial}{\partial x} + v_y \frac{\partial}{\partial y} + v_z \frac{\partial}{\partial z} \qquad ...3.36$$

Equation (3.35) is the well known 'Navier-Stokes' equation and is valid for laminar flow.
For $(\nabla . \tau) = 0$, Eq. (3.34) reduces to

$$\rho \frac{Dv}{Dt} = - \nabla p + \rho g \qquad ...3.37$$

This is the famous Euler's equation which is widely used for describing flow systems in which viscous effects are relatively unimportant.

For turbulent flow the equation of motion can be obtained by replacing v by $\bar{v}$ + v'and p by $\bar{p}$ + p' everywhere they occur. It can be shown that for turbulent flow

$$\rho \frac{D\bar{v}}{Dt} = - \nabla \bar{p} - [\nabla . \tau^{(l)}] - [\nabla . \tau^{(t)}] + \rho g \qquad ...3.38$$

where $\tau^{(l)}$ is the laminar stress tensor and $\tau^{(t)}$ is the turbulent stress tensor, i.e.

$$\tau^{(t)}_{xx} = \rho\, v'_x\, v'_x \;; \qquad \tau^{(t)}_{xy} = \rho\, v'_x\, v'_y \;; \qquad \tau^{(t)}_{xz} = \rho\, v'_x\, v'_z$$

The components of turbulent stress tensor may be measured experimentally.

Solution of Eq.(3.38) requires relationship between the components of the turbulent stress tensor and the time- smoothed velocity gradients. For turbulent systems such a relationship is more complex and is a property of the system.

3.3.3 Semi Empirical Expressions for the Reynolds Stresses

Some of the commonly used semi empirical relationships to $\tau^{(t)}$ are given below :

Boussinesq's Relation

$$\tau^{(t)}_{yx} = -\mu_t \frac{d\bar{v}_x}{dy} \qquad \ldots 3.39$$

Here μ_t is the eddy viscosity which usually depends strongly on position

3.3.3.1 Prandtl's Relation

By assuming that eddies move around in fluid very much as molecules move about in a gas, Prandtl developed an expression for momentum transfer in fluid in which the mixing length plays a role roughly analogous to that of the mean free path in gas kinetic theory.

$$\tau^{(t)}_{yx} = -\rho\, l^2 \left|\frac{d\bar{v}_x}{dy}\right| \frac{d\bar{v}_x}{dy} \qquad \ldots 3.40$$

Here l is the mixing length and the turbulent viscosity is given as

$$\mu_t = \rho\, l^2 \left|\frac{d\bar{v}_x}{dy}\right| \qquad \ldots 3.41$$

Prandtl's model has the following drawbacks :

(i) Specific expressions are required for the mixing length which may not be available for the system of interest.
(ii) The mixing length model implies zero turbulent viscosity at zero length which is not true.
(iii) The model does not describe satisfactorily the complex flow field i.e. recirculatory flow.

To characterize turbulent viscosity in gas stirred liquid bath the following two models have been frequently used :

(i) one equation $k - \varepsilon$ model
(ii) two equation $k - \varepsilon$ model

In one equation model effective turbulent viscosity is determined solving one differential equation which expresses conservations of turbulent energy. The two equation $k - \varepsilon$ model, originally developed by Launder and Spalding*, basically involves two differential equations representing conservation of kinetic energy and dissipation rate of turbulent energy. These two equations in all contain five empirical constants which must be characterized. Different investigators have used different values for these constants.

Considering the efforts involved in solving the partial differential equations and uncertainties involved in characterizing five empirical constants in two equation $k - \varepsilon$ model, several investigators have used rather simple empirical equations for characterizing the turbulent viscosity. Two typical equations are

$$\mu_t = 0.012 (D)^{2/3} H^{-1/3} \rho_l^{2/3} (16 \rho_g \dot{Q}^3 / \pi^2 d_n^4) \quad \ldots 3.42$$

and

$$\mu_t = 5.5 \times 10^{-3} H \rho [(1-\phi) g \dot{Q} / D]^{1/3} \quad \ldots 3.43$$

where

D - bath diameter
H - bath height
ρ_l - density of the liquid in the bath
ρ_g - density of the injected gas
$\dot{Q}$ - gas flow rate
d_n - nozzle diameter
ϕ - gas hold up

3.4 MIXING

Mixing results from a combination of many phenomena, viz. molecular diffusion, convective or bulk flow and turbulent or eddy diffusion. Any one of these mechanisms alone may not be adequate for complete or perfect mixing (uniform mixture drawn to molecular level).

The bulk motion of fluid associated with turbulence in the vessel is responsible for long range mixing. Such bulk motion also helps in disintegrating large size packets into smaller and smaller 'clumps' (eddies). Dispersion of such clumps assists mixing process and constitutes eddy diffusion mechanism of mixing. A smallest size is reached beyond which viscous forces prevent further shearing of clumps. Even at this stage, the liquid is not 'perfectly mixed' and inhomogeneities exist on microscopic scale. Further homogenization (micro mixing) is possible by molecular diffusion only. Micro mixing is very slow, and unattainable in technological processing operations. On the other hand, the macro mixing which results from bulk motion and disintegration of clumps leading to eddy diffusion is comparatively faster.

---

* B.E. Launder and D.B. Spalding : Computer Methods in Applied Mechanics and Engineering, 1974, Vol. 3, pp. 269 - 89

The progressive breakdown of clumps in macro mixing depends on the mode of stirring in the vessel as well as on the amount of input stirring energy. High temperature metallurgical melts are stirred either by gas injection or electromagnetic stirring. We shall confine our discussion to the former mode of stirring only. In gas stirred bath, the gases may be injected either from the top or the bottom of the vessel. It is generally believed that the mixing is more effective when the gas is injected from the bottom.

3.4.1 Mechanism of Stirring in Gas Injected Baths

When a gas is injected into a liquid bath from the bottom, bubbles are formed. These bubbles rise to the top of the bath due to the buoyancy effect. The rising bubbles cause motion of the liquid in the vessel. If the bubbles are spherical in shape and small in size, they slip through the liquid, causing only local movement of the liquid. Such movement of the liquid does not result in the bulk motion in the vessel - hence the mixing in the bath depends mainly on the molecular diffusion. If, on the other hand, large irregular shaped bubbles are formed, these when rise entrain the surrounding liquid with them thus liquid-gas mixture rises from the bottom of the vessel to the top. This rising two phase mixture is called 'plume' (Fig.3.12). Liquid that rises to the bath surface goes down into the bath along the vessel walls, causing gross circulation of the liquid. Such a flow pattern of the liquid in the bath is known as 'Recirculatory Flow'. The overview of this type of flow is shown in Fig.3.12. It has been established that the measure of recirculatory flow promotes mixing in the bath.

At a high gas velocity, bubbles are not formed at the nozzle tip. Instead a continuous gas phase, which is known as 'Gas Jet', moves through the liquid. However, at some distance above the nozzle the jet is disintegrated into a number of smaller bubbles due to turbulence. The bubbles, thus, generated entrain the liquid causing gross circulation in the vessel. This regime of gas velocities is associated with a gas jet followed by a two phase region. Thus, in this region the gas is neither completely in a plume form, nor in a jet form. This configuration, consisting of a gas jet followed by a plume, is known as 'Buoyant Jet' or 'Forced Plume'.

If the gas velocities are still higher and are equal to or greater than sonic velocity, the gas jet extends itself to a much larger distance above the nozzle tip. In this regime the liquid movement is no more due to bubble entrainment, but only due to the momentum associated with the gas jet. Therefore, the flow pattern shown in Fig. 3.12 may not exist.

3.4.2 Characterization of Mixing Phenomena

Mixing in a bath can be characterized using one of the following approaches / models :

Turbulence Recirculation Model :

In this model the velocities of the turbulent flow fields and the dispersion of an added tracer within these are calculated. The calculation is carried out in three steps :

(a) the turbulent flow field is described by the momentum balance equation. The characteristic parameter in this equation is the eddy viscosity.

(b) eddy viscosity is calculated by the $k-\varepsilon$ model

(c) turbulent diffusion of the tracer is calculated by solving the diffusion equation with the eddy diffusivity.

3.4.3 Mixing Time Measurement

Mixing time is one of the frequently used gross integral parameter to characterize the mixing phenomena. Mixing time is the time taken to attain desired level of mixing in the liquid bath. This desired level of mixing is defined in terms of degree of mixing which implies the extent of uniformity in composition desired in the finished mixture.

One of the commonly used techniques of experimentally measuring mixing time is based on what is known as 'Stimulus Response Technique'. In this technique small amount of a suitable tracer is added to the bulk liquid in the form of an impulse and its response to the stirring of the bath (stimuli) is recorded by measuring some easily measurable property of the bath. Based on this principle the following methods have been employed to measure the mixing time in room temperature baths:

(a) A coloured dye is injected into the liquid bath and its spreading patterns are followed by making visual observations or taking photographs.

(b) State of decolourization is traced after addition of a decolouring agent to a dyed liquid bath.

(c) Warm liquid is used as a tracer and the temperature changes in the liquid bath are recorded with the help of thermocouples.

(d) After injecting a tracer impulse, the concentration variation in the bath are recorded by either measuring pH, the electrical conductivity or refractive index.

Without considering details of the mixing process it follows that the mixing times, t_{mix}, are a function of the energy input per unit mass, $\dot{\varepsilon}$. An empirical relationship of the following form describes a large number of plant and model results.

$$t_{mix} = C\,\dot{\varepsilon}^{-n} \qquad \ldots 3.44$$

where C and n are the empirical constants. Mixing time may be correlated with bath diameter (D) and height (H) in the following manner :

$$t_{mix} = [(D^2/H)^2/\,\dot{\varepsilon}]^{n_1} \qquad \ldots 3.45$$

where n_1 is an empirical constant.

3.4.4 Circulation Model

In the circulation model the mixing time is related to the circulation time t_c of a liquid flow in a gas stirred vessel. Circulation time is the average time required for a liquid element to flow once around the vessel. A typical conductivity versus time curve after injection of a tracer would show successive peaks and valleys with gradually diminishing amplitude (Fig. 3.13) - eventually these become almost undistinguishable and a steady state is obtained. The value of t_c can be obtained from such recorder chart by averaging peak to peak or valley to valley time intervals.

Mathematically circulation time

$$t_c = \frac{\text{Volume of the liquid to be mixed}}{\text{Volumetric flow rate of the liquid in the mixing zone}} \qquad \ldots 3.46$$

Since the liquid in the plume is assumed to be well mixed at any instant of time, the volume of liquid to be mixed can be taken as the volume of the liquid outside the plume zone in the vessel. Thus

$$t_c = \frac{A_{OP}\ H}{V_L} \qquad \ldots 3.47$$

A_{OP} - Bath cross-sectional area outside plume

V_L - Liquid recirculatory flow rate

The circulation time is related to mixing time through the following equation

$$t_{mix} = C_i\ t_c \qquad \ldots 3.48$$

where C_i is the circulation number which is defined as the number of circulations a liquid element makes in the vessel before attaining a certain desired degree of mixing. In metallurgical engineering literature the circulation number is often assumed to be a constant, independent of operating conditions and an arbitrary value of 3 is used. Truly speaking both circulation time and circulation number should be functions of operating conditions. Using the experimental measurements of one of our studies following empirical correlations have been obtained :

$$t_o = 83.1\ \dot{\varepsilon}^{-0.664}\ H^{-0.08}\ d_n^{-0.071} \qquad \ldots 3.49$$

and

$$C_i = 3.92 + 0.166 \ln Fr_m - 6.87 \times 10^{-4} (\ln Fr_m)^2 - 0.636 \ln \left(\frac{H}{D}\right) - 0.138 \left(\ln \frac{H}{D}\right)^2 + 0.395 \ln \frac{dn}{D} - 0.037 \left(\ln \frac{dn}{D}\right)^2 \qquad \ldots 3.50$$

where from the modified Froude number is defined as

$$Fr_m = \frac{v_g^2}{g\ h} \left(\frac{\rho_g}{\rho_l - \rho_g}\right) \qquad \ldots 3.51$$

v_g is the gas velocity at the nozzle exit

3.4.5 Two Tank Model

The two tank model is the simplest one of the partial volumes types. Its principle is shown in Fig.3.14. Within the partial volumes the concentration is assumed to be homogeneous. A mass balance leads to the following expressions for the concentration C_1 and C_2 in the two volumes, if the tracer is added into V_1

$$C_1/C\alpha = 1 + V_2/V_1 \exp(-kt) \qquad \ldots 3.52$$

$$C_2/C\alpha = 1 - \exp(-kt) \qquad \ldots 3.53$$

with

$$k = V (V_1 + 1/V_2) \qquad \ldots 3.54$$

and $C\alpha$ is the concentration after complete mixing. The mixing time is defined by a certain approach to the final concentration $C\alpha$, for instance $t = t_{mix}$ if $C_2/C\alpha = 0.95$.

The concept of two tank models can be extended to partial volume models with more than two tanks. Fig. 3.15 shows as an example a model of a gas stirred liquid divided into three partial volumes. The flows are indicated by arrows.

REFERENCES

1. R.B. Bird, W.E. Stewart, and E.N. Lightfoot : Transport Phenomena, Wiley International, New York, 1960.
2. J.T. Davies : Turbulence Phenomena, Academic Press, New York, 1972.
3. G.G. Krishna Murthy, S.P. Mehrotra and A. Ghosh : Metallurgical Transactions B, Vol. 19B, 1988, 839-850.
4. F. Oeters, W. Pluschkell, E. Steinmetz and H. Wilhelmi : Steel Research, Vol.59, 1988, 192-201
5. J. Szekely and O.J. Ilegbusi : The Physical and Mathematical Modelling of Tundish Operations in Materials Research and Engg., Edited by N.J. Grant, MIT Cambridge, U.S.A.

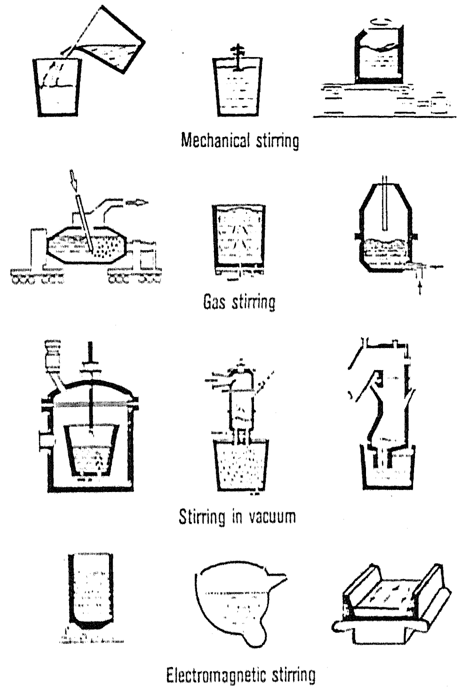
Mechanical stirring

Gas stirring

Stirring in vacuum

Electromagnetic stirring

Fig. 3.1: Different methods for melt stirring

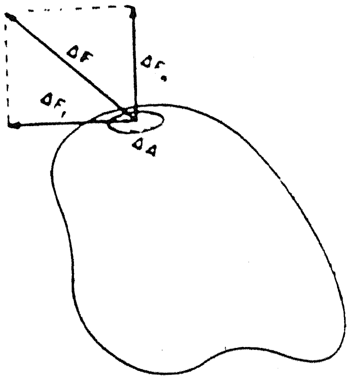
ΔF
ΔF_n
ΔF_t
ΔA

Fig. 3.2: Forces acting on an infinitesimal area on the surface of a fluid

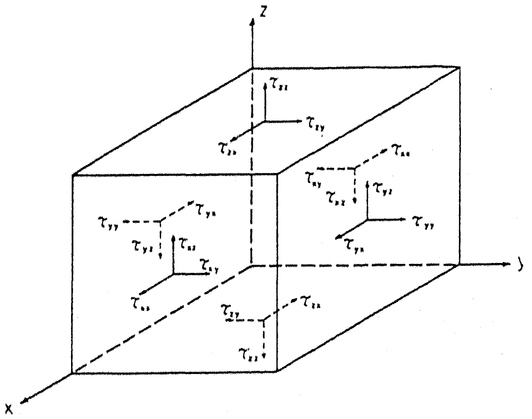
z
y
x
τ_zz
τ_zy
τ_zx
τ_xx
τ_xy
τ_xz
τ_yy
τ_yx
τ_yz

Fig. 3.3: Stresses acting on a fluid stream

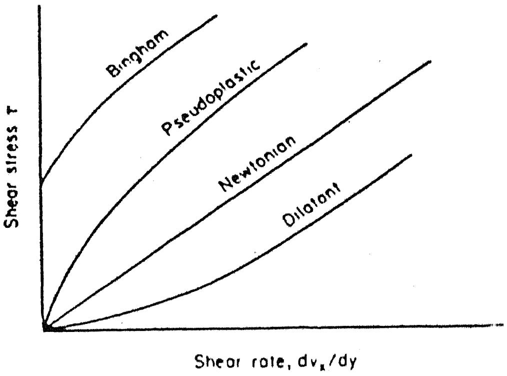

Fig. 3.4: Shear stress plotted against shear rate for Newtonian and non - Newtonian fluids

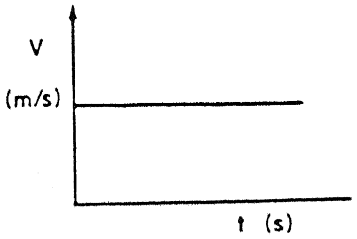

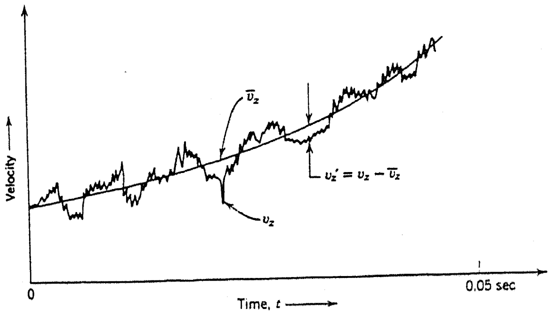

Fig. 3.6: Oscillation of velocity component - about a mean value

Fig. 3.5: Velocity as a function of time at a particular location in a laminar flow

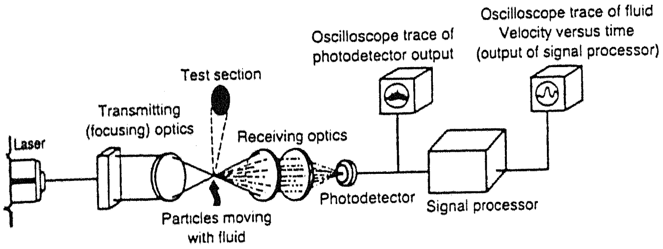
Oscilloscope trace of fluid Velocity versus time (output of signal processor)
Oscilloscope trace of photodetector output
Test section
Transmitting (focusing) optics
Receiving optics
Laser
Photodetector
Signal processor
Particles moving with fluid

Fig. 3.7: Complete dual beam laser doppler velocimeter system

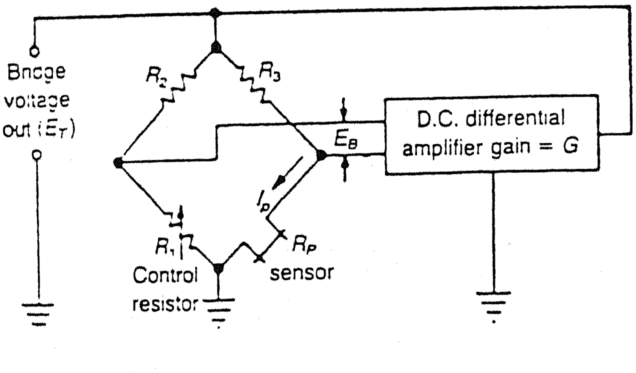
Bridge voltage out (E_T)
R_2
R_3
E_B
D.C. differential amplifier gain = G
I_P
R_1
Control resistor
R_P
sensor

Fig. 3.8: Schematic of constant temperature hot wire anemometer system

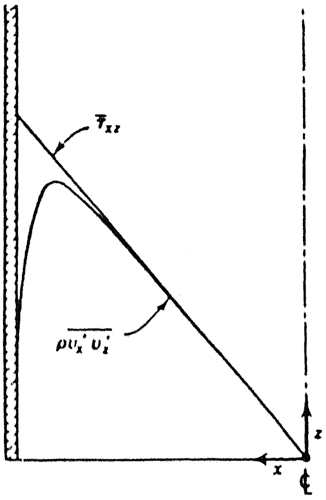

Fig. 3.9: Reynolds stress for flow in a rectangular channel. The quantity τ_{xz} is the sum of $\tau_{xz}^{(l)}$ and $\tau_{xz''}^{(t)}$

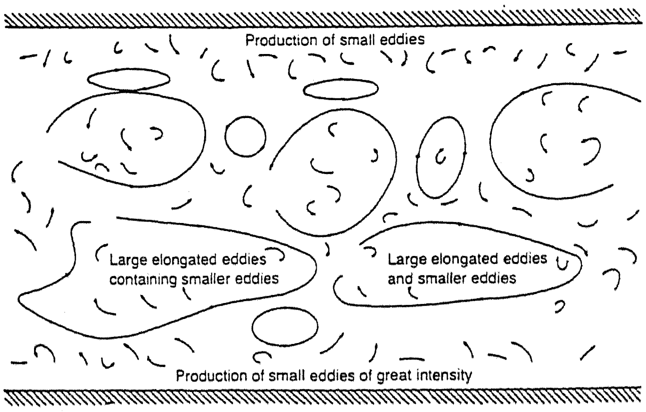
Production of small eddies
Large elongated eddies containing smaller eddies
Large elongated eddies and smaller eddies
Production of small eddies of great intensity

Fig. 3.10: Schematic representation of eddies in pipe flow

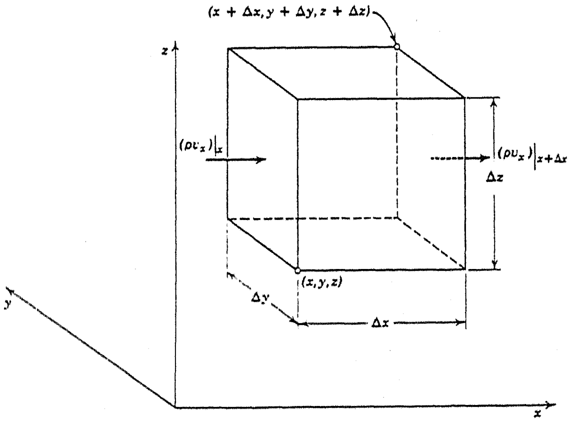
$(x + \Delta x, y + \Delta y, z + \Delta z)$
z
$(\rho v_x)|_x$
$(\rho v_x)|_{x+\Delta x}$
Δz
(x, y, z)
Δy
Δx
y
x

Fig. 3.11: Region of volume $\Delta x \; \Delta y \; \Delta z$ fixed in space through which the fluid is flowing

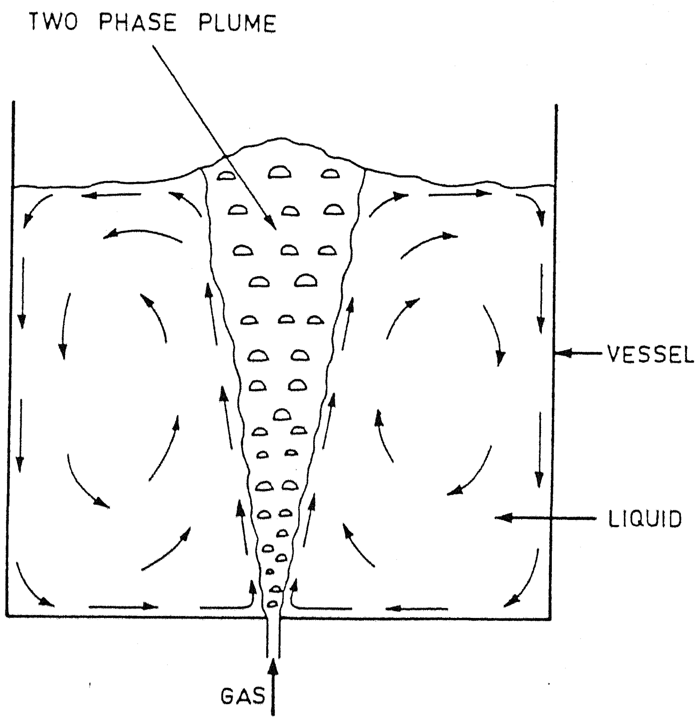
TWO PHASE PLUME
VESSEL
LIQUID
GAS

Fig. 3.12: Flow pattern in a gas stirred liquid bath with a plume

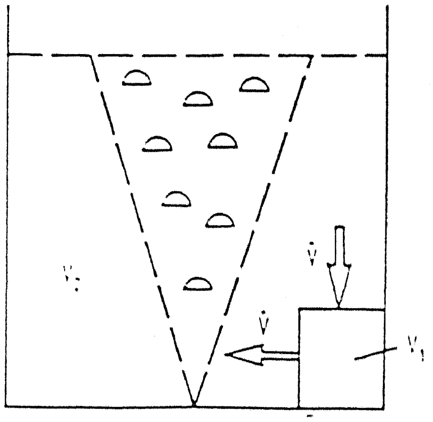
$\dot{V}$
$\dot{V}$
V_2
V_1

Fig. 3.14: Partial volume model

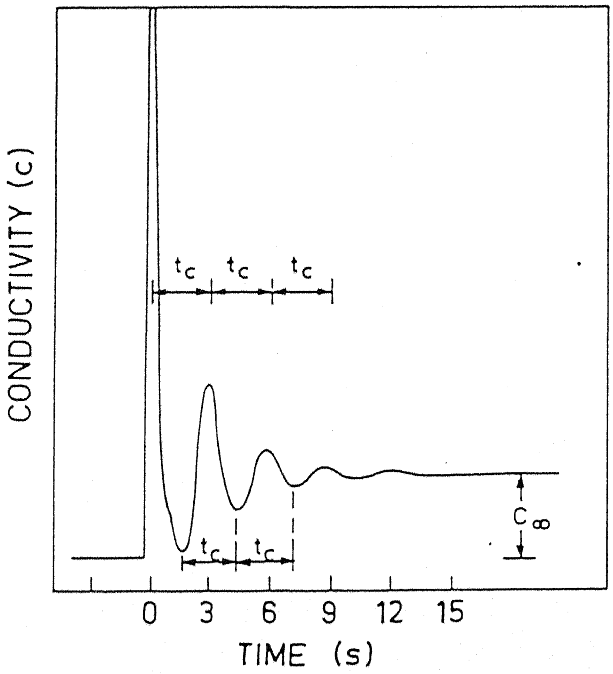

Fig. 3.13: A typical recorder trace of conductivity versus time showing the method of circulation time determination experimentally

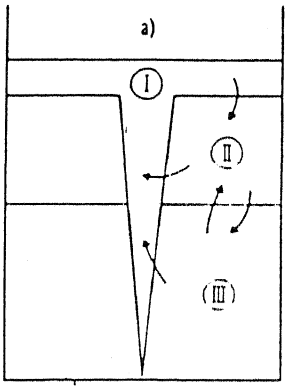

Fig. 3.15: Gas stirred liquid divided into three partial volumes

CHAPTER 4

MASS TRANSFER AND KINETICS

DIPAK MAZUMDAR

4.1 INTRODUCTION

Thermodynamic principles are applied to assess the feasibility of a reaction under a given set of conditions. At high operating temperatures, such as in extraction and refining of metals, the reaction rates are often very fast, so that the system under consideration can be essentially treated at equilibrium. Well known examples are the oxidation of some alloying/inpurity elements during steelmaking. However, most of the processes are not carried out near equilibrium and thus a knowledge of reaction rates, commonly known as kinetics is essential so as to properly analyze the process.

Thermodynamic conclusions, as are well known, independent of the process path, which is not true of kinetics. The rate of reaction or a process is precisely a function of the path, that the process follows during its transition from an initial to the final stage. As the process path depends on a number of details as well as properties of the systems, kinetic predictions, in contrast to thermodynamics, are inexact or at best semi-quantitative.

Since metallurgical systems in general consist of more than one phase, are therefore inherently heterogeneous in nature and hence in evaluating rates of metallurgical processes, one is primarily concerned with the rate of the associated heterogeneous chemical reaction. Consider, therefore, the following slag-metal reaction, viz.,

$$[Mn] + (Fe^{2+}) = [Fe] + (Mn^{2+}) \qquad \ldots 4.1$$

This heterogeneous chemical reaction taking place at the slag-metal interface, consist of several steps, known as ''kinetic steps" These are, for reaction (4.1), as follows :

(i) Transfer of Mn from bulk of the metal phase to the slag-metal interface
(ii) Transfer of Fe^{2+} from bulk of the slag phase to the interface
(iii) Chemical reaction (4.1) at the interface
(iv) Transfer of Fe from the interface to the bulk metal and finally,
(v) Transfer of Mn^{2+} from the interface to the slag phase

Step (iii) is a chemical reaction step and is governed by the laws of chemical kinetics. In much contrast, steps (i), (ii), (iv) and (v) all involve transport of species and hence are mass transfer steps.

The kinetic steps summarized for the reaction (4.1) are in series, and hence, if any one of the five steps is prevented, the overall slag-metal reaction would cease to occur. It is also evident, that the slowest kinetic step influences the overall rate most and consequently, determines the rate of the process. The slowest kinetic step is typically termed as the 'rate controlling or 'rate limiting step'. The conclusions drawn above, would just be reversed if the kinetics steps are in parallel, because there the fastest step influences the overall rate most. However, it is never possible to conceive of a process where all the steps would be in parallel. Consequently, the slowest step in series, would essentially be the rate limiting step.

From the above view point, the slowest step is the most important one and a major subject of all kinetic considerations is to find out what the slowest step is. Needless to say, other steps normally influences the overall process rate to some extent. Moreover, at times, there may be two or more slow steps whose rates might be comparable. However, owing to the complexity of such situations, typically one kinetic step is assumed to control the rate and others are assumed to be infinitely fast, and thus at virtual equilibrium. With such considerations, the rate of a process estimated alone on the basis of the slowest kinetic step would be the highest and naturally greater than the actual observed rate. Consequently, the rate of an overall reaction estimated on the basis of the slowest kinetic step is termed as the virtual Maximum Rate (VMR). The virtual maximum rate thus is a measure of the intrinsic rate of the slowest kinetic step.

4.2 MASS TRANSFER PROCESSES

Mass transfer is concerned with transfer of a chemical species from higher to lower concentration. Mechanisms of mass transfer embody three different modes viz., molecular diffusion, bulk transport via fluid convection and eddy or turbulent diffusion. These are considered below in detail :

4.2.1 Mass Transfer Through Motionless Media

A wide range of mass transfer phenomena in metallurgical operations relate to transfer within solids or equivalent stationary media. For instance, while a steel bar being carburized, a movement of interstitial carbon atoms take place by molecular diffusion (e.g., transport because of concentration gradient) process. It is to be recognized here that with respect to diffusion phenomena through solids there is no coupling of atoms diffusing through a solid with the fluid flow equations. Diffusion process can be conveniently subdivided into steady state and unsteady state processes.

The phenomenological law of diffusion is known as Fick's first law and can be represented as :

$$\text{molar flux} \qquad N_i'' = - D_i A \frac{\partial C_i}{\partial x} \qquad \ldots 4.2$$

$$\text{and mass flux } \dot{n}_i'' = -D_i A \frac{\partial \rho_i}{\partial x} \qquad \ldots 4.2$$

In Eq.(4.2), N_i''/A refers to molar flux of species i across an x (plane normal to x axis. C_i is the molar concentration of species i in moles per unit volume and thus $\partial C_i/\partial x$ represents the corresponding molar concentration gradient. D_i is the diffusion coefficient or diffusivity and has a dimension of L^2T^{-1} . The negative sign on the right hand side essentially implies that concentration decreases along increasing x. Similar interpretations can be made for Eq.(4.3).

Every process analysis dealing with the interchange of mass between various locations in a system, should involve the equation of mass conservation. Hence, the solution to a mass transfer problem must combine the adequate expression of transfer (e.g., Fick's law) with an appropriate mathematical statement of mass conservation. The resulting differential equation is then solved by means of appropriate boundary conditions. Thus, in a 3-dimensional domain mass balance for a species i can be conveniently formulated as :

$$\nabla . \dot{n}_i'' + \dot{r}_i''' = \frac{\partial \rho_i}{\partial t} \qquad \ldots 4.4$$

corresponding expression interms of molar units is :

$$\nabla . N_i'' + R_i''' = \frac{\partial C_i}{\partial t} \qquad \ldots 4.5$$

In Eq. (4.5), $\partial C_i/\partial t$ represents the rate of mass accumulation, while R_i''' is the volumetric rate of mass generation (via any chemical reaction or so). Furthermore, the differential operator ∇ may be conveniently expanded for the three space directions and in different co-ordinate systems by standard mathematical relations.

The boundary conditions as applied to Eqs.(4.4) and (4.5) depend on the physical and chemical characteristics of the system and typically take the following forms :

(a) solute concentration at boundaries known
(b) mass or molar flux of solute through boundary known,
(c) interfacial activities of solute in the two adjacent phases identical and finally
(d) interfacial instantaneous molar fluxes stoichiometrically defined

Eqs. (4.4) and (4.5) in conjunction with the Fick's expression and the appropriate boundary conditions define mathematically the diffusive mass transfer process completely. This presupposes that the diffusivity of the species in the system under consideration is known. Values of diffusion coefficient of different species in widely varying media can be obtained readily from the literature.

4.2.1.1 Pseudo steady state diffusion

Consider the process of oxidation of metals, where the thickness of the oxide layer increases as a function of time. Conceptually, this is clearly a process of unsteady diffusion. However, as most of the oxides are stoichiometric compounds, the overall composition differenced across the growing oxide layer is not appreciable. Consequently, the accumulation terms in Eqs.(4.4) and (4.5) are negligibly small. Therefore, the steady-state versions of Eq.(4.4) and (4.5) is applicable to diffusion across the oxide layer. Similar considerations apply to reduction of metal oxide by any reducing gas. The reduced metal layer which covers the unreduced core of metal oxide is porous and allows diffusion of gases through the pores. However, the pores have little capacity to accumulated gases as compared to the rate of gas supply required to perform reduction. Hence the accumulation term can be conveniently ignored for diffusion across the porous layer.

However, diffusion in the above examples are not steady in a macroscopic sense, since the diffusion path length (thickness across which diffusion is taking place) is a function of time and from this point of view the diffusion is an unsteady process. Therefore, the examples are in between steady and unsteady diffusion and belong to the category of pseudo steady state diffusion.

4.2.2 Mass Transfer in Convective Flow Systems

In the preceding section we were exclusively concerned with metallurgical examples of systems in which there was no bulk motion of the substance through which or across which mass was being transferred. There are, however, a wide variety of systems in which mass transfer mass transfer occurs as a result of both convection and diffusion processes (molecular and/or turbulent diffusion). In any system involving convection, convective components of mass flow generally dominate molecular transport components, except in those regions, such as boundary layers, where the speed of the flow is much reduced. Thus to be able to estimate heat and/or mass transfer rates in connective flow system knowledge of flow is essential.

4.2.2.1 Mass transfer at solid-fluid interface

In the immediate vicinity of the solid-fluid interface, a concentration boundary layer exist in the fluid side during mass transfer between a solid and a fluid. At the solid fluid interface, diffusion is the only mechanism of mass transfer and it can be show that (see Fig. 4.1):

$$(N_i''/A)_{interface} = K_m^i (C_i^s - C_i^b) \qquad \ldots 4.6$$

in which, $K_m^i = \frac{D_i}{\delta_{c,eff}}$. Furthermore K_m^i is the mass transfer coefficient for species i, $\delta_{c,eff}$ is the effective concentration boundary layer thickness. C_i^s and C_i^b refer to surface and bulk concentration of species i respectively. $\delta_{c,eff}$ and hence K_m^i depend on transport properties of fluid (μ, ρ, D etc.), nature of flow (laminar or turbulent), geometry and size of the system. More intense is convection, smaller is $\delta_{c,eff}$ and therefore larger is K_m^i.

To infer mass transfer rates in convective flow systems, typically K_m^i has to be estimated. Towards this, dimensionless numbers are widely employed, which for example include, Reynolds number ($Re = UL/\nu$), Grashoff's number ($Gr = \rho^2 L^3 g \, |\Delta\rho/\rho| / \mu^2$), schmidt number ($Sc = \nu/D$) and sherwood number ($Sh = K_m^i \, L/D_i$). In these, U is a characteristic velocity of the system, ν is the kinematic viscosity of the fluid ($=\mu/\rho$), ρ is the density of the fluid and D_i is the diffusion coefficient of the concerned species.

In general, $Sh = B \, Re^m \, Sc^n$, for laminar forced convection ...4.7

and $Oh = B' Gr^{m1} \, Sc^{n1}$ for laminar free convection ...4.8

In addition, for turbulent flow situation, dimensionless numbers such as turbulent Reynolds number ($Re_t = u'L/\nu$) etc. are also applied.

In Eqs.((4.7) and (4.8) B, B', m, n etc. are constants within ranges of Re,Sc and Gr. These are mostly same for equivalent heat transfer situations many such values have actually been derived from convective hat transfer studies. Some typical mass transfer correlations may be obtained from analogous heat transfer correlations. Only Prandtl number should be replaced by Sc and Nusselt replaced by Sh for this purpose.

4.2.2.2 Mass transfer between two fluids

Reaction between two fluids is exemplified by those of molten metal with molten slag, molten salt or gas. Mass transfer processes between two fluids essentially fall under the surface renewal phenomena, which accounts for the fact that unlike the solid-fluid interfaces considered earlier, interfaces between two fluids are essentially deformable and consequently, velocity, turbulence etc. are not zero at the interfaces between the two fluids.

If the viscosity of one of the fluids is appreciable in comparison to that of the other, it can be conveniently demonstrated that in the high viscosity phase, mass transfer would be exclusively via diffusion process. Moreover, since the surface is getting renewed continuously due to flow at the interface, the diffusion process is essentially unsteady. Further, the geometry of the diffusing medium may be treated as semi-infinite, since exposure time of a fluid packet to the diffusing species is relatively small.

For such a physical situation, starting from the first principle, it can be shown that:

$$K^i_m = 2\left[\frac{D_i}{\pi t_e}\right]^{1/2} \qquad ...4.9$$

in which te is exposure time for mass transfer. Estimation of K^i_m, from Eq.(4.9) allows one to deduce the corresponding mass transfer rates. It is important to mention here that Eq.(4.9) is strictly valid when the flow conditions at the interface is essentially laminar. The mass transfer model represented via Eq.(4.9) is popularly known as "Higbie's surface renewal model".

Application of Higbie's Theory is straight forward provided assumptions are valid and value of t_e is available. However, in practice the flow is turbulent. For such situation Danckwerts proposed another surface renewal theory. He assumed movement of eddy packets to and from interface as cause of surface renewal (e.g., commonly termed as eddy or turbulent diffusion). If eddy clement is assumed to be rigid, the mass transfer taking place within the eddy is therefore by pure diffusion. Similarly, assuming the residence times of eddy elements at the interface to be random, Danckwerts derived that :

$$K^i_m = (D_i S)^{1/2} \qquad ...4.10$$

in which, S is the surface renewal factor and is an experiment alloy determined parameter. It is important to recognize here that both Higbie's and Danckwert's Theory predict that $K^i_m \propto \sqrt{D_i}$, whereas boundary layer theory predicts a more strong dependence of K^i_m on D_i (viz., $K^i_m \propto D_i$).

4.3 THEORY OF REACTION RATES FOR HOMOGENEOUS REACTIONS

4.3.1 Kinetic Laws

The kinetic laws govern relationship between velocity of a chemical reaction and various parameters such as concentration, temperature and pressure. Chemical reactions are specific in nature and, therefore, the rate expressions are determined experimentally. The instantaneous rate of a reaction may be expressed as $-dC_r/dt$ or dC_p/dt where C_r and C_p are the instantaneous concentration of the reactant and the product respectively.

The manner in which the rate of reaction depends on the concentration may be indicated by stating the order of the reaction, which has to be determined experimentally. Thus in a reaction involving A and B as reactants, if it is found experimentally that :

CENTRAL LIBRARY
I.I.T. KANPUR
112509

$$\text{rate} = K\, C_A^a\, C_B^b \qquad \ldots 4.11$$

then, the order of the chemical reaction is (a+b).

In Eq.(4.11), K is the rate constant, which is also known as the specific rate of the chemical reaction. In general, K has been found to increase with increasing temperature. In a limited range of temperature, the variation has been universally found to obey :

$$\log K = A - \frac{B}{T} \qquad \ldots 4.12$$

in which, A and B are two constants.

The rate of a chemical reaction depends on the mechanism (i.e., the path) of the reaction. Therefore, it is essential to obtain much insight into the overall reaction mechanism. The formation of the final products from the initial reactants always takes place by one or more relatively simple steps, in each of which extent of atomic rearrangement is a minimum. The overall chemical reaction may be assumed to be influenced most by the rate of the slowest steps (called the elementary steps). Similarly, the order of a chemical reaction is the order of the rate controlling elementary step.

4.3.2 Law of Mass Action

This states that rate of a chemical reaction is proportional to the product of the active masses of the reacting species. Active mass strictly implies activity. However, typically molar concentration or pressure are also used.

Thus for any reaction,

$$A + B \rightleftarrows C + D \qquad \ldots 4.13$$

according to the law of mass action one may write

$$\text{Rate} = K_f C_A C_B - K_b C_C C_D \qquad \ldots 4.14$$

in which, K_f and K_b are respectively the forward and the backward rate constants which C represents the molar concentration per unit volume.

At equilibrium, obviously, rate = 0 and thus Eq. (4.14) can be conveniently simplified to :

$$K_e = K_f / K_b = \left(\frac{C_C\, C_D}{C_A\, C_B}\right)_{eq.} \qquad \ldots 4.15$$

K_e, in Eq.(4.15) represents the equilibrium constant. In principle, ratios of activity should be employed in Eq.(4.15). However, in view of lack of knowledge on activity or difficulties to use the same, the above approximation is normally accepted.

Rearranging Eqs.(4.14) and (4.15), one may also write :

$$\text{Rate} = K_f \left(C_A C_B - \frac{C_C C_D}{K_e} \right) \qquad \ldots 4.16$$

This is the rate expression for a reversible reaction, which is occurring under conditions close to equilibrium. In contrast, for irreversible reaction (assuming only, forward reaction say),

$$\text{Rate} = K_f C_A C_B \qquad \ldots 4.17$$

One would readily see the resemblance between Eqs.(4.17) and (4.11), mentioned already.

4.3.3 Arrhenius Equation

Equation (4.12) show the dependence of the rate constant with temperature. Arrhenius made further advance is this direction by attempting to explain such a variation. The concept of an activation energy barrier (Fig. 4.2) between reactants and products was thus introduced by Arrhenius to justify the exponential variation of rate constant with temperature, e.g.,

$$K = A \exp(-E/RT) \qquad \ldots 4.18$$

where, E and K are synonymous to E_b and K_f respectively. A, the preexponential in Eq.(4.18) is known as the frequency factor. Physical significance of F_f and E_b are shown in Fig.4.2. Equation (4.18) is the well known Arrhenius equation. This has been successful to correlate K with temperature for a variety of experimental data.

4.3.4 Theory of Absolute Reaction Rates

In view of the success of the Arrhenius equation in chemical kinetics, numerous attempts have been made to interpret the frequency factor (A) and the activation energy (E) from theoretical stand points.

Activation energy of the reaction is determined experimentally by plotting log k as function of 1/T. On the other hand, the frequency factor can be explained fundamentally from the theory of absolute reaction rates. The theory is essentially based on Arrhenius concept of energy barrier and principles of quantum mechanics. Detailed considerations are available in standard texts.

Theory of absolute reaction rates has been applied not only to chemical kinetics but also to a variety of physical rate processes, such as viscous flow, diffusion etc..

4.4 KINETICS OF HETEROGENEOUS CHEMICAL REACTION

As mentioned already, heterogeneity in the characteristics of most metallurgical processes. In section (4.1), a typical heterogeneous chemical reaction and the associated kinetic steps have been considered. There, the desulphurisation chemical reaction essentially occurs at the phase boundary separating the slag and the metal phase. Obviously, the rate of the overall chemical reaction is proportional to the interfacial area. This is in direct contrast to homogeneous chemical reactions, whose rates are proportional to volume. A reaction occurring at interface, is further different from homogeneous reaction from the following view points, e.g.,

(a) adsorption of reactants into the interfacial layer,
(b) chemical reaction amongst the absorbed species, and
(c) desorption of products into the bulk, which is the reverse of the adsorption process

Adsorption refers to incorporation of a species into the interfacial layer, which may be assumed to be few atomic layers thick. Adsorption is classified as physical adsorption and chemical adsorption or chemisorption. In physical adsorption, attractive forces causing adsorption is relatively weak (e.g., typically Vaderwall's type of forces are involved) and is predominant at low temperature. In contrast, in chemisorption (prevalent at high temperature), definite chemical forces are active on the surface and exist between the adsorbed species and the substrate. Heat evolved as a result of such adsorption is of the order of 40 to 400 KJ/mole. The adsorption is essentially irreversible.

The equilibrium relations for the adsorption process at constant temperature are known as adsorption isotherms. Popular adsorption isotherm include :

(a) Langmuir adsorption isotherm (also known as ideal adsorption isotherm and
(b) Gibb's adsorption isotherm

According to Langmuir adsorption isotherm, for a gas adsorbed undissociated on a bare surface site, one can show

$$\frac{\theta}{1-\theta} = K_e \, p \qquad \ldots 4.19$$

in which, θ is the fraction of the site covered, K_e the equilibrium constant for reaction $G + S \rightleftharpoons \underset{\overset{|}{G}}{S}$, and p is the partial pressure of the gas.

When one is concerned with liquid surfaces, Gibb's adsorption isotherm is more appropriate, and accordingly :

$$\Gamma_i = d\gamma / d\mu_i \qquad \ldots 4.20$$

where, μ is the chemical potential of the i being adsorbed in the liquid phase, γ is the interfacial tension, and Γ_i is the excess surface concentration of the adsorbed species (per unit area of the surface). If species i be surface active, then Γ_i is positive and it leads to decrease of γ as μ_i increases.

FURTHER READING

1. R.I.L. Guthrie : Engineering in Process Metallurgy, Oxford Scientific Publications, London & New York, 1990.
2. A. Ghosh and H.S. Ray : Principles of Extractive Metallurgy, Indian Institute of Metals, Calcutta, 1984.
3. A. Ghosh : Monograph on Kinetics of Extractive Metallurgy, I.I.T., Kanpur, 1976.

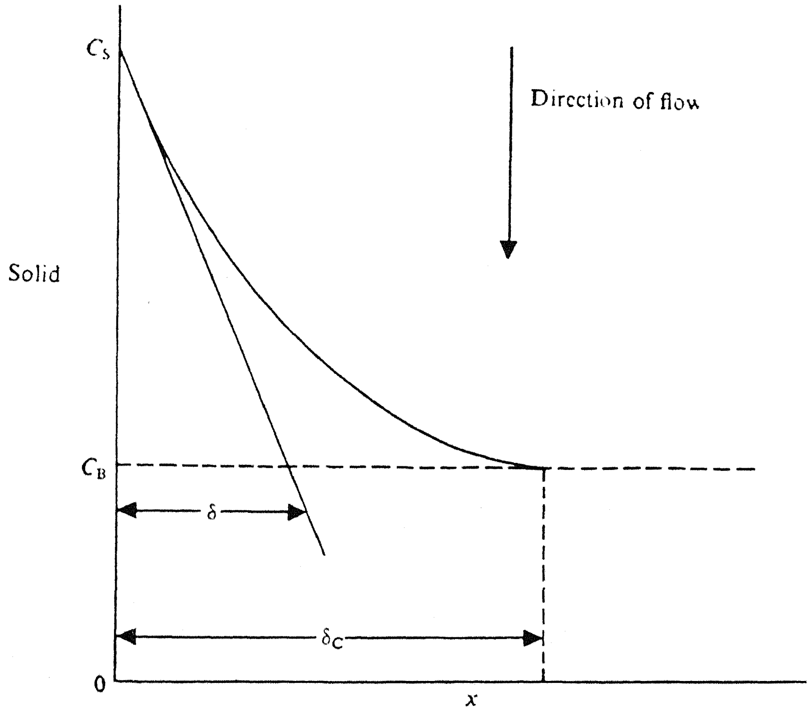
C_S
Direction of flow
Solid
C_B
δ
$δ_C$
0
x

Fig. 4.1 : The concentration boundary layer and the definition of effective concentration boundary layer thickness

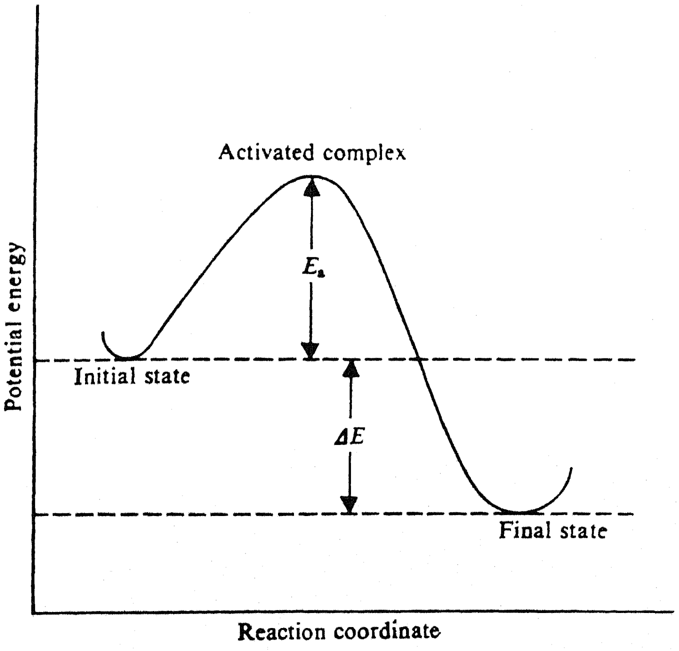
Activated complex
E_a
Potential energy
Initial state
ΔE
Final state
Reaction coordinate

Fig. 4.2 : Energy vs. reaction co-ordinate plot illustrating an activation energy barrier in the path of a process

SECONDARY STEELMAKING PROCESSES

CHAPTER 5

FLUID FLOW AND MIXING IN LADLES

DIPAK MAZUMDAR

5.1 FLUID FLOW IN LADLES

The chemical efficiencies of typical processing operations carried out in steelmaking ladles ladles are intrinsically related to their hydrodynamic performance. Practically, all ladle techniques presently used have one thing in common : most in one way or another employ gas (mostly non-reactive), injected through a submerged lance, porous plug or nozzle to stir the contents of the ladle. It is rather well known that the normal injection of gas into liquid metals is accompanied by the formation of very large bubbles, which are typically spherical cap (or Mushroom) type. In aqueous system, however, at equivalent flow rates, these bubbles could be far smaller and of the pore dimension of the plug. It has also been established that bubbles forming at nozzles or orifices rapidly devolve into a plume of spherical cap bubbles and is particularly typical of numerous processing operations carried out in the steelmaking ladles (1).

The injected gas while rising as a plume to the free surface (the plume results as the bubbles entrains the surrounding liquid during their rise) induces turbulent recirculatory motion of fluid (e.g., steel) within the vessel and this effects mixing, promotes chemical reaction, minimizes temperature and composition inhomogeneities and may aid in inclusion agglomeration and float out. Despite such important role of fluid mechanics in processing ladles, no comprehensive study of hydrodynamics in full scale liquid metal processing ladles can be attempted. This is to be anticipated since high temperature, visual opacity and relatively large sizes of the industrial units often pose serious experimental difficulties. Consequently, aqueous systems have been widely applied to identify the hydrodynamic phenomena at work during ladle refining operations (The basis for use of water as the representative fluid has been discussed elaborately in ch.11). Parallel to this mathematical modelling is often done and extrapolation of this to the actual industrial systems provide useful insight.

5.1.1 Estimation of Macroscopic Flow Variables During Gas Injection into Ladles

The qualitative pattern of the flow at typical flow rates generated in a cylindrical vessel during central injection of gas is shown in Fig.5.1. This shows a recirculating vortex located high in the ladle and displaced toward the outside wall. Thus, a strong outflow of high velocity liquid from the bubble plume passes across the top surface of the liquid, is deflected down the side walls of the ladle, and is then turned back toward the rising plume. It is also readily apparent that most of the high velocity regions are confined to the free surface and the plume region, while elsewhere in the bath, the flow intensity is seen to be rather weak.

The associated field of turbulence viscosity (or diffusivity) is shown in Fig. 5.2 and this shows that higher values are located in the upper liquid regions adjacent to the plumes. The velocity field together with turbulence kinetic energy in ladles during gas injection is of considerable interest and concern from the view point of identifying regions where mixing is at maximum and where alloying addition might at best be introduced. Consequently, it is important to know the distribution of flow parameters in gas stirred ladles as a function of operating variables, such as gas flow rate, liquid depth, vessel radius and so on.

It is well known that ladle processing typically employs low gas flow rates and therefore, the effect of the kinetic power of the input gas ($0.5\ \dot{m}u_o^2$) on the induced flow is considerably less (2) (<<10%).

Indeed, the potential energy afforded by the rising bubbles through the liquid has been identified to be the principal mechanism producing flow recirculation in ladles. Knowledge of the rate of potential energy input or the associated force (viz., the buoyancy) acting on the liquid is necessary, if the ultimate objective is to throw light and draw useful inferences on fluid velocities and turbulence levels in the reactor vessel. It is important to recognize here that input energy in ladles at steady state is dissipated via several mechanisms and this for example, include :

(i) the turbulence energy dissipation loss
(ii) the interphase friction loss (e.g., bubble slippage)
(iii) losses due to the formation of waves and droplets at the free surface as well as friction at the walls and finally,
(iv) losses due to the interaction of the overlying buoyant slag phase with the bulk liquid

The extent of loss of energy due to slag-metal interactions is difficult to quantify and not much is known on this. It has been generally accepted that thermophysical properties of the slag as well the latter's thickness over the bulk phase influences the loss significantly (3). On the other hand, waves and droplet formation at the free surface and friction at the wall put together dissipates only about 10% of the total potential energy input rate.

Thus, considering an ideal no slag situation, the expression of energy balance in gas stirred ladle system can be represented as :

$$E_i = E_{t,D} + E_{e,D} \qquad \ldots 5.1$$

in which, E_i is the rate of potential energy input to the ladle ($= \rho_L\ gQL$), $E_{t,D}$ is the turbulence energy dissipation loss and $E_{s,D}$ is the loss owing to the bubble slippage (viz., the interphase friction).

The potential energy input rate can also be expressed as :

$$E_i = (\rho_L g \alpha V) U_P \qquad ...5.2$$

in which, α is the gas volume fraction in the plume, U_P is the average rise velocity of the plume and V is the volume of the two phase plume. Note that the bracketed quantity in Eq.(5.2) represents the buoyancy force that is exerted on the bulk liquid essentially because of the density deficit in the rising plume with respect to the bulk liquid.

On the basis of Eq.(5.1), one can also write :

$$\eta E_i = E_{t,D} \qquad ...5.3$$

In Eq.(5.3), η represents a fraction governing the rate of generation and dissipation of turbulence kinetic energy in the bath.

An adequate expression, for $E_{t,D}$ can be derived considering any existing turbulence model and this on the basis of the k-ε model, can be represented as :

$$E_{t,D} = 6.038 \frac{\overline{U}^4 \rho_L R^{7/3}}{Q^{1/3}} \qquad ...5.4$$

In Eq.(5.4), $\overline{U}$ is the mean or average speed of recirculation of the bath, R is the vessel radius and Q is the gas flow rate (corrected to mean height and temperature of the liquid).

Thus the appropriate energy balance equation becomes :

$$\eta \rho_L g Q L = 6.038 \frac{\overline{U}^4 \rho_L R^{7/3}}{Q^{1/3}} \qquad ...5.5$$

Taking $\eta = 0.3$ as a typical value for gas stirred ladle (3), one can conveniently derive an appropriate expression for mean speed, $\overline{U}$, in terms of the operating variables as :

$$\overline{U} = 0.81 \frac{Q^{1/3} L^{1/4}}{R^{7/12}} \qquad ...5.6$$

Further more, incorporating the empirical relationship (1), viz.,

$$\frac{\overline{U}}{U_P} (R^{1/3}) = 0.18 \qquad ...5.7$$

into Eq.(5.6), the explicit expression for average plume velocity, U_P can be derived according to :

$$U_P = 4.5 Q^{1/3} L^{1/4} / R^{1/4} \qquad ...5.8$$

As seen from Eqs.(5.6) and (5.8), the mean speed as well as the plume velocity increase according to the third power of the gas flow rate when recirculating flow is induced within the confined mass of liquid in the ladle. Similarly, U_p and $\bar{U}$ are predicted to increase relatively weakly with bath depth (L) and to decrease with vessel radius (R). It is, therefore, apparent that a wider vessel, having more liquid, would slow down the speed. In contrast, for a given gas flow rate, a greater depth of liquid would impart more energy to the liquid increasing the circulation rates.

Some inferences on the turbulence characteristics in the gas stirred ladles can also be made through similar macroscopic considerations (e.g., see ref.1). On the basis of estimated mean speed, average turbulence intensity etc., important estimates can be made of numerous transport processes such as melting, dissolution, dispersion, mixing etc.. It is also important to note, that in view of the relatively small value of η , bubble slippage etc. appear to dissipate quite a significant part of the input energy. Consequently, the size of the bubble in the system and hence the mode of gas injection would exert some influences on the hydrodynamics of the gas stirred ladle system.

5.1.2 The Possible Influences of the Upper Slag Phase on the Fluid Dynamics of Gas Stirred Ladle Systems

The pouring of liquid steel from a furnace into a ladle generally leads to uncontrolled amounts of slag carry over. Being lighter, the slag separates to form an upper phase of variable thickness. It is well known that while the insulating property of the slag are generally beneficial for maintaining liquid steel temperature, its chemical characteristics are often detrimental. During gas injection into ladles, the upper phase interacts in a complex manner (see Fig.5.3) with the bulk liquid steel, and the deformable buoyant slag phase as a result dissipates a considerable part of the input energy (3,4).

Results of comprehensive water model investigation on the dynamics of slag metal interactions in ladles or similar transfer/processing vessels indicate that the slag phase in the immediate vicinity of the plume 'eye' would undergo considerable deformation and this plays a key role in dissipating the input energy. In contrast, the tangential shear generated at the slag-metal interface plays a relatively insignificant role. To issustrate this point further, Fig.5.4 has been included, where the variation in total specific kinetic energy of motion in the bath (i.e., the mean + kinetic energy = $0.5\,\bar{U}^2 + 1.5\tilde{U}^2$) as a function of the specific energy input rate (=rate of potential energy per unit mass i.e., $\rho_L g Q L / \rho_L \pi R^2 L$) has been shown for three different conditions viz., with an overlying phase, no overlying phase and with an wooden block on top of the bulk liquid. It is at once seen that the total energy of motion is drastically reduced in the presence of the overlying slag phase at all specific energy input rate. This dissipation has been attributed to the potential energy required to maintain a deformed oil mass at the oil/water (slag/metal) interface. It is interesting to note that the kinetic energy motion within the ladle is proportionately decreased from the slag free case with increasing gas flow rate (viz., increasing specific energy input rate).

These results from model studies also indicate that a significant portion of the input energy to a gas stirred ladle can be dissipated by an overlying slag phase, during industrial argon/nitrogen stirring operations. This dissipation of input energy in consequence will lead to a decrease in both the mean and turbulence kinetic energies of motion in the bulk steel and may therefore significantly affect the rates of numerous processes viz., alloy melting/dissolution, thermal and particulate mixing etc.. The dissipation, as one can anticipate should be related to the thermophysical properties of the slag and its thickness over the liquid steel. In view of these, the presence of the overlying slag phase would necessarily require a higher specific gas consumption rate so as to lead to compatable rates of various transport processes under equivalent no slag situation.

5.1.3 Application of the Fluid Flow Theories to Industrial Ladle Gas Injection Operations

(i) Estimation of the required protective slag thickness :

During gas injection into ladles, the bubbles escape to the surroundings through an opening created by the plume eye on the overlying slag phase. This leads to the dome shaped structure (typically called the spout) of the slag/air interface, through which considerable amount of thermal energy from the liquid steel normally escapes to the ambient medium. Similarly, the disturbances created in the vicinity of the 'eye' can also lead to significant amount of gas absorption by the bulk liquid steel. In view of these, it is of extreme importance and concern that the required thickness of the protective slag layer be known *a priori* corresponding to a set of specific operating conditions.

Since the kinetic energy of the plume is converted into potential energy at the plume centre line. Therefore, from energy balance point of view, it follows :

$$h_d = \frac{U_p^2}{2g} \qquad \ldots 5.9$$

Consequently, using the previously mentioned plume equation (viz., Eq.(5.8)), it is seen that h_d (height of the dome above the free surface) is approximately 30 cm in 150 t vessel (aspect ratio, L/D =1) at 1 Nm^3 per minute inert gas injection rate. It is to be emphasized here that visual observations of industrial vessel also provide estimates that agrees reasonably well to the values deduced on the basis of Eq.(5.9).

(ii) Inferences of solid liquid mass transfer rates :

A correlation for estimating mass transfer rates in axisymmetric gas bubble driven aqueous system has been proposed recently by the present author (5), e.g.,

$$Sh = 5.81\ (Re_{loc,r})^{0.57}\ (Ti)^{0.82} \qquad ...5.10$$

In the plume region of a gas stirred ladle, Eq.(5.10) can be conveniently represented as :

$$Sh = 5.81\ (d\ U_p\ \rho / \mu)^{0.57}\ (Ti)^{0.82} \qquad ...5.11$$

Incorporating the plume equation into Eq.(5.11) and considering $Ti = 0.3$ as typical of gas stirred ladle system (4), one can readily simplify the preceding equation for $d = 0.01$ m and $D = 2 \times 10^{-9}$ m^2/s to :

$$Sh = 1855\ Q^{0.19} \qquad ...5.12$$

Proceeding further, the explicit relationship between mass transfer coefficient and gas flow rate is obtained as :

$$K_{av} = 3.7 \times 10^{-4}\ Q^{0.19} \qquad ...5.13$$

It is important to note here that the exponent on the gas flow rate, Q, as indicated by Eq.(5.13) is practically equivalent to those deduced experimentally in the plume region of high temperature Fe-C melts (see Fig.5.5).

5.2 MIXING IN LADLES

The intrinsic efficiencies of many chemical processing operations carried out in the present day steelmaking ladles are intricately related to the phenomena of fluid flow and mixing. Mixing in transfer or holding ladles has become particularly important with the developments of processes like continuous casting and secondary steelmaking. To promote mixing in ladles, gas stirring is typically practiced (as this provides a relatively inexpensive source of stirring energy) in which, gas is injected through a porous plug/submerged lance/nozzle. The gas rising as a two phase plume to the free surface, induces a recirculatory motion of liquid and generates turbulence which, in addition to controlling the rate of dispersion and homogenization of alloy additions aids in removing any thermal or particulate inhomogeneities. Therefore, without proper mixing, chemical/thermal and/or particulate inhomogeneities can originate and induce unacceptable variabilities in the final product.

The subject of mixing in processing ladles, is therefore of considerable technoeconimic importance and has justifiably received much attention over the last decade or so (6,7,8). As a result, the influences that the operating variables exert on this important phenomenon is known with reasonable degree of certainty.

5.2.1 The Mixing Phenomena

Mixing results from a combination of many phenomena, viz., molecular diffusion, bulk motion and eddy or turbulent diffusion. Any of these mechanisms alone is not adequate for complete or perfect mixing (e.g., uniform mixing down to the molecular level) even if extremely long period of time is allowed. Consequently, from this point of view, all the three mechanisms are extremely important.

The bulk motion of fluid associated with turbulence in ladle is responsible for long range (viz., macroscopic) mixing. The bulk motion leads to disintegration of large size pockets of fluids into smaller and smaller clumps (called eddies). Dispersion of such clumps in the bulk liquid assists in the mixing process, and constitutes to the eddy diffusion mechanism of mixing. The disintegration of clumps, however, cannot continue indefinitely. Beyond a particular size, viscous forces prevent further shearing of the clumps. Even at this stage, the liquid is not perfectly mixed and inhomogeneities exit on microscopic scale. Further homogenization is possible (viz., micromixing) only by molecular diffusion. The term mixing generally, therefore refers to macro mixing which is the result of the bulk motion and eddy diffusion (viz., the eddying motion) mechanisms.

5.2.2 The Degree of Mixing

In general, mixing times have been used to express the time within which a vessel's liquid contents can reach a state of chemical and/or thermal stability. Various proposals have been made to characterize this state of stability and this essentially follows from the fundamental definition of the degree of mixing, e.g.,

$$\text{Degree of Mixing } (\gamma) = \frac{c - c_i}{c_f - c_i} \qquad \ldots 5.14$$

in which, C_i is the initial uniform concentration, C_f is the final uniform concentration (viz., the bulk concentration) after complete mixing and C is the concentration measured, which obviously is a function of the spatial co-ordinates and time. Clearly, if $C_i \simeq 0$,

$$\gamma = \frac{c}{c_f} \qquad \ldots 5.15$$

and hence any arbitrarily assigned degree of mixing (say 95%) would imply $C = 0.95\ C_f$.

To illustrate this point further, Fig.5.6 shows the variation of C/C_f (= the ratio of local to bulk concentration) at three different locations in a gas stirred bath. There it is readily apparent that the rate of mixing in different regions are markedly different. For example, near the bottom of the ladle, mixing is extremely sluggish, since hydrodynamics and turbulence there are relatively weak. Further more, it is seen by the time region A approaches the 95 pct. mixing mark, the bulk of liquid is practically homogeneous. Consequently, measurements near region A is more representative of the 'bulk 95%

mixing time' for the entire ladle's content than are those derived from locations B and C. It is important to note here that similar conclusion emerges from Fig.5.6, if one considers a 99% mixing criteria instead of 95% . Finally, the definition of degree of mixing is a variable one and the criterion adopted may be specific to a a set of operating conditions depending on the end requirements.

5.2.3 The Influences of Operating Variables on Mixing

A host of variables affect the rate of fluid mixing in ladles, which for example include,

(i) the injected gas flow rate,
(ii) the depth of liquid,
(iii) the vessel radius,
(iv) the mode of gas injection (viz., lance/tuyere/porous plug etc.),
(v) the location of the injector (viz., centre/off centre) and finally,
(vi) the physical characteristics of the overlying slag phase.

Any comprehensive experimental program undertaken on full scale industrial ladles to ascertain the direct influences of the above parameters on mixing times would pose considerable experimental difficulties. Large size of industrial units, high temperature (e.g., ≃ 1600°C) and visual opacity of liquid metal obviously makes such processing units less than convenient case studies. Alternatively, aqueous physical modelling of gas stirred system provides a simple, yet an effective approach for determining the dependence of mixing time on various operating variables.

Nakanishi and Coworkers (9) on the basis of extensive trials on high temperature industrial units as well as on water models of argon stirred ladle claimed that mixing times in reactor vessels follow an universal relationship of the form

$$\tau_m = 12.68 \times 10^3 \, \dot{\varepsilon}_m^{-1/3} \qquad \ldots 5.16$$

in which, τ_m is the 95 pct. mixing time (sec.) and $\dot{\varepsilon}_m$ is the rate of energy input per unit mass of the liquid (W/kg). This relationship has become very popular and widely accepted by the industry (so Fig.5.7). However, Eq.(5.16) implies that the specific shape of the vessel, mode of energy input etc. have no effect on mixing times.

Subsequently, Asai and Coworkers (10) attempted to characterize mixing phenomena in terms of eddy diffusion and fluid convection. On the basis of extensive measurements over different size vessels, an empirical correlation for estimating mixing times has been proposed for gas stirred ladle systems according to :

$$\tau_m = 27.4 \, \dot{\varepsilon}_m^{-1/3} R^{1.96} L^{-1} \qquad \ldots 5.17$$

The authors highlighted the possible influences of vessel geometry and gas injection configuration on mixing times.

More recently, a comprehensive theoretical and experimental investigation has been reported by Mazumdar and Guthrie (11) on mixing times in cylindrical ladles agitated by a centrally rising bubble plume. For specific energy input rate greater than 6 x 10^{-3} W/kg, a correlation for estimating mixing times in cylindrical tanks (0.5 ≤ L/D ≤ 2) during central gas injection has been proposed according to :

$$\tau_m = 25.4 \frac{R^{7/3}}{(\beta\, Q)^{1/3}\, L} \qquad \ldots 5.18$$

in which, β is the fractional depth of lance submergence, Q is the gas flow rate corrected to mean height and temperature (m^3/s), R is the vessel radius (m) and L is the depth of liquid in the ladle (m).

As the energy input rate into the system derives from the potential energy supplied by the rising gas bubbles, the energy input rate per unit mass, $\dot{\varepsilon}_m$ becomes :

$$\dot{\varepsilon}_m = \rho_L\, g\, \beta\, Q\, L \,/\, \rho_L \pi R^2 L \qquad \ldots 5.19$$

with this, Eq.(5.18) can also be rewritten in the form :

$$\tau_m = 37\, \dot{\varepsilon}_m^{-1/3}\, R^{5/3}\, L^{-1} \qquad \ldots 5.20$$

It is instructive to recognize here that Eq.(5.20) is practically equivalent to the one proposed by Asai and Coworkers (viz., Eq.(5.13)), though derived from completely different stand points.

Equation (5.16) further indicates that in addition to the specific energy input rate, the geometry of the vessel (R and L) considerably affects the rate of mixing. It is also clear since mode of gas injection (viz., lance, nozzle or porous plug), as well as the presence of the overlying slag phase determines the rate of specific energy input rate to the system, consequently mixing time is expected to depend on these operating variables as well. Obviously, with the increase in the fractional depth of lance submergence, β , the gas flow rate, Q and the bath depth, L while mixing rate would go up, any increase in the diameter of the vessel in contrast would drastically retard the rates of liquid mixing.

5.2.4 Fundamentals of Mixing Time Calculations in Axisymmetric Gas Bubble Driven Systems

In the presence of a two dimensional velocity field, with no generation, the conservation of a tracer, m_i , is expressed in terms of cylindrical polar co-ordinates, according to :

$$\frac{\partial}{\partial t}(\rho\, m_i) + \frac{\partial}{\partial z}(\rho\, U\, m_i) + \frac{1}{r}\frac{\partial}{\partial r}(\rho r V m_i)$$

$$= \frac{\partial}{\partial z}(\Gamma \frac{\partial m_i}{\partial z}) + \frac{1}{r}\frac{\partial}{\partial r}(r\, \frac{\partial m_i}{\partial r}) \qquad \ldots 5.21$$

The solution to Eq.(5.21) in the presence of a known velocity and turbulence diffusivity field is the essence to the 'theoretical mixing times' (Details of this will be taken up later in the chapter 'Physical and Mathematical Modelling of Secondary Steelmaking Processes'). Thus, the adequacy of Eq.(5.18) can be tested for industrial systems with reference to the equivalent estimates derived via the exact differential model of mixing (viz., Eq.(5.21)).

REFERENCES

1. Y. Sahai and R.I.L. Guthrie : Metallurgical Transactions, Vol. 13B, 1982, pp. 193 - 202.
2. Y. Sahai and R.I.L. Guthrie : Metallurgical Transactions, Vol. 13B, 1982, pp. 125 - 127.
3. D. Mazumdar and R.I.L. Guthrie : Transactions of the Indian Institute of Metals, Vol. 43, No.3, 1990 (in Press).
4. D. Mazumdar, H. Nakajima and R.I.L. Guthrie : Metallurgical Transactions, Vol. 19B, 1988, pp. 507 - 511.
5. D. Mazumdar, S.K. Kajani and A. Ghosh : Steel Research, Vol. 8, 1990 (in Press).
6. J. Mitez and F. Oeters : Canadian Metallurgical Quarterly, Vol. 28, No.1, pp. 19 - 27, 1989.
7. G.G. Krishnamoorthy, S.P. Mehrotra and A. Ghosh : Proceeding, 5th International Iron and Steel Congress, Washington D.C., 1986, pp. 401 - 407.
8. D. Oymo and R.I.L. Guthrie : Proceeding, 4th Process Technology Conference, 1984, pp. 45 - 52.
9. K. Nakanishi, J. Szekely and C.W. Wang : Ironmaking and Steelmaking, Vol. 2, 1975, pp. 115 - 124.
10. S. Asai, T. Okainoto, J. He and I. Muchi : Trans. ISIJ, Vol. 23, 1983, pp. 43 - 50.
11. D. Mazumdar and R.I.L. Guthrie : Metallurgical Transactions, Vol. 17B, 1986, pp. 725 - 733.

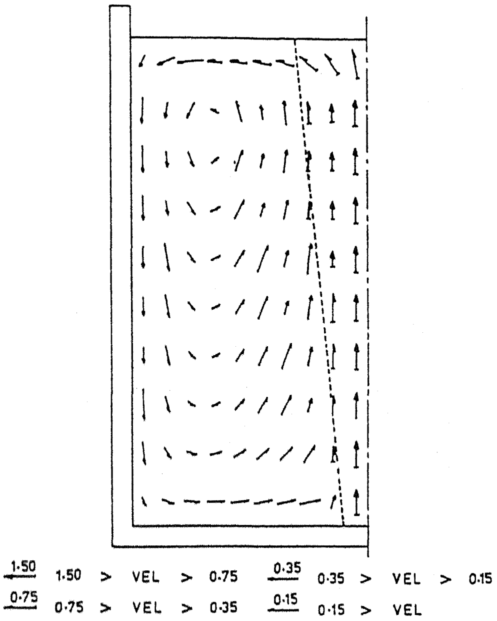
1·50 > VEL > 0·75
0·35 > VEL > 0·15
0·75 > VEL > 0·35
0·15 > VEL

Fig. 5.1 : The velocity field in an argon stirred ladle during axisymmetric gas injection

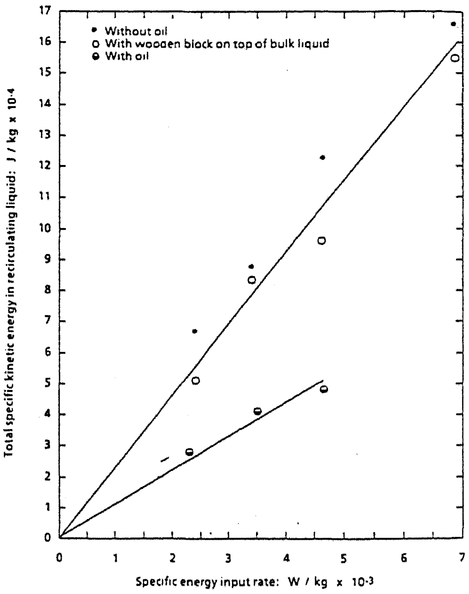

Fig. 5.4 : Energy dissipation by the buoyant slag as a function of specific energy input rate in axisymmetric gas stirred ladle

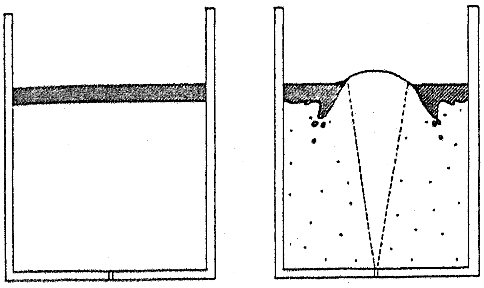

Oil-water system
(*a*) without gas bubbling

(*b*) with gas bubbling

Fig. 5.3 : Phenomena occurring during gas injection in ladles in presence of buoyant slag phase

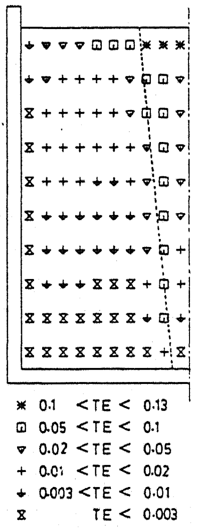
✱ 0·1 < TE < 0·13
⊡ 0·05 < TE < 0·1
▽ 0·02 < TE < 0·05
+ 0·01 < TE < 0·02
↓ 0·003 < TE < 0·01
⧖ TE < 0·003

Fig. 5.2 : The turbulence kinetic energy field in an argon stirred ladle during axisymmetric gas injection

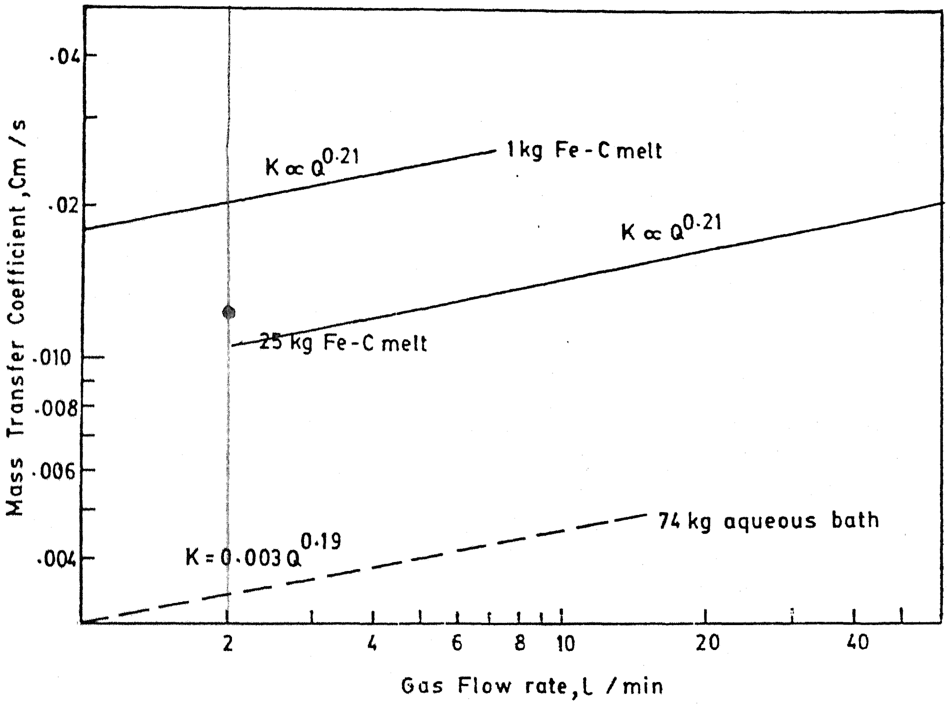

Fig. 5.5 : Variation of mass transfer coefficient as a function of gas flow rate in high temperature and aqueous gas stirred ladles

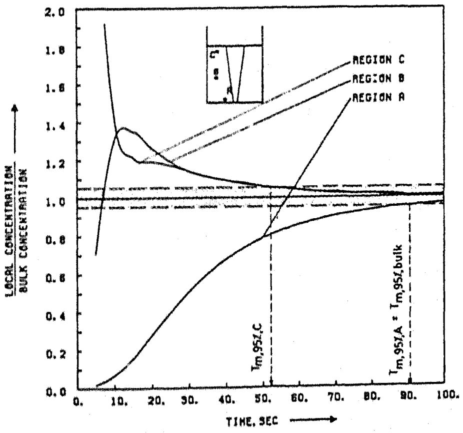

Fig. 5.6 : Rates of mixing in various regions of an aqueous gas stirred cylindrical bath

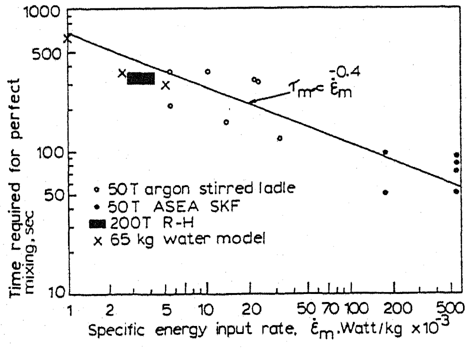

Fig. 5.7 : The universal mixing time correlation of Nakanishi and coworkers (9)

CHAPTER 6

ALLOYING OF STEEL

DIPAK MAZUMDAR

The practice of adding alloying materials to molten steel bath is an integral feature of steelmaking operations. In the industry, where production of large tonnages of various grades of steel are involved, there is considerable interest in trying to achieve optimum steel quality at minimum cost. The problem of reaching this goal is multi-faceted, in that a wide variety of metallurgical, commercial and operating factors enter the picture. While the amount, sequencing and mode of ferroalloy addition will vary from plant to plant, various fundamental factors will determine how quickly these additives will melt, dissolve and incorporated homogeneously into large bodies of liquid metal.

Since the time a cold lump of ferroalloy is projected into the molten steel bath, numerous complex thermal and hydrodynamic phenomena (viz., melting and/or dissolution, dispersion etc.) are involved, till the ferroalloy is completely assimilated into the main bulk of liquid steel. It is first appropriate to review the various thermal events that take place during melting and/or dissolution of typical additions.

6.1 MELTING/DISSOLUTION MECHANISMS

The early stages of an addition's immersion history involve heat transfer from a hot bath of molten steel to a colder solid. Following heat-up of the alloy towards the steel bath temperature and its approach to thermal equilibrium, the addition must dissolve in the steel. If metallic, an addition often follows one of the two main paths before it is mixed into the bath as illustrated in Fig.6.1. For both, there is always a heat transfer stage, involving the formation, growth and subsequent melt back of a solidified shell of frozen bath material. During this time, the temperature of the encased addition rises, tending towards the solidus temperature of the bath. If the solidus temperature of the metal bath is higher then the liquidus temperature of the addition, the latter generally melts inside the solid shell. A liquefied addition will then dissolve and be dispersed into the bulk of the bath following complete (or partial) melt back or collapse of an encasing solidified shell. In literature, such additions whose melting points are lower than the bath melting point are typically called class I (1) alloys. For the steelmaking-addition system, these include, for example ferromanganese, ferrosilicon, silico manganese, ferro chroms etc..

Class II alloys, on the contrary have melting points which are higher than that of the bath. As a result, once the shell is completely re-melted, they remain solid, and must dissolve in the bath as shown in Fig.6.1, via route 2. Dissolution kinetics, being mass transfer controlled, are typically one order of magnitude slower than heat transfer kinetics. Class II alloys, therefore, require considerably longer times than class I alloys to become homogeneously mixed within the bath. Extreme values of addition thermal conductivity, friability, high vapour pressure, heats of mixing, exothermic reactions etc. can somewhat modify the two basic melting/dissolution routes presented in Fig.6.1. For example, exothermic mixing accelerates the dissolution rate of solid titanium in steel by raising the temperature of the dissolving interface (2). Similarly powdered compacts (3), dissolve more rapidly than equivalent sized solid pieces, by virtue of a high surface area to volume ratio once the compact disperses into the melt as particles. Typical examples of this class of alloying additions would include ferro vanadium, ferrotungsten and ferromolybdenum.

It follows from this preamble that the dissolution of a class II alloy is generally slower than that of a class I alloy, and as such often more critical to variations in industrial alloying practices. Incomplete dissolution, non-homogeneous steel etc. may result unless extreme care during processing is taken when class II alloys are added to molten steel bath. Relevant thermo-physical properties of class I and class II ferroalloys are summarized in Tables 6.1 and 6.2 respectively.

6.1.1 Quantitative Prediction of Melting/Dissolution Time

While it is naturally useful to be able to predict how quickly a given ferroalloy of a certain composition, shape and size will melt in a steel bath, the task is complex on account of numerous factors involved for instance, in making accurate prediction for class I ferroalloys, aimed at determining which route will be followed by a given alloy addition and determining how long it will take to melt, it is necessary to describe simultaneous flow of heat through four or five separate regions (viz., the steel shell, the liquid, the mush and solid regions) of the ferroalloy. Such a task is naturally complex in that it requires the simultaneous solution of four or five transient partial differential equations. Similarly, for class II alloys, the mass transfer period following steel shell melt back must be adequately considered. Details of these are outlined elaborately in the literature (for example see ref.3) and hence are not considered here in view of the time constraint.

Since many ferro alloys are produced with wide ranging properties, it is useful to show how one can generalize these results in a simple way. Thus predictions on melting times can be made by completely ignoring any of the thermal phenomena taking place inside the addition, and merely supposing that the melting time is equal to the total heat requirement of the addition divided by the rate at which heat is being supplied from the bath, viz.,

$$T \simeq \frac{\Delta H \rho V_o}{\dot{q}'' A_o} \qquad \ldots 6.1$$

in which, ρ is the addition density, V_o is the volume of addition, A_o

is the initial surface area of addition and ΔH is the heat required to raise unit mass of alloy to 1530°C for route 1 or the alloy's melting point for part II.

Further more, in Eq.(6.1), $\dot{q}''$ is the heat flux to the surface of the addition, which can be conveniently expressed as :

$$\dot{q}'' = h\ (T_B - T_M^s) \qquad \ldots 6.2$$

where, h is the convective heat transfer coefficient, T_B is the bath temperature and T_M^S is the melting point temperature at surface of addition. For a specific alloy addition, the influence of superheat (defined as the difference between the bulk temperature of steel (typically about 1600°C) and its freezing 'point') as well as bath hydrodynamics (on this depends the h value) on the melting kinetics as expressed by Eqs.(6.1) and (6.2) are readily evident. Similarly, as one might anticipate from Eq.6.1, thermophysical properties of additions also affect melting rates considerably.

Apart from bath hydrodynamics, melt superheat etc., various other factors can be important in determining melting kinetics. Among the better known phenomena are those associated with materials having high exothermic heats of solution. The various grades of ferrosilicon represent an important group in this category. Similarly, during projection of an addition into the steel bath, a thin film of gas normally forms around the addition leading to imperfect contact between the solid's surface and the molten bath. This retards the heat transfer rates considerably leading to an increase in overall melting rates. Finally, addition shape, porosity, surface roughness, wettability and a variety of chemical and mechanical features also affect the melting kinetics significantly. In the next section, some basic hydrodynamic factors relevant to addition making techniques are considered.

6.2 HYDRODYNAMIC CONSIDERATIONS

Additions for adjusting melt chemistry are normally made during furnace tapping operations, the most common practice being to throw bags of the various alloys into the eye of the tapping stream or, for higher tonnage operations to mechanically feed them into the teeming ladle via alloy chutes. It has now been well established that while lighter additions (viz., γ = solid-liquid density ratio < 1) such as magnesium, rare-earth silicides, ferrosilicon grades etc. are quite difficult to keep submerged (typical residence time being less than a second), the heavier additions (γ > 1) such as ferroniobium, ferrotungsten etc. would always settle directly to the bottom of the vessel. In much contrast, neutrally buoyant additions ($\gamma \simeq 1$) such as ferrochrome, ferromanganese etc. can undergo prolonged subsurface motion (e.g., remain subsurface) during conventional addition making processes. Such qualitative trends in the trajectories of additions even apply to stagnant or quiescent steel bath.

Subsurface trajectories of additions in steel bath can be conveniently calculated from appropriate force balance equations (4) and hence corresponding submergence time can be estimated. Such trajectory calculations together with appropriate heat transfer considerations can then provide useful inferences on alloys melting subsurface. It's important to recognize here that rates of melting and free dissolution following melting of steel shell (viz., class II alloys) are functions of surface heat and mass transfer coefficients and thus are strongly related to the bath hydrodynamics (viz., flow and turbulence characteristics within the reactor vessel).

Thus, in view of the importance of ladle hydrodynamics in affecting melting/dissolution rates, velocity fields during furnace tapping operations and for porous plug gas stirred situation are of extreme relevance. These for necessary illustrations are shown in Figs. 6.2 and 6.3. For a six minute furnace tapping operation in a 250 ton teeming ladle with a 5° tapper, velocities generated in the bulk of the recirculating liquid range between 0.3 and 1.2 ms^{-1} outside the penetrating jet region. There velocities of $\approx$ 8 ms^{-1} are to be expected following free fall of the steel jet over a 4 m drop from the furnace tap hole into the ladle (5). Similarly, for the case of a typical 250 ton ladle in which gas is injected as a rate of 0.004 $Nm^{3}s^{-1}$, velocities within the rising plume are 1.2 ms^{-1}, while outside, these vary from $\sim$ 1.0 ms^{-1} across the top surface to 0.2 ms^{-1} in the slower recirculating core (6). On the basis of these, depending on the location where any particular addition would undergo melting/dissolution, one can expect considerable variation of associated rates, since velocity is different in different regions and from one configuration to another. Finally, actual trajectories followed by alloy additions dumped into a filled or filling ladle are largely determined by their entry speed, point of impact, the size and most importantly the density.

6.3 MELTING AND DISSOLUTION BEHAVIOR OF SOME ADDITIONS: RESULTS OF PILOT SCALE AND MATHEMATICAL MODEL STUDIES

Figures 6.4(a) through (d) give melting times for spheres of various class 1 alloys immersed in stagnant baths of molten steel. These refer respectively to additions of 80% Fe-Mn, 65% Si-Mn, 50% Fe-Si and Fe-Cr. Referring to these one finds that melting time increases, the larger the addition size as one would normally anticipate. These also show the importance of melt superheat in minimizing melting times. These times, it is to be noted increases exponentially as superheat in the bath approaches zero (At zero superheat, melting times would theoretically be infinite). Under equivalent conditions (size and superheat), the melting times of different additions are different. This is a reflection of different thermal heat (enthalpy) requirements to bring the additions to their respective melting temperatures. It is to be emphasized, that these figures being based on natural convective heat transfer in stagnant baths, are clearly conservative and probably two to four times longer than actual melting times encountered under practical alloy addition processes.

In the case of class II alloys involving mass transfer controlled dissolution processes, natural convective mass transfer rates are considerably smaller than the corresponding heat transfer rates and thus mass transfer process being rate limiting, controls the overall melting/dissolution times. These are clearly obvious from Fig.6.5(a) through (d), which illustrate the dissolution times of some typical class II ferro-alloys such as ferromolybdenum, ferroniobium, ferrotungsten and ferrovanadium. It is obvious, that a stronger convection current in the immediate vicinity of the solid addition enhances the dissolution rates considerably. It is important to mention that these figures also contain the initial thermal period for the steel shell melt back, which is typically about 1% of the total dissolution time.

6.4 INDUSTRIAL CONSIDERATIONS AND ALLOY ADDITION METHODS

A wide variety of methods are available to the industry for making alloy addition to the steel bath. They range from such sophisticated technique as pneumatic injection and bullet shooting to the more mundane procedure of throwing or shovelling. Depending on the addition procedure, the recovery of a particular alloying element may somewhat vary and hence the techniques adopted are of obvious interest and concern.

An alloy's recovery is usually defined as the ratio of the amount left to the amount added. Thus for those additions, made to a filling bath during tapping procedures, a high recovery would indicate minimal losses through : (i) reaction with dissolved oxygen or sulfur in the steel bath, (ii) reaction with air and (iii) reaction with slag. While such a definition of recovery has decided practical merits for making charge calculation, the figures can be a misleading measure of an alloy's efficiency. For example, the recovery of ferrosilicon alloy used in the production of semikilled grades is typically low, perhaps 20% . However, much of the 80% loss is used up quite effectively in lowering the oxygen content of the bath. By contrast, ferro silicon recoveries for fully killed heats can reach as high as 90%, since the amount of silicon then consumed in reducing steel bath oxygen contents becomes only a small fraction of the total amount added. Consequently, efficiency and recovery are not synonymous.

In order to use alloys efficiently and effectively, any premature oxidation through contact with air or slag must be avoided. Ideally, rapid subsurface dispersion and homogenization of the alloy is required and this is particularly difficult to achieve for most of the class I ferroalloys, which normally floats up to the slag metal interface, after an insignificant period of submergence. The serious hydrodynamic problems associated with buoyant additions (Ca, Mg,Fe-Si Si etc.) require, therefore, special attention if subsurface melting is to be achieved in practice and hence premature oxidation through contact with slag is to be avoided. One may note here that class II ferroalloys being heavier than bulk steel, settles to the bottom of the vessel and hence would always undergo subsurface dissolution. Consequently, for buoyant additions the only hope with ordinary addition procedure (throwing or shovelling) is to trap them under the plunging jet, if some subsurface melting is to be expected. Alternatively, special techniques may be adopted to this end. Some of these are described below in nutshell.

6.4.1 Stationary Alloy Ingots

The method involved holding a large rod of solid alloy (Ca, Mg, Al etc.) vertically in a ladle in a similar fashion to a stopper rod-set up . The purpose of this arrangement is to ensure subsurface melting of the addition in the bulk liquid steel. Trials in plant, for aluminium, indicated some higher recoveries by about 10% (7) (e.g., 32% vs. 23%) for low carbon fully killed steel. In terms of efficiency, (100% efficiency 66% recovery), this represented an absolute improvement to about 50% from 35% (see Fig. 6.6).

6.4.2 Wire Feeding

Another way of ensuring subsurface melting is the wire feeding technique. In such cases, the relative motion is provided by the rapid entry of wire into argon stirred ladles. Jet of molten alloy is issued subsurface from the tip of the wire, and thus get assimilated in the bath prior to any reaction with air or slag.

6.4.3 Bullet Shooting

A bullet shooting method (7) developed by Tanoue et al. for Sumito metals, Japan has proved quite successful in promoting subsurface melting of buoyant addition such as Aluminium etc. The work indicated that subsurface melting had been achieved by the use of high entry velocities (~ 50 ms^{-1}) and bullets of high aspect ratio (L/D = 15 : 1).

6.4.4 CAS Process

The conventional argon stirring techniques has important draw backs: (i) reoxidation of liquid steel due to oxidized slag (ii) air oxidation of exposed liquid steel and (iii) inclusion of added alloy in slag during composition adjustment. These drawbacks make argon stirring technique unsuitable as a method for attaining cleaner steel and composition adjustment.

An improved version of this process, the CAS (Composition Adjustment by Sealed argon bubbling) process has solved the above mentioned problems of the conventional argon stirring technique. The new process (see Fig. 6.7) consist essentially of a refractory covered snorkel, which when immersed in a ladle, effectively seals the surface of the liquid steel that becomes exposed when argon gas is injected and permits the addition of ferroalloy without breaking the non-oxidizing atmosphere. The process appears to be a very effective one for making buoyant alloy addition to liquid steel bath (8).

Finally, to enhance the rate of dissolution of class II ferroalloys, it is desirable to crush the lumps of addition to 3 mm ~ 10 mm size range, if these are to completely dissolve during free settling in a 3.5 m deep bath of steel at 1600 °C. Also, the new family of alloys e.g., auto exothermic ferroalloys can be used so as to obtain superior recovery and uniform characteristics (9).

REFERENCES

1. S.A. Argyroponlos and R.I.L. Guthrie : Proceeding Steel making Conference, Chicago, 1982, pp. 156 - 167.
2. S.A. Argyroponlos and R.I.l. Guthrie : Canadian Metallurgical Quarterly, Vol. 18, 1979, pp. 267 - 281.
3. A. Kadaglou : M. Eng. Thesis, Department of Mining and Metallurgical Engineering, McGill University, Montreal, 1983.
4. D. Mazumdar and R.I.L. Guthrie : Applied Mathematical Modelling, Vol. 12(4), 1988, pp. 398 - 401.
5. M. Tanaka : Ph.D. Thesis, Department of Mining and Metallurgical Engineering, McGill University, 1978.
6. Y. Sahai and R.I.L. Guthrie : Metall. Trans. B, Vol. 13, 1982, pp. 203 - 211.
7. R.I.L. Guthrie : Proceeding, Electric Furnace Conference, 1977, pp. 30 - 41.
8. D. Mazumdar and R.I.L. Guthrie : Proceeding, 5th Int. Iron and Steel Congress, Washington, 1986, pp. 1147 - 1158.
9. S.A. Argyropoulos and P.D. Deeley : Proceeding, 24th Annual Conference of Metallurgists, Vancourver, 1985, pp. 139 - 147.

Table 6.1 Physical and thermal properties relevant to class I ferro-alloys

Material	Density $kg\ m^{-3}$	Heat Capacity $J\ kg^{-1}\ k^{-1}$	Thermal Conductivity $W\ m^{-1}\ k^{-1}$	Latent Heat $J\ kg^{-1}$	$T_{solidus}$ K	$T_{liquidus}$ K
Ferromanganese Mn = 79.5% (C = 6.4%) Si = 0.27% Fe: balance	7200.0	700.0	7.53	534654.0	1344.0	1539.0
Silicomanganese Mn = 65.96% Si = 17.07% C = 1.96% Fe: balance	5600.0	628.0	6.28	578783.0	1361.0	1489.0
50% Ferrosilicone Si = 49.03 Al = 1.20% max Fe: balance	4460.0	586.0	9.62	908200.0	1483.0	1500.0
Ferrochrome Cr = 50-58% C = 0.25% max Si = 1.5 max Mn = 0.50 max Al = 1.50 max	6860.0	670.0	6.50	324518.0	1677.0	1755.0

Table 6.2 Physical and thermal properties relevant to class II ferro-alloys

Material, A	Density $kg\ m^{-3}$ (1873 K)	Heat Capacity $J\ kg^{-1}\ K^{-1}$	Thermal Conductivity $W\ m^{-1}\ K^{-1}$	Diffusivity $D_{A/Fe}\ \times 10^{9}\ m^{2}s^{-1}$
Molybdenum	10000.0	310.0	100.0	3.2
Vanadium	5700.0	400.0	50.0	4.1
Niobium	8600.0	290.0	64.0	4.6
Tungsten	19300.0	140.0	115.0	5.9

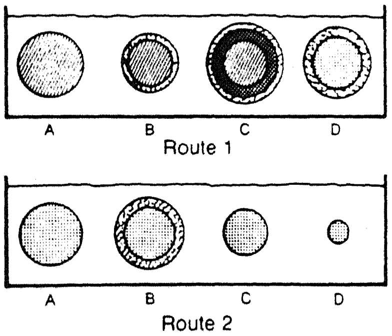
A
B
C
D
Route 1
A
B
C
D
Route 2

Fig. 6.1 : Path taken by alloy additions during melting in the bulk liquid steel

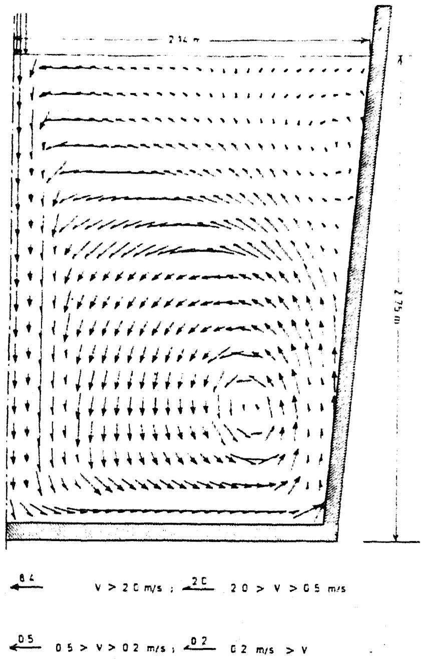
8.4
V > 2.0 m/s ;
2.0
2.0 > V > 0.5 m/s
0.5
0.5 > V > 0.2 m/s ;
0.2
0.2 m/s > V

Fig. 6.2 : Flow fields induced in a 250 ton ladle during furnace tapping operation

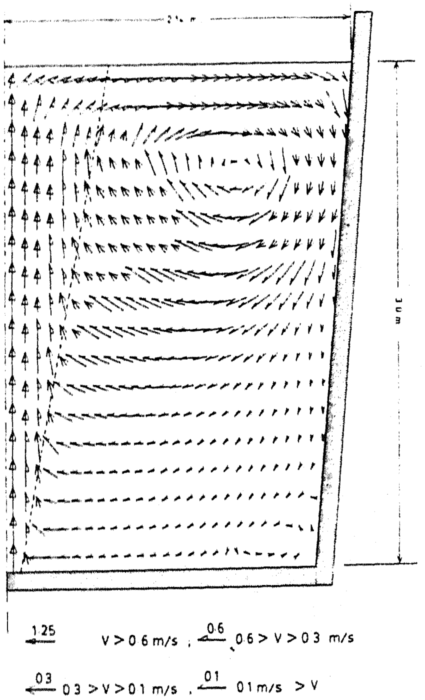
1.25
V > 0.6 m/s ,
0.6
0.6 > V > 0.3 m/s
0.3
0.3 > V > 0.1 m/s ,
0.1
0.1 m/s > V

Fig. 6.3 : Flow field induced in a 250 ton ladle during argon stirring operation

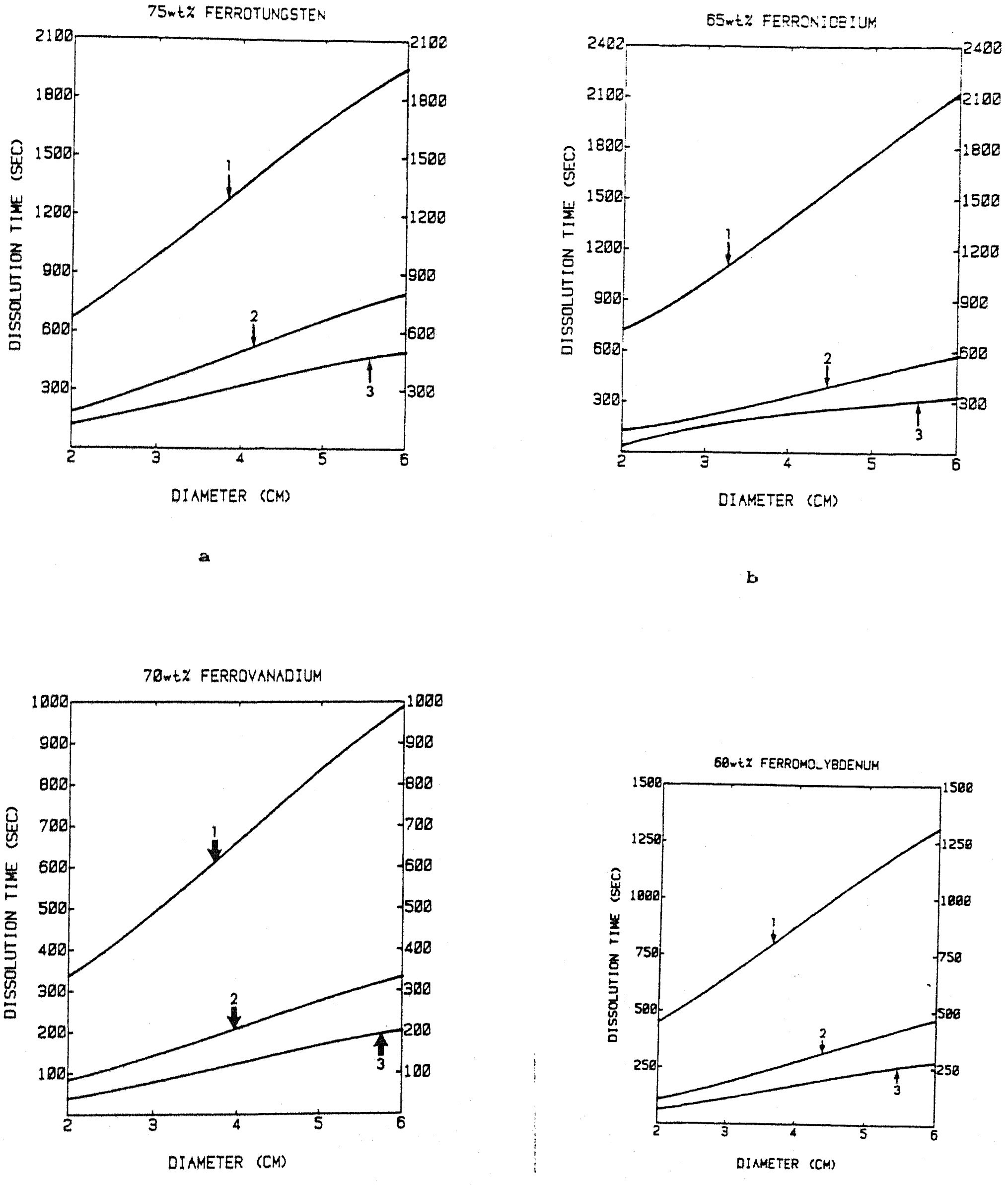

a

b

c

d

Fig. 6.4 : Melting/dissolution of class I ferroalloys in steel

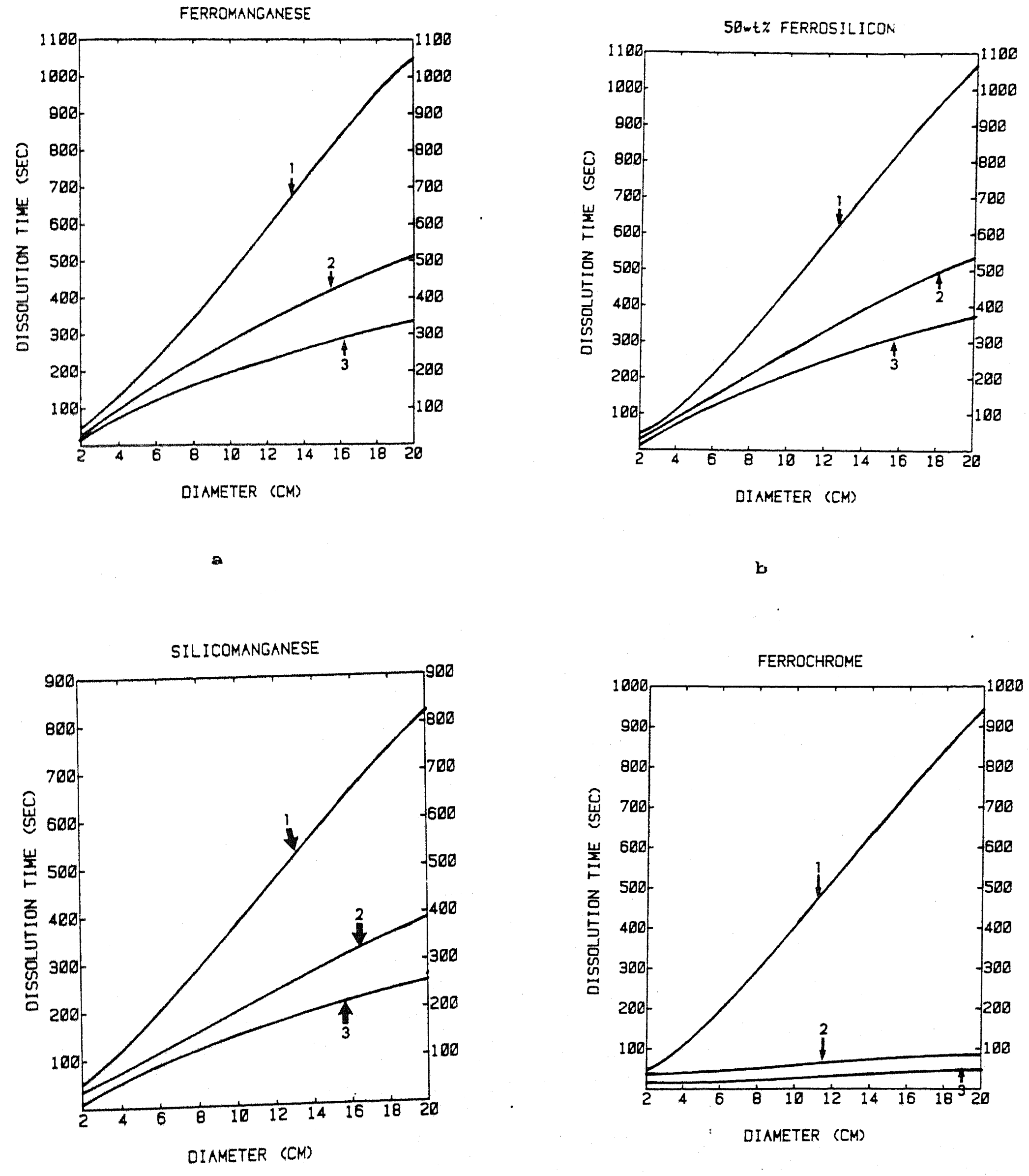

a

b

c

d

Fig. 6.5 : Melting/dissolution of class II ferro alloys in steel

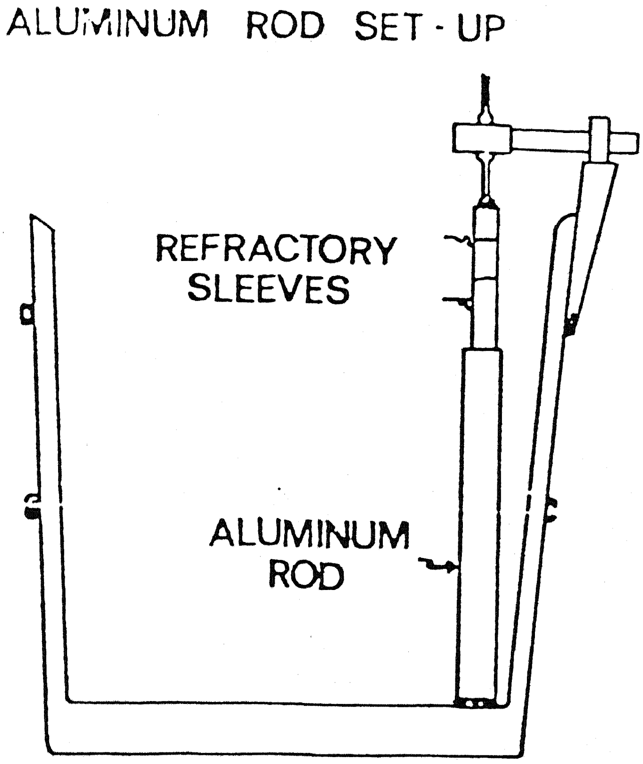
ALUMINUM ROD SET-UP
REFRACTORY SLEEVES
ALUMINUM ROD

Fig. 6.6 : Aluminium rod set up (stationary ingot) for melting aluminium subsurface

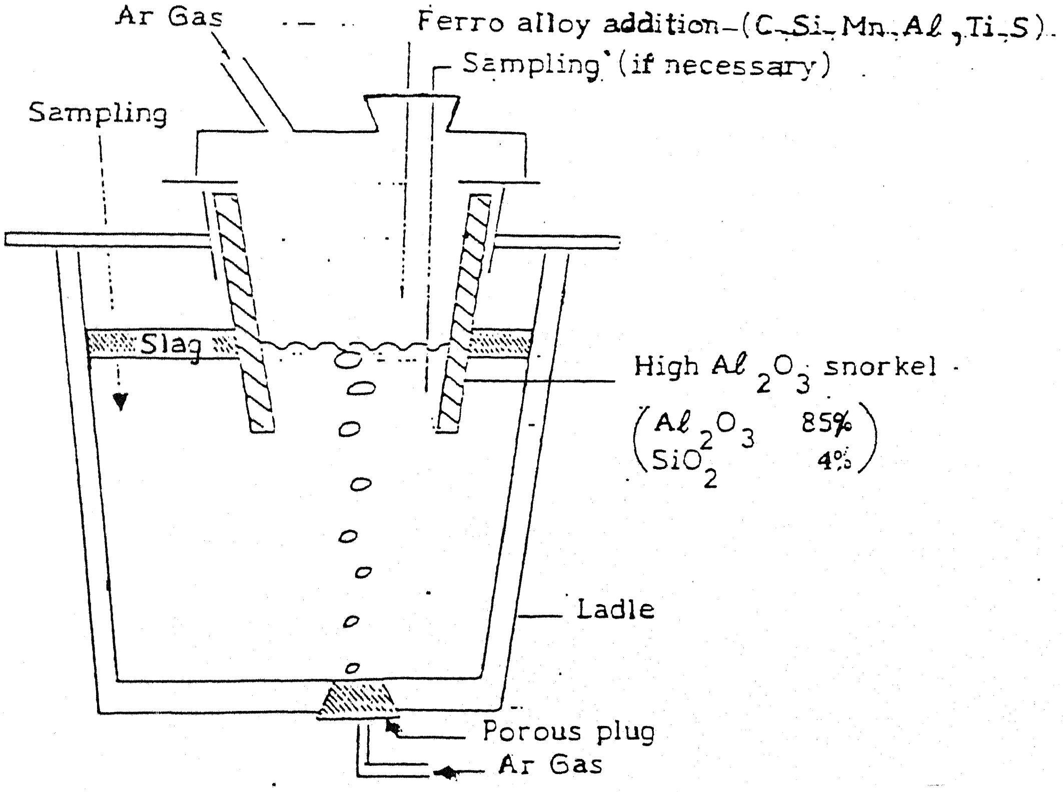
Ar Gas
Ferro alloy addition-(C-Si-Mn-Aℓ-Ti-S)
Sampling (if necessary)
Sampling
Slag
High Aℓ2O3 snorkel
(Aℓ2O3 85%
SiO2 4%)
Ladle
Porous plug
Ar Gas

Fig. 6.7 : The C.A.S. alloy addition practice

CHAPTER 7

DEOXIDATION AND CLEAN STEEL

A. GHOSH

Steelmaking is a process of selective oxidation of impurities in molten iron. During this, however, the molten steel also dissolves some oxygen. Solubility of oxygen in solid steel is negligibly small. Therefore, during solidification of steel in ingot or continuous casting, the excess oxygen is rejected by the solidifying metal. This excess oxygen causes defects such as blowholes and non-metallic inclusions in castings. It also has significant influence on the structure of the cast metal. Therefore, it is necessary to control the oxygen content in molten steel before it is teemed. Actually the oxygen content of bath in the furance is high and it is necessary to bring it down by carrying out `deoxidation' at the end of steelmaking and before teeming the molten metal into ingot or continuous casting mould.

7.1 THERMODYNAMICS OF DEOXIDATION OF MOLTEN STEEL

The dissolution of oxygen in molten steel may be represented by the equation

$$\tfrac{1}{2}\,O_2\ (g) = \underline{O} \qquad \ldots 7.1$$

where O denotes oxygen dissolved in the metal as atomic oxygen.

For the above reaction,

$$K_O = \left\{ \frac{[h_O]}{p_{O_2}^{1/2}} \right\}_{equilibrium} \qquad \ldots 7.2$$

where K_O is equilibrium constant for reaction (7.1), p_{O_2} denotes partial pressure of oxygen in the gas phase in bar, and $[h_O]$ is activity of dissolved oxygen in steel with reference to the 1 wt. pct. standard state.

Again, $$\log K_O = \frac{6120}{T} + 0.15 \quad \text{(ref 1)} \qquad \ldots 7.3$$

and $$h_O = [f_O]\,[W_O] \qquad \ldots 7.4$$

where W_O designates concentration of dissolved oxygen in weight percent and f_O designates activity coefficient of dissolved oxygen in steel. For $\underline{O}$ in pure liquid iron.

$$\log f_O = -\,0.20\,[W_O] \qquad \ldots 7.5$$

The above relations would allow us to estimate W_O in liquid iron at any value of p_{O_2} with which the molten iron would be brought to equilibrium. This value of W_O is nothing but solubility of $\underline{O}$ at that p_{O_2} . However, oxygen tends to form stable oxides with iron. Therefore molten iron becomes saturated with $\underline{O}$ when the oxide starts forming i.e. when liquid iron and oxide are at equilibrium. This oxide, in its pure form, is denoted as Fe_xO, where x is approximately 0.985 at 1600°C. For the sake of simplicity we shall take x equal to 1 often and designate this compound as FeO.

The relevant equation for calculation of solubility of $\underline{O}$ in molten steel is noted below (1).

$$Fe_xO(l) = x\ Fe((l) + \underline{O}\ (wt.pct.)$$

$$\text{and, } \log K_{Fe} = - \frac{6372}{T} + 2.73 \qquad ...7.6$$

$$\text{where, } K_{Fe} = \left\{ \frac{[h_O] \times [a_{Fe}]^x}{(a_{Fe_x O})} \right\}_{equlm} = \text{Equilibrium constant for Eq.(7.6)}$$

$$...7.7$$

Here, a_{Fe} = activity of Fe in metal phase in Raoultian scale $(\simeq 1)$, and (a_{Fe_xO}) denotes activity of Fe_xO in oxide phase.

In case FeO is not pure and it is present in an oxide slag, then $a_{FeO} < 1$, and h_O i.e. solubility of $\underline{O}$ in equilibrium with the slag would be less.

The traditional method of determination of oxygen in steel samples is chemical analysis by vacuum fusion or inert gas fusion apparatus. Here a sample of solidified steel is taken in a graphite crucible and then heated to approximately 2000°C under vacuum or under highly purified inert atmosphere. The steel sample molten and the oxygen contained in it reacts very fast with the crucible and generates carbon monoxide. The quantity of CO is measured by a sensitive instrument such as infrared analyzer and from it the quantity of oxygen in the sample is estimated. This apparatus has been made quite accurate and fast.

Quite often, especially in industrial molts, the bath not only contains dissolved oxygen but also oxide particles. The above method of determination gives the total oxygen content, which is the sum of dissolved O and oxygen in inclusions. This hampered progress of our understanding about the behaviour of oxygen in steelamking and deoxidation till the development of immersion oxygen sensors based on materials such as ZrO_2 doped with CaO or MgO or Y_2O_3 and ThO_2 doped with Y_2O_3 during the decade of 1960. Thereafter this has become quite a popular tool for measurement of dissolved oxygen content in molten steel both in the laboratory as well as in industry. Excellent reviews are available in literature on the principles and details of such sensors (2,3).

There are various designs available in market now a days. For the sake of illustration, Fig.7.1 shows the sensor employed by Fruehan et al (6) schematically. The ZrO_2 (CaO) or ThO_2 (Y_2O_3) disk serves as the solid electrolyte and at high temperature it is an ionic conductor with O^{2-} as the only mobile ionic species. Cr, Cr_2O_3 mixture is the reference electrode. This assembly is immersed in liquid steel. Molten steel constitutes the other electrode. A molybdenum Al_2O_3 cerment dips into it and the electrical circuit is completed by platinum lead wires connected to measuring circuit. These sensors can be used only once, i.e. they are disposable type. Immersion time required is at the most a minute or so. Efforts are going on to develop sensors that can be continuously immersed in liquid steel for longer period. Laboratory successes have been reported.

Such sensors behave as reversible galvanic cells. Since the solid electrolyte conducts oxygen ions only, the cell E.M.F. is related only to the difference of chemical potentials of oxygen at the two electrodes.

$$\mu_{O_2} \text{ (liquid steel)} - \mu_{O_2} \text{ (reference)} = -ZFE \qquad ...7.8$$

where μ_{O_2} designates chemical potential of oxygen, F is Faraday's constant, Z is valency (4 here) and E is cell E.M.F.

The galvanic cell in Fig.7.1 may be represented as :

$$\underset{\text{(reference)}}{Cr(s) + Cr_2O_3(s)} \;\Big|\; ZrO_2 \text{ (CaO)} \;\Big|\; \underline{O} \text{ (in liq.steel)} \qquad ...7.9$$

Here μ_{O_2} (reference) = RT ln p_{O_2} (ref)

$$= \Delta G_f^{\,o} \text{ for formation of } Cr_2O_3(s) \qquad ...7.10$$

and μ_{O_2} liq.steel) = RT ln p_{O_2} (in equil.with liq.steel)

$$= 2RT \ln \frac{[h_O]}{K_O} \text{ (from Eq.7.3)} \qquad ...7.11$$

Therefore, knowing ΔG^o_f (Cr_2O_3) and K_O from literature, the

cell E.M.F. allows us to calculate $[h_O]$. As discussed in the next section, $[f_O]$ can be estimated from chemical analysis of steel. Therefore content of dissolved oxygen (i.e. W_O) can be obtained from Eq. (7.4).

In pure liquid iron, solubility of oxygen is governed by Eqs. (7.6) and (7.7). However in molten steel, there are other more reactive alloying elements such as C, Si and Mn and the oxygen solubility is governed by reaction with one or more of these elements.

It has been well established that carbon content of steel has considerable influence on bath oxygen content at the end of heat in steelmaking furnaces. The reaction is :

$$\underline{C} + \underline{O} = CO\ (g); \quad K_{CO} = \frac{p_{CO}}{[h_C]\ [h_O]} \qquad \ldots 7.12$$

Fig. 7.2 shows relationship between dissolved carbon and dissolved oxygen in molten steel bath (4). The equilibrium line corresponding to p_{CO} = 1 atm at 1600°C is lower than the range found in both BOH and BOF steelmaking. Similar findings have been reported by others.

7.1.1 Thermodynamics of Simple Deoxidation

Deoxidation of liquid steel is carried out mostly in ladle, tundish and mould. Even in furnace, deoxidizers are often added into the mtal bath directly. In all these cases, the product of deoxidation, which is an oxide or a solution of more than one oxide, forms as precipitates.

Deoxidation never takes place at constant temperature. Temperature of molten steel keeps dropping from furnace to mould. Addition of deoxidizer also causes some temperature change due to heats of reaction. However we shall consider it as isothermal. This would not affect our considerations of deoxidation equilibria since it is only the final temperature at which the equilibrium is supposed to be attained which is ofimportance, and thermodynamically it would not make any difference if the process is presumed to take place at that temperature.

Deoxidation may be carried out by addition of one deoxidizer only. This is being termed as **simple deoxidation**. In contrast we may use more than one deoxidizer simultaneously and, in that case, it will be termed as **complex deoxidation**. In this section we will discuss simple deoxidation. A deoxidation reaction may be represented as

$$x\ [M] + y\ [O] = (M_xO_y) \qquad \ldots 7.13$$

where M denotes the deoxidizer and M_xO_y is the deoxidation product. The equilibrium constant (K'_M) for reaction (3.9) is given as :

$$K'_M = \left(\frac{(a_{M_xO_y})}{[h_M]^x\ [h_O]^y} \right)_{\text{at equil.}} \qquad \ldots 7.14$$

Again, as in Eq. (2.20),

$$h_M = f_M \cdot W_M \text{ and } h_O = f_O \cdot W_O \qquad \ldots 7.15$$

If the deoxidation product is pure, then $a_{M_xO_y}$ = 1. Also in very

dilute solutions, f_M and f_O may be taken as 1. In that case, Eq. (7.14) may be rewritten as

$$[W_M]^x \; [W_O]^y = \frac{1}{K'_M} = K_M \qquad \ldots 7.16$$

where K_M is known as `deoxidation constant'.

Obviously $[W_M]$ and $[W_O]$, as already understood, are wt.pct. of $\underline{M}$ and $\underline{O}$

respectively at equilibrium with pure oxide. It may be noted that K_M is like `solubility product' in an aqueous solution. It is a measure of solubility of the compound M_xO_y in molten steel at the temperature under consideration.

As in Eq. (7.6), variation of K_M with temperature may be represented by an equation of the type :

$$\log K_M = -\frac{A}{T} + B \qquad \ldots 7.17$$

where A and B are constants. Eq. (7.17) shows that as T increases, log K_M and hence K_M also increases. In other words, solubility of M_xO_y in molten steel increases with temperature. Since, in deoxidation, we are interested in lowering concentration of oxygen with addition of as little deoxidizer as possible, an increases of temperatutre would adversely affect the thermodynamics of the process.

Experimental determination as well as thermodynamic estimation of K_M for various deoxidizers have been going on for the last 4 or 5 decades. With advancement in science and technology, more accurate values are being found with progress of time. This has led to a number of compilations, some old and some new where efforts have been made to put down the most acceptable values. It is still going on and discrepancies still exist, especially with more reactive elements such as Al, Zr, Ce, Ca etc. Table 7.1 presents such a compilation. It is based on suggested values of Jacquemot et al (5) and Ghosh and co-workers (6,7).

It may be noted that all oxide products are definite compounds except for deoxidation by manganese, where the product is either a solid or a liquid solution of FeO-MnO of variable compositions. The underlying reason for this behaviour is the fact that manganese is a weak deoxidizer (Fig. 2.1). Stability of MnO, although greater than that of FeO, is not drastically different from the latter.

For deoxidation by Mn, it is in a way more appropriate to consider the reaction

$$(MnO) + [Fe] = [Mn] + (FeO) \qquad \ldots 7.18$$

Fe and Mn form an ideal solution (i.e. one which obey's Raoult's law). Same is true of the MnO-FeO slag. Therefore $a_{MnO} = X_{MnO}$, $a_{FeO} = X_{FeO}$, and $h_{Mn} = W_{Mn}$. Noting that a_{Fe} 1, the equilibrium constant for reaction (7.18), i.e.

$$K_{Mn-Fe} = \frac{[h_{Mn}] \times (a_{FeO})}{(a_{MnO})} = \frac{[W_{Mn}]\ (X_{FeO})}{(X_{MnO})} \qquad \ldots 7.19$$

where X denotes mole fraction. Eq. (7.19) shows that $\frac{X_{MnO}}{X_{FeO}}$ in deoxidation product would be proportional to W_{Mn} at constant temperature. Fig. 7.3 shows the relationship. The oxide product is liquid at low $\frac{X_{MnO}}{X_{FeO}}$ and solid at high value.

Taking the activity coefficients, viz. f_O and f_M as 1, one would be able to calculate the relationship between $[W_M]$ and $[W_O]$ using Eq. (7.16) and Table 7.1 for many deoxidizers. Such calculations would be all right at very low values of W_M. At higher ranges, it would give approximate values only, since f_M and f_O, esspecially f_O may deviate somewhat from 1. For more precise calculations, therefore, first order interaction coefficients (e^j_i) are to be considered. The relationship between activity coefficients and interaction coefficients follow from Chapter 2, and are as noted below.

$$\log f_M = \sum_j e^j_M \cdot W_j \qquad \ldots 7.20$$

$$\log f_O = \sum_j e^j_O \cdot W_j \qquad \ldots 7.21$$

where j denotes all the alloying elements present in liquid steel. For example, if the steel contains C and Mn, then

$$\log f_O = e_O^O \cdot W_O + e_O^C \cdot W_C + e_O^{Mn} \cdot W_{Mn}$$

Some values of interaction coefficients are tabulated in Table 2.2 (8).

Taking logarithm of Eq. (7.16), we have

$$\log W_O = -\frac{1}{y}\log K_M - -\frac{x}{y}\log W_M \qquad \ldots 7.22$$

In a $\log W_O$ vs. $\log W_M$ plot, Eq. (7.22) would yield a straight line with a slope of $- x/y$. However such linearities are not always expected if rigorous equations such as Eqs. (7.14), (7.15), (7.20), and (7.21) are employed, as shown by the calculated $\log W_O$ vs. $\log W_M$ curves for various deoxidizers in Fig. 7.4.

Fig. 7.4 shows that Mn is the weakest deoxidizer of all, and Al, Zr, etc. are very powerful. Deviation from straight line for Mn deoxidation is caused by variable composition of deoxidation product as well as the fact that the liquid FeO-MnO changes to solid FeO-MnO at higher manganese content. Deoxidizer such as Al, Ti, Zr etc. exhibit a minimum in solubility of oxygen. This behaviour is due to the large negative value of e^{M}_{O} (see Table 2.2) for these elements and the situation has been analyzed by several workers, such as Ghosh and Murty (7) and such minima have been quantitatively explained. On the basis of their exercise, the following analytical equation was proposed to describe the curves.

$$\log K_M = x\,(\log W_M + e_M^{M}\,.\,W_M) + y\,(\log W_O + e_O^{M}\,.\,W_M + r_O^{M}\,.\,W_M^{2}) \qquad ...7.23$$

where r_O^{M} is second order interaction coefficient

Unlike conventional deoxidizers, the allkaline carths, viz. Ca and Mg, are gaseous at steelmaking temperatures (p_{Mg} = 25 atm and p_{Ca} = 1.8 atm at 1600°C). Moreover they are sparingly soluble in molten steel. Solubility of Mg is 0.1 wt.pct. at p_{Mg} = 25 atm and that of Ca is 0.032 wt.pct. at p_{Ca} = 1.8 atm at 1600°C. As a result of this poor solubility, the equilibrium relationships by these elements and dissolved oxygen is difficult to determine experimentally.

7.1.2 Complex Deoxidation

As already stated if more than one deoxidizer is added to the molten steel simultaneously, it is known as complex deoxidation. Some important complex deoxidizers are Si-Mn, Ca-Si, Ca-Si-Al etc.

Complex deoxidation offers the following advantages and are being employed increasingly for better quality product.

(a) The dissolved oxygen content is lower in complex deoxidation as compared to simple deoxidation from equilibrium considerations. Consider deoxidation by silicon.

$$K_{Si} = \frac{[h_{Si}]\,[h_O]^2}{(a_{SiO_2})} = \frac{[W_{Si}][W_O]^2}{(a_{SiO_2})} \qquad ...7.24$$

If only ferrosilicon is added, then the product is pure SiO_2, i.e. a_{SiO_2} = 1. On the other hand, simultaneous addition of ferrosilicon and ferromanganese in suitable ratio leads to formation of liquid MnO-SiO_2. Consequently, a_{SiO_2} is less than 1 and hence $[W_{Si}]\,[W_O]^2$ is less than that obtained by simple ferrosilicon addition. At a fixed value of W_{Si}, therefore, W_O would be less in the latter case.

(b) The deoxidation product, if liquid, agglomerates easily into larger sizes and consequently floats up faster making the steel cleaner. This is what happens in many complex deoxidation such as in the example presented above.

(c) Properties of inclusions remaining in solidified steel can be made better by complex deoxidation, thus yielding a steel of superior quality. This will be discussed again in appropriate place later.

Equilibrium calculations involving complex deoxidation requires data on activity vs. composition relationships in the binary or ternary oxide systems of interest besides K_M and e_i^j . For activity in oxide (i.e. slag) systems, general discussions in Chapter 1 may consulted. For complex deoxidation, the desired product should be within this liquid field. Thermodynamic calculations involving complex deoxidation should aim at the following:

(a) Estimation of weight percentages of deoxidizing elements and oxygen remaining in molten steel when equilibrium is attained.

(b) Estimation of composition of the deoxidation product in equilibrium with the above.

Rigorous calculations pose difficulties due to two reasons. First of all, the activity vs. composition data in oxide systems are not available in the form of equations. Secondly, interaction of more than one deoxidizer calls for an iterative procedure for solution of equations (7.20) and (7.21). Therefore it is necessary to use computer-oriented method. A major challenge is minimization of calculation errors. Thukdogan (9) has carried out thermodynamic analysis for complex deoxidation by Si-Mn. Bagaria, Brahma Deo and Ghosh (10) carried out thermodynamic analysis of simultaneous deoxidation by Mn + Si + Al. Ghosh and Naik (11) have done the same for deoxidation systems : Ca + Si + Al and Mg + Si + Al. Readers may refer to those for details. Some salient findings by Ghosh and Naik are being presented below.

Calculations were performed in the range where the deoxidation product is liquid $CaO\text{-}SiO_2\text{-}Al_2O_3$ slag in the ternary diagram (see Fig.2.3) at two temperatures, viz. 1550°C and 1600°C. Fig.7.5 presents some results of calculations for Ca-Si-Al system as log W_O vs. log W_M (M = Si or Al) curves for 3 compositions of liquid deoxidation products. The dotted curves are based on rigorous calculations taking into consideration all interaction coefficients. For the solid curve h were taken the same as wt.pct. i.e. the interaction coefficients were ignored. The two curves differ by about 20 pct. Thermodynamically the complex deoxidizer was found to be at the most an order of magnitude more powerful as compared to simple deoxidation by Al or Si.

The above exercise is important from the point of view of industrial application. Ignoring of interactions, i.e. taking h_i = W_i

simplifies calculation procedure in a significant way. The above analysis shows the kind of error one may encounter is tolerable for many applications. It is also possible to predict thermodynamically the sequence of precipitation of deoxidation product provided the process is treated as reversible. This issue is pertinent for deoxidation where the product composition varies.

Example 7.1 Consider determination of dissolved oxygen in liquid steel by oxygen sensor with $Cr-Cr_2O_3$ reference electrode at 1600°C. What would be the value of h_O, if the EMF of the cell is +100 mV? Calculate also dissolved aluminium content. Ignore solute-solute interactions.

Solution: Combining Eqs.(7.8), (7.10) and (7.11),

$$\Delta G_f^o \ (Cr_2O_3) \text{ per mol } O_2 - 2RT \ln \frac{h_O}{K_O} = -ZFE \qquad \text{Ex.7.1}$$

From Table 2.1, at 1600°C (1873K), $\Delta G_f^o = -422.7 \times 10^3$ J mol^{-1}

$R = 8.316$ J mol^{-1} K^{-1}, $Z = 4$, $F = 96{,}500$ J volt^{-1} gm.equiv^{-1}, $E = 0.1$V

From Eq.(7.3), $K_O = 2615$ at 1873K.

Putting in values and solving, $h_O = 0.0116$

From Table 7.1, for $2\underline{Al} + 3\,\underline{O} = Al_2O_3(s)$; $K_M = 3.32 \times 10^{-14}$

$$= [W_{Al}]^2\,[W_O]^3.$$

W_O is nothing but h_O in the above equation, since solute-solute interactions have been ignored in arriving at it.

Putting in values, and solving, $W_{Al} = 1.46 \times 10^{-10}$ wt% .

Example 7.2

Consider deoxidation by addition of ferromanganese (60%Mn) to molten steel at 1600°C. The initial oxygen content is 0.04 wt.pct. It has to be brought down to 0.02 wt.pct. Calculate the quantity of ferro-manganese required per tonne of steel. Manganese content of steel before deoxidation is 0.1 wt. pct.

Solution: Consider the reaction:

$$(MnO) = [Mn] + [O] \ ; \ K_{Mn} = \frac{[h_{Mn}]\ [h_O]}{(a_{MnO})} \qquad \text{...Ex.7.2}$$

As noted earlier h_{Mn} may be taken as W_{Mn} and a_{MnO} as X_{MnO}.

Assuming also that $h_O = W_O$;

$$\text{So,} \quad \frac{[W_{Mn}]}{(X_{MnO})} = \frac{K_{Mn}}{[W_O]} \qquad \text{...Ex.7.3}$$

From Table 3.1, $\log K_{Mn} = - \dfrac{11070}{T} + 4.526$

i.e. at 1600°C (1873 K), $K_{Mn} = 0.0413$
Noting that the final $W_O = 0.02$ wt.pct.,

Therefore, $$\frac{[W_{Mn}]}{(X_{MnO})} = 2.065 \qquad \text{...Ex.7.4}$$

Now from Eq. (7.19), again

$$\frac{[W_{Mn}]}{(X_{MnO})} = \frac{K_{Mn-Fe}}{(X_{FeO})} \qquad \text{...Ex.7.5}$$

From Table 7.1, $\log K_{Mn-Fe} = - \dfrac{9370}{T} + 4.330$ (assuming the product to be solid MnO-FeO)

i.e. at 1873 K, $K_{Mn-Fe} = 0.212$

Therefore combining Eqs. (Ex.7.4) and (Ex.7.5)

$(X_{FeO}) = 0.10$

or, $(X_{MnO}) = 1 - (X_{FeO}) = 0.9$

or, $[W_{Mn}] = 1.86$ wt.pct.

Now total quantity of Mn required

= Mn required to form MnO
= Mn required to increase Mn-content of bath from 0.1 wt.pct. to 1.86 wt.pct.

Now, Mn required to form MnO/tonne of steel

$$= \frac{\text{Quantity of oxygen removed/tonne of steel}}{\text{Atomic mass of oxygen}} \times X_{MnO} \times \text{Atomic mass of manganese}$$

$$= \frac{(0.04 - 0.02) \times 10^{-2} \times 10^{3} \times 0.9 \times 55}{16}$$

= 0.62 kg/tonne steel

Mn required to increase Mn-content of bath

$= (1.86 - 0.1) \times 10^{-2} \times 10^{3} = 17.6$ kg/tonne of steel

Total Mn-required = 17.6 + 0.62 = 18.22 kg

$$\text{Total ferromanganese required} = 18.22 \times \frac{100}{60} = 30.4 \text{ kg (Ans.)}$$

From Fig.7.3 it is confirmed that the assumption of solid FeO-MnO as the deoxidation product is correct.

Example 7.3: Consider deoxidation of molten steel by aluminium at 1600°C. The bath contains Mn-1% , C-0.1% . The final oxygen content is to be brought down to 0.001 wt.pct. Calculate residual aluminium content of molten steel assuming that [Al] - [O] - Al_2O_3 equilibrium is attained. Also take into account all interaction coefficients.

Solution: The deoxidation product has been taken as Al_2O_3 (s) already. For the reaction

$$Al_2O_3(s) = 2[Al] + 3[O];$$

$$K_{Al} = [h_{Al}]^2 [h_O]^3 = 2.5 \times 10^{-14} \text{ at } 1600^\circ C \text{ (Table 7.1)}$$

or, $\log K_{Al} = 2 \log h_{Al} + 3 \log h_O$

$$= 2 [\log W_{Al} + e_{Al}^{Mn} \times W_{Mn} + e_{Al}^{C} \times W_C + e_{Al}^{O} \times W_O + e_{Al}^{Al} \times W_{Al}]$$

$$+3[\log W_O + e_O^{Mn} \times W_{Mn} + e_O^{Al} \times W_{Al} + e_O^{C} \times W_C + e_O^{O} \times W_O] \quad \text{...Ex.7.6}$$

From Table 2.2, $e_{Al}^{Mn} = 0$, $e_{Al}^{C} = 0.091$, $e_{Al}^{O} = -6.6$, $e_{Al}^{Al} = 0.045$, $e_O^{Mn} = 0.021$, $e_O^{C} = -0.45$, $e_O^{O} = -0.2$, $e_O^{Al} = -3.7$.

Noting that $W_{Mn} = 1$, $W_C = 0.1$, $W_O = 0.001$ and substituting the values in Eq.(Ex.7.6), we obtain

$$\log 2.5 \times 10^{-14} = 2 \log W_{Al} + 3 \log 0.001 - 12 W_{Al} - 0.07 \quad \text{...Ex.7.7}$$

Taking 1st guess as $W_{Al} = 0.01$, a trial and error solution yields:

$$W_{Al} = 5.75 \times 10^{-3} \text{ wt.pct.}$$

as the residual aluminium in the bath.

Example 7.4: Consider deoxidation of molten steel by simultaneous addition of ferromanganese and ferrosilicon at 1600°C. If the residual W_O and W_{Si} are respectively 0.01 and 0.1 wt. pct., determine the composition of the deoxidation product and W_{Mn} in steel at equilibrium with the above conditions. Ignore interactions amongst elements in molten steel.

Solution: Consider the reaction:

$$(SiO_2) = [Si] + 2[O]$$

$$K_{Si} = \frac{[h_{Si}]\,[h_O]^2}{(a_{SiO_2})} = \frac{[W_{Si}]\,[W_O]^2}{(a_{SiO_2})}$$ (since Henrian behaviour for Si and O) ...Ex.7.8

Now, $K_{Si} = 2.39 \times 10^{-5}$ at 1600°C (Table 7.1),

$W_{Si} = 0.1$, $W_O = 0.01$.

This yields $a_{SiO_2} = 0.418$

Assuming the deoxidation product as $MnO-SiO_2$, using diagram (1), wt.pct. SiO_2 in deoxidation product = 37.5 pct. and therefore MnO content is 62.5 pct. Also a_{MnO} is approximately 0.3.
Again, consider the reaction ;

$$(MnO) = [Mn] + [O]$$ ...Ex.7.9

for which $K_{Mn} = 0.0413$ at 1600°C.

$$K_{Mn} = 0.0413 = \frac{[W_{Mn}]\,[W_O]}{(a_{MnO})}$$

Substituting values for a_{MnO} and W_O, W_{Mn} becomes 1.24 wt. pct.
Therefore: (a) Deoxidation product contains 37.5 wt. pct. SiO_2 and 62.5 wt. pct. MnO.

(b) Wt. pct. Mn in steel = 1.24

7.2 KINETICS OF DEOXIDATION OF MOLTEN STEEL

In Sec.7.1, we were concerned with dissolved oxygen only. However in industrial deoxidation practice both dissolved as well as total oxygen (i.e. dissolved oxygen + oxygen present in deoxidation products) are of importance. Even if the former is low, presence of entraped deoxidation products gives rise to inclusions (i.e. dirtiness) in solidified steel. Therefore the products of deoxidation should be separated out from the molten steel before the latter solidifies, if a clean steel is desired. Therefore the subject of deoxidation kinetics is concerned with deoxidation reaction as well as separation of deoxidation products.

Studies of deoxidation kinetics started seriously from 1960 (12) and are still continuing. Factors controlling the rates have been established reasonabl well from theoretical considerations as well as from experiments conducted in laboratory and plant. Availability of new equipments and techniques were of considerable help. In almost all studies prior to 1970, only total oxygen could be determined by sampling and vacuum fusion analysis. Later investigators also employed immersion oxygen sensors for determination of dissolved oxygen in molten steel. Advent of electron probe microanalyser allowed rapid and easy determination of chemical composition of inclusions in steel. Development of quantimet brought about a method of rapid determination of inclusion size, number etc. By 1970 and even earlier thermodynamic parameters for important deoxidation reactions were available with a fair degree of confidence.

The basic behaviour pattern of oxygen and inclusions from furnace to solidification during steelmaking may be visualized with the help of Fig. 7.6 due to Plockinger and Wahlster (12). The dissolved oxygen content descreases rapidly upon deoxidation in the ladle and keeps on decreasing all the way. Inclusion content in liquid steel becomes quite high in ladle upon deoxidation followed by decrease due to separation of deoxidationproduct. Since solid steel has negligible solubility for oxygen, the dissolved oxygen in liquid steel also upon solidification could give rise to inclusions. Therefore the expected inclusion content in solid steel would always be higher in solid than in the liquid. For understanding of the factors influencing the rates, a number of fundamental investigations have been carried out from 1960 onwards. These have been done mostly in the laboratory under controlled conditions. Therefore, we shall first of all discuss the findings of laboratory experiments.

Laboratory investigations have been carried out mostly with a small melt (of the order of a kg. of steel) and under inert atmosphere. High frequency induction furnaces were normally employed for maintaining steel molten at the desired temperature. If the steel is directly heated by a high-frequency power, then eddy current flows through it. This eddy current and the magnetic field of the induction coil generate force, which causes flow and circulation of molten steel. This is known as induction stirring. On the other hand, if the ceramic crucible containing the steel is surrounded by a hollow cylinder of graphite or molybdenum then the eddy current flows through the latter primarily and heats it up. Then the steel is heated up indirectly by radiative and convective heat transfer from the hot cylinder. In this case, induction stirring of molten steel may be made negligibly small and the bath would be a quite one.

Discussions of deoxidation kinetics as conducted in laboratory may be subdivided into:

(a) kinetics of deoxidation reaction
(b) kinetics of elimination of deoxidation products from liquid steel.

7.2.1 Kinetics of Deoxidation Reaction

It consists of the following steps (or `stages' if you so wish to call them).

(a) Dissolution of deoxidizer into molten steel.
(b) Chemical reaction between dissolved oxygen and deoxidizing element at phase boundary or homogeneously.

(c) Nucleation of deoxidation product.
(d) Growth of nuclei principally by diffusion.

Rates of deoxidation reaction have been followed by many investigators (13,14) by monitoring the change in dissolved oxygen content of molten steel ($\underline{O}$) with time. Fig. 7.7 shows dissolved $\underline{O}$ as well as total oxygen content of molten steel as function of time for deoxidation by electrolytic manganese. It shows that the dissolved $\underline{O}$ decreases much more rapidlythan the total oxygen. This behaviour pattern has been found by all investigators. Turkdogan et al (2) found deoxidation reaction with Si to be complete more or less within 2 minutes. Olette et al carried out deoxidation by addition of aluminium shots as well as by injection of liquid aliuminium (Fig.7.8) and found most of the reaction to be complete within 1 minute (14).

A scrutiny of Figs.7.7 and 7.8 reveal grossly 2 stages. Initially the dissolved $\underline{O}$ decreases rapidly in first 30 secs or so. This is followed by the second stage which exhibits a much slower rate of decrease of $\underline{O}$. This behaviour pattern has been explained as due to very fast speed of the three kinetic steps (b) and (c) and (d) which is responsible for the rapid initial rate, and reasonably fast speed of step (a).

Let us now try to present the supporting logic as well as experimental evidence for the above mentioned explanation. The reaction

$$x\,[M] + y\,[O] = (M_xO_y) \qquad \ldots 7.13$$

would take place mostly either on the surface of the added deoxidizer or on the surfaces of (M_xO_y) particles. Therefore it is primarily a **phase-boundary reaction**. No one has been able to determine the rate of the actual phase boundary reaction step (step b). However at high temperature it is mostly very fast, and has been assumed to be so here. Homogeneous reactions of course are faster even.

Mechanism of dissolution of deoxidizer would depend on its melting point. The common deoxidizers, viz. ferromanganese, ferrosilicon and aluminium, all melt below 1500°C. Therefore they melt and dissolve. Rate of melting depends on the heat requirement as well as rate of heat transfer to the deoxidizer. Dissolution of ferromanganese is endothermic. On the other hand, dissolution of ferrosilicon is slightly exothermic but its melting point is higher than that of ferromanganese. Therefore on overall count, both would perhaps melt at about the same rate. Aluminium is expected to melt faster due to its much lower melting point.

After melting the dissolution of deoxidizer requires its mixing and homogenization in the molten steel bath. It would depend on intensity of fluid convection due to density differences (free convection) as well as stirring from other sources (such as induction stirring). However the whole process of dissolution may be delayed if tenacious oxide films form around the dissolving deoxidant. Chipman and his coworkers found difficulties of dissolving silicon in molten iron and attributed it to a tenacious film of silica.

Chipman attributed some observed slowness in deoxidation reaction to formation of stable oxide films formed on the interface of regions with a high content of deoxidizing agent and a high content of oxygen. Grethen and Phillippe (15) have presented photomicrograph of such film of MnO. Al_2O_3 in deoxidation system: Al-Fe-Mn. As Fig.3 shows, Olette et al demonstrated (3) that injection of liquid aluminium into molten steel gives faster deoxidation in comparison to addition of Al as shots. As we know it is being commercially practised as well.

Deoxidation involves formation of new phase (i.e. the deoxidation product) as a result of the reaction (3.9). New phases form by what are known as processes of **nucleation and growth**. Nucleation is the process of formation of a small embryo of the new phase which is capable of growth. Such an embryo (also called critical nucleus) consists of a small number of molecules and has a dimension of the order of ten Angstrom or so.

Again, two mechanisms of nucleation are possible :

(a) **homogeneous** nucleation which takes place in the matrix as such, and

(b) **heterogeneous** nucleation, which takes place with the aid of a **substrate**.

According to the classical theory, the work required to form a spherical nucleus homogeneously is

$$\omega = 4\pi r^2 \gamma + \frac{4}{3} \pi r^3 (\Delta G/v) \qquad ...7.25$$

where γ is the interfacial tension between liquid steel and deoxidation product, r is the radius of the nucleus, ΔG is the change in free energy for reaction (7.13) per mole and v is the molar volume of the deoxidation product (i.e. the new phase). γ is positive, whereas ΔG is negative.

from Eq. 2.6,

$$\Delta G = \Delta G^o + RT \ln Q$$

$$= - RT \ln K'_M + RT \ln Q = RT \ln \frac{Q}{K'_M} \qquad ...7.26$$

where Q is known as activity quotient.

For pure deoxidation product, in accordance with Eq. (7.16), we may write

$$\frac{J}{K'_M} = \frac{\{[W_M]^x [W_O]^y\}_{equilibrium}}{[W_M]^x [W_O]^y} \qquad ...7.27$$

Since ΔG is negative, $J/K'_M < 1$. The inverse of J/K'_M (i.e. $\frac{K'_M}{J}$) is known as **supersaturation ratio** (X) and is larger than 1. More negative ΔG is, higher is X.

Therefore, for higher rate of nucleation, the supersaturation is also to be higher. Investigators tried to estimate supersaturations required for `reasonable' rates of nucleation for the common deoxidation systems (16).

Values of this critical supersaturation as estimated by different workers ranged between 10^3 to 10^8 for strong deoxidizers (Al, Zr, Ti), 500-4000 for manganese silicate and 200-20000 for silica. Such supersaturations are attainable in the initial stages of deoxidation by strong deoxidizers, but not so much with weak dioxidizers.

According to Sano et al (17) rapid homogeneous nucleation is possible during the initial stage of deoxidation even by Mn and Si. Moreover in the melt, exogeneous oxide particles are likely to be present always. These particles would serve as substrates for heterogeneous nucleation, which is easier because of less energy required.

Anyway, to sum up the situation, it has been concluded by various workers that rapid nucleation of deoxidation product is possible when the deoxidizer is added. This has made rapid initial decrease of dissolved oxygen content possible. However as a result of reaction, the supersaturation in melt also comes down drastically. Therefore nucleation ceases after some time.

Growth of deoxidation product occurs by a number of mechanism. All of them would be considered later in connection with their particle size. However, the growth by diffusion alone can contribute to the reaction and consequent lowering of dissolved oxygen. It has been analyzed by Turkdogan (16), Sano et al (17), Lindberg and Torsell (18). The essential conclusion is that growth by diffusion also is expected to be extremely rapid, taking hardly a few seconds for completion. This is in view of very large number of nuclci formed (of the order of 10^5-10^7 nuclei/cm^3 of melt).

From the above discussions, it is evident that the deoxidation reaction accompanied by simultaneous nucleation and growth should be complete and equilibrium will attain within few seconds. However the assumption by all the above workers (16-18) had been that the dissolution and homogenization of the deoxidizer are instantaneous. Since this is not expected, dissolved oxygen decreases more slowly (Figs. 7.7 and 7.8). Dissolution is perhaps more or less complete during the initial stage, but the mixing and homogenization process even in the laboratory experiments take a few minutes and this seems to be the primary cause for slow decrease of dissolved oxygen content during the second stage although as Fig. 7.8 shows dissolution of solid may have some role to play here also. There have been many investigations on mixing both in laboratory and in industry in connection with other processes.

7.2.2 Kinetics of Removal of Deoxidation Products from Molten Steel

As Fig. 7.7 shows the total oxygen content of molten steel decreases more slowly than the dissolved oxygen content. It has been observed universally. It may take 10/15 minutes even in laboratory melts to remove the total oxygen adequately. This behaviour pattern demonstrates that the removal of deoxidation products from melt is a slow process and is really the most important kinetic step controlling steel cleanliness.

Growth by diffusion is expected to be complete essentially in seconds. Sample calculations (18) demonstrate that the deoxidation products can assume a size of at best 1-2 microns (1 micron = 10^{-3} mm). This is because there are too many nuclei in the melt and, hence, each one has limited growth. In contrast, microscopic observations of solidified steel reveal presence of a large number of inclusions of size even above 50 microns. Therefore there are other mechanisms of growth which play important role.

Example 7.5: Calculate the absolutely maximum size of deoxidation product as a result of growth of critical nuclei by diffusion alone. Assume the deoxidatiuon product to be silica, number of critical nuclei(z) per $cm^3 = 10^6$ and initially the melt contains 0.15 wt. pct. silicon and 0.03 wt. pct. oxygen. Temperature = 1800K. Ignore all interaction coefficients.

Solution: The absolutely maximum size would be obtained only if a very long time is allowed and the system attains equilibrium.

$$SiO_2(s) = [Si]_{wt\%} + [2O]_{wt\%} ;$$

$$\Delta G^o \text{ at 1800K} = 43000 \text{ cals/mole} \qquad \text{...Ex.7.10}$$

$a_{SiO_2} = 1$, and hence

$$\Delta G^o = - RT \ln K = - RT \ln [W_{Si}] [W_O]^2$$

Hence, $[W_{Si}] [W_O]^2 = 6 \times 10^{-6}$ ...Ex.7.11

From reaction stoichiometry

$$W_{Si} - W_{Si}^o = \frac{28}{32} (W_O - W_O^o) \qquad \text{...Ex.7.12}$$

where $W_{Si}^o = 0.15$ wt. pct. and $W_O^o = 0.03$ wt. pct.

$$\text{or,} \quad W_{Si} = 0.875 W_O + 0.124 \qquad \text{...Ex.7.13}$$

Substituting W_{Si} from Eq.(Ex.7.13) into Eq.(Ex.7.11) and solving by iteration, $W_O = 0.007$ wt. pct.

Material balance for oxygen

oxygen in 10^6 nuclei+ residual oxygen in 1 cm^3 of melt

= initial oxygen in 1 cm^3 of melt

i.e.

$$10^6 \times V \times \frac{32}{25} + 7.16 \times 0.007 \times 10^{-2} = 7.16 \times 0.03 \times 10^{-2} \qquad \text{...Ex.7.14}$$

where V is volume of one particle of SiO_2, 25 is molar volume of SiO_2 in cm^3 and 7.16 is density of liquid iron in gms cm^{-3}.

Solving Eq.(Ex.7.14) for V and assuming the particle to be spherical, radius (r) of particle is equal to 6.7×10^{-4} cm. i.e. 6.7 microns. Since growth by diffusion takes places for a short time, actual radius will be less than this.

Kinetics of removal of deoxidation products from molten steel consists of the following steps:

(a) growth,
(b) movement through molten steel to surface or crucible wall,
(c) floating out to surface or adhesion to crucible wall.

Sano et al (17), Lindborg and Torsell (18) carried out fundamental investigations with laboratory melts. Out of these the latter has received wide acceptance because their theoretical analyses were supported by inclusion counting and size analysis. Besides diffusion, they considered the following additional mechanisms of growth.

(a) **Ostwald Ripening (i.e. diffusion - coalescence):** According to this mechanism, larger particles of deoxidation product grow at the cost of smaller ones. However this mechanism does not have any significant contribution to growth of deoxidation product.

(b) **Stokes Collision:** In a quiet fluid and at very low Reynold's no. (i.e. laminar flow), a spherical particle of solid, at steady state, moves according to the Stoke's law of settling and its terminal velocity (v) is given as

$$v = \frac{g\, d^2 \,(\rho_s - \rho_f)}{18\mu} \qquad \text{...7.28}$$

where g is acceleration due to gravity, d is diameter of the particle, μ is viscosity of the fluid, ρ_s and ρ_f are densities of solid and fluid respectively. This equation may be applied even to motion of gas bubbles and liquid droplets provided these are small in size (less than a millimeter or so). Since deoxidation products are lighter than molten steel, they move upwards. Equation (7.28) shows that $v \propto d^2$, other factors remaining constant. Therefore particles of different sizes would move at different speeds. During this process many of them are likely to collide with one another. Lindborg and Torsell (18) assumed that they would coalesce and form one particle as soon as they collide. This is the mechanism of growth by Stokes Collision.

(c) **Gradient Collision:** Suppose the melt is not quiet and there is some stirring and consequent turbulent flow. Then the liquid moves in irregular eddies. The minimum size of such eddy under conditions of Torsell's experiments was estimated as 300 microns. Since inclusion sizes were much smaller than this, it was assumed that any oxide particle would move along with the eddy in which it is contained. Since different eddies have different velocities (both in magnitude and direction) they would all the time collide enhancing the chances of collision of deoxidation products leading to their coalescence and growth.

Example 7.6: Liquid steel is being deoxidized by addition of ferrosilicon at 1600°C. The deoxidation product is globular silica. Calculate the time required for particles of diameter 5 micron and 50 micron to float up through a depth of 10 cm and 2 meters.

Given: Densities of liquid steel and silica are 7.16×10^3 and 2.2×10^3 $\mathrm{kgm^{-3}}$ respectively.

Viscosity of liquid steel = 6.1×10^{-3} $\mathrm{kg\ m^{-1}\ s^{-1}}$

$g = 9.81\ \mathrm{ms^{-2}}$

Solution: Assume that the particles have steady, terminal velocity given by Stokes Law from the beginning.

$$\text{Then time to float up } (t) = \frac{\text{Depth of steel } (L)}{v}$$

$$= \frac{L \times 18\,\mu}{gd^2\,(\rho_s - \rho_f)} = \frac{18\mu}{g\,(\rho_s - \rho_f)} \times \frac{L}{d^2}$$

If d is expressed in micron (10^{-6}m) and time in minute

$$t = \frac{18\mu}{g\,(\rho_s - \rho_f)} \times \frac{10^{12}}{60} \times \frac{L}{d^2} \qquad \text{...Ex.7.15}$$

$$= \frac{18 \times 6.1 \times 10^{-3} \times 10^{12}}{9.81 \times (7.16-2.22) \times 10^3 \times 60} \times \frac{L}{d^2}$$

$$= 3.6 \times 10^4 \times \frac{L}{d^2} \text{ min} \qquad \text{...Ex.7.16}$$

Calculations yield

L (in m)	=	0.1	0.1	2	2
d (in micron)	=	5	50	5	50
t (in min)	=	150	1.5	3×10^{3}	30

These theoretical expectations were confirmed by laboratory experiments (18) as shown by Fig.7.9 for silicon deoxidation. Very little oxygen (total) is removed in the 1st stage because the particles are small and they do not float out rapidly. Then particles grow rapidly due to collision and start floating out rapidly giving rise to rapid oxygen removal in the 2nd stage. Since most large particles float out at this stage, further floatation and removal in the 3rd stage is slow.

It has been well-established that stirring helps in the removal of deoxidation products (14,17,19). A stirring contributes faster growth of oxide particles and hence help the removal of deoxidation product. There are workers who are of the view that a recirculatory motion of bath such as in induction stirring actually makes floating out of inclusions difficult (15) but Miyashita et al (19) on the other hand, have shown that even in induction stirring the rate of floating out of inclusions is much larger than that predicted by Stokes' Law (Fig.7.10).

In 1957, E. Plockinger et al (12) demonstrated that, contrary to the ideas of the time, primary inclusions rich in alumina could be eliminated several times more quickly than silicates at comparable sizes. It was subsequently shown by some other investigators that the chemical nature of deoxidation product has significant influence on its removal. Since the particle can interact chemically with the melt at the interface only, it was apparent that interfacial phenomena cannot be ignored. One of the most decisive experiments was by Negi et al (20) who found that addition of little surface active agent such as tellurium to molten steel accelerated elimination of oxide inclusions (alumina, mullite and zirconia).

Interfacial phenomena can influence all stages, viz. growth, movement and floating out/removal of deoxidation products. Previously it used to be believed that only a liquid deoxidation product is capable of growth to a large size since they coalesce together upon collision. Discovery of large coral-like alumina clusters violates this contention (21). Some investigators (13,21) have claimed that small alumina particles coalesce together upon collision due to the fact that molten iron does not 'wet' alumina. Therefore alumina-alumina interface has considerably less energy as compared to alumina-iron interface. Some other investigators also have supported this view broadly. Singh (22) explained nozzle blockage in aluminium deoxidized melts by a mechanism similar to that found by Olette. Ofcourse this view has been questioned by some others who are of the opinion that these clusters may form during solidification in interdendritic space. However even if it occurs in dendritic cavities during solidification there is no doubt that these form primarily in melt itself.

Agglomeration of inclusions takes place by flocculation (i.e. establishing contact) and coalescence. Lindborg and Torsell (18) assumed these to be instantaneous. Kazakevitch and Olette (21) have tried to elucidate the mechanism. First of all, contact is established at some points. Coalscence takes place by drainage of molten steel out of the region between the two particles due to capillary forces. Coalescence is easy in case of liquid deoxidation product. For solid particles, it happens by sintering (20).

It was recognised quite some time back that the oxide particles may almost come up to the free surface of molten steel. However it is likely to take a little more time or face difficulties in actually floating out on the surface if the interfacial forces are not favouralbe. Similarly a particle may come in contact with the crucible wall, but may face difficulties in actually getting stuck on to the crucible wall if interfacial forces are not favourable. This is specially important for stirred melts since the particles are not likely to stay long near free surface or crucible wall, and are likely to be swept back into the melt. Therefore a number of workers studied these aspects (15).

Kazakevitch et al (21) have elucidated the fundamental considerations for **emergence** at free surface of melt and at slag-metal interface. Emergence at a free surface can take place if

$$\Delta G_{29} < 0, \text{ where}$$

$$\Delta G_{29} = \gamma_p - \gamma_m - \gamma_{pm} \qquad \ldots 7.29$$

γ_p is surface tension of the deoxidation product, γ_m is the surface tension of molten steel and γ_{pm} is interfacial tension between the deoxidation product and molten steel. On the other hand, if there is a slag layer on metal surface, then the condition for emergence is

$\Delta G_{26} < 0$,

where $\Delta G_{26} = \gamma_{ps} - \gamma_{ms} - \gamma_{pm} \qquad \ldots 7.30$

where γ_{ps} and γ_{ms} are interfacial tensions at particle-slag and metal-slag interfaces respectively. If calculations are carried out then it would be found that ΔG is mostly negative for all systems. Actually it is a question of how strongly negative it is. More negative is ΔG, easier would be emergence and hence removal of the oxide particles. Since slags would wet the deoxidation product, ΔG_{30} is always expected to be more negative as compared to ΔG_{29}. Therefore a slag cover on molten steel ought to help in removal of deoxidation product, and experimental findings support this (23).

Nakanishi et al (24) deoxidized liquid iron containing 300 ppm of oxygen by aluminium in laboratory high frequency induction furnace using crucibles of different materials. Extremely low concentration of oxygen (12 to 14 ppm) were obtained with SiO_2 and CaO crucibles, whereas oxygen was higher (34 to 42 ppm) for Al_2O_3, ZrO_2 and MgO crucibles. X-ray microanalysis of SiO_2 and CaO crucibles after deoxidation revealed an increase of Al_2O_3 concentration on their surfaces. These observations have been corroborated by other investigation and are caused by interfacial forces.

To sum up, for production of clean steels with low oxygen content upon deoxidation,

(a) the deoxidation product should be chemically very stable and should preferably be liquid,

(b) the melt should be stirred,

(c) the interfacial forces should be favourable for elimination of the oxide particles.

It is to be also noted that extensive investigations have been carried out on particle size distribution, nature and morphology of inclusions in steel as affected by deoxidation practice. However inclusions also arise during teaming and solidification. Hence this topic would be discussed later.

7.2.3 Deoxidation on Industrial Scale

Deoxidation is carried out in industry in furnaces, ladles, runners and even in moulds. It is beyond the scope of the present write up to describe all these. These fundamentals of deoxidation thermodynamics and kinetics as established through laboratory experiments do apply to industrial situations as well. However the conditions in the latter are different from laboratory in a number of ways, and is much more complex. Here it is intended to discuss these very briefly.

An industrial vessel is much larger in size as compared to a laboratory crucible. Therefore,

(a) The deoxidation products take much longer time to float up or to come in contact with lining.
(b) Mixing and homogenization of bath is much more difficult as compared to laboratory situation.

In addition to the above the following have to be kept in mind.

(a) An industrial melt is contaminated by presence of exogeneous oxide particles coming from refractory linings and slag.

(b) There may be a thin layer of slag covering the free surface of the metal.

As discussed earlier stirring assists in faster growth of oxide particles through gradient collision. It also helps in faster rise of the oxide particles. Hence, for production of cleaner steel, stirring of molten metal in the bath by inert gas purging has been widely adopted. Trials carried out in a 140t melt demonstrated that (25) that the oxygen content of melt decreased more rapidly as stirring was increased. However the acceleration of the process tends towards a limit as the stirring power increases because it increases the risk of reentrainment of oxide particles from surface to the interior of the melt. Similar findings have been reported bgy some others. Therefore stirring should be optimum.

Ghosh and Choudhary (26) carried out deoxidation by ferromanganese and ferrosilicon in 6t and 1t electric are furnaces. Their findings point out that deoxidation equilibria could be attained within 10 minutes after addition of deoxidizers if only stirring of bath by CO evolution was reasonable.

Therefore mixing, homogenization, nature of flüid motion in the melt is of crucial importance for proper dioxidation practice. Other strategies are also adopted by industries. One such strategy isto obtain liquid deoxidation product by proper sequence of addition of Si, Mn and Al. Liquid deoxidation products tend to coalesce and grow rapidly upon collision and hence eliminated faster. Injection of synthetic slag powders, sizing of deoxidizers, and synchronization of their addition with tapping in ladle deoxidation are some of the other strategies one may think of. The location of addition should be such that the deoxidizer disperses quickly throughout the melt.

Many experimental and plant studies (19) have shown that the rate of separation of deoxidation products in stirred melts can be represented by an equation of the form

$$C_t = C_o \exp(-kt) \qquad \ldots 7.31$$

where C_o is the initial concentration of inclusions, C_t the concentration of inclusions at time t, and k the apparent separation constant. k obviously would depend on stirring.

However Eq.(7.31) should be taken only as an approximate quide. For example, Suzuki et al(27) measured total oxygen content as function of time in ladle stirred by argon. Their data are presented in Fig.7.11. The mean curve is also superimposed on the data. Employment of Eq.(7.31) on their data at stirring times of 4 minutes and 10 minutes yielded values of k equal to 2.7×10^{-3} s^{-1} and 1.7×10^{-3} s^{-1} respectively. These are significantly different. It is to be borne in mind that total oxygen content of liquid steel also includes dissolved oxygen content in addition to oxide particles. Moreover some reentrainment of particles also occurs. So even after prolonged stirring a steady value of oxygen content remains in the melt.

From the above considerations, a more appropriate equation is

$$\triangle W_o = [\triangle W_o]_i \exp(-kt) \qquad \ldots 7.32$$

where $\triangle W_o$ is difference of wt.pct. total oxygen at time t after stirring and that at steady state. In Fig.7.11 if the steady value is taken as approximately 30 ppm, the values of k evaluated at stirring times of 4 mins and 10 mins are 4.9×10^{-3} s^{-1} and 4.2×10^{-3} s^{-1} respectively. These are much closer to one another.

7.2.4 Concluding Remarks

A new technique that is being tried now is filtering of molten steel by using porous filter of ceramics. It is a challenging problem for ceramic technologists and its success is yet to be ascertained.

7.3 CLEAN STEEL (28,29)

Inclusions are non-metallic particles embedded in the matrix of metals and alloys. It may be stated that inclusions have been generally found to be harmful to mechanical properties and corrosion-resistance of steel. This is more so for high-strength steels for critical applications. Therefore production of `clean steel' has received considerable attention. However no steel can be freed from inclusions. The number of inclusions has been variously estimated to range between 10^{10} - 10^{15} per tonne of steel. Therefore we can talk about cleaner and cleaner steel, but not clean steel (strictly speaking). Again the yardstick of cleanness depends on how one assesses it. For example, most of the inclusions are submicroscopic. Therefore a microscopic examination cannot faithfully assess cleanness.

Above considerations lead to the conclusion that cleanness is a vague and relative term. Which steel is clean and which steel is dirty, can be found only when we know its applications and consequent property requirements and then we know the corresponding limiting size, frequency of occurence and properties of inclusions. It is also to be recognised in this connection that a complementary strategy to make inclusions relatively harmless is to modify them. This is known as **inclusion modification**. The subject of inclusion modification shall be dealt with in a subsequent chapter.

This section shall be concerned with factors contributing to cleanness of steel only. It is to be noted in this connection (28) that inclusions of larger size (may be called **macroinclusions**) are much more harmful and ought to be eliminated. On the other hand, presence of **microinclusions** can be tolerated. As a matter of fact the latter can even be beneficial. They can, for example, restrict grain growth, increase yield strength and hardness, and act as nuclei for precipitation of carbides, nitrides etc.

The critical inclusion size is not fixed but depends on many factors. Broadly speaking, it is in the range of 5 to 50 microns. Inclusions are mostly oxides and sulphides and sometimes oxysulphides. Their distribution and intensity of occurence in ingots and continuously cast sections would depend primarily on :

(a) non-metallic particles coming with molten metal during teeming,

(b) inclusions originating during freezing inside mould due to deoxidation etc.

and (c) ability of non-metallic particles to float up.

Fundamentals of floating up of particles through a liquid bath have been discussed in sec.7.2. However, in solidifying steel, entrapment of particles by the dendrite arms is a major factor. Since phenomena during casting are not going to be discussed in this course, it will be skipped.

7.3.1 Factors Affecting Occurence of Non-Metallic Particles in Liquid Steel in Mould

The factors are :

(a) products of deoxidation and desulphurization of liquid steel in ladle; deoxidation has already been discussed; reaction of sulphur and formation of sulphide inclusions shall be taken up later.

(b) oxygen pick up by teeming stream from air and consequent formation of oxide,

(c) erosion of refractories coming into contact with liquid steel in ladle, teeming nozzle and stopper,

(d) entrapment of slag particles in ladle.

Inclusions arising out of (a) are known as **endogeneous** inclusions. These are small, numerous, rather uniformly distributed and typical of the steel in which they occur. Sec.7.2 has discussed fundamentals related to endogeneous inclusion formation.

Inclusions arising out of other factors are known as **exogeneous** inclusions. These are larger in size, scarce and haphazard in occurence. Table 7.2 (30) shows the findings of Pickering's investigations. The approximate relative volumes of exogeneous inclusions from refractory erosion were found to be much more than those of endogeneous inclusions. McLean (31), in a recent review, also asserted that erosion of refractory linings of nozzles, stoppers, runners etc. as a serious source of large inclusions. Besides he quotes several investigators who have found macroinclusions of size larger than 100 micron also originate from reoxidation of steel stream during teeming. In one study, 60-65% of inclusions were eliminated by argon shielding. Reoxidation products tend to form inclusions richer in weaker oxides (e.g. FeO, MnO). This has been observed by many investigators (32).

Table 7.2 : Average Sizes and Relative Abundance of Inclusions (30)

	Type of inclusion	Avg.diameter, micron	Approx.relative volume
1.	Alumina spinel and CaO.6 Al_2O_3 (other than clusters)	5	1
2.	Other calcium aluminates	27	160
3.	Secondary deoxidation products	32	260
4.	Primary deoxidation products (Si-killed)	49	940
5.	Erosion of silicates (Al-killed steel)	64	2100
6.	Erosion of silicates (Si-killed steel)	107	9800

REFERENCES

1. J.F. Elliott, M. Gleiser and V. Ramakrishna, **Thermochemistry for steelmaking**, Vol.2, Addison-Wesley Publishing Corp, Reading, Mass. U.S.A., 1963.
2. E.C. Subbarao ed., **Solid electrolytes and their applications**, Plenum Press, New York, 1980.
3. R.J. Fruehan, L.J. Martonik and E.T. Turkdogan, Trans. AIME, 245 (1969), 1501 - 09.
4. G.M. Cohen, Opean Hearth Proceedings, AIME, 57 (1974), 336.
5. A. Jacquemot, C. Gatellier and M. Olette, IRSIDE RE 289 (1975) - Casting and Solidification of Steel ECSC No. 6210 - 50.
6. A. Ghosh and P.N. Chaudhary, Trans. IIM, 38 (1985), 31.
7. A. Ghosh and G.V.R. Murty: Trans. ISIJ, 26 (1986),629.
8. G.K. Sigworth an d J.F. Elliott, Metal Science, 8 (1974), 298.
9. E.T. Turkdogan, in **Chemical Metallurgy of Iron and Steel**, Iron and Steel Inst. London,(1973), 153.
10. A.K. Bagaria, Brahma Deo and A. Ghosh, **Proceedings of International Symposium on Modern Developments in Steelmaking**, Amit Chatterjee and B.N. Singh ed., Jamshedpur, (1981), 8.1.1.
11. A. Ghosh and V. Naik, Tool and Alloy Steels, 17 (1983), 239 - 44.
12. E. Plockinger and M. Wahlster, Stahl Eisen, 80 (1960), 659.
13. E.T. Turkdogan, in **Chemical Metallurgy of Iron and Steel**, Iron and Steel Inst., London, (1973), 153.
14. M. Olette and C. Gatellier in Information Symposium on **Casting and Solidification of steel**, IPC Science and Technology Press Ltd., Guildford, U.K., (1977), 8-61.
15. E. Grethen and L. Phillippe, in **Production and Application of Clean Steels**, Iron and Steel Inst., London, 1972
16. E.T. Turkdogan, JISI, 204 (1966), 14-19.
17. N. Sano, S. Shiomi and Y. Matsushita, Trans. ISIJ, 7 (1967), 244.
18. U. Lindborg and K. Torssell, Trans. AIME, 242 (1968), 94.
19. Y. Miyashita et al, in Proceedings 2nd Japan-USSR joint symposium on physical chemistry of metallurgical processes, Iron and Steel Inst., Tokyo, 1969, 101.
20. K. Nogi and K. Ogino, Canad Met. Qtly, 22, No.1 (1983), 19-28.
21. P. Kozakevitch and M. Olette, in Ref.15, p.42.
22. S.N. Singh, Met. Trans., 2 (1971), 3248.
23. K.P. Bziva and V.V. Averin, in Ref.19, p.113.
24. K. Nakanishi et al, in Ref.19, p.50.
25. T.A. Engh and N. Linskogh, Scand J. Met. (1975), 49.
26. A. Ghosh and P.N. Chaudhary, Trans. IIM, 38 (1985), 31.
27. K. Suzuki, K. Kitamura, T. Takenouchi, M. Funazaki and Y. Iwanami, Ironmaking Steelmaking (1982), 33.
28. R. Kiessling and N. Lange, **Non-metallic Inclusions in Steel**, The Metals Soc., London, 1978.
29. Iron and Steel Inst.,**Production and Application of Clean Steels**, London, 1972 (also Subsequent Proceedings).
30. F.B. Pickering, in ref. 29, p.75.
31. A. McLean and I.D. Sommerville, in Proceedings of **International Symposium on Modern Developments in Steelmaking**, ed. A.Chatterjee and B.N. Singh, Jamshedpur, (1981), pp.739-55.
32. S.K. Banerjee, T. Mukherjee and A. Ghosh, Trans.IIM, 36 (1983),459.

Table7·1 : Values of K_M for some deoxidizers

Deoxidant	Deoxidation product	Concentration range of $M(W_M)$, if any	$\log_{10}K_M$	(K_M) 1600°C
1	2	3	4	5
Al	Al_2O_3	above 10^{-5}	$-\frac{58473}{T} + 17.74$	3.32×10^{-14}
B	B_2O_3			1.5×10^{-8}
C	CO (g)		$-\frac{1168}{T} - 2.07$	2.05×10^{-3}
Ce	Ce_2O_3		$-\frac{68500}{T} + 19.6$	10^{-17}
	$FeCr_2O_4$	below 3.0	$-\frac{45796}{T} + 18.83$	2.39×10^{-6}
Cr	Cr_2O_3	3.0 - 8.0	$-\frac{45531}{T} + 20.25$	8.72×10^{-5}
	Cr_3O_4	above 8.0	$-\frac{48850}{T} + 21.45$	2.23×10^{-5}
	Liq.FeO-MnO solution	below 0.2	$\log K_{Mn} = -\frac{8780}{T} + 3.445$	0.0585
			$\log K_{Mn-Fe} = -\frac{6525}{T} + 2.948$	0.29
Mn	Solid FeO-MnO solution	above 0.2	$\log K_{Mn} = -\frac{11070}{T} + 4.526$	0.041
			$\log K_{Mn-Fe} = -\frac{6980}{T} + 2.91$	0.15
Nb	$FeNb_2O_6$	below 0.4	$-\frac{88300}{T} + 36.76$	4.1×10^{-11}
	NbO_2	0.4 - 5	$-\frac{32780}{T} + 13.92$	2.6×10^{-4}
Si	SiO_2		$-\frac{27893}{T} + 10.27$	2.4×10^{-5}
Ti	Ti_3O_5	0.0004 - 0.4	$-\frac{90727}{T} + 29.15$	5.45×10^{-20}
	Ti_2O_3	above 0.4	$-\frac{55751}{T} + 17.9$	2.06×10^{-12}
V	FeV_2O_4	below 0.2		1.32×10^{-7}
	V_2O_3	above 0.2	$-\frac{42198}{T} + 17.0$	2.2×10^{-6}
Zr	ZrO_2		$-\frac{41258}{T} + 11.86$	6.8×10^{-11}
Ca	CaO		$-\frac{32903}{T} + 7.56$	9.84×10^{-11}
Mg	MgO		$-\frac{32027}{T} + 8.47$	2.35×10^{-9}

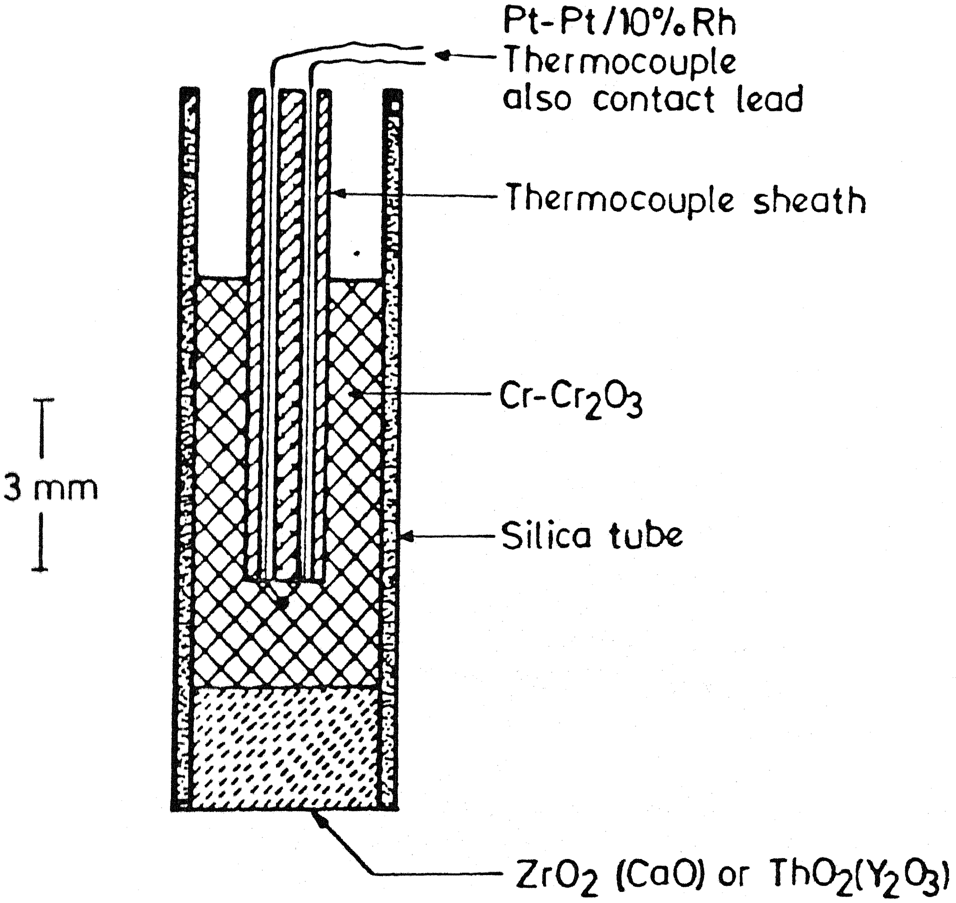
Pt-Pt/10%Rh Thermocouple also contact lead
Thermocouple sheath
$Cr-Cr_2O_3$
3 mm
Silica tube
ZrO_2 (CaO) or $ThO_2(Y_2O_3)$

Fig. 7.1 : Schematic diagram of oxygen sensor[6]

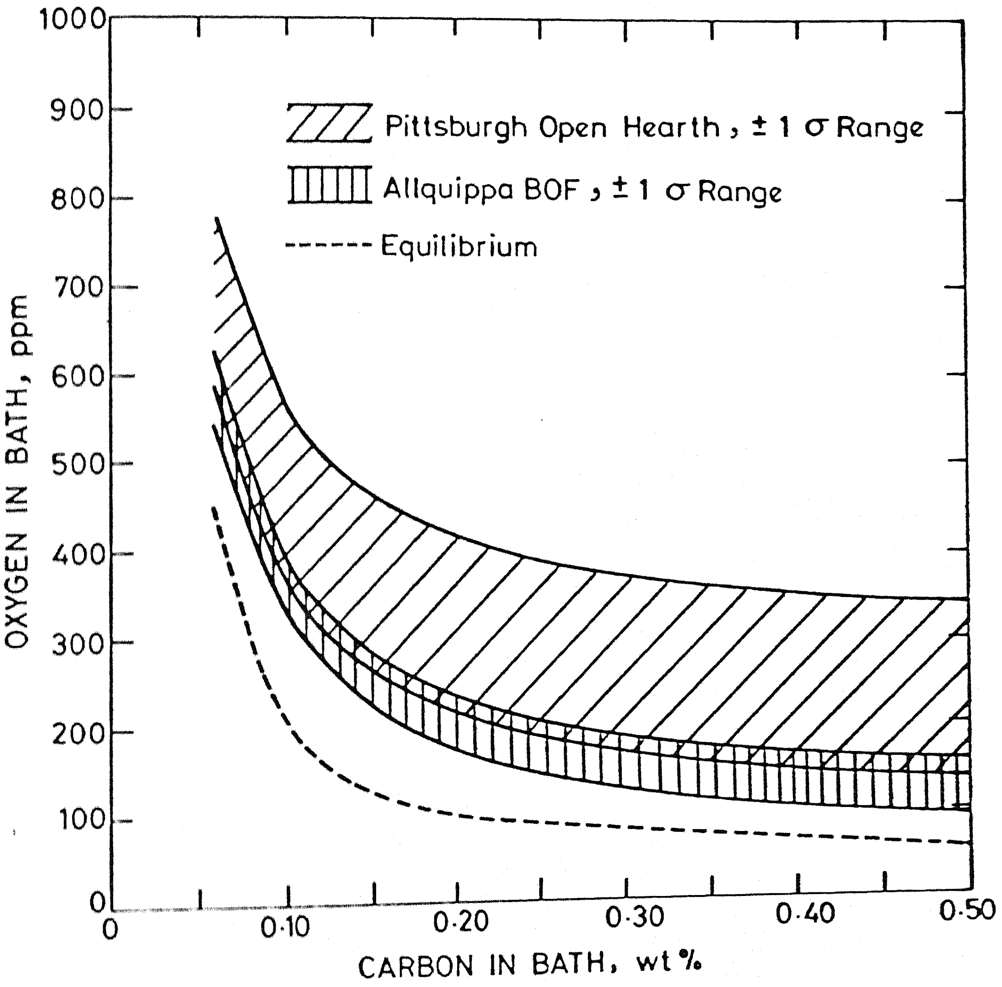

Fig. 7.2 : Relationship between dissolved oxygen and carbon in molten steel during tapping from furance

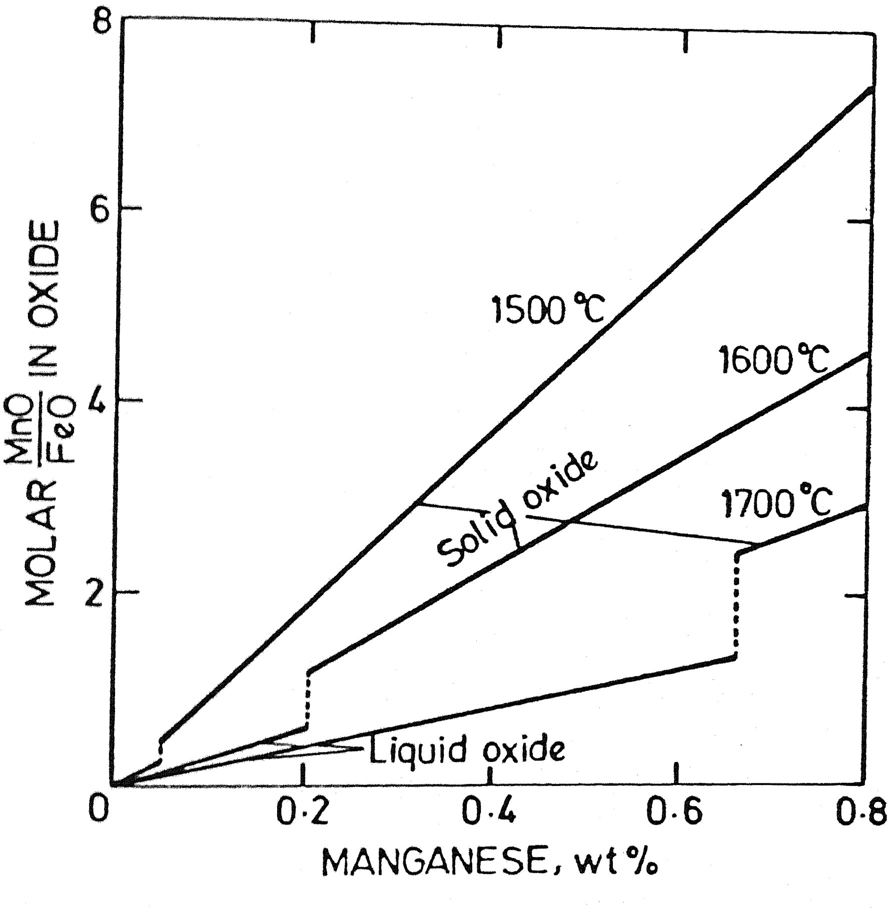

Fig. 7.3 : Composition of liquid or solid FeO - MnO solution in equilibrium with liquid iron containing manganese and oxygen

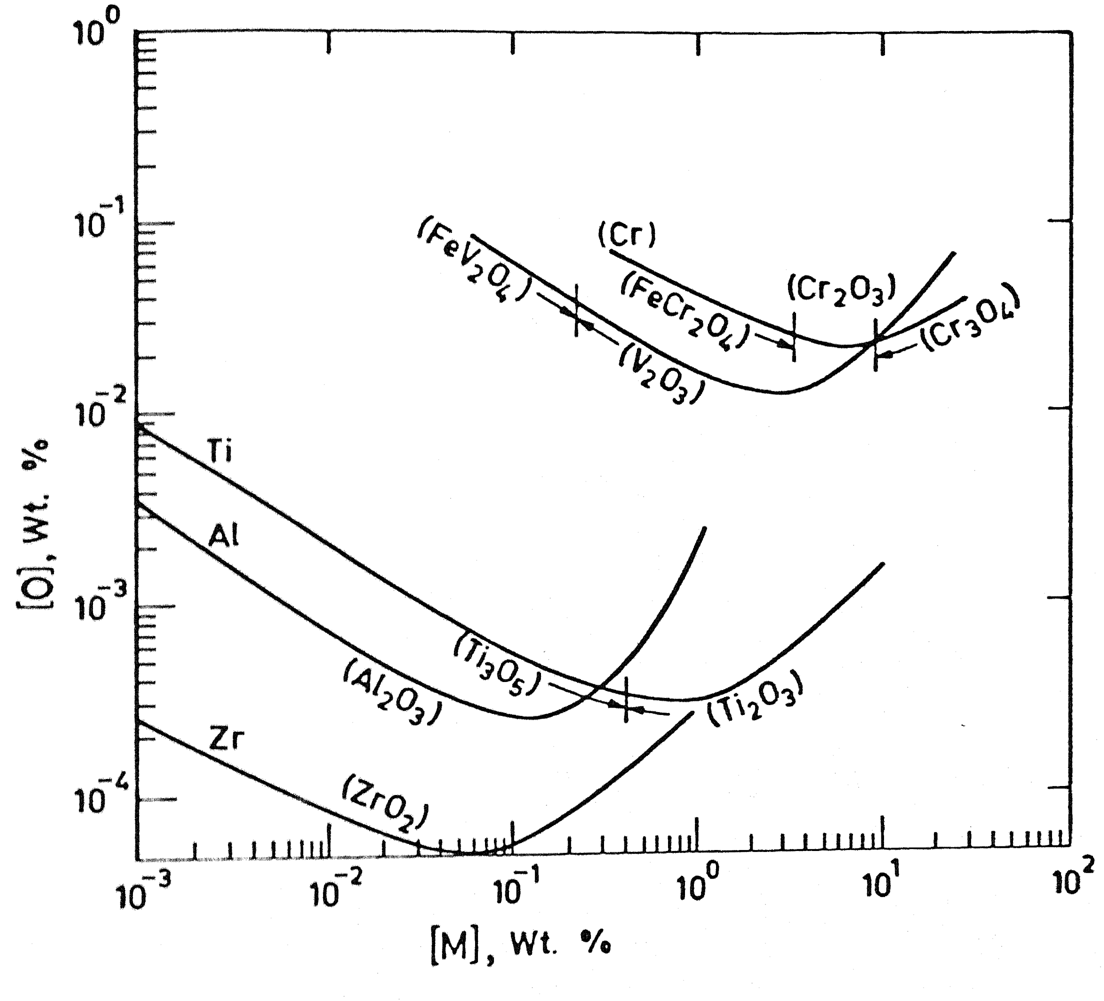

Fig. 7.4 : Deoxidation equilibria in liquid iron at 1600°C

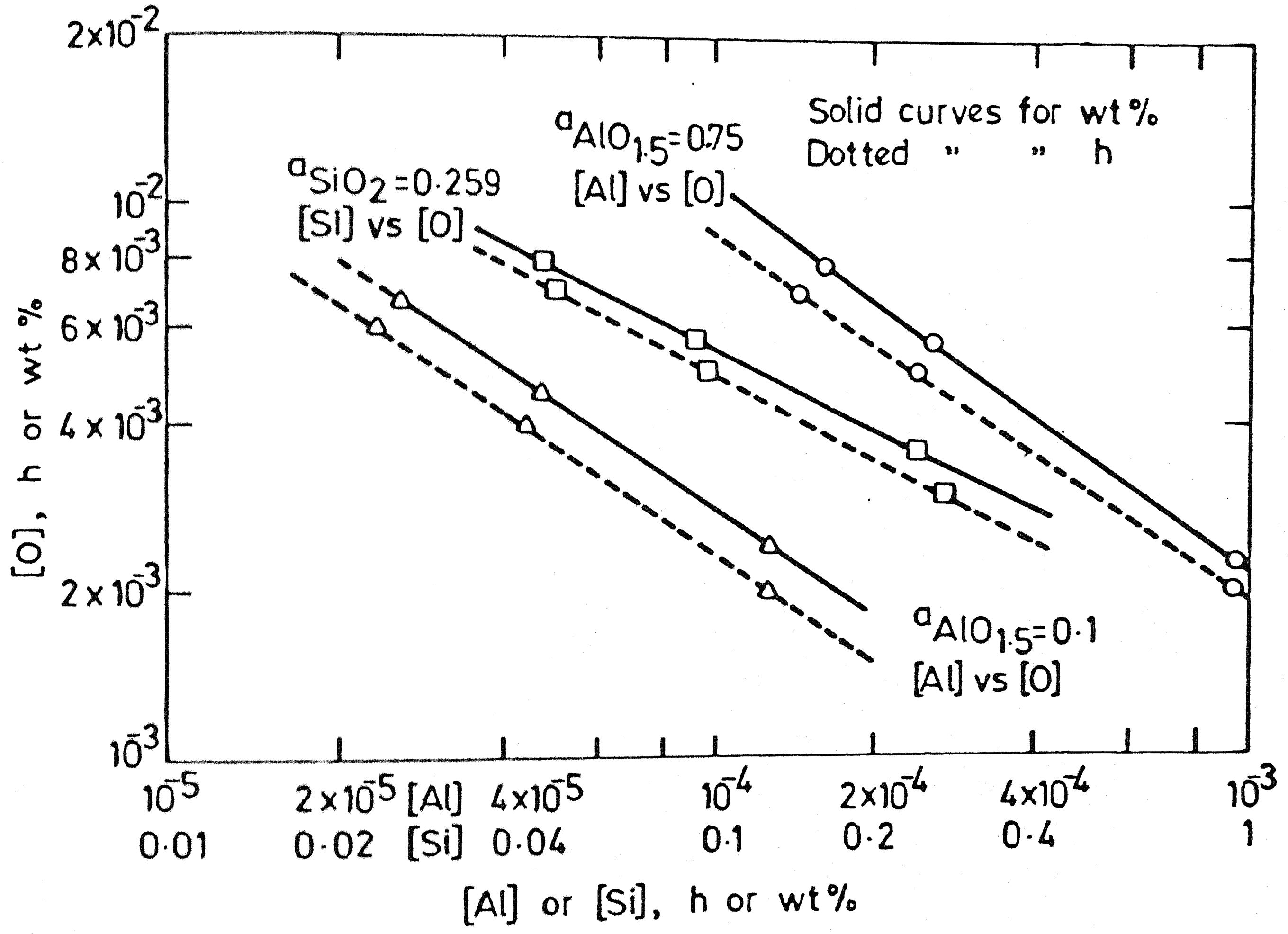

Fig. 7.5 : Some [Wt.% O] vs. [Wt.% M] and [h_O] vs. [h_M] relationship for [Al] - [O] - Al_2O_3 and [Si] - [O] - SiO_2 equilibria for deoxidation by Ca - Si - Al at 1600°C

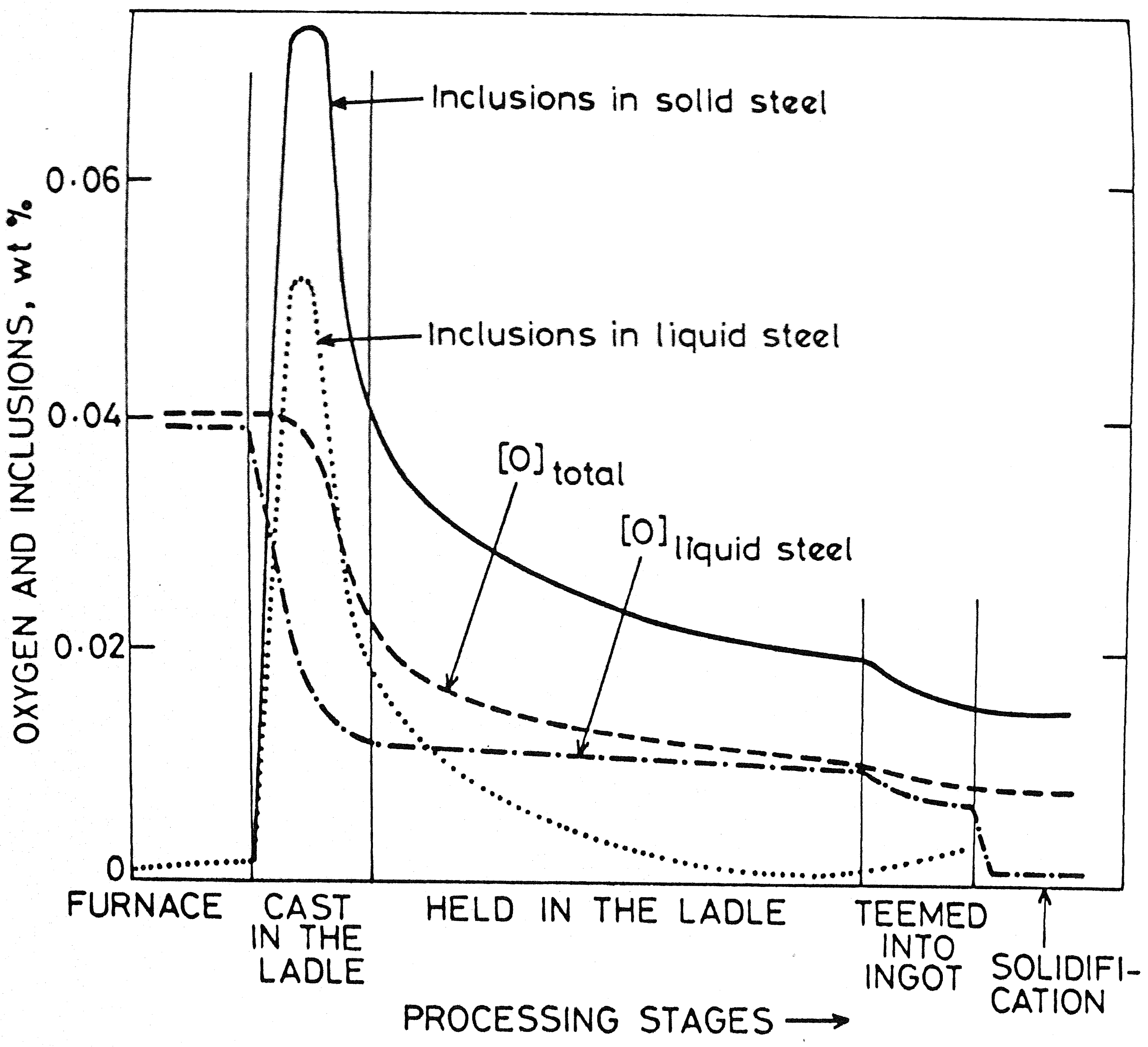

Fig. 7.6 : Phenomena of deoxidation by precipitation

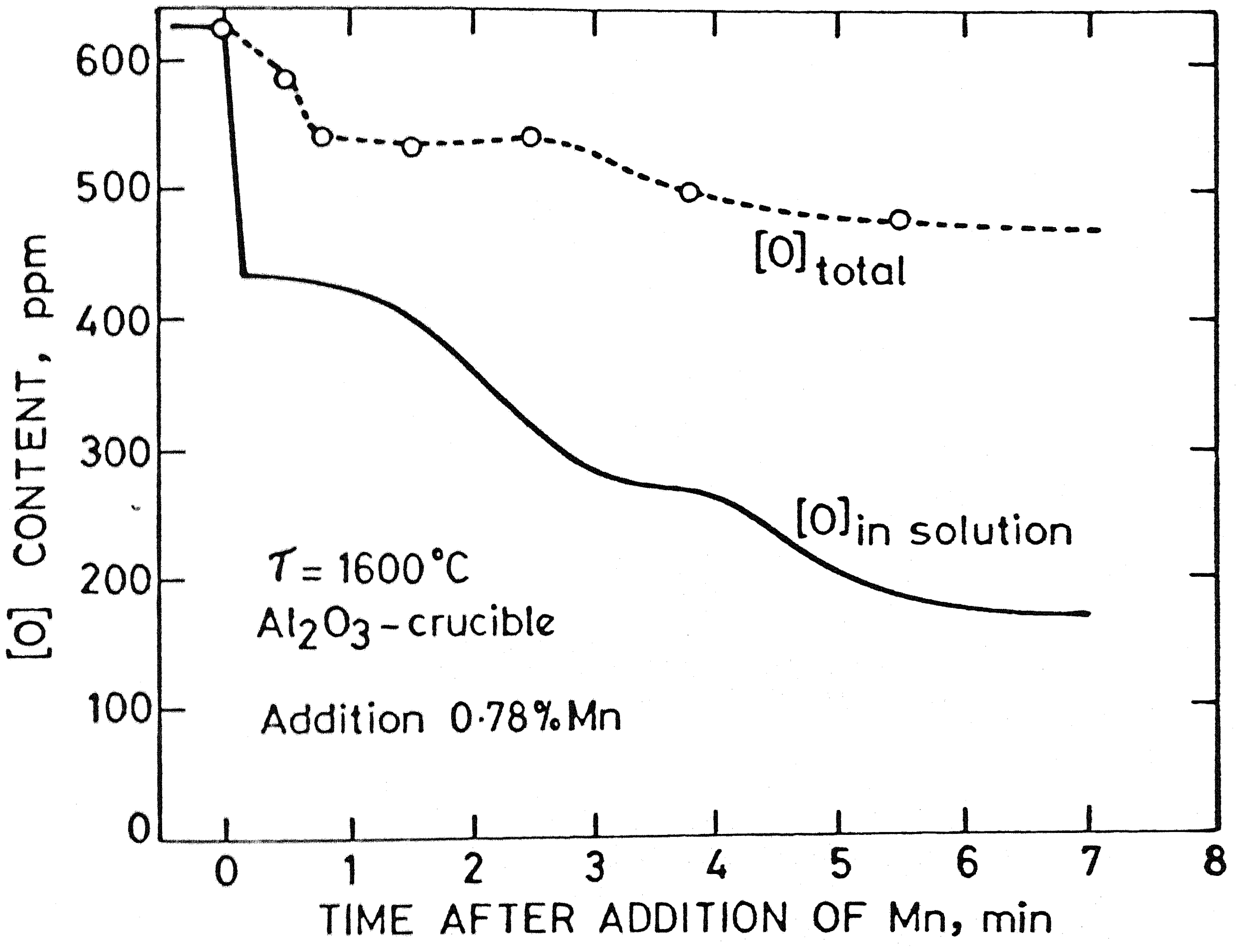

Fig. 7.7 : Oxygen concentration curve following the addition of electrolytic manganese

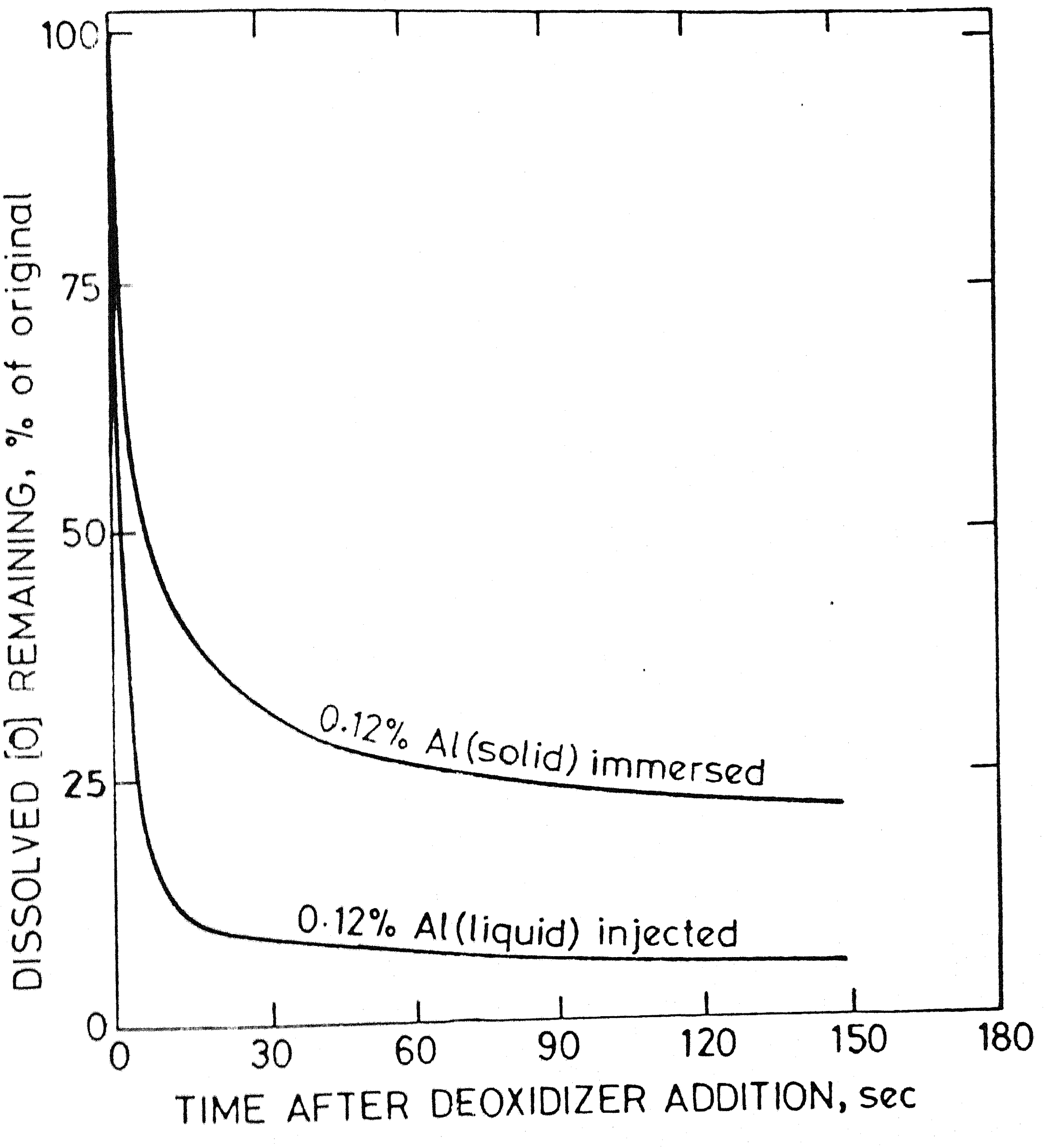

Fig. 7.8 : Effect of method of introduction aluminium on dissolved oxygen in molten steel

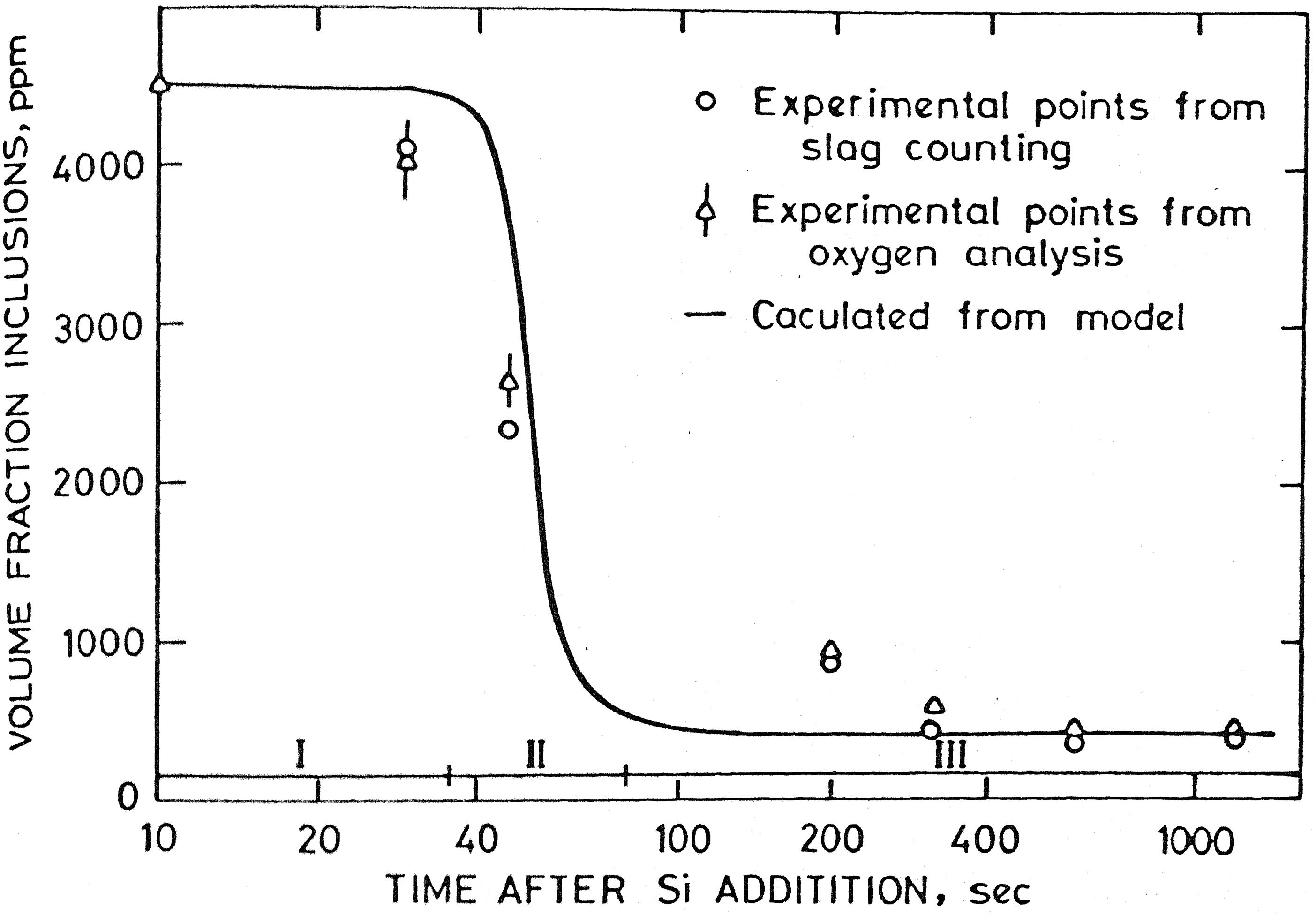

Fig. 7.9 : Total inclusion content vs. time, calculated as well as experimental (Lindborg and Torsell)

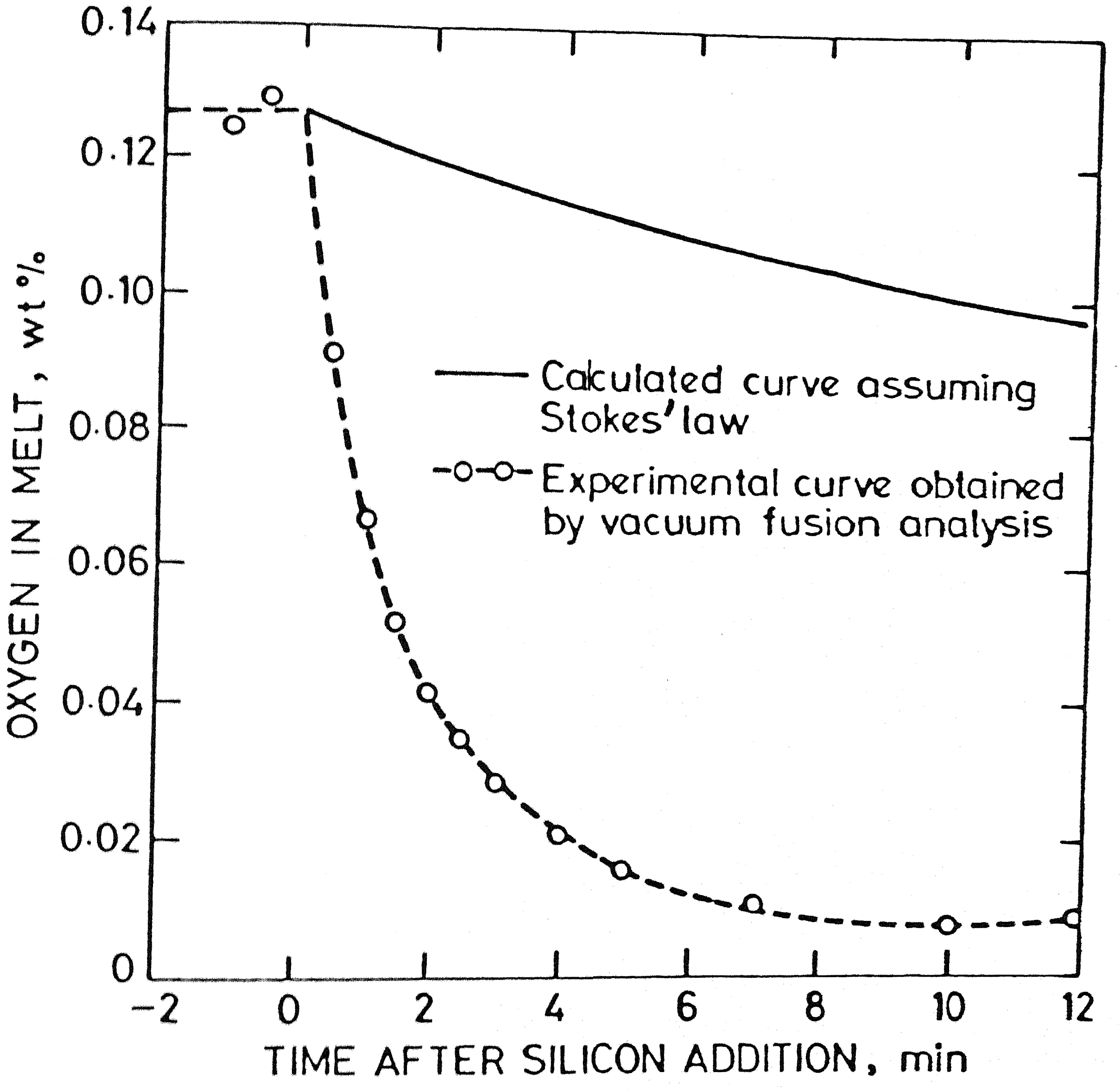

Fig. 7.10 : Change of oxygen content in the stirred iron melt obtained by calculation assuming Stokes' law, and that by vacuum fusion analysis

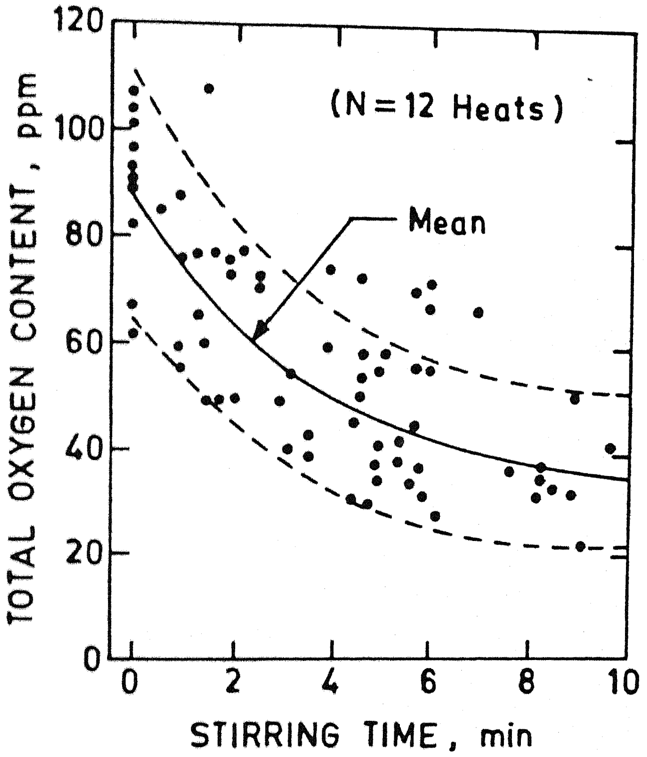

Fig. 7.11 : Total oxygen content of moltent steel as function of time in argon stirred ladle

CHAPTER 8

DEGASSING AND DECARBURISING OF STEEL

N. K. BATRA

8.1 DEGASSING OF STEEL

8.1.1 INTRODUCTION

The word degassing implies the removal of dissolved gases such as hydrogen and nitrogen from the liquid bath before casting. These gases have got limited solubilities in the liquid iron but very little in the solid iron as shown in Fig.8.1. Concentrations of the gases in the liquid near the solid-liquid interface during the solidification stages of steel may build up to such an level that gas bubbles are formed and if the same cannot leave the bath due to the net work of dendrites in the solidifying mass, the bubbles give rise to blow holes. The phenomenon is similar to that of CO formation in semikilled and rimmed steel. Such blow holes are detrimental to the soundness and mechanical properties such as strength, toughness etc. of steel. Similarly if the gases are present as supersaturated solution in solid state, the material may crack even under reduced stress conditions.It is very time consuming, expensive and difficult to get rid of these gases in the solid state, and the best way to have low gases in the finished steel is to control the contents of these gases in the liquid state itself. As there may be some unavoidable pick up of gases during tapping and teeming operations in atmospheric air, it is advisable to degasify the liquid steel in the furnace or ladle to levels below the specified values for the finished steel.

8.1.2 Basic Principles

Molecules of diatomic gases such as hydrogen and nitrogen tend todissociate and go into solution as atoms in the liquid iron as follows:

$$H_2(g) = 2\underline{H} \qquad \ldots 8.1$$

$$K_H = f_H\,[\text{wt.\% H}]^2/p_{H_2} \qquad \ldots 8.2$$

$$\log K_H = -\frac{3810}{T} - 3.18 \qquad \ldots 8.3$$

and

$$N_2(g) = 2\underline{N} \qquad \ldots 8.4$$

$$K_N = \frac{f_N^{\,2}(\text{wt.\% N})^2}{p_{N_2}} \qquad \ldots 8.5$$

$$\log K_N = -\frac{376}{T} - 2.492 \qquad \ldots 8.6$$

f_H, f_N are the activity coefficients of hydrogen and nitrogen in liquid iron, and have the unit values of 1.0 in very dilute solutions. p_{H_2} and p_{N_2} are the partial pressures of hydrogen and nitrogen respectively.

A number of thermodynamic studies are reported in the literature which are aimed at finding the activity coefficient values in presence of alloying elements in liquid iron. The results are summarized in terms of interaction parameters which may be used to find f_H and f_N as follows:

$$\log f_H = \sum_j e_H^j \,(\text{wt.\% } j) \qquad \ldots 8.7$$

$$\log f_N = \sum_j e_N^j \,(\text{wt.\% } j) \qquad \ldots 8.8$$

values of interaction parameters for species of interest are summarized in Table 8.1. The computed solubilities of hydrogen and nitrogen at various partial pressures of these gases at 1600°C and 1700°C are plotted in Fig. 8.2. The effects of alloying elements in steel on the solubility limits of these gases at 1 atm pressure are shown in Figs. 8.3 and 8.4. In general, solubilities tend to fall with rising levels of silicon and carbon but increase with increase in contents of other elements which form stable nitrides or hydrides.

8.1.3 Nitrogen Control

The principal source of nitrogen contamination is the atmospheric air, though it may also be present to some extent in the charge for steelmaking or alloy steelmaking. The Basic Bessemer process suffered mainly because of the increased and unavoidable nitrogen pick up near the end of refining. In Oxygen Steelmaking, the problem of nitrogen pick up does not arise due to the use of pure oxygen for refining purposes, and a blanket provided by the slag cover at the top. Control of nitrogen in electric arc furnace steelmaking is more difficult as the slag may be pushed back by the force of arc, and temperatures in the vicinity of the arc are very large. It is important to maintain a certain degree of carbon boil which helps to remove the absorbed nitrogen gas by lowering the partial pressure of nitrogen gas above the bath. A materials balance gives the following :

$$P_{N_2} = \frac{\frac{1}{28}(d\underline{N}/dt)}{\frac{1}{28}(d\underline{N}/dt) + \frac{1}{12}(d\underline{C}/dt)} = \frac{f_N^2\,[\underline{N}]^2}{K_N} \qquad \ldots 8.9$$

or simplifying and by taking $(d\underline{N}/dt) \ll (d\underline{C}/dt)$

$$\frac{1}{\underline{N}^2}(d\underline{N}/dt) = \frac{28}{12}\,\frac{f_N^2}{K_N}\,(d\underline{C}/dt) \qquad \ldots 8.10$$

Steady conditions may be reached when the rate of nitrogen removal equals the rate of nitrogen pick up by the bath. Under the reducing slag conditions, one must take into account the tendency of nitrogen pick up while determining its duration and purpose of controlling other elements such as sulphur and oxygen in steel.

Against the solubility limit of around 0.045% , the actual nitrogen contents of the commercial steels may vary from 0.003 to 0.006% . Further lowering of nitrogen is made possible in the secondary refining units by lowering the partial pressure of N_2 gas and by maintaining certain degree of agitation to the bath. The most common vacuum treatment processes used in the steel industry are shown in Fig. 8.5. In the early applications of vacuum degassing, it was observed that nitrogen is not very effectively removed, as the reaction rate (i.e. equation 8.4) is strongly influenced by surface active solutes such as sulphur and oxygen. Results as obtained by Pehlke are plotted in Fig. 8.6 to show the detrimental effects of oxygen on the rate of nitrogen removal from the bath. Swish and Turkdogan has reported that rate of nitrogen removal is inversely proportional to the oxygen content of the bath.

8.1.3 HYDROGEN CONTROL

The primary sources of hydrogen are water vapours in the atmospheric air, and the water content of the wet refractory lining, mould lining, slaked lime and scrap etc. The dissociation of H_2O in the gas phase gives rise to hydrogen in steel as follows :

$$H_2O\ (g) = 2\underline{H} + \underline{O} \qquad \ldots 8.11$$

$$K_{OH} = \frac{f_O f_H^2\ [\text{wt.\% H}]^2 [\text{wt.\% O}]}{p_{H_2O}} \qquad \ldots 8.12$$

$$\log K_{OH} = -\frac{10390}{T} - 0.16 \qquad \ldots 8.13$$

The amount of hydrogen absorbed would depend upon the oxygen content of bath and partial pressure of H_2O gas, the maximum value being limited by the reaction 8.1 at unit partial pressure of hydrogen gas. The results of computations are plotted in Fig. 8.7. Against the solubility limit of 25 ppm (.0025 wt.%) actual hydrogen levels in commercial steel are of the order 3 to 8 ppm. A part of hydrogen absorbed is removed during CO boil i.e.

$$(d\underline{H}/dt) = \frac{2}{12}\ \frac{f_H^2\ \underline{H}^2}{K_N}\ (d\underline{C}\ /dt) \qquad \ldots 8.14$$

In some sensitive steels and alloy steels, the upper limits on hydrogen contents of steel are specified to be below 3 ppm and degassing of steel is necessary to get such low levels of hydrogen.

The principal methods of hydrogen removal are the same as that used for nitrogen removal i.e. by argon purging of bath or the use of vacuum systems shown in Fig. 8.5. Unlike nitrogen, the adsorption and desorption of hydrogen are reported to be rapid and reaching equilibrium. The following equation may be used to determine the rate of hydrogen removal by argon purging (assuming $V_{Ar} >> V_{H_2}$)

$$V_{H_2} = -112(d\underline{H}/dt)W = V_{Ar}\frac{f_H^2 (\underline{H})^2}{K_H} \qquad ...8.14$$

where W is weight of bath in tons and V_{Ar} is the flow rate of argon in Nm^3/min. If there is a fall in temperature due to argon purging, the same must be taken into account while calculating the value of K_H using equation 8.3. The normal rate of purging gas is around .01 Nm^3/ton/min whereas only 0.0005 to 0.001 Nm^3/ton/min is required to promote homogenization. It may be important to mention here that once the steel bath is degassed, it has a tendency to pick up hydrogen again rapidly if it is allowed to come in contact with any source of hydrogen.For this reason it is very important to ensure that any additions made after degassing are completely dry and the mold lining as well as casting fluxes are free of any dampness. Best results on vacuum degassing are reported in case of unkilled steel where the vigorous CO evolved during solidification acts as both homogenising medium and scavenger for the residual gases in steel.

8.2 DECARBURISATION OF STEEL

8.2.1 Introduction

The effective decarburisation of steel bath with minimum losses of iron or other valuable elements such as manganese and chromium is key to the success of any steelmaking, alloy steelmaking and secondary steelmaking processes. The sources of carbon are many fold i.e. blast furnace iron, high carbon and medium carbon ferro alloys, graphite electrodes etc. whereas the desired levels of carbon in the finished product may vary over a range depending upon the nature of the product produced. In some categories of steel such as soft iron, annealed dynamo steel, special deep drawing steel, austinitic stainless steel, and high chromium alloy steel etc,the specified carbon levels are very low i.e. 0.01 to .04 pct. Generally there are no practical difficulties in refining high carbon steel either in basic oxygen steelmaking or electric are furnace steelmaking but problems arise while decarburising steel to very low levels of carbon. In many cases, the opening carbon analyses of the bath is kept to be around 0.5 pct. greater than that of the finished steel so that due advantages is taken of the carbon boil period in homogenizing the bath as well as degassing of steel to some extent as mentioned before.

8.2.2 Production of Low Carbon Plain and Low Alloy Steels

Removal of carbon occurs at the cost of an oxidizing medium i.e. O_2 lancing, iron ore additions, mill scale, Mn ore etc. As carbon level falls, oxygen level in bath builds up i.e.

$$[\underline{C}] + [\underline{O}] = CO\,(g) \qquad \ldots 8.15$$

$$K_{CO} = \frac{p_{CO}}{[\underline{C}]\,[\underline{O}]}\;\frac{1}{f_o}\;\frac{1}{f_c} \qquad \ldots 8.16$$

$$\log K_{CO} = \frac{1224}{T} + 2.048 \qquad \ldots 8.17$$

Carbon oxygen plots at various partial pressures of carbon monoxide gas are shown in Fig. 8.8. As oxygen level builds up, FeO content of the slag increases

$$[\underline{O}] + [Fe] = (FeO) \qquad \ldots 8.18$$

$$K_{FeO} = \frac{\gamma_{FeO}\; N_{FeO}}{f_o [wt.\%\; \underline{O}]} \qquad \ldots 8.19$$

$$\log K_{FeO} = \frac{6323}{T} - 2.737 \qquad \ldots 8.20$$

In secondary steelmaking, use is made of the dependence on the pressure of the carbon-oxygen reaction so that oxygen level does not rise to give high iron losses even at low carbon values. As a matter of fact, if carbon and oxygen in the bath are 0.04 and 0.05 pct. respectively to start with, no further oxidizing medium is needed in lowering the levels of both elements to 0.01 pct. by maintaining the partial pressure of CO gas at around 0.05 atm. If starting levels of carbon are greater than 0.04 pct., additional oxygen supply becomes necessary to bring carbon levels to around 0.01 pct. and the final oxygen level would depend upon the partial pressure of CO gas prevailing in the system. There are various ways in which the partial pressure of CO gas can be reduced for bulk decarburization of bath :

(i) Argon or nitrogen purging of bath in the ladle
(ii) Use of mixed or inert gases in bottom blowing or combined blowing converters
(iii) Vacuum treatment units.

Low carbon steels produced at reduced pressures, would not require much of further deoxidation before tapping. This in turn minimizes the formation of non-metallic inclusions in the solidified steel as a result of complex reactions occurring between the alloying elements and residual oxygen during the solidification stages of steel, and thus would produce much cleaner steels.

8.2.3 Decarburising of High Chromium Melts

Chromium and manganese have got higher affinities for oxygen than iron, and if present in the melts, would get oxidized to slag when an oxidizing medium is added to achieve decarburisation of steel. Earlier methods of refining with ore additions were limited to low chromium levels. Soft but expensive low carbon ferro-chromium alloys were added to get the right composition after the decarburization. The advent of oxygen lancing in 1940's enabled to use cheaper grades of high carbon ferro-chrome alloy and the alloy steel scrap as sources of chromium in the charge. Very high temperatures of 1800°C or more could be rapidly obtained by blowing oxygen, and it minimized the oxidation of chromium in the melt. Final adjustments of the bath at the end of the oxygen blow could still be done by adding low carbon scrap or ferro-alloys. Further, much of the oxidized chromium in the slag got reverted to metal in the subsequent reducing period where ferro-silicon and lime were added to the furnace with some means of stirring the bath. This period promoted desulphurisation of metal but made difficult removal of any phosphorus from the charge. The oxidation and reduction reactions can be understood by considering the following :

$$Cr_3O_4 + 4\underline{C} = 3\,\underline{Cr} + 4\,CO\,(g) \qquad \ldots 8.21$$

$$\log \frac{[\%\,Cr]}{[\%\,C]} = -\frac{13800}{T + 4.21[\%\,Ni]} + 8.76 - 0.925 \log p_{CO} \qquad \ldots 8.22$$

$$Cr_3O_4 + 2\,\underline{Si} + 4\,CaO = 2\,(2\,CaO.SiO_2) + 3\,\underline{Cr} \qquad \ldots 8.23$$

$$\log\,(\%\,Cr)_{slag} = 1.283 \log\,[\%\,Cr] - 0.748 \log\,[\%\,Sc] - 1.709\left(\frac{\%CaO}{\%\,SiO_2}\right) - 0.923 \qquad \ldots 8.24$$

The results in the reducing period are affected a great deal by the lack of vigorous stirring of the bath. It was a common practice to resort to refurnacing and reladling of metal to homogenize the bath, promote slag-metal reactions and to reduce the wear on the refractories. Coolants in the form of scrap etc. were often used to cool the bath just after the oxygen blow.

Equation 8-22 is plotted in Fig.8.9 which shows that high chromium levels of over 15 pct. can be retained in the bath while decarburising below 0.05 pct. carbon at temperatures above 1900°C. The amount of silicon in the melt prior to oxidation was kept below 0.25 pct. to avoid excessive wear of the refractory lining material. The technology of oxidizing the bath at very temperatures and subsequent reduction of the slag helped in the bulk production of austinitic grade of stainless steal at relatively low costs. The process has since been discarded in favour of more versatile processes which relied on the reduced pressure of carbon monoxide for batter recovery of chromium instead of high and difficult to handle temperatures. This may be visualized from the equation 8-22 itself and or the plots shown in Fig.8.10. The means of refining high chromium melts under reduced pressure conditions are discussed below.

8.2.4 Argon - Oxygen Decarburisation

An argon oxygen decarburising vessel is schematically shown in Fig.8.11. A mixture of argon and oxygen is blown through the tuyeres to effect removal of carbon at low p_{CO} . During finished stages, at the end of blow, pure inert gas may be blown to mix metal and slag for increased recovery of chromium and also to keep the tuyeres open. A typical log sheet for production of stainless steel in an A.O.D. vessel is shown in Table 8.2 where O_2 to Argon ratio is changed from 3.0 to nil in three steps. As long as carbon content is high, partial pressure of CO gas need not be reduced to retain chromium in metal and high O_2 to Ar ratio may thus be employed. With O_2 to argon ratio of 1 to 3, p_{co} will be close to 0.4 and at temperature of 1700°C, Cr to C ratio in the melt is computed to be 178 i.e. 15% Cr can be retained in melt at the carbon level of 0.084%. It is desirable to have silicon at 0.20 percent maximum to reduce the lining wear, reduce time, and excessive temperature increase to some extent. In the early stages of blow, argon may be replaced by low cost nitrogen. If necessary alloy or cooling scrap can be added at intermediate stages to lower the bath temperature and to reduce the wear on the refractory. As such, there is no need to resort to refurnancing and reladling of metal as practiced earlier. Any chromium in slag is stripped by adding silicon bearing agents and lime from the top and blowing argon from the bottom for vigorous stirring of bath. Recovery of chromium from the charge is as high as 98 pct. and that of manganese is in the charge 85 to 90 pct. If extra low sulphur (0.005%) in the alloy steel is required, the same may be attained by removing the first slag and building up another reducing slag with constant argon stirring of bath.

The life of the bottom or submerged tuyeres is affected adversely by the high oxygen to argon ratio during blowing. For treatment of high carbon (over 1.5 pct.) melts, top lanced oxygen blowing facilities are incorporated in the process to enhance the rate of decarburisation. Argon or argon-oxygen mixture are still blown from the bottom tuyeres to maintain homogenization of the bath during the period of oxygen refining by top blowing. As carbon is reduced and low p_{CO} becomes important for retaining chromium in the bath, top lancing is discontinued and the practice reverts to the conventional mixed gas technique. Thermal efficiency of the process may be improved by burning a part of CO gas to CO_2 by using a sub sonic lance of instead of supersonic lance used in LD steelmaking. Mixing to the bath is aimed independently by the bottom blowing of gas. This helps to incorporate more cold metal and scrap in the change without needing to melt the same in an arc furnace or cupola. Experience gained with the bottom and combined oxygen steelmaking at various parts of the world has helped to develop the AOD process for the effective decarburisation of high chromium melts at much lower costs.

8.2.5 Vacuum Oxygen Decarburisation

Schematic of the vacuum decarburising vessel is shown in Fig.8.12. In many ways at is similar to the argon-oxygen process in providing a reduced partial pressure of CO gas to minimize chromium oxidation. In design, it is an essentially a modified ladle degassing unit except for the addition of a lance for injecting oxygen into the bath. Table 8.3 compares the performance and design features of the VOD units with these of the AOD units. The required low p_{co} is attained by the reduction of total pressure above the bath rather than by dilution of CO gas by argon. Argon gas in VOD units is passed for providing agitation and breaking the slag cover. Silicon content in the charge to the ladle vessel is kept below 0.25 percent to help control the rise in temperature and minimize the refractory wear. The rate of oxygen injection to the vacuum vessel would depend upon the rate at which the gases can be pumped out from the system. High carbon melts would require high rates of oxygen injection for rapid decarburisation and it may be done without resorting to vacuum in the ladle or converter till carbon levels below 0.5 pct. are achieved. The major advantages of a VOD unit over on the AOD units are as follows:

(i) Much lower pressures of CO gas can be attained which favours decarburesation of bath to very low carbon levels and increased recovery of chromium.
(ii) The overall consumptions of argon gas and reducing mix are less.
(iii) Heat efficiency is better due to less heat being carried away by the flue gases.
(iv) Better control of the process by measuring the analysis and volume of flue gases and taking bath samples.

It has got the following disadvantages:

(i) Cost of the vacuum plant may be high.
(ii) There are difficulties in removing the slag and making fresh reducing slag to produce very low sulphur alloy steel as the VOD installations are not provided with a means of slag disposal.

Typical changes in the temperature and composition in the VOD ladles and VOD converter processes are shown in Fig.8.13. The choice between the two depends upon the initial carbon content of the change as mentioned before. Nippon Steel Corporation at Yawata works have used the VOD process in combinaton with basic oxygen furnaces for steelmaking for the production of ferritic stainless steels since 1971. The convention practice of LD steelmaking resulted in an increased consumption of BOF refractory, reduced metal yields, lower heat efficiency and productivity due to the need to remove phosphorus rich slag after first blow. Further improvements were made around 1980's by incorporating the dephosphonsation treatment of hot metal by soda ash injection technique prior to decarburisation in the top and bottom blowing oxygen converters. Final refinement is done in the VOD vessels. Advantage is taken of the high speed decarburisation suppressing chromium oxidation through the top and bottom dilution blowing (i.e. O_2 + Ar) and slag reduction by using bath agitation. Ferro-alloys and scrap charges are preheated before hand to around 300 C in 10 min. by using the bottom blowing tuyeres as oxy-fuel burners. In comparison to AOD process, decarburisation rate in the new process is reported to be 3 times or more at high and medium carbon contents. The flow rates of gases used for top and bottom blowing are summarized in Table 8.4. The treatment time in the VOD units have been reduced for 150 min. to 70 min. by resorting to better refining in the new process. Integrated chromium yield improved for 91.6% to 95.6% with overall lowering of cost by 13% .

8.3 SOLVED EXAMPLES

Example 8.1 : Steel bath at 1600°C contains 0.4 pct. carbon which is being decarburised at the rate of 0.25 pct./hour. Initial nitrogen and hydrogen contents are reported to be 60 ppm and 10 ppm respectively. If the nitrogen and hydrogen pick up from the atmosphere are ignored during carbon boil, find composition of bath after 1 hour of refining. Ignore any changes in the temperature of the bath.

Solution

Initial carbon $C_i = 0.4\ \%$

Change in carbon = $\Delta C_i = 0.25\%$

Final carbon in metal $C_f = 0.4 - 0.25 = 0.15\%$.

Using interaction parameters in Table 8.1 and ignoring the effect of dissolved oxygen as an approximation

$$\log f_H = .009 \quad \text{or} \quad f_H = 1.02$$

$$\log f_O = -0.0675 \quad \text{or} \quad f_O = .856$$

$$\log f_C = .0213 \quad \text{or} \quad f_C = 1.05$$

Solving equation(8.14), ($p_{N_2} << p_{CO}$, $p_{H_2} << p_{CO}$ and $p_{CO} = 1$ atm.)

$$N_f = \frac{1}{\frac{1}{N_i} + \frac{28}{12}\,\frac{f_N^2}{K_N}\,\Delta C_i}$$

$$N_i = 0.006\%$$

Using equation(8.6) $K_N = \frac{1}{403}$

Putting values

$$N_f = .0021\% \quad \text{or 21 ppm}$$

Similarly $H_i = .001\%$ or $K_H = 163745^{-1}$

$$H_f = \frac{1}{\frac{1}{H_i} + \frac{2}{12}\frac{f_H^2}{K_H} C_i} = 0.00012\% \text{ or } 1.2 \text{ ppm.}$$

From equation (8-16) and (8-17)

$$O_f = \frac{p_{co}}{K} \frac{1}{[C_f]} \frac{1}{f_o} \frac{1}{f_c} = 0.0147\% \ .$$

Bath composition after 1 hour : [C] = 0.15% [O] = 0.0147%
[N] = 21 ppm
[H] = 1.2 ppm

Example 8.2 : Steel bath at 1650°C contains .05 pct. C, 40 ppm nitrogen and 8 ppm hydrogen to start with under the atmosphere of CO gas at 1 atm pressure. Argon is than purged through the bath at the rate of 0.01 Nm^3/hr/ton. Determine the bath composition in the bath as a function of time. Ignore any changes in temperature of bath and take activity coefficients of hydrogen, nitrogen, carbon and oxygen at unity for simplicity.

Solution

$T = 1923$ K $\qquad C_i = 0.05$

$K_{CO} = 484 \qquad K_H = (144970)^{-1} \qquad K_N = (487)^{-1}$

Using equation 8-16, $O_i = 0.0414\%$.

$N_i = 0.004 \qquad H_i = 0.0008$

General rate equations (1 ton steel basis):

$$\dot{n}_{CO} = -\frac{10}{16}\frac{d[O]}{dt} \quad \text{k moles/min}$$

$$\dot{n}_{H_2} = -\frac{10}{2}\frac{d[H]}{dt} \quad \text{k moles/min}$$

$$\dot{n}_{N_2} = -\frac{10}{28}\frac{d[N]}{dt} \quad ,,$$

$$\dot{n}_{Ar} = \frac{0.01}{22.4} \quad ,,$$

$$\dot{n}_T = \dot{n}_{CO} + \dot{n}_{N_2} + \dot{n}_{H_2} + \dot{n}_{Ar}$$

$$p_{CO} = \frac{\dot{n}_{CO}}{n_T} = K_{CO} \quad [C]\ [O]$$

$$p_{H_2} = \frac{\dot{n}_{H_2}}{n_T} = [H]^2/K_H$$

$$p_{N_2} = \frac{\dot{n}_{N_2}}{n_T} = [N]^2/K_N$$

Oxygen is lost by its reaction with carbon,

$$[C] = C_i - [O_i - [O]]\ \frac{12}{16}$$

$$= 0.019 + 0.75\ [O]$$

$$\frac{\dot{n}_{CO}}{\dot{n}_{H_2}} = \frac{p_{CO}}{p_{H_2}} = \frac{k_{CO}}{[H]^2}\ [0.019 + 0.75\ [O]]\ [O]\ K_N$$

$$= \frac{2}{16}\ \frac{d[O]}{d[H]}$$

$$\frac{d[O]}{[O]\ [0.019 + 0.75[O]]} = k_{CO}\ k_N\ 8 \times \frac{d[H]}{[H]^2}$$

$$\frac{1}{.019}\ [\ \frac{1}{[O]} - \frac{0.75}{0.019 + 0.75(O)}]\ d[O] = 0.026\ \frac{d[H]}{[H]^2}$$

$$\text{or} \quad \ln \frac{[O]}{[C]} / \frac{O_i}{C_i} = -5.074 \times 10^{-4}\ [\ \frac{1}{H_f} - \frac{1}{H_i}\ ]$$

$$\text{or} \quad H_f = \frac{1}{883 - 1970.6\ \ln \frac{[O]}{[C]}}$$

Similarly, for nitrogen

$$\frac{d[O]}{[O]\ [0.019 + 0.75[O]]} = k_{CO}\ k_N\ \frac{16}{28}\ \frac{dN}{N^2}$$

$$N_f = \frac{1}{232.7 - 92.7\ \ln \frac{[O]}{[C]}}$$

Also

$$-\frac{10}{16}\ \frac{d[O]}{dt} = k_{CO}[O]\ 0.019 + [O]]\ [\frac{0.01}{22.4} - \frac{10}{16}\ \frac{d[O]}{dt} - \frac{10}{28}\ \frac{d[N]}{dt} - \frac{10}{2}\ \frac{d[H]}{dt}]$$

Solving

$$[\frac{10}{16}]\frac{1}{0.019}[\ln\frac{[O]}{[C]} - \ln\frac{O_i}{C_i}] = k_{co}[\frac{0.01}{22.4}t + \frac{10}{16}[O_i - [O]]$$

$$+ \frac{10}{28}[N_i - [N]] + 5[H_i - [H]]$$

or

$$t = -28.2 - 152\ln\frac{[O]}{[C]} + 1400[O_i - [O]] + 800[N_i [N]]$$

$$+ 11200[H_i - [H]]$$

Results of computations

[O]	[C]	[H]	[N]	t	t^*
%	%	%	%	min	min
0.0414	0.05	0.0008	0.004	0	0
0.03	0.0415	0.00066	0.0038	38.0	21.2
0.02	0.034	0.00052	0.0035	85.6	52.4
0.01	0.0265	0.00036	0.0031	169.6	120

---

* By assuming $P_{Ar} >> P_{CO} > P_{H_2} > P_{N_2}$

REFERENCES

1. C.R. Taylor (ed), Electric Furnace Steelmaking, Iron and Steel Society, USA, 1988.
2. R.D. Pehlke and J.F. Elliot, Trans. AIME, 227, (1963) 844.
3. J.H. Swisher and E.T. Turkdogan, Trans. AIME 239, (1967) 602.
4. M.E. Plockinger and O. Etterich (ed), Electric Furnace Steel Production, John Wiley and Sons (1985).
5. N. Sato, H. Aoki, S. Murakami, N. Moritama and T. Kohtani, Proc. Steelmaking, Vol.68, Detroiet (1985), 253.

Table 8.1 Interaction parameters of interest

$$\text{Log } f_i = \sum e_i^j \,[\text{wt \% } j]$$

	e_i^j			
J	i			
	C	H	N	O
C	0.14	0.06	0.13	- 0.45
Cr	- 0.024	- 0.0022	- 0.047	- 0.04
H	0.67	-	-	- 3.1
Mn	- 0.012	- 0.0014	-0.02	- 0.021
N	0.11	-	-	0.057
Ni	0.012	-	0.01	0.006
O	- 0.34	- 0.19	0.05	- 0.20
P	0.051	0.011	0.045	0.062
S	0.046	0.008	0.007	- 0.133
Si	0.08	0.027	0.047	- 0.131

Table 8.2 Vessel log: Argon Decarburization

Time, Min.		Temp °C	O_2/A(N_2)	Gas Flow Nm^3/hr	
				O_2	A or N_2
0	Charge liquid metal (slag free) Weight 150 metric tons 1.62 C, .54 Mn, 18 Si, .028 S, 17.00 Cr, 6.80 Ni. Add 2290 kg Dolomite lime	1564			
4	Begin stage 1 blow Adjust chemistry 2320 kg H.C. FeCr, 1640 kg FeMn, 2480 kg Ni briquettes		3	5100	1700(N_2)
24	Complete stage 1 blow				
25	Begin stage 2 blow	1686	1	3400	3400(N_2)
44	Complete stage 2 blow, C .50				
48	Begin stage 3 blow		1/3	1700	5100(A)
63	Complete stage 3 blow	1708			
70	Add reductant mix and stir 3820 kg FeCrSi 1830 kg lime 195 kg spar Sample: .032 C, 1.25 Mn, .35 Si .03 N, .015 S, 18.25 Cr, 8.39 Ni				2500(A)
78	Slag off Make final additions 458 kg, FeSi, 32 kg graphite				
104	Tap Ladle temperature	1600 1540			

Table 8.3 Design and performance indices of decarburising using for treating high chromium melts

		Process		
		VOD	AOD	VODC
Volume	m^3/ton	0.22	0.4 - 0.7	0.5
Initial C content	(%)	max. 1.8, usually < 1	1.5 - 3.0	1.5 - 3.0
Starting temperature	(°C)	about 1600	about 1520	1520
Max. oxidizing rate dc/dt	(%C/min)	0.006-0.03	0.04 or 0.08[a]	0.08
Oxygen flow rate	(m^3_n/t min)	0.2-0.70	0.3-0.75 or 1.2[a]	1.2
Argon flow rate	(m^3_n/t min)	.0005- .0010	.15-.5	.01
Slag basicity	(%CaO/%SiO_2)	1.2-2.0	1.2-1.5	1.2-1.5
and for secondary slag			2	2
Sulphur distribution	(%S)/[%S]	about 100	about 100	about 100
and for secondary slag			200	200
Treatment temperatures	(°C)	1600/1700	1550/1700	1600/1700
Treatment time from fill to end of tapping	(min)	about 140	about 90	about 90
Oxygen consumption	(m^3_n/t)	about 15-20	about 30	about 30
Oxygen efficiency (CO)	(%)	20 - 60	30 - 90	50 - 80
Gas consumption - argon and nitrogen	(m^3_n/t)	about 0.8	15 - 25	1.0
Reduction silicon	(kg/t)	about 5-8	10 - 18	about 10
Lime	(kg/t)	20 - 35	70 - 100	40 - 50
Chromium output	(%)	98	98	98

[a] With lancing

Table 8.4 Blow patterns for ferritic stainless steel making at Yawata works of Nippon Steel Corporation in 150 ton converter

Charge to Converter

Hot Metal (S = 0.0022 %, P = 0.015 %, C = 5.3 %)	40.0 %
High Carbon Ferro Chromium	30.0 %
Medium Carbon Ferro Chromium	14.0 %
Stainless Steel Scrap	08.0 %
Other Scrap	08.0 %

Blow Pattern

Sl. No.	Time of blow	% C at end of blow	Blow of gases (Nm^3/min/ton) Top blow O_2	Top blow Ar	Bottom blow O_2	Bottom blow Ar
1.	preheating of scrap 10 min	–	1.0	0.33 (air)	0.16	0.106 (N_2)
2.	First blow, 17 min	0.74	3.17	–	0.17	–
3.	Second blow, 4 min	0.25	1.75	0.87	0.113	0.057
4.	Argon blow, 5 min	0.25	–	–	–	0.17

Final Analyses

	T	C	Cr	Si
Before VOD	1680	0.25	16.2	0.10
After VOD	1600	0.02	16.2	0.10

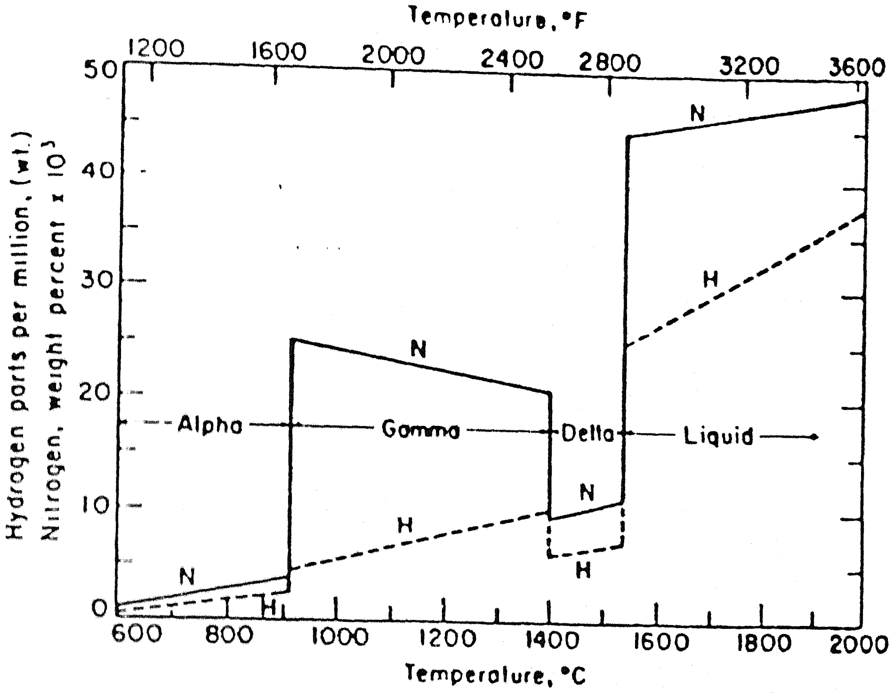

Fig. 8.1 : Effect of temperature on the solubilities of nitrogen and hydrogen in iron at 1 atmosphere pressure of each gas

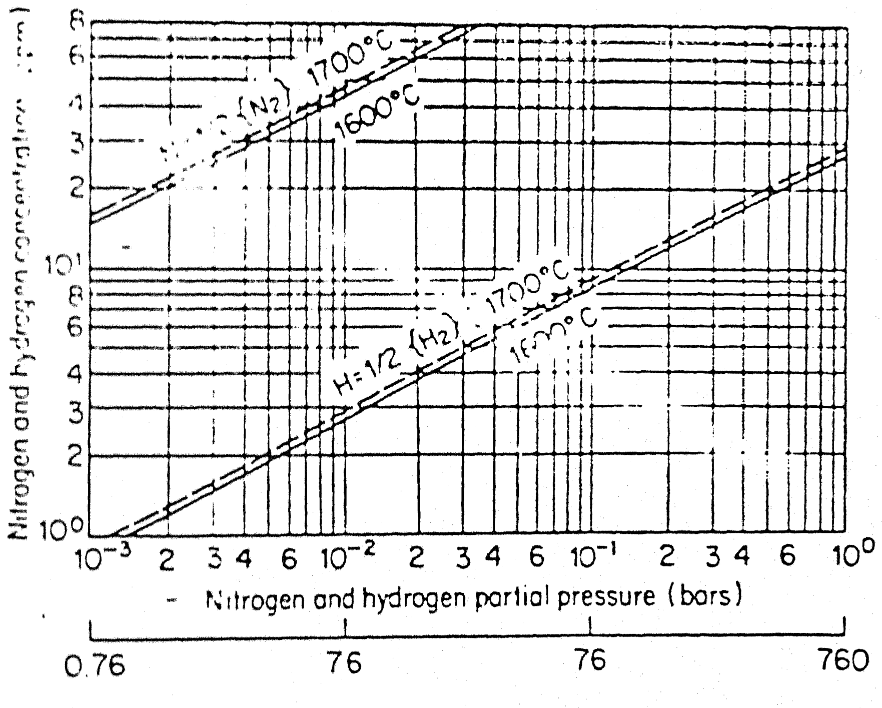

Fig. 8.2 : Solubility of hydrogen and nitrogen in iron melts at 1600 and 1700°C

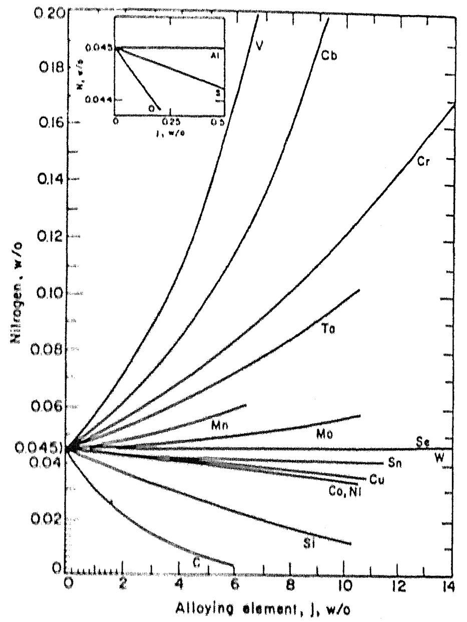

Fig. 8.3: Solubility of nitrogen in liquid iron alloys at 1600°C (2912°F) and 1 atmosphere of $N_2(g)$

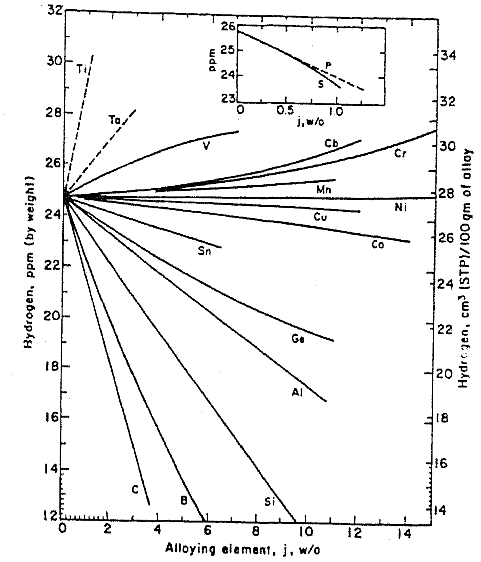

Fig. 8.4: Solubility of hydrogen in liquid iron alloys at 1600°C (2912°F) and 1 atmosphere of $H_2(g)$

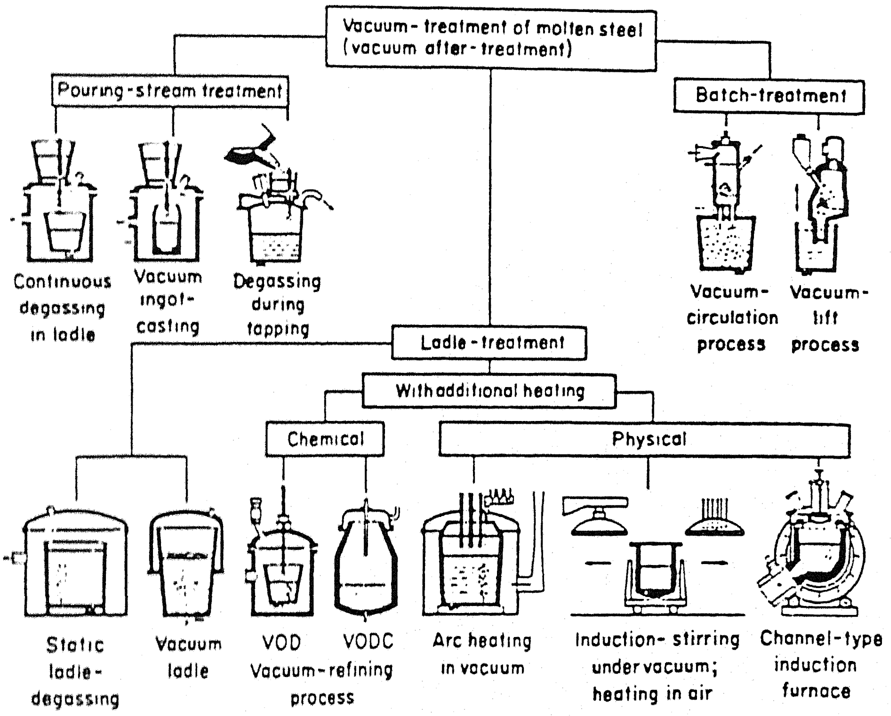
Vacuum-treatment of molten steel (vacuum after-treatment)
Pouring-stream treatment
Batch-treatment
Continuous degassing in ladle
Vacuum ingot-casting
Degassing during tapping
Vacuum-circulation process
Vacuum-lift process
Ladle-treatment
With additional heating
Chemical
Physical
Static ladle-degassing
Vacuum ladle
VOD
VODC
Vacuum-refining process
Arc heating in vacuum
Induction-stirring under vacuum; heating in air
Channel-type induction furnace

Fig. 8.5 : Survey of the most common vacuum-treatment processes used in the production of steel and castings

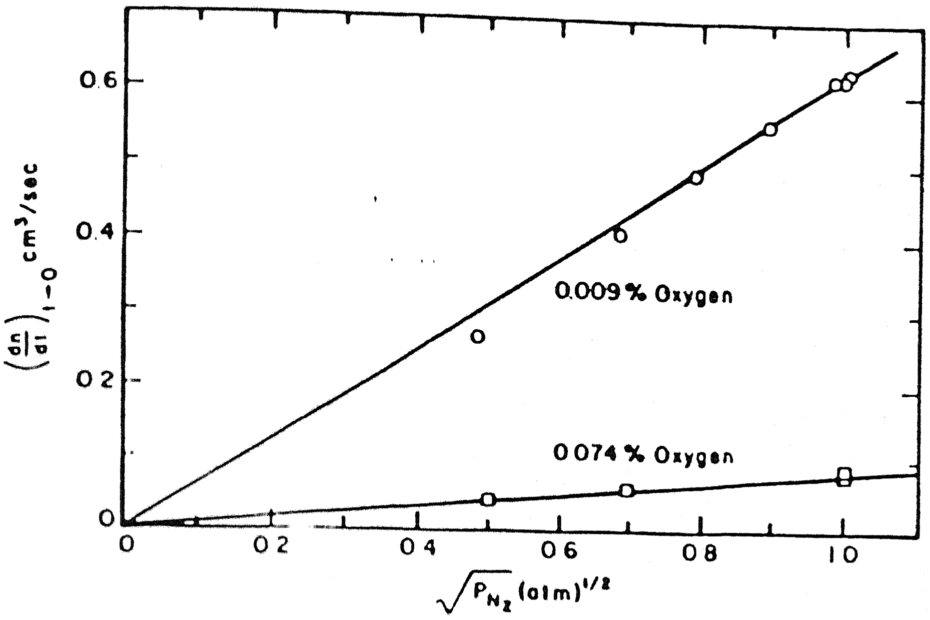

Fig. 8.6 : Initial rate of nitrogen absorption as function of $p_{N_2}^{1/2}$

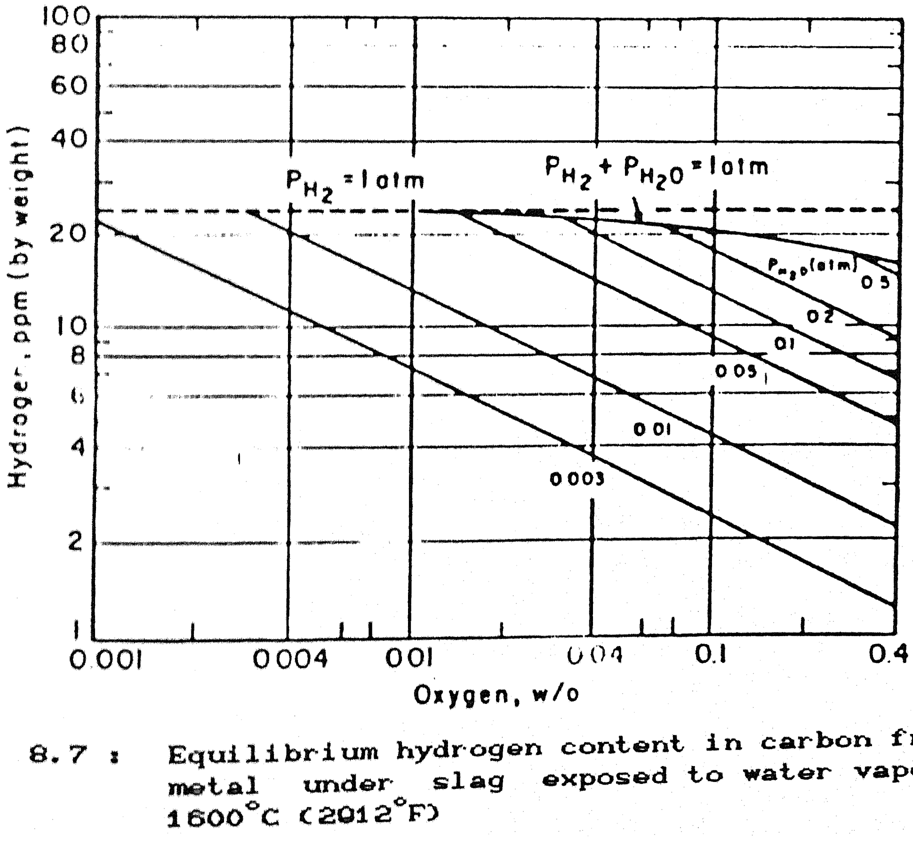

Fig. 8.7 : Equilibrium hydrogen content in carbon free metal under slag exposed to water vapor, 1600°C (2012°F)

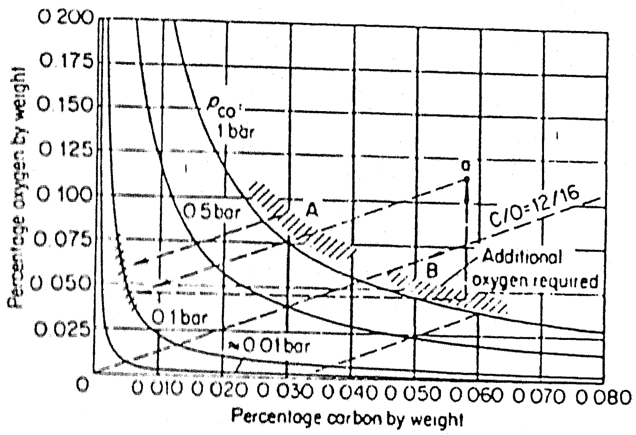

Fig. 8.8 : Relationship between carbon and oxygen content of melt at various p_{CO}.

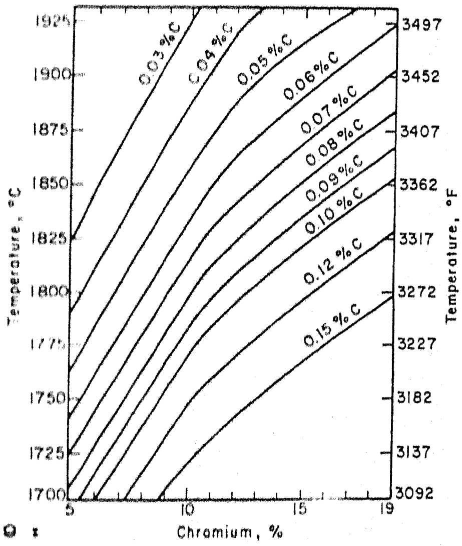

Fig. 8.9 : Relation among chromium, carbon, and temperature in oxygen - saturated bath

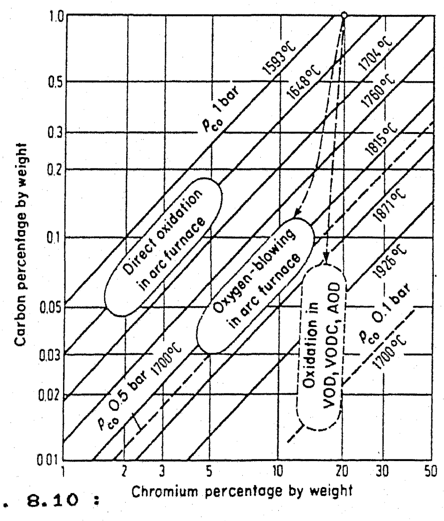

Fig. 8.10 : Final contents for carbon - chromium temperature equilibria for decarburizing high - chromium melts

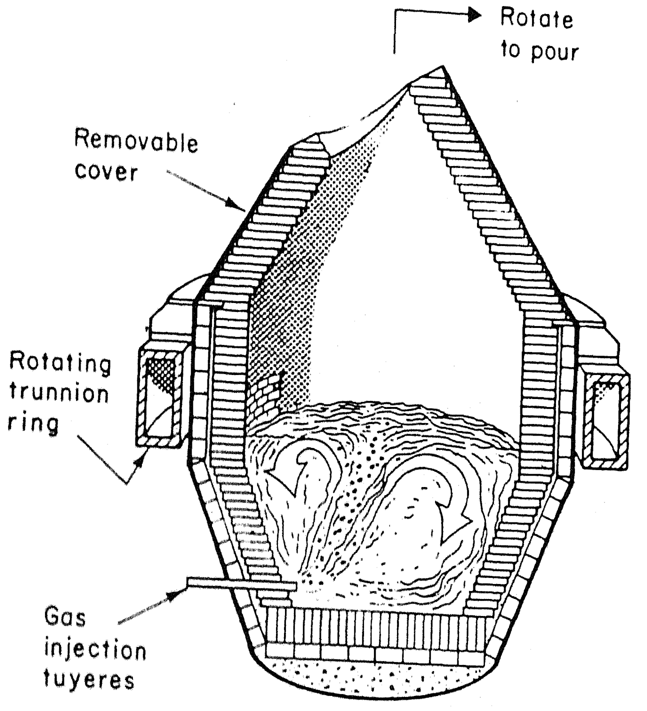
Rotate to pour
Removable cover
Rotating trunnion ring
Gas injection tuyeres

Fig. 8.11 : Argon - oxygen decarburizing vessel

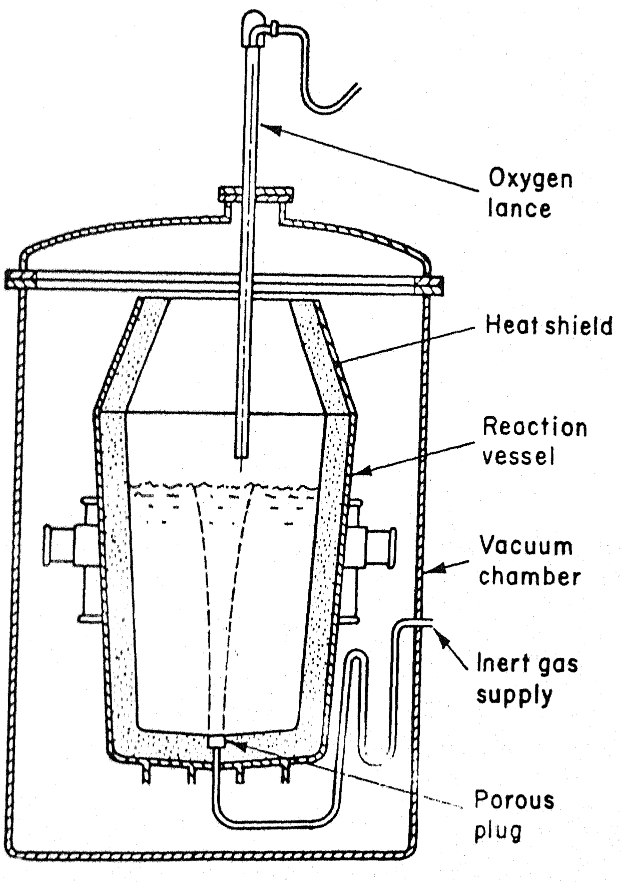
Oxygen lance
Heat shield
Reaction vessel
Vacuum chamber
Inert gas supply
Porous plug

Fig. 8.12 : Vacuum decarburizing vessel

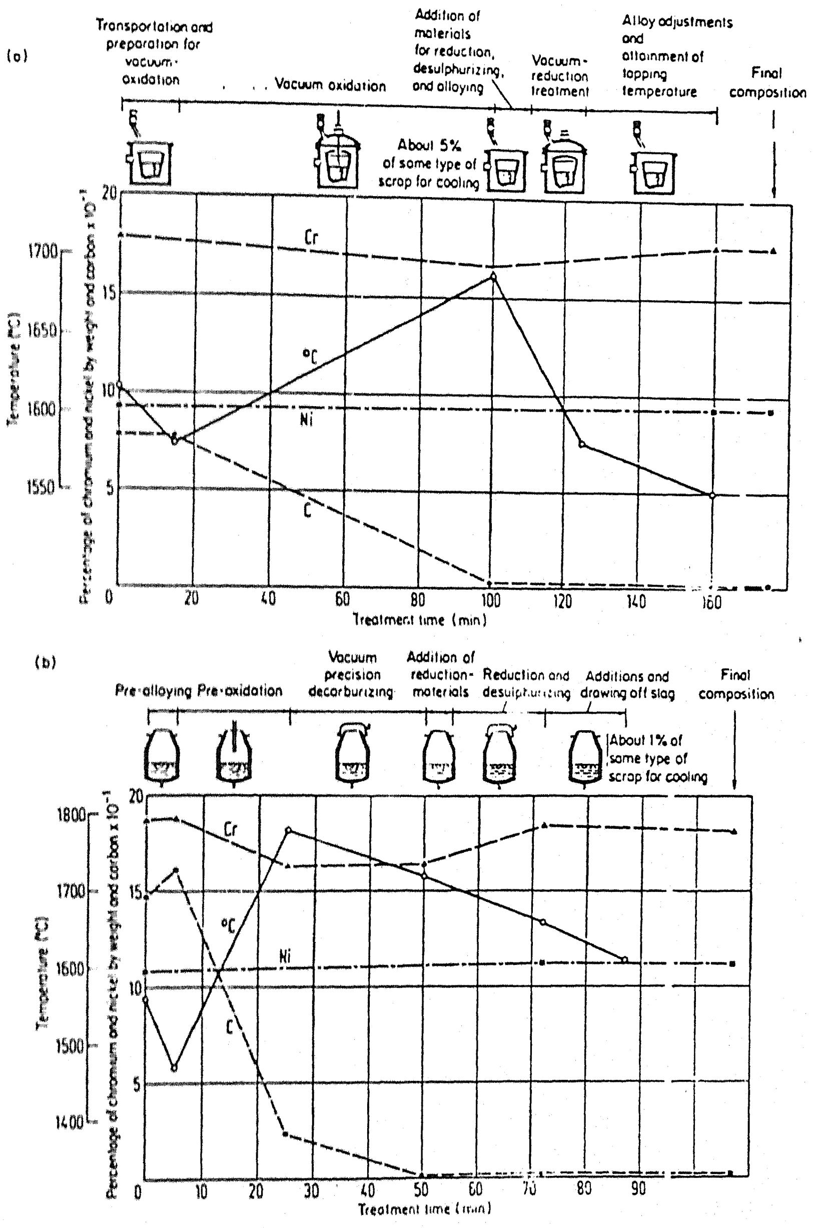

Fig. 8.13 : Changes in temperature and chemical composition during treatment of a high - chrome melt in (a) the VOD process and (b) the VODC process

CHAPTER 9

THERMODYNAMICS AND KINETICS OF DESULPHURIZATION REACTION

A. GHOSH

As stated in chapter 1, synthetic slag treatment and powder injection processes of molten steel in ladle were started in late 60 s and early 70 s with the objective of lowering sulphur content of steel to a low level demanded by many applications. This led to the development of what is known as **Injection Metallurgy** (IM). Low sulphur steel can be obtained by treatment of the melt in ladle by desulphurizing agents either by injection into melt as powder along with a carrier gas (Ar or N_2), or by simple addition. Additions can be made under a synthetic slag cover. Vacuum degassers may additionally be employed. However some inert gas stirring is always required.

Various calcium-bearing agents are employed such as calcium silicide, synethetic premelted slags of either $CaO-Al_2O_3-SiO_2$ or $CaO-Al_2O_3$ or $CaO-Al_2O_3-CaF_2$ type, calcium-barium alloys. Occasionally rare earth metals are also added for inclusion modification.

This chapter is concerned with thermodynamic and kinetic aspects of desulphurization reactions in secondary steelmaking. Injection metallurgy will be dealt with in chapter 10.

9.1 THERMODYNAMIC ASPECTS

9.1.1 Thermodynamics of Sulphur in Liquid Steel

At steelmaking temperatures sulphur is a stable gas, the most predominant molecule being S_2. The dissolution of sulphur in molten steel may be represented by the equation

$$1/2\ S_2\ (g) = \underline{S} \qquad \ldots 9.1$$

For the above reaction,

$$K = \left[\frac{[h_s]}{p_{s_2}^{1/2}} \right]_{equilibrium} \qquad \ldots 9.2$$

where K is equilibrium constant for reaction (9.1), p_{s_2} denotes partial pressure of sulphur in the gas phase in bar, and h_s is activity of dissolved sulphur in steel with reference to 1 wt.pct. standard state.

$$\text{Again, } \log K = \frac{6829}{T} - 1.152 \text{ (ref.1)} \qquad \ldots 9.3$$

The interaction coefficients describing influence of some common solutes (j) in liquid steel on activity coefficient of sulphur dissolved in liquid steel (i.e. e_S^j) are noted below at 1600°C (2)

j	=	Al	C	Mn	S	Si	Ti
e_S^j	=	0.035	0.11	−0.026	−0.028	−0.063	−0.072

The solubility of sulphur in molten steel is also very high.

9.1.2 Thermodynamics of Reaction of Sulphur

Ca and Ba form CaS and BaS respectively upon reaction with sulphur, whereas cerium forms several sulphides (3) out of which CeS is the stablest one at steelmaking conditions. Ce also forms an oxysulphide, Ce_2O_2S. All these compounds are solids at steelmaking temperatures. It may be noted from thermodynamic data on these compounds from any standard text (4,5) that all these elements form very stable sulphides as well as oxides (see also ch.2). Therefore they are both strong deoxidizers as well as desulphurizers and would form both oxides and sulphides.

Again these compounds would not necessarily be present in pure form. For example, addition of Ca-Si leads to formation of $CaO-SiO_2$ type deoxidation product as discussed earlier in ch.7, sec.7.3. However we do not propose to get involved into these complexities and consider the overall reaction as

$$\underline{S} + (MO) = \underline{O} + (MS) \qquad \ldots 9.4$$

For the limiting case of unit activities of MO and MS (i.e. assuming pure MO and Pure MS), the equilibrium constant (K_{MS}) for reaction (9.4) is

$$K_{MS} = \frac{[h_O]}{[h_S]} \cong \frac{[w_O]}{[w_S]} \qquad \ldots 9.5$$

The values of K_{MS} for different systems can be calculated from free-energy of reaction. Fig.9.1, resproduced from Turkdogan (6) shows the pattern. Ba is the strongest desulphurizer and Mg the weakest with Ca and Ce lying in between.

Studies carried out at MEFOS, Sweden (7) on Ca-Si injection in argon-purged ladles showed that presence of a proper slag at the top of the melt is important to prevent resulphurization during processing. It has also been stated that the slag-metal equilibrium with respect to sulphur is closely attained. An empirical equation for sulphur distribution between slag and metal has been suggested as

$$\frac{(W_s)}{[W_s]} = \frac{118.4\ B - 205}{(W_{FeO})_t} \qquad \ldots 9.6$$

$$\text{where B = Basicity index of slag} = \frac{W_{CaO} + 1.4\ W_{MgO}}{W_{SiO_2}} \qquad \ldots 9.7$$

and W is weight percent.

Holappa (8) has reviewed the theoretical basis for sulphur removal in ladle treatment by slag-metal reaction. If MO and MS are not pure, then it is better to utilize the general ionic form of desulphurization reaction, viz.

$$[S] + (O^{2-}) = (S^{2-}) + [O] \qquad \ldots 9.8$$

$$K_s = \frac{(a_s^{2-})\,[h_o]}{[h_s]\,(a_o^{2-})}$$

or,

$$(K_s)\,(a_o^{2-}) = \frac{(a_s^{2-})\,[h_o]}{[h_s]} \qquad \ldots 9.9$$

If we substitute (a_s^{2-}) by wt.pct. sulphur in slag i.e. (W_s), then we may use a modified value of K_s (let it be K'_s). Then

$$K'_s\,(a_o^{2-}) = \frac{(W_s)\,[h_o]}{[h_s]} = C'_s \qquad \ldots 9.10$$

where C'_s is known as **modified sulphur capacity.**

Sulphur capacity of slag (C_s), i.e. the ability of a slag to absorb sulphur was defined originally by Richardson (9) as :

$$C_s = (W_s)\,(p_{O_2} / p_{S_2})^{1/2} \qquad \ldots 9.11$$

where (W_s) is wt.pct. sulphur in the slag in equilibrium with a gas having partial pressures of oxygen and sulphur as p_{O_2} and p_{S_2} . Values of C_s for various slags are available in slag Atlas (10).

Its usefulness stems from the fact that C_s is a property of slag, and at a fixed temperature it is determined solely by slag composition. Higher is the value of C_s , better is desulphurizing ability of the slag. Fig.9.2 shows C_s values for some typical slag systems of interest in secondary steelmaking. Superiority of CaO-CaF$_2$ slag is obvious.

C_s is determined by equilibrating the slag with a gas mixture having known oxygen and sulphur potential. However it is the slag-metal equilibrium which is of interest. This requires use of modified C_s (viz. C'_s) as defined in Eq.(9.10).

The relationship between C_s and C'_s is

$$\log C_s = \log C'_s + \frac{936}{T} - 1.375 \qquad \ldots 9.12$$

At 1600°C, $C'_s = 7.5\ C_s$.

Another parameter that is of interest is **equilibrium sulphur** partition ratio between slag and metal (L_s), where $L_s = (W_s)/[W_s]$. From Eq.(9.10) if $[h_s]$ is taken as $[W_s]$,

then $$L_s = \frac{(W_s)}{[W_s]} = \frac{C'_s}{[h_o]} \qquad \ldots 9.13$$

h_o in liquid steel is typically determined by presence of deoxidizer especially dissolved aluminium. One may relate h_o to FeO-content of slag as well. However it has been found more appropriate to relate it to the former. Fig.9.3 shows L_s as function of CaO content of slag and aluminium content of metal for CaO-Al_2O_3 slag (11). Therefore, for good desulphurization generally Al content of more than 0.020% is recommended (8).

9.1.3 A Note On Temperature and Composition Dependence of C_S and L_S

The thermodynamic relationship between L_s and W_{Al} may be derived as follows.

From Eqs.(9.12) and (9.13),

$$\log L_s = \log C'_s - \log h_o = \log C_s - \frac{936}{T} + 1.375 - \log h_o \qquad \ldots 9.14$$

Again, from Table 7.1 (ch.7),

$$\log K_{Al} = \log [h_o]^3 [h_{Al}]^2 = -\frac{58473}{T} + 17.74 \qquad \ldots 9.15$$

or, $$\log h_o = \frac{1}{3}\left[-\frac{58473}{T} + 17.74 - 2 \log W_{Al}\right] \qquad \ldots 9.16$$

if it is assumed that $h_{Al} = W_{Al}$.

Combining Eqs.(9.14) and (9.16),

$$\log L_s = \log C_s + \frac{2}{3} \log W_{Al} + \frac{18555}{T} - 4.538 \ldots 9.17$$

An important issue is variation of L_s with temperature at a fixed slag composition.In addition to Eq.(9.17) we should also know how C_s varies with temperature. A simplified approach to this issue is to recognize that it is CaO in slag which is the predominant desulphurizer. For the reaction,

$$CaO(s) + \underline{S} = CaS(s) + \underline{O} \qquad \ldots 9.18$$

$$\log K_{CaS} = -\frac{5140}{T} + 1.191 \text{ (ref.12)} \qquad \ldots 9.19$$

This does not match with that reported by Zhang and Toguri (13). However Eq.(9.19) is being accepted since it is consistent with Fig.9.1.

Again, $$K_{CaS} = \frac{(a_{CaS})\ [h_O]}{(a_{CaO})\ [h_S]} \qquad \ldots 9.20$$

Proceeding similarly as in derivation of Eq.(9.10) we may write

$$m\ K_{CaS}\ (a_{CaO}) \;=\; (W_S)\ .\ \frac{[h_O]}{[h_S]} = C'_S \qquad \ldots 9.21$$

where m is a constant of proportionality.

Combining Eqs.(9.12), (9.19) and (9.21),

$$\log C_S = \log m + \log (a_{CaO}) - \frac{4204}{T} - 0.184 \qquad \ldots 9.22$$

In the limited temperature range of secondary steelmaking it seems good enough to assume a_{CaO} to be independent of temperature at a fixed slag composition. Therefore, if C_S is known at one temperature from a diagram such as Fig.9.2, it can be estimated at any other temperature. Further refinement on this can be made by invoking regular solution assumption for a_{CaO} .

For application of thermodynamics to predict slag-metal sulphur distribution under equilibrium, use of diagrams as in Fig.9.2 is somewhat inconvenient. Therefore attempts are being made to analytically represent C_S and L_S as function of slag composition. Tsao et al (14) carried out equilibrium measurements. With the help of their own data as well as those of others they have proposed the following correlation by data fitting through statistical regression analysis.

$$\log C_S = 3.44\ (X_{CaO} + 0.1\ X_{MgO} - 0.8\ X_{Al_2O_3} - X_{SiO_2}) - \frac{9894}{T} + 2.05 \qquad \ldots 9.23$$

This may be useful for prediction purposes within a factor of 2 to 3. Also it is not applicable to CaF_2-bearing slags. Gaye et al (15) employed the following correlation arrived at by Duffy et al (16) on the basis of **Optical Basicity Index.**

$$\log C'_S \;=\; B/D + 2.82 - \frac{13300}{T} \qquad \ldots 9.24$$

where $B = 5.62\ W_{CaO} + 4.15\ W_{MgO} - 1.15\ W_{SiO_2} + 1.46 W_{Al_2O_3}$

and $D = W_{CaO} + 1.39\ W_{MgO} + 1.87\ W_{SiO_2} + 1.65 W_{Al_2O_3}$

The conclusion drawn by them is that the domains of liquid slag compositions leading to high L_S are rather limited, and the efficiency of sulphur removal treatment will rely on the ability to reach these domains. The aimed compositions should be close to CaO-saturation.

They also recommend that, in using Eq.9.24, calcium present as CaF_2 should be subtracted in slag analysis.

9.1.4 Solved Examples

Example 9.1 : Fig.9.2 presents values of sulphur capacity for some slags at 1600°C. Compare these with predictions based on Eqs.(9.23) and (9.24) mole at fraction of CaO of 0.6 for CaO + SiO_2, CaO + Al_2O_3 systems.

Solution : Values of C_s as read off from Fig.9.2 are noted below. As for calculation from Eq.(9.23), $X_{CaO} = 0.6$ in all cases. $X_{SiO_2} = 0.4$ for CaO − SiO_2 slag, and $X_{Al_2O_3} = 0.4$ for CaO − Al_2O_3 slag.

In CaO − SiO_2 at 0.6 mole fraction CaO

$$W_{CaO} = 100 \times \frac{0.6 \times 56}{0.6 \times 56 + 0.4 \times 60} = 58.3$$

or, $W_{SiO_2} = 100 - 58.3 = 41.7$

In CaO − Al_2O_3 at 0.6 mole fraction CaO,

$$W_{CaO} = 100 \times \frac{0.6 \times 56}{0.6 \times 56 + 0.4 \times 102} = 45$$

or $W_{Al_2O_3} = 100 - 45 = 55$

Substituting these values in Eq.(9.24) allows calculation of C_s by noting that $C_s = C'_s / 7.5$.

	Values of C_s		
	Fig. 9.2	Eq. (9.23)	Eq. (9.24)
CaO − SiO_2	5.0×10^{-4}	2.85×10^{-3}	7.89×10^{-4}
CaO − Al_2O_3	2.7×10^{-3}	5.38×10^{-3}	1.99×10^{-3}

Hence Fig.9.2 and Eq.(9.23) are giving differing values. But Eq.(9.24) is matching reasonably with Fig.9.2.

Example 9.2 : At 1600°C and for CaO − Al_2O_3 slag of mole fraction of CaO equals to 0.6,

(a) Calculate desulphurization efficiency of slag (i.e. $[W_o]/[W_s]$ ratio),

(b) Compare the above with that of pure CaO,

(c) Calculate the value of L_s if liquid steel contains 0.01 wt.pct. Al, and compare with Fig.9.3.

(d) Calculate wt.pct. sulphur in metal.

Assume wt.pct. of sulphur in slag to be 1. Ignore interactions of other solute elements.

Solution :(a) From Eq.(9.13), and taking $h_o = W_o$ in metal phase,

$$\frac{[h_o]}{[W_s]} = \frac{[W_o]}{[W_s]} = \frac{C'_s}{(W_s)} \qquad \text{...Ex. 9.1}$$

Now, $(W_s) = 1$, and $C_s = 2.7 \times 10^{-3}$ (Fig.9.2).

From Eq.(9.12) at 1600°C, $C'_s = 7.5\ C_s$.

Putting in values,

$$\frac{[W_o]}{[W_s]} = 2.03 \times 10^{-2}$$

(b) From Fig.9.1, for CaO - CaS system at 1600°C,

$$\frac{[W_o]}{[W_s]} = 2.5 \times 10^{-2}$$

Therefore the slag with 1 pct. sulphur is as powerful a desulphurizer as pure CaO.

(c) Putting in values, i.e. $C_s = 2.7 \times 10^{-3}$,

$W_{Al} = 0.01$, and $T = 1873$ K in Eq.(9.17),

$\log L_s = 1.467$, i.e. $L_s = 29.2$

Fig.9.3 gives L_s approximately equal to 20 for 45 wt.pct. CaO and at 1650°C.

For comparison, L_s is to be estimated at 1650°C (1923 K) with the help of Eq.(9.17). But before that C_s is to be estimated at 1650 °C using Eq.(9.22).

From Eq.(9.22),

$$\log(C_s)_{1923K} - \log(C_s)_{1873K} = -4208\left(\frac{1}{1923} - \frac{1}{1873}\right) \qquad \text{...Ex. 9.2}$$

$$= 0.0585$$

$$\log(C_s)_{1923K} = \log(2.7 \times 10^{-3}) + 0.0585$$

$$= -2.510$$

Putting in values in Eq.(9.17),

$$\log(L_s)_{1923K} = -2.510 + \frac{2}{3}\log 0.01 + \frac{18555}{1923} - 4.538$$

$$= 1.2745$$

i.e. L_s at 1923K (1650°C) = 18.8

This matches closely with the value in Fig.9.3.

(d) $$L_s = \frac{(W_s)}{[W_s]} = 29.2 \text{ (from part c)}$$

Since $(W_s) = 1$, $[W_s] = \frac{1}{29.2} = 0.034$ pct.

This is not good. Hence operating conditions are to be altered (higher CaO in slag or higher Al in metal or lower temperature or combinations there of). This type of conclusion was arrived by Gaye et al (15) as mentioned before.

9.2 KINETIC ASPECTS

General aspects of kinetics and mass transfer have been briefly reviewed in chapter 4. A useful approach that has found application in dealing with rates of industrial processes is to treat the rate equation as that of **first order, irreversible** reaction. Coming specifically to transfer of a solute from liquid metal to slag, the rate of transfer (r_i) is given as :

$$r_i = k\,A\,C_i \qquad \ldots 9.25$$

where k is rate constant, A is slag-metal interface area, and C_i is instantaneous concentration of solute i per unit volume of liquid metal.

Again, from material balance,

$$r_i = -V_m \frac{dC_i}{dt} \qquad \ldots 9.26$$

where V_m is volume of liquid metal and t is time.

Combining Eqs.(9.25) and (9.26) and integrating,

$$[C_i]/[C_i^o] = \exp\left(-\frac{kA}{V_m}t\right) = \exp(-k a_s t) \qquad \ldots 9.27$$

where C_i^o is initial concentration and $a_s = \frac{A}{V_m}$ is specific interface area of metal phase. Sometimes it is more appropriate to replace C_i by $(C_i - C_e)$ in Eq.(9.25) (i.e. assuming rate equation to be **first order, reversible**). C_e is concentration of solute i in liquid metal at equilibrium with slag.

With the above modification, Eq.(9.27) is to be rewritten as :

$$[C_i - C_e]/[C_i^o - C_e] = \exp(-ka_s t) \quad \ldots 9.28$$

At low concentrations, $W_i \propto C_i$. With this in mind, Eq.(9.27) may be rewritten for sulphur as

$$[W_e]/[W_e^o] = \exp(-ka_s t) \quad \ldots 9.29$$

and Eq.(9.27) as

$$[W_e - W_s^*]/[W_e^o - W_e^*] = \exp(-ka_s t) \quad \ldots 9.30$$

It may be noted that Eq.(9.29) gives an idea of extent of sulphur removal from liquid steel whereas Eq.(9.30) gives an idea of approach of the system towards equilibrium with slag. According to Gaye et al (15), equation of the type of 9.29 is more appropriate for sulphur reaction.

A is not geometrical surface area, but is usually much larger than that due to slag-metal emulsification, surface waves etc. This causes uncertainty in ascertaining value of A also. Therefore experimental data typically yield values of either kA or ka_s parameter. Obviously larger is ka_s , faster is refining. At high temperature k mostly means mass transfer coefficient (k_m) since mass transfer is usually slower as compared to rates of interfacial reaction (15).

In slag-metal sulphur reaction in secondary steelmaking, there is always stirring by injected bubbles of argon. Mass transfer across gas stirred slag-metal interface has been a subject of investigation of last 30 years in connection with various steelmaking processes. Several cold model, hot model and theoretical studies have been made in connection with ladle metallurgy as well. Kim et al (17) have reviewed it. Broadly speaking, kA is proportional to Q^n, where Q is volumetric flow rate of gas and n is the exponent. One may write it also as $\dot{\varepsilon}^n$, where $\dot{\varepsilon}$ is the rate of energy dissipation (see chs. 3 and 5).

Both desulphurization in plant scale ladle as well as water model studies show that the exponent n exhibits abrupt changes depending upon value of Q. This is demonstrated by Fig. 9.4, which shows 3 regimes. In the 1st regime (at lowest Q), the oil layer simulating slag was found to be calm. Regime II (middle one) was found to start when the oil layer near the edge of the plume eye continuously formed ligaments and disintegrated into droplets. In regime III, the entire oil layer was in droplet form dispersed in water. Authors also formulated dimensionless numbers and established criteria for change over from one regime to another.

Gaye et al (15) have advocated use of the following mass transfer correlation for slag-metal sulphur reaction in ladle metallurgy.

$$k_m = C\,(D_s \cdot Q/A)^{1/2} \qquad \ldots 9.31$$

where the constant C has been evaluated as 500 $m^{-1/2}$ from plant data. Eq.(9.31) is in accordance with Danckwerts' surface renewal theory of mass transfer. However it is not known whether the exponent 1/2 is obeyed only in a limited range of Q or not. D_s is diffusion coefficient of sulphur in liquid steel.

Several studies have been carried out on reaction and reactor kinetics in connection with injection metallurgy. Since it is the subject matter of chapter 10, not much discussion is intended except to note a few points briefly.

(i) When CaO powder is injected into the melt, it tends to form an impervious layer of CaS on it and further reaction is slowed down. Therefore injection of synthetic slag powder is preferable since it melts when it comes into contact with liquid steel.

(ii) Calcium silicide (Ca-Si) is employed to add calcium metal into the melt. Metallic Ca boils at 1491 °C under 1 bar pressure. Its vapour pressure as function of temperature is given as (18).

$$\log p^{o}_{Ca}\ \text{(in bar)} = 4.55 - 8.03 \times 10^{3}/T \qquad \ldots 9.32$$

Value of p^{o}_{Ca} at 1600 °C turns out to be 1.83 bar. This is quite high and is likely to lead to instant, violent vapour formation.

Mellberg et al (19) have discussed it. If Ca is alloyed with Si, then

$$p_{Ca} = p^{o}_{Ca} \times a_{Ca} \qquad \ldots 9.33$$

where a_{Ca} is activity of calcium in Ca-Si. Fig.9.5 presents Ca activity as function of mole fraction of Ca in Ca-Si alloys at 1600 °C. It may be noted that thermodynamic value p_{Ca} over the alloy as per Eq.(9.33) is lower by a factor of few thus bringing it much below atmospheric pressure. This allows time for calcium to dissolve in liquid steel and participate in reaction to a significant extent.

However solubility of calcium in liquid iron is very low (0.025 ± 0.008 wt.pct. according to ref.19). Therefore silicon is expected to dissolve into the melt much faster than calcium. So, shortly after injection, the liquid Ca-Si alloy would get depleted in silicon. Consequently its vapour pressure goes up leading to instant vaporization of residual calcium. This is the explanation of some loss of calcium.

REFERENCES

1. C.W. Sherman, H. Elvander and J. Chipman, Trans. AIME, 188 (1950), 340.
2. G.K. Sigworth and J.F. Elliott, Metal Science, 8 (1974), 298.
3. A. Vahed and D.A.R. Kay, Met. Trans. B, 7B (1976), 375.
4. J.F. Elliott, M. Gleiser and V. Ramakrishna, **Thermochemistry for Steelmaking**, Vols.1 and 2, Addison-Wesley Publishing Corp, Reading, Mass, USA, 1963.
5. O. Kubaschewski, E. Ll.Evans and C.B. Alcock, **Metallurgical Thermochemistry** (4th Ed), Pergamon Press, New York, 1967.
6. E.T. Turkdogan, **Physical Chemistry of High Temperature Technology**, Academic Press, New York, 1980, p.388.
7. G. Carlsson, in Proc. Int.Sym. on Modern Developments in Steelmaking, ed. A. Chatterjee and B.N. Singh, Jamshedpur, 1981, p.643.
8. L.E.K. Holappa, Int.Met.Reviews, 27 (1982), 53.
9. F.D. Richardson, **Physical Chemistry of Melts in Metallurgy**, Vol.2, Acad Press, London, 1974.
10. Verein Deutscher Eisenhuttenleute, **Slag Atlas**, Verlag Stahleisen mBH, Dusseldorf, 1981.
11. R.J. Fruehan, **Ladle Metallurgy Principles and Practices**, Iron & Steel Soc., USA, 1985, ch.2.
12. G. Carlsson, Y.Y. Dong and D. Jorgensen, Scand J. Met., 16 (1987), 50.
13. X.F. Zhang and J.M. Toguri, Canad Met. Qtly, 26 (1987), 117.
14. T. Tsao and H.G. Katayama, Trans. ISIJ, 26 (1986), 717.
15. H. Gaye, P.V. Riboud and J. Welfringer, Proceedings PTD, 5th Int. Iron & Steel Cong., Vol.6, Washington DC, 1986, p.631.
16. J.A. Duffy, M.D. Ingram and I.D. Sommerville, Trans. Faraday Soc. I 74 (1978), p.1410.
17. S.H. Kim, R.J. Fruehan and R.I.L. Guthrie, Steelmaking Proc., Iron & Steel Soc., USA (1987), 107.
18. E. Schurmann and R. Schmid, Arch. Eisenh (1975), 773.
19. P.O. Mellberg and S. Gustafsson, Proc. Symp on Injection Met.,Shanghai, 1982.

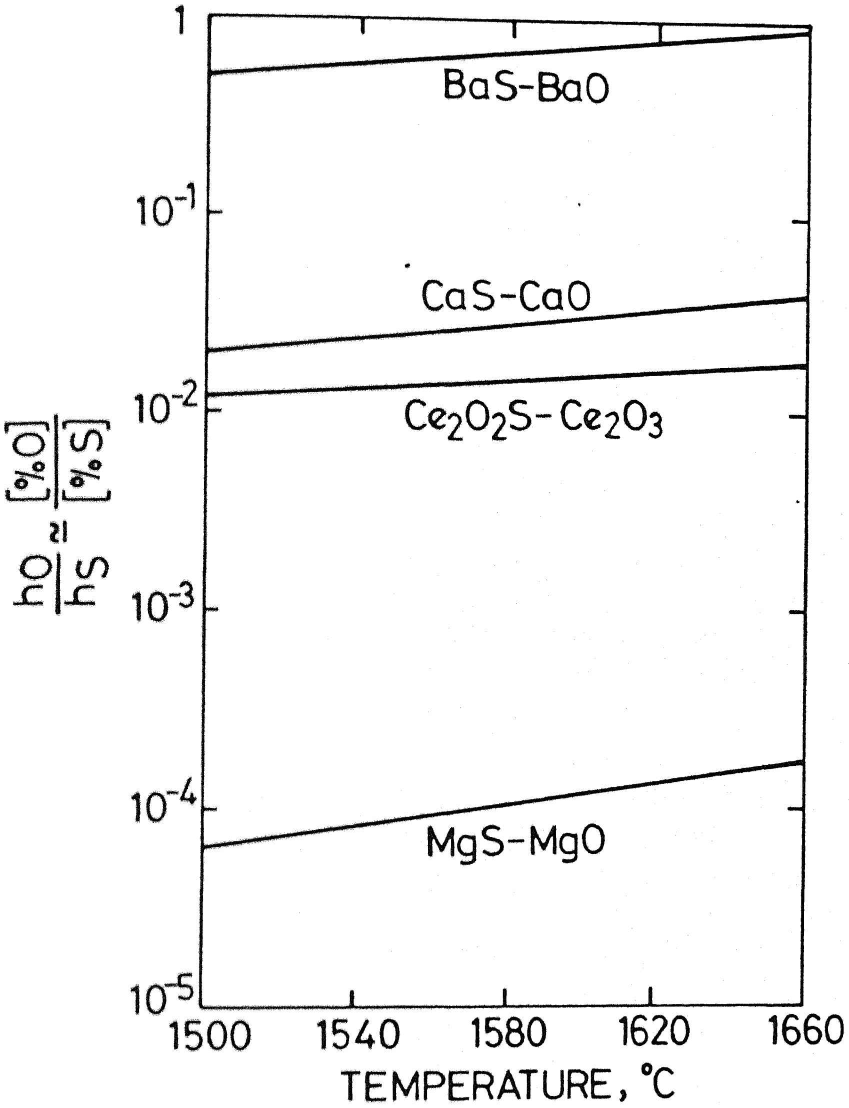

Fig. 9.1 : Oxygen/sulphur activity ratio in liquid iron for the indicated sulphide - oxide equilibrium at 1600°C

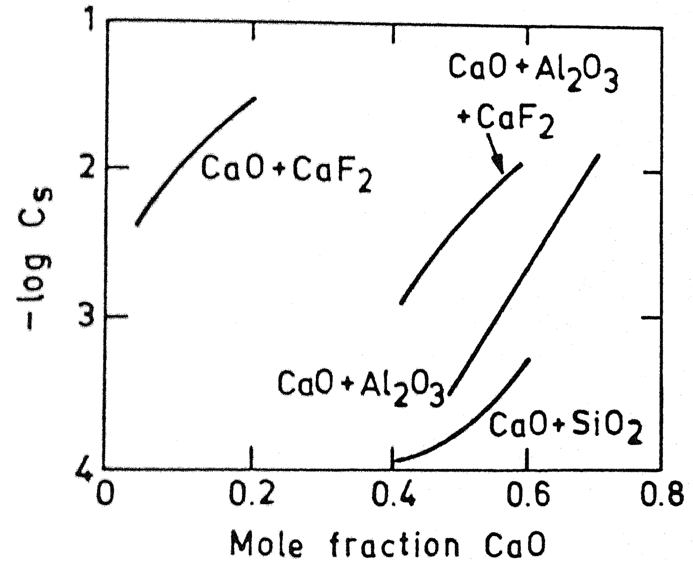

Fig. 9.2 : Sulphide capacities of selected slags at 1600°C[17]

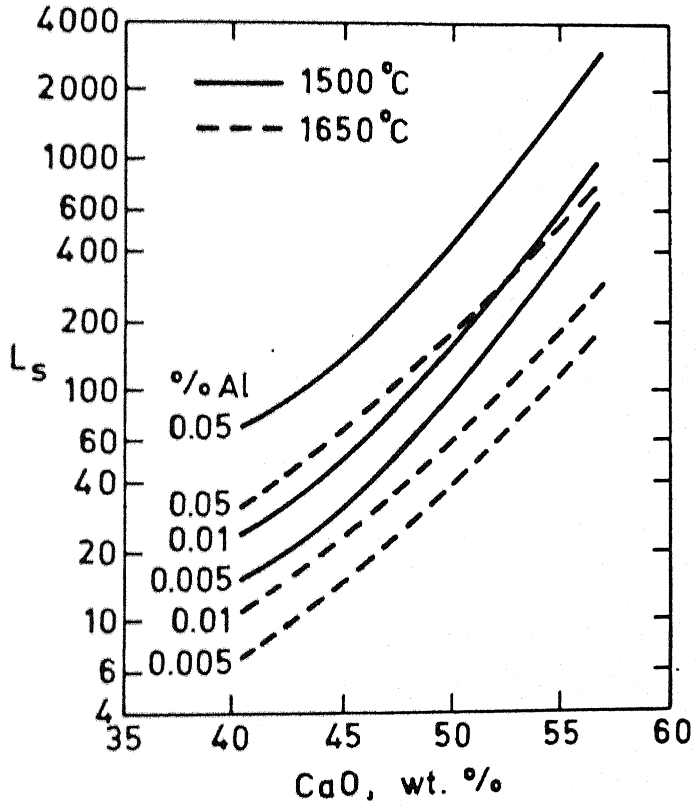

Fig. 9.3 : Sulphur partition ratio between slag and metal for Fe - Al alloys in equilibrium with $CaO - Al_2O_3$ slags (E.T. Turkdogan, Arch. Eisenwuttenwesen, 54 (1983), 1)

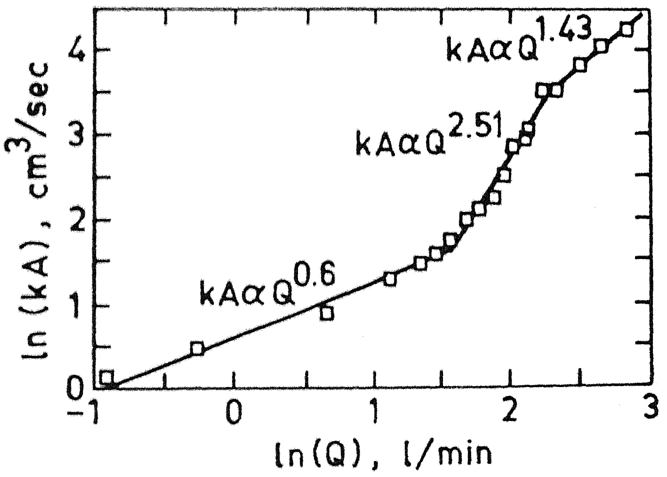

Fig. 9.4 : kA vs. gas flow rate for mass transfer between two liquids in vessel stirred by axisymmetric gas injection from bottom

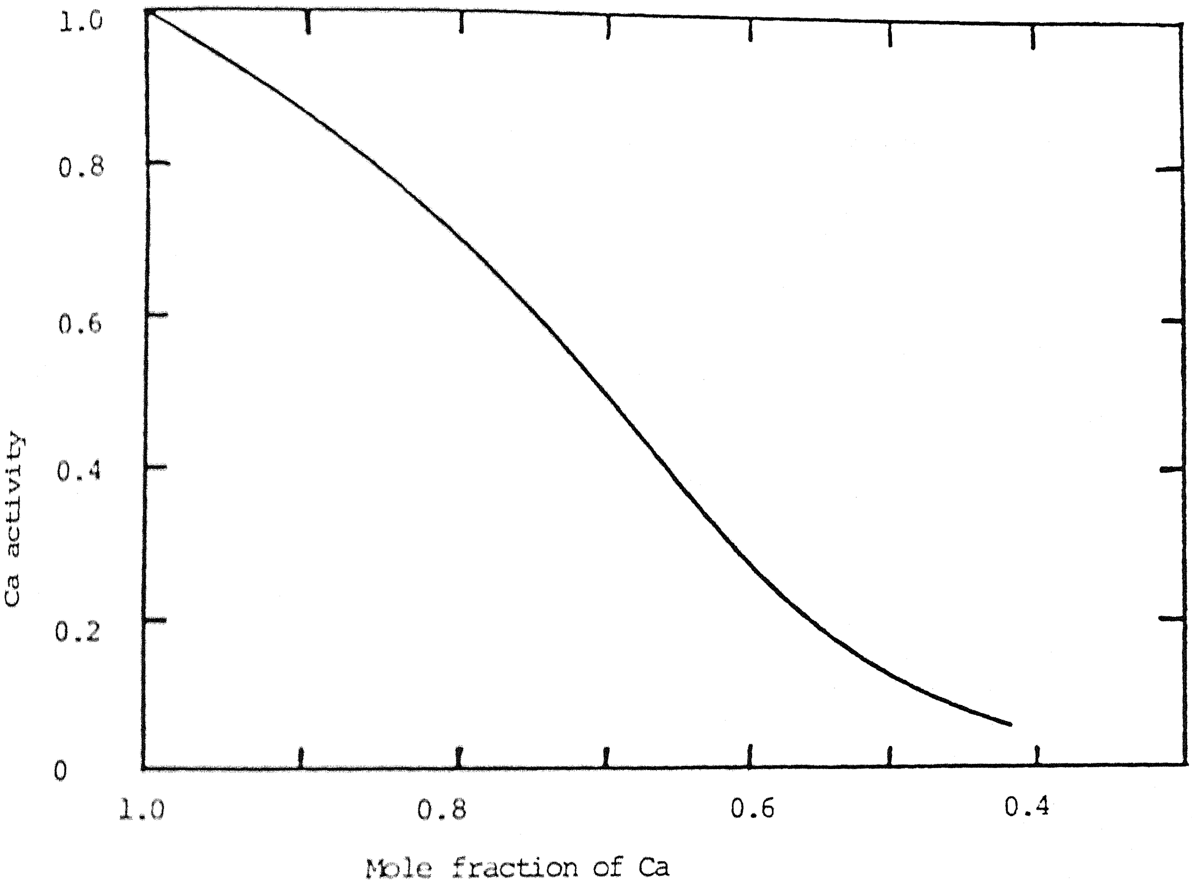

Fig. 9.5 : Estimated Ca - activity at 1600°C in Ca - Si alloys

CHAPTER 10

INJECTION METALLURGY

S.C. KORIA

10.1 INTRODUCTION

The growing demand for steels with improved mechanical propertie for various applications has placed a major task before steelmakers t search new ways and means to produce steels with extra low level c basic impurities (i.e. carbon, sulphur, phosphorous, oxygen, hydroge and nitrogen) and with low amount of inclusions (oxide, sulphide etc. consistently and economically in existing steelmaking reactors. I this context, injection metallurgy, including powder injection and ga injection and the various supporting technologies such as systems t cut off slag flow into teeming vessels, suck top slag off out of ladl and system to compensate heat loss of the melt in the ladle has foun growing acceptance since it calls for less expensive investment, hanc operation and quicker processing at reasonable reaction efficiency fc a wider span of heat size. The application of these techniques eithe singly or in combination in the metallurgical reactors has mac possible to achieve any level of basic impurities insteel. It i claimed that a total basic impurity level of less than 70 ppm can b achieved with the following specification of each element :

$$C \le 20,\ O \le 10,\ H \le 0.7,\ N \le 15,\ S \le 5 \text{ and } p \le 15 \text{ ppm}$$

Application of injection has so far been to 3 sectors refining, i.e., hot metal pretreatment, converter blowing of hot met and ladle processing of resulting steel. The application has been do with powder injection and/or gas injection in combination with some the supporting technologies for better control of refining towar extra low impurity concentrations.

Fig. 10.1 illustrates the process routes for some grades of ste utilizing the different injection metallurgy techniques. In t Fig.10.2 the various techniques of injection metallurgy a illustrated.

In this chapter main emphasis has been given to the gas injecti and gas/solid powder injection. Other supporting technologies for t growth of injection metallurgy are briefly touched upon.

10.2 GAS INJECTION

10.2.1 Purpose

Inert gases like nitrogen and argon are injected into steel me in order to generate the flow field in the bath which is conducive

(a) for bath homogenization w.r.t. concentration a temperature

(b) to enhance the rate of slag/metal reaction such as deS for synthetic slag treatment
(c) for removal of non-metallic inclusions
(d) to enhance the rates of dissolution of metal and ferro-alloys additives with improved alloy yield and composition control within narrow limits
(e) for hydrogen and nitrogen removal.

10.2.2 Gas Injectors and Locations

Fig.10.3 shows the various injectors used for gas injection purposes. There are linear injectors where channels are either drilled into the bricks or this pipe set in the refractory. Note particularly the similar concept of the double tuyere on the left and the multiple hole brick on the right where two separated flow circuits have been implemented.

There are canned bricks on the porous bricks and the so called permeable elements where the gas flow section has been considerably increased by sandwiching the refractory bricks. Recently spiral type of tuyeres are also advocated to be used (3).

The gas injector are located either at the base of the vessel centrally or non-centrally or top of the vessel submerged in the bath or side of the vessel. Porous plugs are normally placed at the bottom of the vessel. Straight type of tuyeres could be placed at top and bottom.

It is important to note that the gas injectors of any type are submerged into the bath so that the gas jet enters directly into the bath.

10.2.3 Phenomena of Gas Discharge into Liquids

Two different flow phenomena are observed in front of the tuyere when a gas is discharged into a liquid body : at low flow rates, the gas is dispersed into discrete bubbles indicated by periodic pressure oscillations in the supply pipe. The frequency of the pulses is within a range of 8 to 25 per second, depending on the specific gas/liquid system. When the gas flow rate exceeds a characteristic limit, the gas leaving the orifice becomes a continuous flow. The gas bubbles are released from an elongated free space formed in front of the tuyere. In this case pressure fluctuations are irregular and only of small amplitude. Accordingly, two different flow regimes are of concern : **bubble flow at low and jetting flow at high discharge rates.**

The bubbling-jetting transition of gas jets into liquid was analysed by the present author using the theory of the compressible fluid flow. For one dimensional steady flow of gas the dynamics of the mass flow rate is given by (4-6).

$$\frac{\dot{m}}{A} = \rho v = \text{constant throughout the flow} \qquad \ldots 10.1$$

intense as can be seen in Figs. 10.5 and 10.6, the stirring action is small near the bottom of the ladle and intense at the top surface of the melt. An asymmetrically placed bubble plume gives velocities near the bottom which might be of an order of magnitude greater than for a symmetrically placed plume.

In an experimental work the liquid velocity induced by gas injection has been studied by the technique of dissolution (9-12). The liquid velocity ratio i.e. velocity at bottom (u_b)/velocity at the surface (u_s) was found to depend upon the location of the gas injecting lance i.e. top or bottom and whether they are placed symmetrical or asymmetrical to the bath (9-12).

The following results were obtained : For bottom injection

$$\frac{U_b}{U_s} = [\exp(0.744 (\frac{r_n}{R}) - 0.833)]^{1.4286} \qquad ...10.4$$

For top injection

$$\frac{U_b}{U_s} = [\exp(0.676 (\frac{r_n}{R}) - 0.8496)]^{1.4286} \qquad ...10.5$$

r_n is the radial location of the nozzle and R is bath radius, i.e. $r_n/R = 0$ for central location of lance. Putting $r_n/R = 0$ in eqs. 9.4 and 9.5 we get $(U_b/U_s)_{Bottom} = 0.305$ and $(U_b/U_e^n)_{Top} = 0.297$. It is explicit in the equations that off-centre injection increases the U_b/U_s for top and bottom injection.

A stirring pattern of the type in Fig.10.5(a) may be useful for slag/metal reaction e.g. des by synthetic slag where higher velocity at the interface between slag and metal is required. Whereas a stirring pattern of the type in Figs.9.5b and 9.5c may be useful to enhance the dissolution rates of the dense additives which settle at the bottom.

Correct stirring is of the utmost importance. It should be known when to stir what and how vigorously, for the adequate promotion of transfer rates, and when just to move the melt slowly for homogeneisation.

There are metallurgical reactions which require strong mixing of metal and slag (e.g., deS and deP), whereas other require gentle mixing at the metal/slag interface and maintenance of an unbroken slag layer (e.g. deoxidation and inclusion removal) (13). Vigorous mixing of metal and slag is achieved by gas stirring, less disturbance at the metal/slag interface can be obtained with RH.DH and induction stirring. The demand for gently stirring would be necessary when slag carryover can not be controlled : any turbulent flow in the neighborhood of the slag/metal phase boundary activates interfacial mass transfer, leading to the reduction of slag by deoxidizing elements, phosphrous reversions and oxygen and nitrogen pick up from the atmosphere.

In the reference (8) the following specific gas injection rates are given :

Stirring	< 5 N l min^{-1}t^{-1}
Lime steel deS	14 N l min^{-1}t^{-1}
VAD deS	< 2 N l min^{-1}t^{-1}

10.2.5 Gas Induced Stirring Power

The stirring power is expressed in terms of ''Watts". (1 Watt = 1 joule/ s = kg m^2/s^3).

The stirring power induced by gas injection into the steel bath at the height H given by : P = Power through expansion at unaltered pressure (p) (This is due to the heating of the gas from T_o to some temperature (T_L) + power through isothermal expansion (pv^8 (This is due to the rise of the gas bubbles, and during their rise the ferrostatic pressure decrease which causes the bubbles to expand).

By evaluating both the contribution one arrives at the following expression :

$$p = 371 \; Q \; T_L \; [(1 - \frac{T_o}{T_L}) + \ln \frac{p_1}{p_2}] \qquad ...10.6$$

In the expression Q is in Nm^3/sec. T_L in k. and $p_1 = p_2 + \rho_L \, g \, H$. ρ_L = density of liquid, H = height of bath and p_2 is atmospheric pressure.

For H = 3 m, p_2 = 101.3 k p_a and $T_o = T_L$ = 1873K (e.g.), we get p = 411.7 Q T_L. By decreasing the pressure (i.e. p_2) above the melt surface as is done in VAD or VOD treatment, the mixing power increases. For p_2 = 79.9 kpa ; p = 472.7 Q T_L and for p_2 = 13.3 k pa, p = 1039.05 QT_L. A decrease in the atmospheric pressure to 0.13 p_2 an increase in power is 2.5 times that at atmospheric pressure.

This calculation illustrates clearly the effectiveness of vacuum as a technique in the injection metallurgy.

10.2.6 Recirculation Rate in Gas Stirred Ladles

The mass flux M (in ton/sec) of entrained steel passing through the top section of the bubble plume is given by the following semi-empirical equation :

$$M = 13.3 \; (H + 0.8) \; [\ln (1 + \frac{H}{1.48})]^{0.5} \; Q^{0.381} \qquad ...10.7$$

With water model experiments, the relationship

$$\dot{M} = 10.65\ (H + 1.46)^{1.127} \times [\ln (1 + \frac{H}{1.46})]^{1.127}\ Q_{l}^{0.549} \qquad \ldots 10.8$$

In the Eq. 10.8 Q_l is in $m^3 sec^{-1}$ at temperature T and the pressure p of the nozzle exit.

With H = 2.5 m, Q = 600 NL min^{-1} and Q_l = 1496.8 (l min^{-1}) one obtains $\dot{M}$ = 7.5 ton/sec and 6.6 ton/sec. The recirculation time of a 185 ton melt is then about 25s; for a 60 ton melt, it is about 50-20s, when the gas flow rate increases from 20 to 200 NL min^{-1}.

10.3 GAS/SOLID POWDER INJECTION TECHNOLOGY OR INJECTION LADLE METALLURGY

10.3.1 Overview

In recent years the pneumatic injection of powders into iron and steel has become a very successful way to accomplish deS, deSi, deP, modification of oxide inclusions and provide sulphide shape control. The major advantages of powder injection are :

1. the interfacial area of the injected particles in contact with the melt is much greater than a top slag and therefore reactions by injection are faster.
2. the carrier gas generally keeps the ladles well mixed; precisely controlled.
3. the rate and total quantity of reagent can be precisely controlled.
4. a wide variety of powders can be injected so that (i) sequential operations of refining or alloying can be accomplished during a heat or (ii) reagents can be substituted to take advantage of new reagents or changes in relative price of reagents.
5. the atmosphere can be controlled, for example, to eliminate oxygen, which allows powerful desulphurisers such as Mg, Ca and CaC_2 to be used; and finally.
6. injection stations and the associated equipments are not excessively expensive.

10.3.2 Concept of Permanent and Transitory Contact Modes

For reactions occuring between two immiscible phases, the two different models are (14):

(i) Permanent contact (ii) Transitoric contact.

In the permanent mode of contact the slag phase is permanently in contact with the liquid phase during the entire period of treatment. The efficiency of extraction of an impurity by this mode would depend upon the partition coefficient of the impurity, amount of slag/ton of steel, slag basicity and composition, interfacial area, time of contact and the mixing condition. A kinetic expression can be obtained which incorporates the effects of all the above mentioned parameters (14):

$$(W_x)_p = \frac{[X]_o}{[X]} = \frac{1 + \eta^* Y}{1 + \eta^* Y \exp\left[- \frac{1 + \eta^* Y}{\eta^* Y}\right] . \frac{\beta.F.t}{v}} \qquad ...10.9$$

where, $[X]_o$ = initial concentration of the impurity in the metal, η^* = equilibrium value of the partition coefficient, Y = amount of slag/ton of steel, β = mass transfer coefficient, F = interfacial area, t = time of contact, v is volume of melt.

The maximum efficiency of the permanent contact reactor is obtained by 10.9. For $\beta.F.t/v \longrightarrow \propto$ i.e. $t = t_{equilibrium}$ we get.

$$[W^*]_p = 1 + \eta^* Y \qquad ...10.10$$

when $\eta^* Y$ is very large i.e. when the slag capacity is very large,

$$[W^*_x]_p = \exp\left[\frac{\beta.F.t}{v}\right] \qquad ...10.11$$

In transitoric mode of contact, the phases after contact during the rising of the mixture no longer react. The slag phase may or may not be removed from the system. The following kinetic expression can be obtained(14).

$$(W_x)_T = \exp\left(\frac{\eta^* Y}{\eta^* Y + \beta \frac{A}{v} . t} . \beta \frac{A}{v} . t\right) \qquad ...10.12$$

The maximum efficiency of the transitory mode of contact is given by.

$$[W^*_x]_T = e^{\eta^* Y} \qquad ...10.13$$

Dividing Eqs. 5 and 6 we get.

$$\frac{[W^*_x]_T}{[W^*_x]_p} = \frac{e^{\eta^* Y}}{1 + \eta^* Y} \qquad ...10.14$$

The above equation shows that for any value of $\eta^* Y$, the transitoric mode of contact is more effective. This is explained by the fact that the used (ssaturated) slag in the case of transitoric contact is leaving the system. The efficiency of transitoric contact mode is illustrated in the following:

Consider desulphurization of hot metal (C = 3.3%, S = 0.08% and Si = 1.3%) by injection of CaC_2 powder. The melt temperature is 1427°C (15):

The deS reaction is

$$CaC_2 + [S] = CaS + 2[C] \qquad ...10.15$$

$$\ln K = \frac{43100.5}{T} - 13.3 \qquad ...10.16$$

By assuming a_{CaC_2} & $a_{CaS} = 1$, we may write.

$$[wt\ \%\ S] = \frac{[f_c \times wt\ \%\ C]^2}{f_s\ .\ K} \qquad ...10.17$$

$$\text{Log } f_c = e_c^C\ [wt\ \%\ C] + e_c^S\ [wt\ \%\ S] + e_c^{Si}\ [wt\ \%\ Si]$$

$$= 0.14 \times 3.3 + 0.046 \times 0.082 + 0.08 \times 1.3 \qquad ...10.18$$

$$f_c = 3.71 \qquad ...10.19$$

$$f_s = 2.74 \qquad ...10.20$$

$$[wt\ \%\ S] = \frac{3.71^2 \times 3.3^2}{2.74 \times 171653.86}$$

$$= 3.186 \text{ ppm.}$$

This is the value of S attainable in metal by transitoric mode of contact under equilibrium conditions.

Eq^m permanent reaction is

$$[S] + (O^{2-}) = (S^{2-}) + [O] \qquad ...10.21$$

$$K = \frac{(wt\ \%\ S) \times r_{S^{2-}} \times [a_o]}{[wt\ \%\ S] \times f_s \times a_{O^{2-}}} \qquad ...10.21$$

It is known that $r_{S^{2-}}$ is practically independent of sulphur concentration in slag and $a_{O^{2-}}$ is a function of slag basicity. For a top slag of a given composition (hance basicity)

$$[wt\ \%\ S] = \frac{K'\ [a_o] \times (wt\ \%\ S \text{ soluble in slag})}{f_s} \qquad ...10.22$$

where K' is equilibrium quotient $= \dfrac{r_{S^{2-}}}{K\ a_{O^{2-}}}$

The value of K' has to be determined. In anexpt with 80% CaC_2 + 20% $CaCO_3$ powder injection, the resulting slag after deS was CaO = 53.4%, SiO_2 = 18% , Al_2O_3 = 6.8% , FeO = 13% and MgO = 4.9% , (S) = 4% . The value of K' was found to be 80. Putting K' = 80 in the above expression we get.

$$[wt\ \%\ S] = 29.62\ [a_o] \times (wt\ \%\ S)_{\text{soluble in slag}}$$

For $(\text{wt \% S}) = 4.5$ and $[a\ ] = 1 \times 10^{-4}$ we get $[\text{wt \% S}] = 0.0133\%$ at equilibrium. Further decrease in $[a_o]$ is better for deS.

In the actual experiments, the sulphur content of the hot metal after deS was nearing close to the value calculated by equilibrium permanent contact (15).

Despite, the fact remains that the transitoric mode of contact is an efficient mode to produce steels with lower impurities. In the transitoric mode of contact, the slag droplets or injection of solid powder take part in the reaction directly. The transitory reaction provides the initial driving force towards reaching the quilibrium for permanent reaction.

10.3.3 Problems

The main disadvantage of powder injection is that the residence time of the particles is quite short (a few seconds); thus the reagent efficiencies are often very poor. The trajectories of the particles are of fundamental importance to these processes. For reagents such as lime and calcium carbide, the particles must be in contact with melt for reaction to occur. In contrast to this, Mg and Ca vaporize when injected into iron and steel. Other alloying elements such as Al, C, Si, Ca, Mg, B, Se, Ti havedensities lower than liquid steel whereas others such as Ce, Mo, Pb, W, Zr, Cr, Co are heavier than liquid steel. Elements with extremely low or high densities as well as strong oxygen affinity are difficult to introduce into the bath.

During the injection of alloys there is a temperature drop at the lance tip due to the expansion of the gas and heat transfer to the alloy. This might lead to the formation of deposits at the lance tip for elements with a high enthalpy and heat conductivity. The deposits occur often during injection of Mg or Ca. The deposits lead to a constriction of the feed lance and sometimes to complete blocking. The growth of deposits may be avoided by constructional changes in the lance and the choice of suitable process parameters. Injection of C does not give such problems.

10.3.4 Materials for Reactions and Alloying by Injection with Carrier Gas

The main purpose of particle injection is the feeding of a fine grained material deep into the molten steel.

The optimum powder size is determined as a compromise between fine powders (creating theoretically large interfaces, but may choke the nozzle or remain entrapped within the bubble or being carried away by the dust collecting system) and course powder (creating small reaction surfaces, but having a greater chance to leave the gaseous envelop and to react with the steel bath, but with shorter reaction times due to greater buoyancy. Nominal particle sizes less than 2 mm, usually 0.1 to 0.5 mm are recommended. The powders can be mechanically mixed, or premelted and granulated.

All alloys, slags, etc. can be injected. Some examples (16):

Desulphurization :

CaO, $CaO + Al$, $CaO + CaF_2 + Al$, $CaC_2 + CaCO_3 + CaC_2 + CaO$, $CaSi$, CaC_2, $Mg + CaO$, Miochmetal.

Deoxidation:

CaSi, CaSi Ba, Ca Si Mn.

Sulphide modification:

Ca Si, Ca Zr

Dephorphorisation:

$CaO + CaF_2 + Fe_2O_3$

Nitrogen removal:

Fe Zr, Si Zr

Alloying purposes:

Si	from FeSi75
N	from $CaCN_2$
C	from graphite powder
Ni	from Ni-oxide
M_o	from M_o - oxide, and so on.

The more sophisticated injection of powder under the steel bath surface has a number of advantages, e.g. CaSi- injection results in

(a) Change from two slag practice to single slag practice in EAF
(b) Posssibility to buy scrap and pI with higher S contents
(c) Possibility to produce low S steel
(d) Avoiding of Al cluster problem in the nozzle for Al- treated steels.

Working with powder of reactive materials requires special precautions because of risks for dust explosions. The tendency of powder material to explode is connected with the following factors :

(a) Particle size (b) Particle structure (c) The quantity of particles in the air (d) Its reactivity to oxygen (e) The humidity of the material by side reactions (f) Content of non combustible material (g) Required energy to ignite a dustair mixture of the material.

10.3.5 Equipment of Injection

Figure 10.7 shows the different types of dispensers (16).

For injection under the metal surface consumable or fireclad lances or tuyeres can be used.

The pusher dispenser is the simplest one in design. The pusher operates best with flowable powders, those powders having the property of self feeding. The pusher dispenser will not operate properly with powders contg. more than 15% of a -200 mesh fraction.

In the fluidizer dispenser, a wide range of powders at high powder to gas ratios can be transported. It is possible also to use for non flowable powders with a big tolerance concerning grain size. The shape of the powder particles does not affect the flowability to any great extent.

The vibratory dispenser has its best use for applications requiring low and close control of powder flow rate.

A typical application is the injection of Mg powder into iron in uncovered ladle where a high and non-uniform Mg -flow rate can cause violent explosionlike reactions. Vibratory dispensers can transport flowable and to a considerable extent nonflowable powders and operate at low powder to gas ratios.

The friction by the particles in the equipment sometimes causes problems particularly when they are needle shaped materials with high quartsite content. This problem can be solved by using powder <0.1 mm. In generall the friction problem and the wear can be solved by chosing suitable particle sizes, and optimal gas speed which should be above a certain minimum level.

10.3.6 Powder Conveying Modes

Gas-solids powder transfer systems are generally designed as either Dilute OR Dense phase conveying modes.

Dilute phase systems are normally low pressure and characteristically handle low solids loadings having high gas velocities. These systems have comparatively lower pressure losses per unit length of conveying line in comparison to the dense phase design.

Dense phase systems operate with higher pressure losses and with high solids loadings. Due to such high loadings, such systems are operated at low velocities to minimize solids degradation and line erosion. Less gas is needed to transport a given mass of solid in dense phase conveying.

The dense phase systems do not provide truly continuous conveying. There are two reasons for this; firstly, plugs of material interspersed with slugs of air. Secondly, the conveying is often operated as a batch process. The second problem can be avoided if two hoppers are used in parallel. At any one time, one hopper can feed the material into the pipeline and the other can be refilled. The problem of intermittant flow could be circumvented by discharging the pipeline to a storage vessel and then using, say, a rotary value at the vessel bottom to feed material continuously to the process.

The physical properties of the powder such as density, vapour pressure, m.p.t. etc. would decide the type of conveying modes. For example, Ca,Mg being lighter than liquid steel and also their b.p.t. is lower than steel melt temperature, they must be injected at high velocities into the bath i.e. in dilute conveying mode. Similarly various fluxes for deS can be injected.

Fig.10.8 shows the pneumatic conveying regimes for horizontal and vertical flow of powders.

10.3.7 Interaction Between Powder Jet and Liquid

When the gas carrying the solid particles enters the liquid, the particles proceed in almost a straight line at constant velocity within the cone angle of the particle jet, while the gas loses its velocity. The jet velocity decay is at first governed by the liquid entrainment : inertia causes the velocity to decrease rapidly. A low momentum jet is quickly dissipated by the buoyancy force and spreads readily and lightly leden jets penetrate less deeply than heavily laden jets. The gas jet breaks up into a could of bubbles that rise through the liquid owing to vuoyancy, and, as this happens, particles trapped in the bubble hit the gas/liquid interface.

Fig. 10.9 shows the uncoupled and coupled flow (17). For uncoupled flow, the gas and particles separate at the lance tip on contact with the liquid, the gas rising as bubbles. For coupled flow, gas and particles move together for some distance into the liquid. As the jet velocity decays, the coupling force decreases, and the gas then separates from the particles, spreads away from jet axis and particles, and leaves the jet.

If the liquid wets the solid particles completely, the particles are immersed in the liquid spontaneously and without creating a surface depression at the interface. The stripped particles travel two to three times as for as the gas jet and could hit the bottom of the ladle with vertical injection and deeply immersed injection lances.

Fig. 10.10 shows the different possible regimes in injection of gas and gas/powder mixtures into the liquid (17). In this figure, the amount of liquid entrained in the downward portion of the jet trajectory is small, so that there is little chance for liquid-particle reaction. On the other hand, there is ample opportunity for solid/gas reaction at progressively higher temperatures along the jet axis. Solid/gas jet configuration is harful for mixtures which react exothermically with each other such as pulverised coal-air mixtures because of potential lance damage. However, endothermic materials such as CaC_2 - $CaCO_3$ for hot metal deS are well suited to this regime.

This configuration (Fig.10.10) is also very good for materials which react exothermically with the liquid such as iron oxide material for hot metal deSi because the reaction zone is far from the lance tip.

Some materials for injection are coarse; for example Mg and CaSi are too dangerous to handle as fine powders. These particles require larger gas velocities than fine particles for pneumatic conveying. On the other hand, particles which are easily wetted by the liquid, such as ferro-alloys or specially coated reagents, may cross the gas/iron interface so that either a particle liquid jet or particles settling as individual will prevail. In both the cases there is an intimate contact of liquids with solid and gas phase reaction is suppressed in favour of liquid phase reactions. Unfortunately the particles contact close to the lance with the possibility of damage due to exothermic reactions.

Granules that vaporize explosively such as Mg in iron or Ca in steel can also damage the lance. Lance clogging can be eliminated by either mixing the grtanules with fine powders to make a jet as in the time-may process or by moving to higher flow rates where choked flow can be obtained.

10.3.8 Typical Injection Practice Sequence (18)

The sequency is for a steel contg. 0.02 - 0.03% S in BOF or EF with a final aim of S less than 0.005% S

1. Some type of slag retention should be used.
2. Steel must be aluminium killed with an aims of 0.03 to 0.05 pct. Al in the ladle. Oxygen sensor measurements are useful.
3. Synthetic top slag should be added prior or during tap. For example 10 kg CaO or 2 kg CaF_2/ton of cteel can be used.
4. Measure slag corryover at this point. For excessive amount of slag, additional aluminium should be added to reduce the slag or increase CaS; should be injected.
5. CaSi is injected. 56 kg/min using 0.42 m^3/min to 0.57m^3/min Argon. Typically about 2.72 kg/ton is injected. Therefore for a 200 ton heat, around 544 kg CaSi is required in 8-10 minutes.
6. After injection a gentle argon stir at 0.14 m^3 min^{-1} for around 2 min will help float out inclusions.
7. Trim additions of Al and Mn may be needed at this point. An oxygen sensor may be used to estimate Al.

Variations

(a) flux may be injected instead CaSi
(b) CaO may be injected before CaSi to produce a stiff top slag if a ladle cover is not used
(c) smaller amount of CaSi can be used if only oxide modification for casting purpose is desired.

10.3.9 Conclusions

Injection ladle metallurgy technique is extremely effective for deS, oxide shape control and sulphide shape control. However, it is necessary to avoid steelmaking slag carryover and excessive splashing caused by high argon flow rates. The processes causes usually an increase in hydrogen and nitrogen contents and it may be difficult to control the aluminium content. The biggest disadvantage may be the temperature loss ogf about 24°C to 38°C associated with the process. Therefore, any attempt to utilize injection metallurgy technique should also consider the development of supporting technoloies such as avoiding slag-carryover, compOensation for heat losses, shrouding the metal streams and vacuum facility. The consolidation of all these technologies will help producing clean steels with low amount of basic impurities.

REFERENCES

1. E. Hees : Meetallurgical Plant and Technology Vol.47, No.2, (1990), p.26
2. P.H. Dauby : 4th Process Techn. Conference, Chicago, Illinois (1984), p.3
3. F. Oeters, W. Pluschkell, E. Steinmetz and H. Wilhelmi: Steel Research, Vol.59, No.5 (1988) p. 192
4. S.C. Koria : Steel Research, Vol.59 (1988) p.104
5. S.C. Koria : Ironmaking & Steelmaking , Vol.16 (1989) p.21
6. S.C. Koria : Steel Research, Vol.60 (1989) p. 60
7. G. Carlsoon and E. Burstrom : Scand. Jl. of Met., Vol.15 (1986) p.298
8. K.W. Lange : International Materials Reviews, Vol.33, No.2(1988) p.53
9. S.C. Koria and C.D. Khai : Trans. IIM (1988)
10. S.C. Koria and C.D. Khai : Trans. IIM (1989)
11. S.C. Koria and C.D. Khai : Gas Induced Stirring in Liquid Bath, Video Film, IIT Kanpur, India. The Film can be obtained from the said address
12. S.C. Koria : Steel Research, Vol.59, No.11 (1988) p.484
13. S.C. Koria and M.R.R.I. Shamsi Ironmaking and Steelmaking, No.6 (1990) To appear
14. E. Steinmetz : Archiv fur das Eisenhuttenues, Vol.39, No.6 (1968) p.421
15. U.B. Pal and B.V. Patil : Ironmaking & Steelmaking, Vol.13, No.6 (1986) p.294
16. A. Wikander : Powdered alloys for injection; In SCANINJECT I Intern. Conference on Injection Met.Luka, Sweden, June 9-10, 1977, p.3.1
17. L.R. Farias and G.A. Irons : Met. Trans. Vo.16B, June 1985, p.211
18. R.J. Fruehan : Ladle metallurgy, Principles and Practice, ISS of AIME, 1985

Table 10.1 Information on initiation of jetting mode of injection in liquid (5)

System	Bath height, m	Lance diameter, mm	P_b/P^*	$\dot{m}/A$, g cm^{-2} s^{-1}	Remarks
Air/water	1·2	4	1·116	53·01	Variation of kinetic pressure on jet axis as function of downstream distance. Kinetic pressure was constant at $x/D \leqslant 2$
Air/water	1·27	0·396	. . .	51	High speed photography
Air/water	0·50	4·0	1·048	31·51	Coalescence of gas packets. Lack of sharp pressure peaks and prevention of gas accumulation in lance
Nitrogen/water	0·40	. . .	1·038	40	High speed photography was used to determine steady jetting type of behaviour
Nitrogen/water	0·50	2·0	1·048	47·16	High speed photography; spreading of jet near orifice was key parameter
Nitrogen/mercury	0·20	2·0	1·26	56·59	
Helium/water	0·50	2·0	1·048	20·66	
Air/water	0·6	1·0	1·058	46·82	Gas concentration was 99% just downstream of gas injecting lance
Air/water	0·6	2·0	1·058	40·32	
Argon/steel	0·17	1·0		54.58	No penetration of liquid into lance was observed
Argon/steel	0·17	1·0		59.32	
Nitrogen/steel	0·17	1·0		47.25	
Helium/steel	0·17	1·0		16.87	

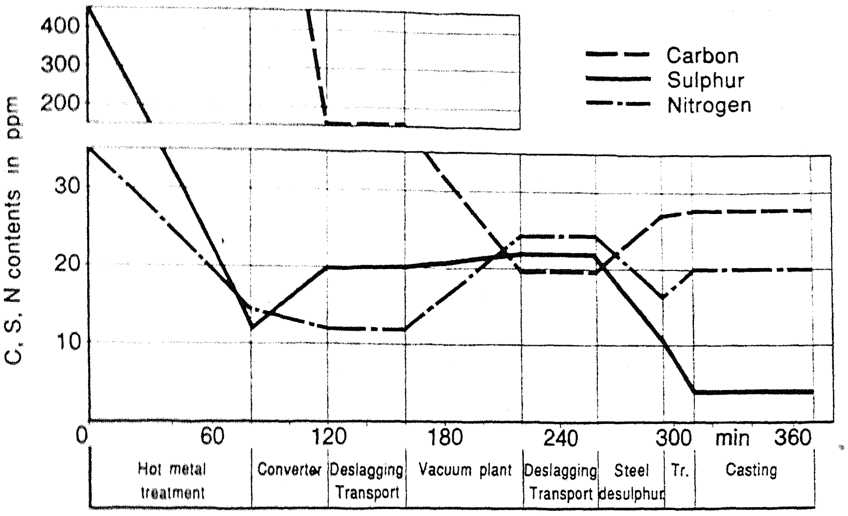

Fig. 10.1a : Evolution of multi-stage process route for an electric sheet steel grade with >3% Si using injection metallurgy

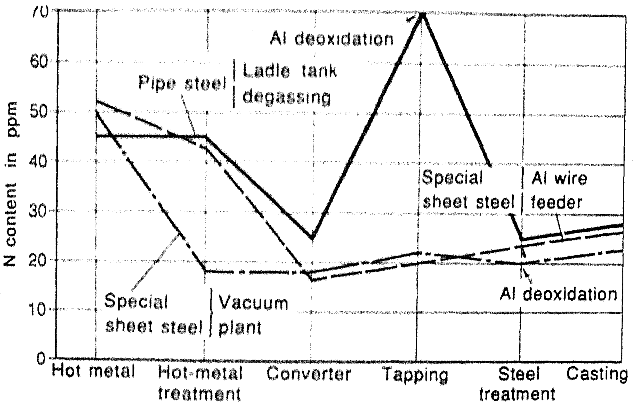

g. 10.1b : Variation of nitrogen content. Process routes with different hot metal treatment and Al deoxidation

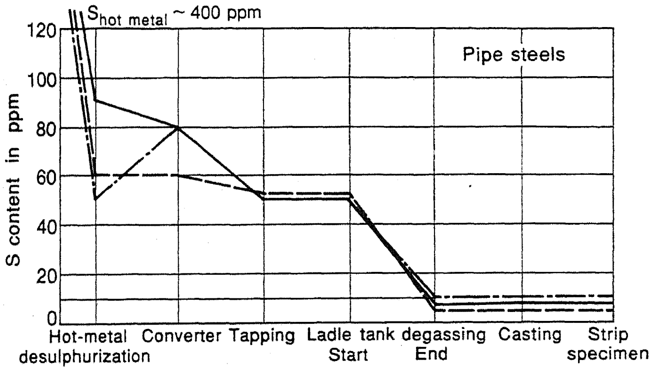

Fig. 10.1c : Process routes for hot metal desulphurization

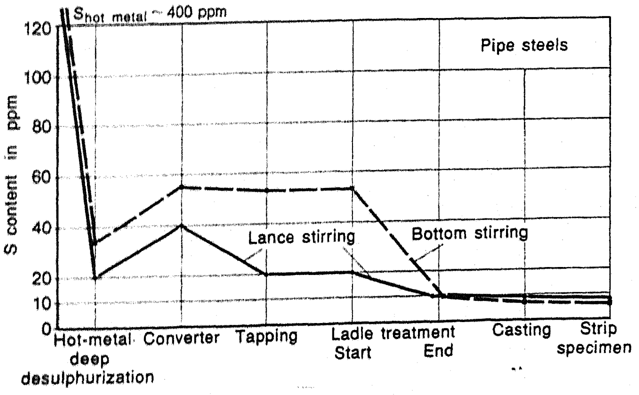

Fig. 10.1d : Process routes for hot metal desulphurization

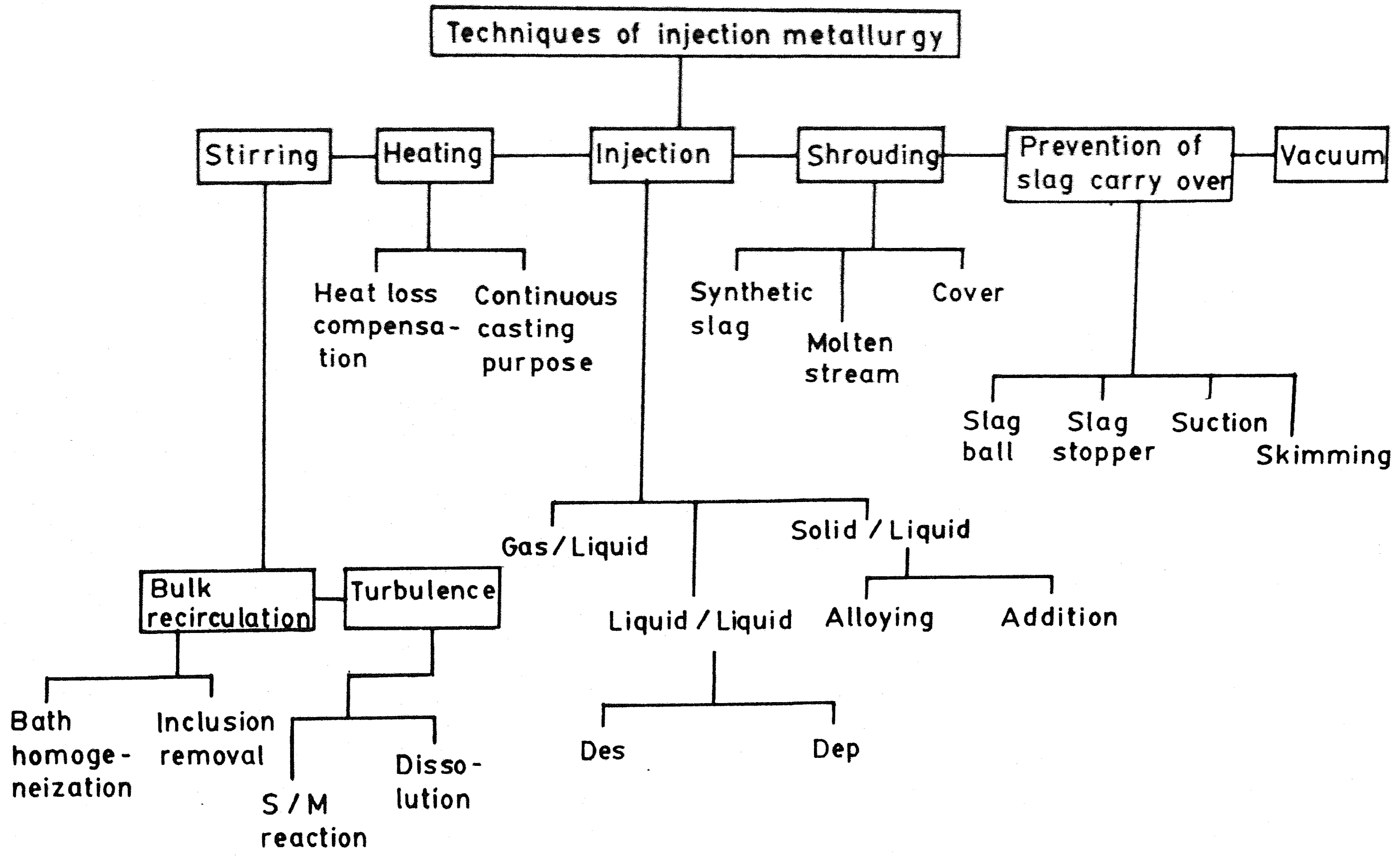
Techniques of injection metallurgy
Stirring
Heating
Injection
Shrouding
Prevention of slag carry over
Vacuum
Heat loss compensation
Continuous casting purpose
Synthetic slag
Molten stream
Cover
Slag ball
Slag stopper
Suction
Skimming
Gas/Liquid
Liquid/Liquid
Solid/Liquid
Alloying
Addition
Des
Dep
Bulk recirculation
Turbulence
Bath homogeneization
Inclusion removal
S/M reaction
Dissolution

Fig. 10.2 : Injection metallurgy techniques and their role for clean steel production

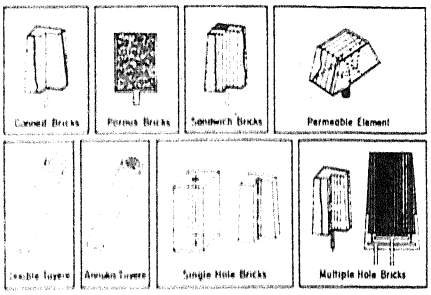
Canned Bricks
Porous Bricks
Sandwich Bricks
Permeable Element
Flexible Tuyere
Annular Tuyere
Single Hole Bricks
Multiple Hole Bricks

Fig. 10.3 : Example of injectors used in mixed gas blowing

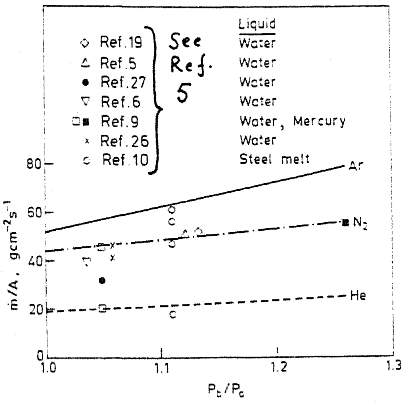

Fig. 10.4 : Variation of mass flux of gas for onset of jetting of liquids as function of ratio back pressure/liquid ambient pressure

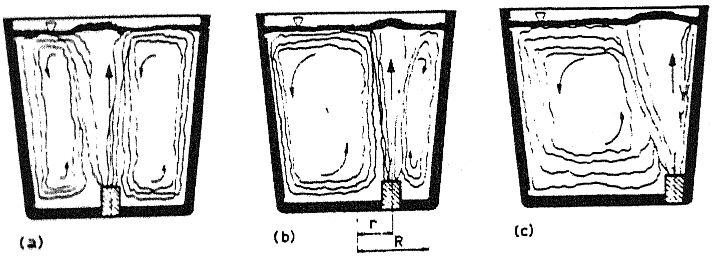

a central, b off-centre, $r/R = 0{\cdot}5$; c edge, $r = R$

Fig. 10.5 Different positions of porous plug and resulting flow pattern

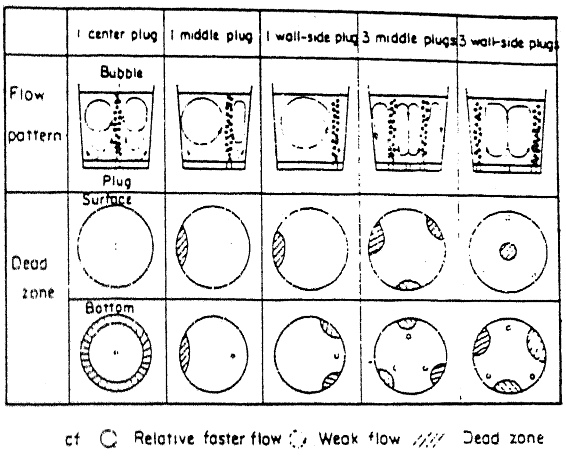
1 center plug
1 middle plug
1 wall-side plug
3 middle plugs
3 wall-side plugs
Flow pattern
Bubble
Plug
Dead zone
Surface
Bottom
cf
Relative faster flow
Weak flow
Dead zone

Fig. 10.6 Flow patterns in ladles for various injection configurations

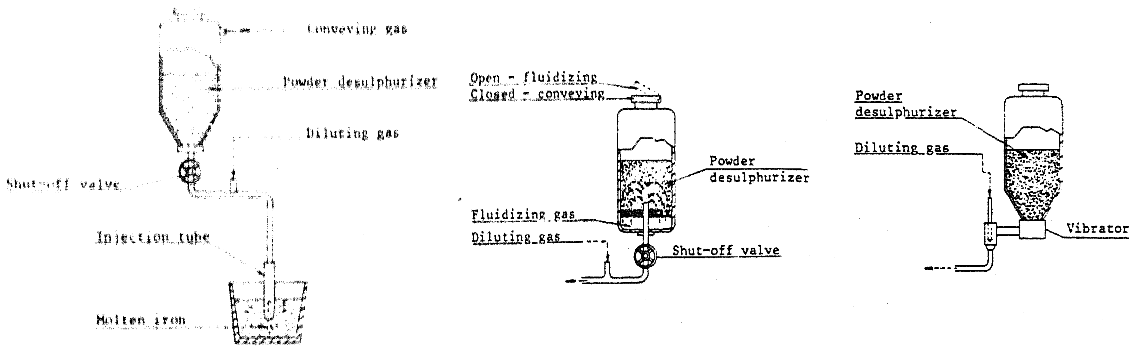
Conveying gas
Powder desulphurizer
Diluting gas
Shut-off valve
Injection tube
Molten iron
Open - fluidizing
Closed - conveying
Powder desulphurizer
Fluidizing gas
Diluting gas
Shut-off valve
Powder desulphurizer
Diluting gas
Vibrator

Pusher dispenser **Fluidised bed dispenser** **Vibratory dispenser**

Fig. 10.7 Different types of powder dispensers

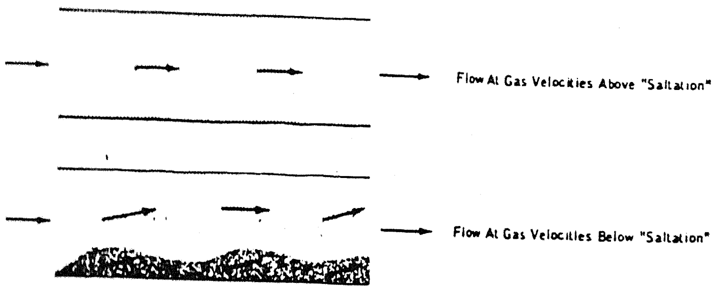
Flow At Gas Velocities Above "Saltation"
Flow At Gas Velocities Below "Saltation"

a. Horizontal dilute phase conveying

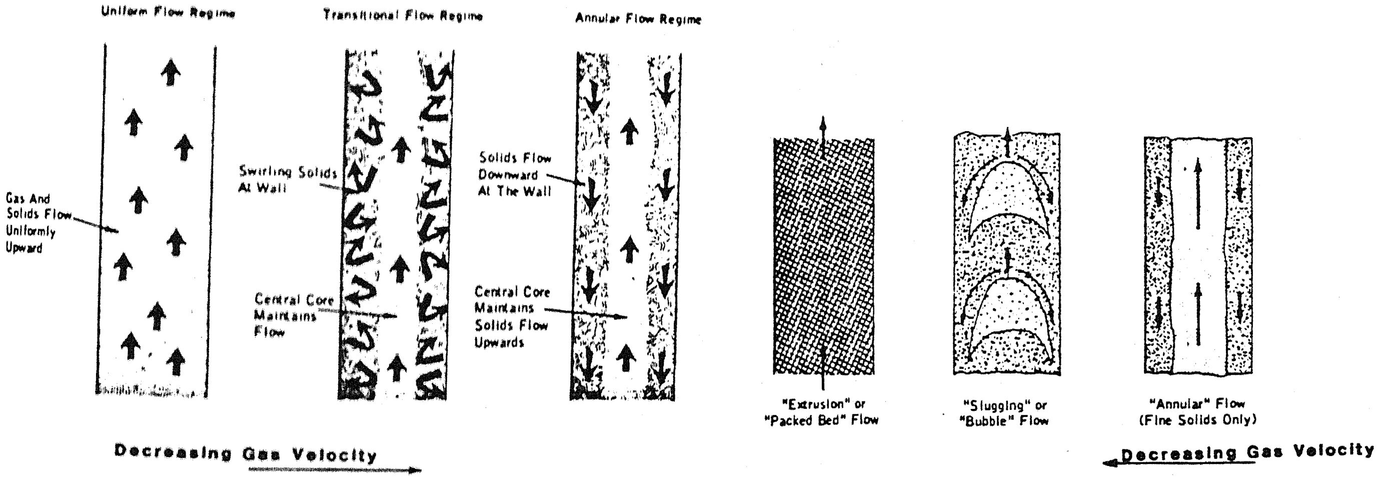
Uniform Flow Regime
Transitional Flow Regime
Annular Flow Regime
Gas And Solids Flow Uniformly Upward
Swirling Solids At Wall
Central Core Maintains Flow
Solids Flow Downward At The Wall
Central Core Maintains Solids Flow Upwards
Decreasing Gas Velocity
"Extrusion" or "Packed Bed" Flow
"Slugging" or "Bubble" Flow
"Annular" Flow (Fine Solids Only)
Decreasing Gas Velocity

b. Vertical dilute phase conveying

c. Vertical dense phase conveying

Fig. 10.8 Pneumatic transport of powder regimes

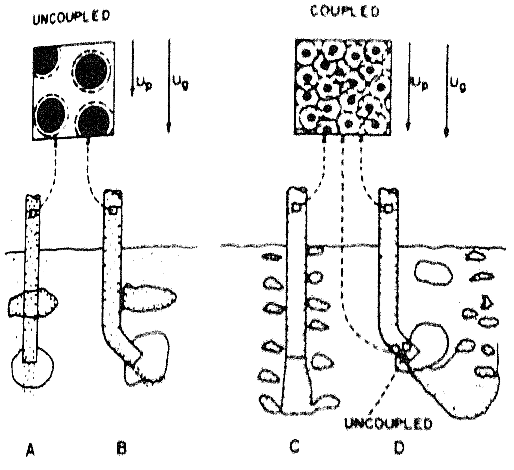
UNCOUPLED
COUPLED
u_p
u_g
u_p
u_g
UNCOUPLED
A
B
C
D

A) Coarse particles injected straight downward are uncoupled so that bubbles form.

B) Coarse particles injected at an angle segregate to the bottom of lance and bubbling is produced

C) Fine particles injected straight downward are coupled with the gas and therefore form jets which penetrate until their momentum is dissipated. Bubbles with particles inside rise from this point

D) Fine particles injected at an angle segregate to the bottom of the lance and therefore a jet of particles and some gas penetrates into the bath. At the lance tip most of the gas is in the top part of the lance and therefore the gas is uncoupled from the powder and therefore bubbles form at the lance tip as well

Fig. 10.9 Schematic diagram illustrating the coupling between gas and solid phases for various configurations

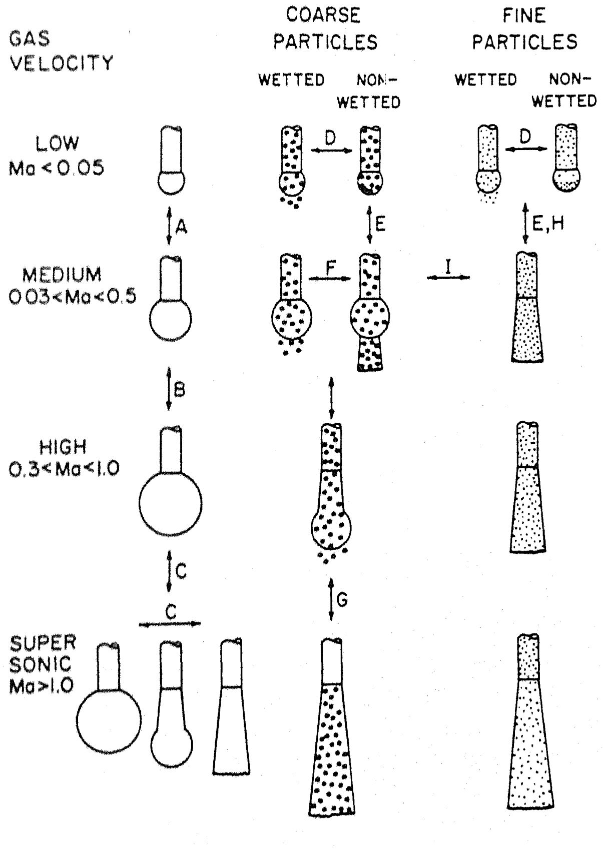
GAS VELOCITY
COARSE PARTICLES
FINE PARTICLES
WETTED
NON-WETTED
WETTED
NON-WETTED
LOW Ma<0.05
D
D
A
E
E,H
MEDIUM 0.03<Ma<0.5
F
I
B
HIGH 0.3<Ma<1.0
C
C
G
SUPER SONIC Ma>1.0

Fig. 10.10 Schematic representation of the regimes of gas and particle flow in liquids

CHAPTER 11

PHYSICAL AND MATHEMATICAL MODELLING OF SECONDARY STEELMAKING PROCESSES

DIPAK MAZUMDAR

11.1 PHYSICAL MODELLING

The physical modelling studies reported in the metallurgical literature have been carried out in connection with the development of new, or adapted, steelmaking processes. The laboratory modelling of slag/metal/gas flows have most frequently used water as the modelling medium to represent the liquid metal. The validity for using water in place of molten steel has been demonstrated repeatedly over the years by many researchers. For the present purposes, it is sufficient to note that the most important single property in this context apart from its ubiquity, is that its kinematic viscosity (= molecular viscosity/density) is essentially equivalent to that of molten steel at 1600°C (i.e., within 10 pct.). Flow visualisation experiments in aqueous systems using dyes or other tracers, have therefore proved to be very helpful in developing a qualitative understanding of various flows. Similarly, more detailed information on flow characteristics have also been possible by measuring velocity fields by tracking the motion of neutrally buoyant particles, hot wire or hot film anemometry and lately by laser doppler anemometry. In addition, measurements of residence time distribution to characterise mixing in water model experiments using dye, acids or KCl salt solution have proved very popular.

Having realised the advantages of using water as the representative fluid, it is now appropriate to discuss the general problem of how to model or characterise metallurgical processes. As a foreword, it is perhaps self evident but important to note, that if the same forms of dimensionless differential equations apply to two or more such metallurgical operations, and if an equivalence of dimensionless velocity, temperature, pressure or concentration etc. fields also exist between the two, than either becomes a faithful representation of the other; i.e., one can be used as a model of other. This is a general statement of the need for similarity between a model and a prototype which requires that there be constant ratios between corresponding quantities.

11.1.1 Physical Modelling Principles (1)

The states of similarity between a model and a full scale system would normally include geometrical, mechanical, thermal or chemical similarity. Mechanical similarity is further subdivided into requirements of static, kinematic and dynamic similarity between a model and its prototype. These are discussed below in detail.

(a) Geometrical similarity :

A basic requirement of any effort to model a full scale system or prototype is that the two be geometrically similar. Obviously, both must derive from the same generic species - a small feathered bird could certainly not replace its full scale human equivalent. Two bodies are said to be geometrically similar, when for every point in one body, there exist a corresponding point in the other. Such point to-point geometrical correspondence normally allows a single characteristic linear dimension to be used in representing the sizes of a model and prototype. For instance, a cylindrical model ladle in the laboratory can be represented by its diameter D, and compared to its equivalent full scale counterpart by noting its relative size or scale according to :

$$\lambda = \frac{D_m}{D_p} \qquad \ldots 11.1$$

In which, λ is called the geometrical scale factor. Note $\lambda = 1$ essentially suggests that the laboratory model is having exactly the same dimensions as the full scale industrial system. On the basis of these, liquid steel at position r_p, z_p and θ_p would then correspond to liquid in the model at r_m, z_m and θ_m, its equivalent location, according to (see Fig. 11.1).

$$\theta_p = \theta_m \quad \text{and} \quad \frac{r_m}{r_p} = \frac{Z_m}{Z_p} = \frac{D_m}{D_p} = \lambda \qquad \ldots 11.2$$

(b) Mechanical similarity :

For systems of interest to process metallurgist, in addition to geometric similarity, mechanical similarity is a common requirement. As previously mentioned, mechanical similarity comprises static similarity, kinematic similarity and dynamic similarity.

b1 Static similarity

Static similarity is concerned with solid bodies or structures which are subjected to loads and is chiefly of interests to mechanical and structural engineers, since in modelling of secondary steelmaking processes this has no relevance, consequently it is mentioned here.

b2 Kinematic similarity

The requirement of kinematic similarity may be stated as follows : geometrically similar moving systems are kinematically similar when corresponding particles trace out geometrically similar paths in corresponding intervals of time. The concept is illustrated diagrammatically in Fig.11.1 . This shows an alloy addition being dropped into a filling ladle of steel during a tapping operation. In order that the low-temperature analogue on the right be a true representation, it is necessary that model alloy addition (a wooden sphere in water having the same density ratio as the ferro-alloy addition in steel) move through the water such that :

$$\frac{r_{m,t}}{r_{p,t}} = \frac{Z_{m,t}}{Z_{p,t}} = \frac{\theta_{m,t}}{\theta_{p,t}} = \frac{t_m}{t_p} = C_t \qquad \ldots 11.3$$

we shall return to this example later, when we take up the application of the modelling principles.

b3 Dynamic similarity

Dynamic similarity is concerned with the forces which accelerate or retard moving masses in dynamic systems. It requires that the corresponding forces acting at corresponding times at corresponding locations in the model should also correspond. Before we proceed further, it is worthwhile considering the typical forces met in fluid flow systems viz., pressure, inertial, gravity and viscous forces and their appropriate dimensional representation.

Pressure force, F_p = pressure X cross-sectional area or PL^2

Inertial force, F_i = mass X acceleration or $\rho U^2 L^2$

Gravity force, F_g = weight of fluid or $\rho g L^3$

Viscous force, F_μ = tangential shearing stress X area or μUL

Dynamic similarity requires that at a given point,

$$\frac{F_{p,m}}{F_{p,p}} = \frac{F_{i,m}}{F_{i,p}} = \frac{F_{g,m}}{F_{g,p}} = \frac{F_{\mu,m}}{F_{\mu,p}} = C_F \qquad \ldots 11.4$$

i.e., the polygons of forces for corresponding particles or fluid elements must be geometrically similar between model and full scale.

As a further consequence, it follows that corresponding ratios of different forces in model and prototype should be equal; i.e., for inertial/viscous force equivalence,

$$\frac{F_{i,m}}{F_{\mu,m}} = \frac{F_{i,p}}{F_{\mu,p}} \qquad \ldots 11.5$$

or, dimensionally

$$\left[\frac{\rho\ U^2 L^2}{\mu UL}\right]_m = \left[\frac{\rho\ U^2 L^2}{\mu UL}\right]_p \qquad \ldots 11.6$$

and finally,

$$N_{Re,m} = N_{Re,p} \qquad \ldots 11.7$$

similarly, for inertial/gravity force equivalence:

$$N_{Fr,m} = N_{Fr,p} \qquad \ldots 11.8$$

under such conditions, the dependent grouping, telling no what the overall pressure drop along the flow system is, will again bear a constant ratio such that,

$$N_{Eu,m} = N_{Eu,p} \qquad \ldots 11.9$$

In Eqs. (11.7), (11.8) and (11.9) N_{Re} , N_{Fr} and N_{Eu} respectively represents the various dimensionless groups (viz.,the Reynolds number, the Froude number and the Euler number) that characterises the state of fluid motion in moving systems.

(c) Thermal similarity

In modelling heat transfer operations, thermally similar systems are those in which corresponding temperature differences bear a constant ratio to one another at corresponding positions. When the systems are moving, kinematic similarity is a pre-requisite to any thermal similarity. Heat transfer rates by conduction, convection and/or radiation to a certain location in the model must bear a fixed ratio to the corresponding rates in the prototype. This situation can be expressed algebraically as :

$$\frac{\dot{Q}_{r,m}}{\dot{Q}_{r,p}} = \frac{\dot{Q}_{k,m}}{\dot{Q}_{k,p}} = \frac{\dot{Q}_{c,m}}{\dot{Q}_{c,p}} = C_Q \qquad \ldots 11.10$$

where subscripts r,k and c refer to heat transfer by radiation, conduction, convection respectively and Q represents quantities of heat transferred per unit of time.

(d) Chemical similarity

For adequate chemical similarity to be achieved between a model and a prototype, it is normal that dynamic and thermal similarity be first satisfied : the former since mass transfer and chemical reaction usually occur by convective and diffusive processes during motion of reacting material through the system, and latter since chemical kinetics are normally temperature dependent. Consequently, chemically similar systems may be defined as those in which corresponding concentration differences bear a constant ratio to one another at corresponding points within the geometrical system of interest.

11.1.2 Successful Modelling

The objective of the physical modeller is to achieve geometrical, mechanical, thermal and chemical states of similarity between a model and the full scale system (prototype). His objectives are achievable provided certain criteria are met. These criteria, as has been mentioned already, are that ratios of like quantities (forces, heat flows, mass flows) should correspond on a point to point to basis within the physical domain of interest. Starting with the governing equation, it is possible to deduce what corresponding conditions are needed for a model.

Having carried out such an analysis, as will be demonstrated subsequently, that only one ratio of corresponding quantities can be satisfied in practice. It is then up to the skill of the physical modeller to decide which is the most important criteria requiring his attention. Fortunately, some latitude is generally allowable in the less sensitive force ratios, since they will have little bearing on modelling phenomenon. The trick is to decide which factors can be ignored in setting up the model.

11.1.3 Case Illustrations

(a) Hydrodynamic modelling of ladle flows (2)

Hydrodynamic studies on ladle flows are often not concerned with thermal and chemical similarity effects, consequently the equivalence between a model ladle and a full scale system can be adequately described via the geometric and the dynamic similarities. Geometric similarity provides the necessary means for scaling the characteristic physical dimensions of the system, while dynamic similarity entails the correspondence among various forces (e.g., inertial, viscous, body forces and etc.) acting on the system. It is through consideration of these forces that the required criterion between the model and the full scale systems can be established.

In any flow system, the balance between various forces acting on a fluid element can be described via the Navier-Stokes equation. For a multidimensional flow situation, under steady state conditions, the force balance in tonsorial form can be expressed as :

$$\frac{\partial}{\partial x_j}(\rho\, u_j u_i) = -\frac{\partial p}{\partial x_j} + \frac{\partial}{\partial x_j}\left(\mu \frac{\partial u_i}{\partial x_j}\right) + F_i \qquad \ldots 11.11$$

The non-dimensional equivalence of Eq.(11.11),is typically represented as :

$$\frac{1}{N_{Eu}} = \phi\,(N_{Re}\,,\,N_{Fr}) \qquad \ldots 11.12$$

Equation (11.12) states that the ratio of the pressure force to the kinetic energy contained in the fluid (e.g., N_{Eu}) in a flow system is a function of the inertial, viscous and body (viz., the buoyancy, in the present situation) forces. It is therefore apparent that to achieve similar ratios of pressure force to kinetic energy in the model and in the full scale systems, the Reynolds (= inertial force/viscous force) and the Froude (= inertial force/buoyancy force) number equivalence must be maintained between the two. Nevertheless, with typical laboratory scale water models employed in fluid studies (e.g., $\lambda \simeq 0.1$ to 0.4), it is impossible to regard both Reynolds and Froude similarity simultaneously. This essentially follows since kinematic viscosity of steel at 1600°C is practically equivalent to that of water at the room temperatures. As a consequence to this, the influence of one of these dimensionless groups on the induced flow has to be ignored as a first approximation. Assuming flows in typical gas stirred ladles to be dominated largely by the inertial forces (viz., considering $N_{Re} \gg N_{Fr}$), the dynamic similarity criterion between model and full scale ladle systems can be derived from Eq.(11.12) according to :

$$(N_{Fr})_m = (N_{Fr})_{f.s} \qquad \ldots 11.13$$

It is to be mentioned here that a large number of investigations carried out to date support the above conviction and indicate that flows in bubble stirred ladles are by and large predominated by inertial rather than turbulence viscous forces. Equation (11.13) under the assumptions mentioned already, suggests that to establish dynamic similarity between model and full scale systems, the ratio of the inertial to the buoyancy forces in these systems must be identical. To quantify these forces in gas stirred ladle systems in terms of relevant expressions, Fig. 11.2 has been included in the text. This illustrates schematically the gas injection system (viz., Fig.11.2(a)) and a corresponding idealized representation (viz., Fig.11.2(b)) applied to infer the various forces. Referring to these, it is readily seen that the buoyancy force acting on the system can be conveniently expressed as :

$$\text{Buoyancy force} = (\rho_L - \rho_g)\, g\, \alpha\, (\pi r_e^2 L)$$

$$\simeq \rho_L\, g\, \alpha\, (\pi r_e^2 L) \qquad \ldots 11.14$$

in which, r_e represents the radius of the idealized plume (Fig.11.2(b)) and has been deduced assuming the latter to be essentially cylindrical in shape having a volume equivalent to that of the actual near conical geometry (e.g., Fig.11.2(a)). Equivalent expression for inertial force is however, not readily apparent. This follows as the expression for inertial force embodies a characteristic velocity scale as well as a characteristic length scale (see also latter) and these as one might anticipate, are not straight forward in a recirculating flow system, such as the one under present consideration. Towards this, it is to be recognised here that in the plume region alone flow is practically unidimensional and therefore, considering the average plume radius as the characteristic dimension, the required expression for the inertial force can be derived. The inertial force acting on the system can then be represented as :

$$\text{Inertial force} = \rho_m U_p^2 (\pi r_e^2) \qquad \ldots 11.15$$

Incorporating Eqs.(11.13) and (11.14) in Eq. (11.15), the dynamic similarity criterion for the gas stirred ladle systems is expressed as :

$$\left(\frac{\rho_m U_p^2}{\rho_L g L \alpha}\right)_m = \left(\frac{\rho_m U_p^2}{\rho_L g L \alpha}\right)_{f.s} \qquad \ldots 11.16$$

Incorporating the continuum approach to represent the mixture density, ρ_m, in the two phase plume region viz., $\rho_m \simeq \rho_L(1-\alpha)$, Eq.(11.16) can also be written in the following form, viz.,

$$\left(\frac{U_p^2(1-\alpha)}{g L \alpha}\right)_m = \left(\frac{U_p^2(1-\alpha)}{g L \alpha}\right)_{f.s} \qquad \ldots 11.17$$

Furthermore, assuming volume fraction of gas, α, to be equal in the model as well as in the full scale systems, Eq.(11.17) is readily simplified to :

$$\left(\frac{U_p^2}{gL}\right)_m = \left(\frac{U_p^2}{gL}\right)_{f.s} \qquad ...11.18$$

Equation (11.18) derived on the basis of Froude dominated flow phenomena is the key to the modelling of ladle gas injection operations. It is instructive to recognise here, that a criterion such as equality of modified jet Froude number (viz., $N'_{Fr} = \frac{U_o^2}{gL} \cdot \frac{\rho_L}{\rho_L - \rho_g}$) between the model and the full scale systems is not applicable to the present situation, since under ladle flow conditions the kinetic energy of the incoming gas is considerably less (typically about 7-10 pct.) than the potential energy afforded by the rising bubbles. Moreover, in the bubbling regime the hydrodynamic conditions at the orifice or the nozzle is not critical to the bulk flow recirculation induced. Hence a dimensionless number embodying orifice characteristics (e.g., d_o, u_o etc.) has clearly no relevance to the present investigation. In this context, it is seen that incorporating $\bar{U}$, the mean speed of liquid recirculation in Eq.(11.15), though a dimensionally correct expression for inertial force is obtained, the resultant expression, nonetheless, would not be physically meaningful. To express further the equivalence in Eq.(11.18) is terms of the operating variables Q,L and R, the macroscopic equation for estimating the plume rise velocity, U_p, proposed by Mazumdar and Guthrie (ch.5) can be adopted, e.g.,

$$U_p = 4.5\, Q^{1/3} L^{1/4} R^{-1/4} \qquad ...11.19$$

Equation (11.19), as has been demonstrated produces results that are consistent with experimental measurements reported in the literature. Thus, substituting U_p from Eq.(11.19) into Eq.(11.18), the following expression is obtained in terms of the relevant operating variables, viz.,

$$\left(\frac{Q^{2/3}\, L^{1/2}\, R^{-1/2}}{gL}\right)_m = \left(\frac{Q^{2/3}\, L^{1/2}\, R^{-1/2}}{gL}\right)_{f.s} \qquad ...11.20$$

and finally, in terms of the geometric scale factor, λ, $\left(= \frac{L_m}{L_{f.s}} = \frac{R_m}{R_{f.s}}\right)$, the explicit equation between the model and the full scale gas flow rates becomes :

$$Q_m = \lambda^{3/2}\, Q_{f.s} \qquad ...11.21$$

Thus, on the basis of Eq.(11.21) and geometrical similarity, a water model ladle with the required scale factor can be conveniently proposed. To illustrate this, Table 11.1 has been included, which shows the characteristics of a 150 ton gas ladle and those corresponding to a 0.33 scale model ladle. With reference to Table 11.1 it is instructive to note, that it is not necessary to scale down the lance diameter, since, hydrodynamic conditions at the orifice or nozzle are known to be not critical to the overall flow recirculation induced. It is however, important to ensure that similar gas flow regimes (e.g., bubbling into liquid) prevail in both prototype and model and thus while selecting the gas injection lance for the water model ladle, this needs to be emphasized. Finally, as seen, the modelling exercise ignores the presence of any overlying buoyant slag phase in either full scale or model systems.

(b) Fluid flow and ferro-alloy hydrodynamics in ladle tapping operations

Referring to Fig.11.3, we see that a jet of liquid steel issues from the tap hole of a Basic Oxygen Furnace and plunges through a height, H, into a filling bath of steel. That most important factors governing the resulting flow field are, by reference to the turbulent form of the Navier Stokes Equation, forces due to inertia, to gravity, to friction and possibly to surface tension. We therefore require equivalence of forces between model and prototype, such that .

$$Re_m = Re_p \quad \text{or} \quad \left(\frac{\rho UL}{\mu}\right)_m = \left(\frac{\rho UL}{\mu}\right)_p \qquad \ldots 11.22$$

and

$$Fr_m = Fr_p \quad \text{or} \quad \left(\frac{U^2}{gL}\right)_p = \left(\frac{U^2}{gL}\right)_p \qquad \ldots 11.23$$

and perhaps

$$We_m = We_p \quad \text{or} \quad \left(\frac{\rho U^2 L}{\sigma}\right)_m = \left(\frac{\rho U^2 L}{\sigma}\right)_p \qquad \ldots 11.24$$

Choosing water as the low temperature analogue fluid, we have the condition that $(\rho/\mu)\text{water} = (\rho/\mu)\text{steel} \simeq 10^{6}\ m^2 s^{-1}$. We see therefore that a water model satisfying Reynold's criteria would need a characteristic velocity (i.e. jet entry velocity into the ladle) such that

$$U_m = \frac{U_p}{\lambda} \simeq \frac{U_p}{0.15} \qquad \ldots 11.25$$

However, if we are to satisfy the Froude Criteria, we have

$$\left(\frac{U^2}{L}\right)_m = \left(\frac{U^2}{L}\right)_p \qquad \ldots 11.26$$

$$\text{or} \quad U_m = \lambda^{1/2} U_p \qquad \ldots 11.27$$

Obviously both conditions cannot be met with $\lambda = 0.15$. The question is which one should we adopt? If we consider the numerical value of the Reynolds Number for steel entering a 4m diameter ladle at $10\ ms^{-1}$

$$Re_p \simeq \frac{7000 \times 10 \times 4}{0.007} \simeq 4 \times 10^7 \qquad \ldots 11.28$$

where ρ = 7000 kg m^{-3}, $\mu = 7 \times 10^{-3}$ kg $m^{-1}s^{-1}$ (or mPas). This indicates that the ratio of inertial to molecular viscous forces are enormous, and that the flow is therefore inertial force rather than viscous force dominated.

By contrast, the numerical value of the Froude relationship

$$Fr_p \doteq \frac{U_o^2}{gL} = \frac{10^2}{9.81 \times 4} \simeq 2.5 \qquad \ldots 11.29$$

is close to unity where the characteristic length scale is taken to be the vessel diameter. The jet entry velocity, U_o, is governed by the height of drop from the furnace and the ferrostatic head in the emptying B.O.F. furnace. The result indicates that inertial and potential forces are of the same order of magnitude and therefore of equal importance.

Finally,we should consider surface tension forces which appear in the Weber Number as a ratio of inertial/surface tension forces. Again,

$$We = \frac{\rho U_o^2 L}{\sigma} \simeq \frac{7000 \times 100 \times 4}{1.63} \simeq 1.7 \times 10^6 \qquad \ldots 11.30$$

where the surface tension of steel, at 1600 dynes/cm, translates to 1.63 kg s^{-2}. Evidently with inertial forces almost two million times greater than surface tension forces, we can neglect the latter, at least in terms of bulk movement of steel.

One difficulty with this analysis is the phenomenon of air entrainment. Air is entrained into liquid steel surrounding the impact zone of the plunging jet. In fact, significant quantities can be drawn in to (a) create very dirty reoxidised steel, and (b) considerably modify flow patterns within the ladle. However, this entrainment phenomenon is not likely to be surface tension related at full scale, but rather Froude based. Definitive studies have yet to be performed. Summarizing these arguments, we conclude that the operation of tapping a furnace into a ladle should be modelled on a Froude Basis.

For modellers with lingering doubts, a full scale aqueous model would be needed: under such conditions, equality of both Fr and Re groups between model and prototype would be satisfied, since both $\lambda^{1/2} = 1$ and $\lambda^{-1} = 1$.

Recommendation

A 0.15 scale model of the tapping operation should be built, wherein lengths, L, velocities, U_o, entry flow rates, Q_o, and fill-ing times, t, should be modelled such that :

$$L_m = \lambda L_p \qquad \text{e.g. } D_m = 0.15 \times 4.0 \text{ m} = 0.60 \text{ m}$$

$$V_m = \chi^3 V_p \qquad V_m = 0.15^3 \times 37.7 \text{ m} = 0.127 \text{ m}^3$$

$$U_m = \lambda^{1/2} U_P \qquad U_m = 0.15^{1/2} \times 10 = 3.88\ m/s^{-1}$$

$$Q_m = \lambda^{5/2} Q_P \qquad Q_m = 0.15^{5/2} \times 0.11 = 9.6 \times 10^{-4}\ m^3 s^{-1}$$

$$t_m = \lambda^{1/2} t_P \qquad t_m = 0.15^{1/2} \times 360 = 140\ s$$

Ferro-Alloy Hydrodynamics

To model particle trajectories of alloy additions in liquid steel, a little background information on heat transfer to alloy additions is needed. One finds that all alloys dropped into steel baths, no matter their actual thermal properties and melting points, freeze a shell of steel around them. This leads to the phenomenon of a molten ferro-alloy core contained within a frozen steel shell as discussed in ch.6. Consequently, the hydrodynamic simulation involves treating the motion of a buoyant lump (sphere for simplicity) of relatively constant diameter as it moves through a swirling flow of liquid steel.

We will use the differential equation technique to determine what important parameters need to be considered, and therefore how we should set about modelling particle behaviour in flowing fluid.

Applying Newton's Second Law of Motion, therefore, which states that the sum of the applied forces acting on a body is equal to the product of the body's mass and acceleration, we have, taking z positive downwards,

$$m_s \frac{dU}{dt} = F_B + F_A + F_D + F_g \qquad \ldots 11.31$$

where

$$F_g = \rho_s V_s g$$

$$F_B = -\rho V_s g$$

$$F_D = -C_D\, 1/2\, \rho\, U_r |U_r| \left(\frac{\pi d_s^2}{4}\right)$$

$$F_A = +C_A \rho V_s \frac{dU_p}{dt}$$

The only force worthy of extra comment is the added mass force, F_A. This force is a measure of the resistance experienced by an accelerating or decelerating submerged body during its translation through a fluid. Evidently, acceleration of a body through a high density liquid such as molten steel is considerably more difficult than the same body's acceleration through a gas, for instance. For a sphere, the coefficient of proportionality, C_A, the added mass coefficient is 0.5, and $F_A = 0.5 \rho V_S \frac{dU}{dt}$.

Substituting for the various forces, and collecting like terms, we can write the following differential equation :

$$(M_s + M_A)\frac{dU}{dt} = F_g + F_B + F_D \qquad \ldots 11.32$$

or

$$(\rho_s + C_A \rho) V_s \frac{dU_P}{dt} = \rho_s g V_s - \rho g V_s - \frac{1}{2}\rho |U_r| U_r C_D \frac{\pi d_s^2}{4} \qquad \ldots 11.33$$

or

$$\frac{dU}{dt} = \frac{(\rho_s - \rho)g}{(\rho_s + C_A \rho)} - \frac{3\rho |U_r| U_r C_D}{4 d_s (\rho_s + C_A \rho)} \qquad \ldots 11.34$$

defining $\gamma = \rho_s / \rho$

$$\frac{dU}{dt} = \frac{(\gamma - 1)g}{(\gamma + C_A)} - \frac{3}{4}\frac{|U_r| U_r C_D}{d_s(\gamma + C_A)} \qquad \ldots 11.35$$

or simplifying and reducing to dimensionless form

$$\frac{d_s}{U_r^2}\frac{dU}{dt} = \frac{(\gamma - 1)\, g\, d_s}{(\gamma + C_A)\, U_r^2} - \frac{3}{4}\frac{C_D}{(\gamma + C_A)} \qquad \ldots 11.36$$

For the ferro-alloy in liquid steel to be modelled by a particle travelling through water, this general equation must apply to both systems and there must be a correspondence of like quantities or forces. Denoting the real system by subscript 1, and the model by subscript 2, (and dropping the solid, s, subscript) we require a correspondence of quantities such that

$d_2 = K_d d_1$

$U_{r,2} = K_{Ur} U_{r,1}$

$\gamma_2 = K_\gamma \gamma_1$

$C_{A,2} = K_A C_{A,1}$

$C_{D,2} = K_C C_{D,1}$

$t_2 = K_t t_1$

We can write for System 1 :

$$\frac{d_1}{U_{r,1}^2}\frac{dU_{P,1}}{dt_1} = \frac{(\gamma_1 - 1)}{(\gamma_1 + C_{A,1})}\frac{g\, d_1}{U_{r,1}^2} - \frac{3}{4}\frac{C_{D1}}{\gamma_1 + C_{A,1}} \qquad \ldots 11.37$$

And for System 2 in terms of 1:

$$\frac{K_d}{K_{U_r} K_t} \frac{dU_{P,1}}{dt_1} = \frac{(K_\gamma \gamma_1 - 1)}{(K_\gamma \gamma_1 + K_A C_{A,1})} \frac{gK_d d_{S,1}}{K_{U_r}^2 U_{r,1}^2} - \frac{3}{4} \frac{K_C C_{D,1}}{(K_\gamma \gamma_1 + K_A C_{A,1})}) \qquad ...11.38$$

For these two differential equations to be numerically identical as required for a perfect model, we need $K_A = 1$, $K_C = 1$, $K_\gamma = 1$, and $K_d / K_{U_r}^2 = 1$. Consequently, provided the added mass coefficient is identical for both large and small spheres, the drag coefficient C_D is numerically equivalent (true provided Reynold's Number > 10^4 or more), the solid/liquid density ratio is the same, and Froude modelling is adopted ($\frac{K_d}{K_{U_r}^2} = \frac{d_2/d_1}{U_2^2/U_1^2} = 1$), we can achieve a perfect correspondence between model and prototype, in which times are equivalent, as well as are particle trajectories.

Recommendation

A 0.15 scale model requires that the particles entering the aqueous analogue be scaled, together with entry velocities and density ratios. Hence

$$d_m = \lambda D_P \quad \therefore \quad d_m = (0.15 \times 20) \text{ to } (0.15 \times 200) \text{ mm} = 3\text{mm to } 30\text{mm}$$

$$\gamma_m = \gamma_P \quad \therefore \rho_m = 0.3 \; \rho_{H_2O} \text{ to } 0.9 \; \rho_{H_2O} = 300 \text{ to } 900 \text{ kg m}^{-3},$$

and entry velocities should be scaled according to Froude Criteria, as for plunging jet.

11.2 MATHEMATICAL MODELLING

Recent efforts in the mathematical modelling of secondary steelmaking processes have largely concentrated on turbulent recirculatory flows. Such flows play an important role in determining the rates of various transport processes such as slag-metal reactions, alloy dissolution, mixing and so on carried out in the reactor vessels (viz., R.H. Vacuum degasser, argon stirred ladle, C.A.S. method of alloy addition etc.). Since direct measurements of flow variables in prototype metallurgical reactors are difficult and often impracticable to obtain (high temperature, visual opacity and large sizes of industrial unit essentially preludes this), recent mathematical modelling has tended to precede industrial verification.

The mathematical models aim at solving appropriate partial differential equations governing the transport of mass, momentum and other scalar flow properties (e.g., turbulence kinetic energy).

mathematical formulation of different phenomena of relevance to the secondary steelmaking as well as the methods used to solve the set of p.d. e's are briefly described in the following sections.

11.2.1 The Turbulent Fluid Flow Model

The relevant hydrodynamic equations describing turbulent flow of liquid are, in vectorial form, the equation of continuity :-

$$\nabla . U = 0 \qquad ...11.39$$

and motion -

$$\frac{DU}{Dt} = -\frac{1}{\rho} \nabla.p + \frac{1}{\rho}\nabla(\tau_{lam} + \tau_{turb}) + \bar{f} \qquad ...11.40$$

In Eq.(11.39), no spatial accumulation of liquid can occur as the liquid is essentially in compressible. Similarly, within any differential volume element of fluid, the convective terms (appearing on the left hand side of Eq.(11.40) must be balanced by the pressure terms, the laminar (τ_{lam}) and turbulent (τ_{turb}) viscous shear stresses, and the body force term, $\bar{f}$. The body force term may include the force of gravity (e.g., filling ladles), buoyancy forces (e.g., gas stirred ladles), electromagnetic forces (e.g., induction stirring) and the like. Solutions to Eqs.(11.39) and (11.4) for any specific case with appropriate boundary conditions yield the predicted velocity field.

It is readily seen that the velocity field can be extracted from Eq.(11.40), provided the distribution of τ_{turb} in the flow domain is known, as often, τ_{lam} and $\bar{f}$ are exactly known for any given flow situation. The turbulence shear stress is related to an unknown parameter the turbulence viscosity, μ_{turb} via the gradient of the relevant velocity component. Consequently, in essence, Eq.(11.40) can be visualised to embody the parameter turbulence viscosity μ_{turb} and a knowledge of the distribution of this latter parameter is desirable if Eq.(11.40) is to be solved. Estimation of μ_{turb} essentially follows from an appropriate turbulence model and to this end, the k - ε model, originally proposed by Rodi and Spalding (3), has been the most widely accepted one. The model has been successful in predicting turbulence behaviour of a large number of flow systems. According to this model, the turbulence viscosity, μ_{turb} , is given by :

$$\mu_{turb} = C_{\mu} \rho k^2 / \varepsilon \qquad ...11.41$$

and is obtained by the solution of two additional partial differential equations, one for turbulence kinetic energy, k, and the other for the rate of dissipation of turbulence kinetic energy, ε. The model has been applied for simulating hydrodynamics of various secondary steelmaking processes such as argon stirred ladle (4,5), CAS alloy addition procedure (6) and so on.

It is instructive to note here, that the flow equations and the equations in the turbulence models are mutually coupled (viz., the flow depends on k and ε via μ_{turb} while k and ε themselves depend on the flow). Thus the flow equation together with k and ε equations constitute a system of simultaneous partial differential equations. Further, examination of Eq.(11.40) also indicates the flow equations are essentially non-linear. Consequently, it is not possible to solve the equations of the turbulence flow model analytically and thus, numerical method will have to be applied to this end. Moreover, in developing a method for solving Eq.(11.40), the real difficulty lies in deducing the unknown pressure field, since there is no explicit equation for pressure. Pressure is indirectly specified via the continuity equation since, once the correct pressure field has been obtained and substituted into the equation of motion, the resulting predicted velocity field must satisfy the continuity equation (viz., Eq.(11.39)). However, ways to determine the pressure field constitute an extremely fascinating area of research where significant efforts have been ongoing for the last two or three decades. It's impossible to address the relevant aspects of numerical solution of turbulent Navier - Stoks equations (Eq.(11.40) during this short time and hence for necessary appraisal of the subject interested readers are referred to the well acclaimed text book of Patankar (7).

11.2.2 Model of Single Particle - Liquid Interactions

The hydrodynamic interaction of a solid addition with a liquid is of major concern in secondary steelmaking operations. For instance, the hydrodynamics of projected lumps of ferro-alloy additions etc., into filling ladles of steel is of interest, in view of the large tonnage used in the primary conditioning of raw steel and their critical role in determining the chemical characteristics, or grade, of each heat of steel. One is therefore interested in understanding how and where the solid being projected into the bath moves as a function of time. Such information coupled with data on melting and dissolution kinetics, chemical reaction rates etc. are needed before a clear understanding and appreciation of these operations can be gained.

A macroscopic approach based on Newton's second law of motion can be adopted in determining a projected addition's subsurface motion through a liquid from first principle according to :

$$\frac{d}{dt}(M\bar{U}_p) = \sum F \qquad \ldots 11.42$$

Equation (11.25), for the trajectory of a spherical object in translation through a fluid can also be described as (8) :

$$(M_s + C_A M_A)\frac{d\bar{U}_p}{dt} = M_s g\,(\frac{\rho_p}{\rho} - 1) - \frac{C_D}{2} R^2_p \rho \bar{U}_r |\bar{U}_r| \qquad \ldots 11.43$$

In Eq.(11.43), M_s is the mass of sphere $(= \frac{4}{3} \pi R_p^3 \rho_p)$, U_p is the instantaneous velocity of the sphere while $\bar{U}_r$ is the relative velocity between the particle and the bulk fluid. It is through the drag force term ($F_D \alpha \bar{U}_r^2$) that the fluid's motion the vessel exerts an influence on the trajectory of submerged particles. Obviously, the distribution of flow parameters within the vessel must first be specified, before subsurface trajectory of alloy additions can be predicted via Eq.(11.43). Furthermore, it is readily apparent that the initial condition to Eq.(11.43) and the hydrodynamics of the vessel will characterise one alloy addition procedure from another, though the subsurface trajectory for different physical situations are essentially governed by Eq.(11.43).

11.2.3 Model of Mixing or Dispersion in a Recirculating Flow Domain

Thermal, particulate or liquid mixing phenomena are essentially governed by similar p.d.e's and these, in terms of a general variable , can be represented according to :

$$\frac{\partial \phi}{\partial t} + \nabla \cdot (U \phi) = \nabla \cdot (\Gamma \text{ grad } \phi) + S_\phi \qquad \ldots 11.44$$

In which, U is the velocity, Γ is the turbulence exchange coefficient (= eddy kinematic viscosity) and S_ϕ is the source term (of generation or depletion). Because of the coupling of Eq.(11.44) with the flow and turbulence, it is implicit that the distribution of U and Γ in the flow domain must first be known, before Eq.(11.44) is solved for ϕ , the dependent variable. Referring to Eq.(11.44), it is seen that if $\phi = M_i$, $\Gamma = D_E$ (the eddy deffusivity) and $S_\phi = 0$, then Eq.(11.44) would essentially dictate the conservation of a species 'i' in a differential volume element and hence on solution would provide the distribution of the species in the flow domain. Thus the specific meaning of ϕ (temperature, concentration etc.) depends on the prescription of S_ϕ as well as on the imposed initial and boundary conditions to Eq.(11.44).

11.2.4 Case illustrations

(a) Axisymmetric gas stirred ladle systems

Equations (11.39) through (11.44) together with the associated boundary conditions can be solved numerically to provide estimates of numerous phenomena (flow, turbulence, alloy motion, mixing or dispersion etc.) of interest to the steelmakers. This is particularly important since experimental investigations on high temperature steel processing ladles are often impracticable and provide serious threat. Indeed empirical study aimed at process optimization would require several thousand heats. Alternatively, required informations can be conveniently deduced via the mathematical models presented already.

Consider therefore, the solution of Eqs.(11.39) and (11.40) in conjunction with the k - ε turbulence model for industrial gas stirred ladle systems. Assuming that the distribution of F, the body force generated via gas injection (viz., the buoyancy force), is known within the flow domain (4), the fluid flow equations can be solved conveniently to derive the flow characteristics of gas stirred systems. As a typical example of the model's capabilities in this respect, predicted recirculatory flow field generated in typical 150 ton teeming ladle (viz., Table 11.1) at a gas flow rate of 0.0188 m^3/s and 50 pct. lance submersion are presented in Fig.11.4. The predicted velocity field clearly shows the strong recirculatory vortex characteristic of the axisymmetric gas injection system. As seen, plume velocities of about 1.1 ms^{-1} would be observed and steel flow down the side walls would exhibit velocities of approximately 0.35 m/s.

Similarly, Table 11.2 presents the numerically calculated average recirculation speed, $\bar{U}$ and the average plume velocities, U_p as a function of fractional depth of lance submergence. These are defined as :

$$\bar{U} = \frac{\int_0^L \int_0^R \sqrt{u^2 + v^2}\; 2\pi r \; dr \; dz}{\int_0^L \int_0^R 2\pi r \; dr \; dz} \qquad \ldots 11.29$$

and

$$U_p = \frac{\int_0^{r_c} \int_0^L \sqrt{u^2 + v^2}\; 2\pi r \; dr \; dz}{\int_0^{r_c} \int_0^L 2\pi r \; dr \; dz} \qquad \ldots 11.30$$

Although the flow patterns generated in these cases are very similar, one can note that increasing the lance depth by 20 to 25 pct. causes liquid steel recirculation rate to increase by about 8 to 15 pct.. This in turn is expected to enhance the associated rate of heat and mass transfer in the gas stirred system.

(b) The C.A.S. alloy addition procedure

Steel flows generated in a 150 ton C.A.S. ladle at a gas flow rate of 0.0188 m^3/s are presented in Fig.11.5. Marked differences with equivalent flows in central gas injection (viz., Fig.11.3) is readily apparent. The flow field in Fig.11.5 two contra-rotating recirculating vortices that are characteristic of the C.A.S. system. As can be seen plume velocities would be about 1.2 m/s, while upward flows of steel along the vertical side walls would be about 0.05 m/s. It is, however, interesting to note that steel flow down the wall of the central refractory cylinder would exhibit velocities as high as 0.5 m/s. The high momentum of outward flowing steel associated with this high velocity can be expected to cause hydro dynamic erosion of the refractory cylinder lining. This, in turn could represent a source of inclusions.

Figure 11.6 shows flow fields generated under equivalent conditions in a C.A.S. ladle with a taper of 5^{o}, tapered rather than vertical cylindrical walls being more typical of industrial practice. Two points worth noting here are, first a small secondary recirculation zone near the junction of the surface with the side walls and second, the lower position of the recirculating vortex in the bulk compared with previous predictions in a vertical cylindrical ladle. These differences essentially result from the inclination of the side walls, even though this is only 5^{o} . None the less, the overall nature of flow pattern in this case is practically equivalent to those in vertical cylindrical wall ladle.

Predicted trajectories (via. Eq.(11.43)) of four typical spherical additions (85 mm diameter) (Al, Fe-Si, Fe-Mn and Fe-Nb) in the cylindrical 150 ton C.A.S. ladle is shown in Fig.11.7. These clearly show that buoyant additions such as Al and Fe-Si would instantaneously resurface and would proceed to melt within the central slag free region under inert atmosphere. Further more, the presence of high velocities coupled with enhanced bath turbulence would promote melting and dissolution rates of such buoyant additions considerably. It is clear that the initial steel shell around the addition would melt back and release the molten alloy content into the inert slag free region, which will be then gradually dispersed into the bath. As mentioned in ch.6, one should note that melting times of there buoyant additions are only a fraction of complete alloy mixing times.

Ferromanganese and additions with similar densities, on the other hand, may undergo subsurface melting, rather than melting within the central slag free region. Similarly, they may fall out of primary recirculating loop into the bulk of the liquid steel, and then gradually float up to the slag-metal interface. If the alloy's content is released from within the steel shell, in the vicinity of the slag-metal interface, it is clear that a portion could react with any oxidizing slag present, leading to a poor recovery of such additions.

Heavier additions such as ferro-niobium will settle to the bottom and only then gradually melt and be dispersed. However, since the bottom part of the ladle's contents is relatively quiescent, such additions will typically experience considerably longer mixing times. First hand calculations indicate that about 600 seconds of dissolution time is required for 85 mm dia spherical particle (ch.6). One further notes that such additions after a prolonged dissolution times takes about 400 seconds (e.g., Fig.11.8) to become completely dispersed into the bulk steel.

Dispersion behaviour (deduced via Eq.11.28) of molten additives in a 150 ton C.A.S. ladle at a gas flow rate of 0.0188 m^3/s is shown in Fig.11.8. At this gas flow rate, about 400 seconds bubbling is needed to disperse the dissolved additions homogeneously within the bath. Further more, it can be seen that the rate of transfer of dissolved additions from the central baffled region to the slag-metal interface (viz., mixing curve for region C) is extremely sluggish. Consequently, such addition techniques have the potential for slowing fading and in improving recovery rates of buoyant additions such as aluminium and ferro-silicon (4,6).

REFERENCES

1. R.I.L. Guthrie : Engineering in Process Metallurgy, Oxford Scientific Publication, Oxford University Press, New York, 1989.
2. D. Mazumdar : Metallurgical Transactions, Vol. 21B, 1990, pp. 925 - 928.
3. B.E. Launder and D.B. Spalding : Computer Methods in Applied Mechanics and Engineering, Vol. 3, 1974, pp. 269 - 284.
4. D. Mazumdar and R.I.L. Guthrie : Ironmaking and Steelmaking, Vol. 12, No.6, 1985, pp. 256 - 264.
5. D. Mazumdar and R.I.L. Guthrie : Metallurgical Transactions, Vol. 17B, 1986, pp. 725 - 733.
6. D. Mazumdar and R.I.L. Guthrie : Proceeding, 5th International Iron and Steel Congress, Washington D.C., 1986, pp. 1147 - 1157.
7. S.V. Patankar : Numerical Fluid Flow and Heat Transfer, Hemisphere Publishing Co. Inc.,, New York, 1980.

Table 11.1 Characteristic of a full scale system and the model

	Full Scale 150 Ton Teeming Ladle	Model 0.30 Cylindrical Tank of Plexiglas
Height, (m, as filled)	3.04	0.93
Diameter, (m)	3.65	1.12
Nozzle diameter, (mm)	20.28	6.35
Gas flowrate*, ($m^3 s^{-1}$)	1.88×10^{-2}	6.8×10^{-4}
Liquid	steel	water

* Corrected to mean height and temperature of the liquid

Table 11.2 Variation of average plume velocity and average bath recirculation speed as a function of fractional depth of lance submergence

Fractional Depth of Lance Submergence	Average Plume Velocity, $m\ s^{-1}$	Average Bath Recirculation Speed, $m\ s^{-1}$
0.50	0.92	0.136
0.75	1.06	0.156
0.95	1.14	0.167

Vessel diameter = 3.65 m, liquid depth = 3.04 m, and gas flow rate = $1.88 \times 10^{-2}\ m^3 s^{-1}$.

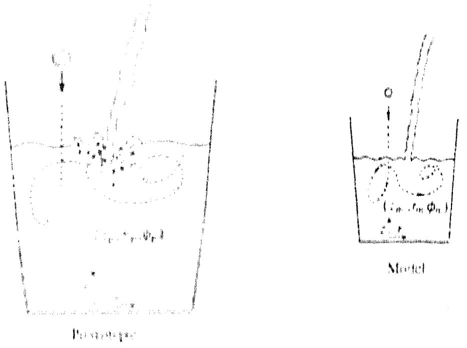
Prototype
Model

Fig. 11.1 : Illustration of a model and a prototype for alloy addition

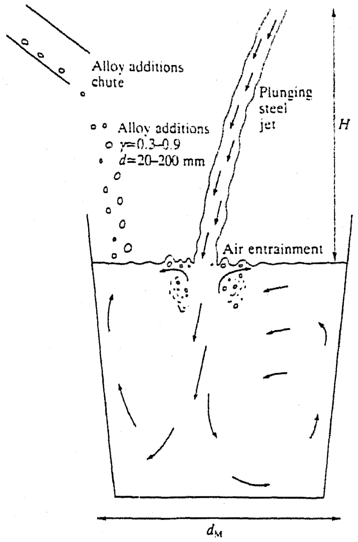
Alloy additions chute
Plunging steel jet
Alloy additions
γ=0.3–0.9
d=20–200 mm
H
Air entrainment
d_M

Fig. 11.2 : Typical alloy addition practice in ladles

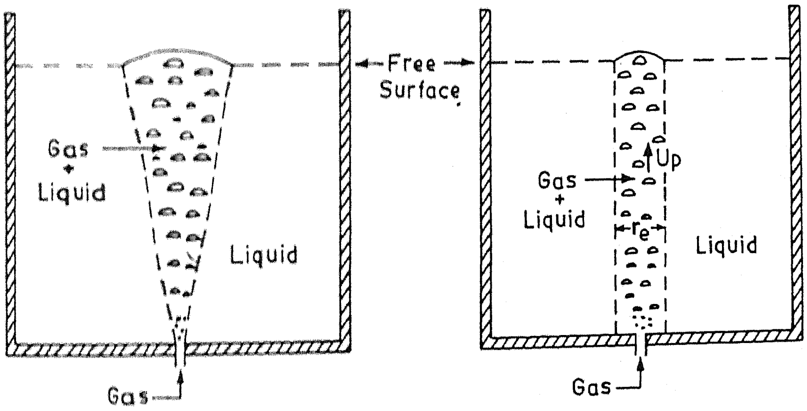
Free Surface
Gas + Liquid
Liquid
Gas
Up
r_e
Gas + Liquid
Liquid
Gas

Fig. 11.3 : Representation of argon stirred ladle applied to inter various forces acting on the system

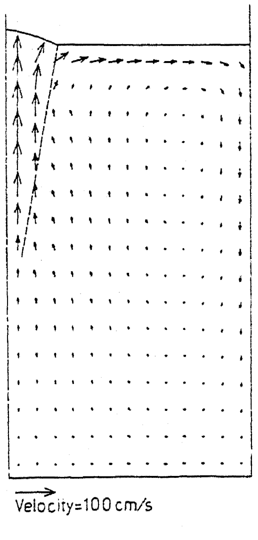

Fig. 11.4 : Flow field induced in a 150 ton ladle during central argon injection

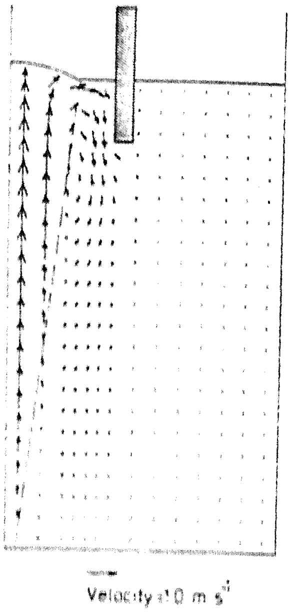
Velocity : 1.0 m s⁻¹

Fig. 11.5 : Flow field induced in a 150 ton ladle during C.A.S. operation

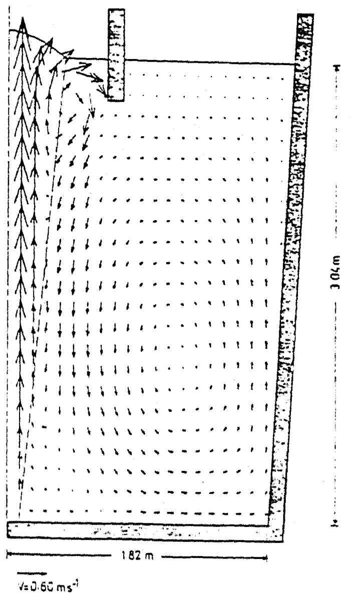
1.82 m
3.04 m
V=0.60 ms⁻¹

.Fig. 11.6 : Flow field induced in a 150 ton ladle with 5° tapper during C.A.S. operation

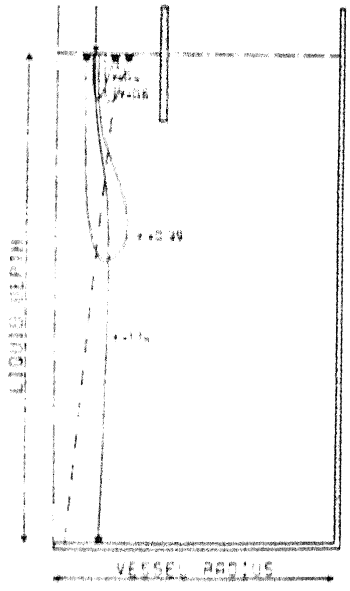
LIQUID DEPTH
VESSEL RADIUS

Fig. 11.7 : Alloy additions' trajectories in a 150 ton C.A.S. ladle

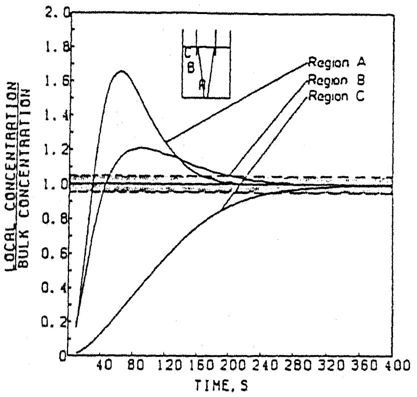

Fig. 11.8 : Mixing rates in various regions of a 150 ton C.A.S. ladle

CHAPTER 12

MISCELLANEOUS TOPICS

A. GHOSH

Attempts have been made in this course to organise subject matters into several distinct topics in the previous chapters. However it was found that this is not completely possible. In view of limited time available in the course as well as importance of some other topics in addition to all those presented in the previous chapters, it was decided to incorporate some miscellaneous topics of importance at the end as presented below.

12.1 GAS ABSORPTION DURING TAPPING AND TEEMING FROM SURROUNDING ATMOSPHERE

It has been known from as early as 1950s that oxygen is absorbed by molten steel during teeming from the surrounding air. From then onwards many investigators have reported it. McLean and Sommerville (1) have reviewed this recently. Since the oxygen is picked up just before casting, the resulting inclusions do not get separated well and lead to additional dirtiness in the solidified steel. The problem is more serious in continuous casting because of faster freezing and consequently less time available to inclusions for floating up. It is of relevance to ingot casting as well if we wish to produce clean steel.

It has been found that the product of such reoxidation generally forms macroinclusions (above 100 micron or so) which are harmful to the properties of steel. Also they are richer in iron and manganese oxides. Extent of oxygen absorption during tapping is of the order of 10-20 ppm (2) whereas it exhibits a wide range of 10-1000 ppm (i.e. 0.001-0.1 pct.) during teeming depending conditions.

Therefore it has been widely accepted that if we really desire clean steel, especially in continuous casting the teeming stream ought to be shielded from the surrounding air by inert gas. This is known as stream protection and is a widely adopted practice in continuous casting. It is rarely practiced for ingot casting because of adverse cost-to-benefit ratio. Therefore it is important to understand mechanism of such absorption and the variables that influence it so as to minimize it in industrial practices.

Nitrogen pick up is much slower than oxygen pick up, but is significant too. During tapping nitrogen pick up may be as large as 40 ppm (3) and during teeming it may go up to 150 ppm (1). Some reoxidation also takes place from the ferrous oxide/silicate slag coating on ladle refractory lining. However this is a different subject.

12.1.1 Mechanism of Gas Absorption During Pouring of Liquid : General Comments :

Geometrically speaking, this is a case of a liquid stream falling freely into a pool of the same liquid through a gaseous atmosphere. As shown in Fig.12.1 schematically,the absorption of gas can take place (4).

(a) through the surface of the falling stream,
(b) at the surface of the pool, and
(c) via entrainment as bubbles inside the molten pool.

Theoretical analysis as well as experimental work with water model have shown that the last mechanism, viz. absorption via entrainment is the predominant one. Szekely (5) theoretically estimated the extent of oxygen absorption by a stream of molten steel from air during teeming. He assumed the stream to be laminar and smooth, and that the air gets dragged into the pool of liquid steel by frictional drag at stream surface. The entrained air forms bubbles inside the liquid metal pool and all the oxygen from such bubbles are absorbed by metal. Szekely calculated the oxygen absorption $(\Delta \underline{O})$ as 26.5 ppm using industrial data. These agreed well for laminar streams.

However many investigators (1) found very large quantities of oxygen pick up and these were ascribed to turbulence and rough surfaceof stream. Therefore, here we have a situation where the physical characteristics of the stream is of considerable importance. In addition it was found that under certain circumstances the stream becomes unstable and breaks up into droplets. Such droplets increase the specific surface area of liquid metal enormously and lead to significant absorption of gas even before the teeming stream plunges into the liquid metal pool.Kumar and Ghosh (4) carried out a cold model experiment where water simulated liquid metal and CO_2 simulated air. They found that the rate of absorption of CO_2 by water increased by an order of magnitude when the falling water stream disintegrated before plunging into the pool of water. Extensive oxygen and nitrogen pick up in fraction of a second during free fall of droplets of liquid iron have been experimentally measured (1).

Meaningful experiments for understanding of mechanism are very difficult with liquid steel. Therefore investigators carried out experiments with water models (1,4). In such experiments visualization of the stream and the pool, still as well as movie photographic studies have been done. In addition rates of entrainment of air as well as rates of gas absorption have been determined.

Since gas absorption increases very significantly if the stream breaks up as droplets, prediction of conditions under which the stream is expected to break up before plunging is an important issue. It has been observed that, if at all, it breaks up only at a distance from the nozzle exit. This distance may be designated as **stream break up length** (l_b). Actual break up takes place if $H > l_b$, where H is the height of the nozzle exit from the surface of liquid pool. It has been established that l_b depends upon nozzle geometry (i.e. length/diameter ratio of nozzle etc.), teeming rate, and motion of fluid in the tank.

Actually the stream has some perturbation when it comes out of the nozzle. This perturbation gets accentuated during its free fall and eventually leads to break up.

Perturbation theory has been used to analyze the situation (6). A very important conclusion is that thinner stream at low velocity tends to break up most easily, i.e. one characterized by low value of l_b . Experimental observations confirm the same. However the conclusions should not be generalized as the data have been obtained over a limited condition.

A number of water model studies directed their attention to mechanism of gas entrainment by rough and turbulent stream (1), and a general picture has emerged. With increasing velocity of the stream, the stream Reynold's no. ($Re_s = \frac{d \rho_0 v_0}{\mu}$) increases. Above a certain value of Re_s, the stream starts to exhibit turbulence. Level of turbulence, i.e. intensity of turbulence of the stream is one of the key factors. It has been proposed that there are 4 distinct mechanisms as follows (1).

(a) At very low Re_s smooth, laminar stream as Szekely assumed (5).

(b) At higher Re_s stream surface becomes rough, but the surface of the pool remains reasonably smooth with a nice vortex at plunge point.

(c) At still higher Re_s both stream and pool surface become rough and the INDUCTION TRUMPET Fig.12.1) i.e. the cavity around the plunge point, has violent boil like motion.

(d) At still higher Re_s stream break up takes place.

It has also been established that the wavy nature of roughness of the stream surface drags gas pockets along with it. Mechanical interaction at the plunge point on liquid pool surface leads to entrainment. The rate of entrainment becomes one or two orders of magnitude higher under this condition. It has been found that the rate of entrainment increases with increasing v_0 and H, and depends upon nozzle geometry etc. Some quantitative relations also have been proposed (6).

Assuming 100 pct. absorption of gas from entrained bubble, the fractional increase of gas content in liquid ($\Delta[G]$) is given as

$$\Delta[G] = \frac{\rho_g \dot{v}_g}{\rho_l \dot{v}_l} \qquad \ldots 12.1$$

where ρ_g and ρ_l are densities of gas and liquid respectively, $\dot{v}_g$ is volumetric rate of gas entrainment, $\dot{v}_l$ is volumetric liquid pouring rate.

Choh et al (2,3) applied the above equations for estimation of oxygen absorption during teeming as well as tapping from converter utilizing also the theoretical analysis and experimental results (6). They have prepared nomographs for predicting oxygen absorption during teeming and tapping. They have also shown that these are in reasonable agreement with experimental data of some other investigators.

Regarding nitrogen, it has already been mentioned that the rate of absorption is lower than that of oxygen, but significant pick up occurs during tapping and teeming. Pehlke and Elliott (7), in their pioneering laboratory investigation on rate of nitrogen absorption and desorption by liquid iron found that the rates were retarded significantly if the melt contained dissolved oxygen and/or sulphur. Fig.12.2 shows variation of apparent rate constant (a measure of rate) as function of oxygen content of melt, as an example. They explained their results in the following way. Dissolved oxygen and sulphur had already been found to lower surface tension of liquid iron, i.e. they are surface active and prefer to segregate at the surface layer of the melt. Pehlke and Elliott proposed that such blockage of surface by O and S atoms were responsible for lowering of rates of nitrogen absorption and desorption. Since then many investigators have worked on it and the above findings and interpretations have been confirmed.

Therefore, nitrogen pick up during tapping and teeming is expected to be more in deoxidized and desulphurized melts. It has been confirmed by data (1,3). Sommerville (1) found nitrogen pick up during free fall of droplet of molten steel through nitrogen atmosphere decreasing with increasing wt.pct. S in melt in a manner similar to that shown in Fig.12.2. Fig.12.3 (3) shows how nitrogen content in steel increased during tapping from an 80t converter. Again the retarding effect of oxygen is evident. The calculated values assuming 100 pct. absorption were 40 ppm, which matched with converter data at very low oxygen content, but not in heats containing higher wt.pct. oxygen.

Very little information is available about the influence of physico-chemical processes occurring inside molten steel on mass transfer controlled absorption during pouring of liquid except that by Kumar et al (4). It is also likely that presence of strong oxide and nitride forming elements such as Al, Ti would influence the pick up. However informations in literature in this connection are yet to searched.

Not much information about absorption of hydrogen from atmosphere in teeming could be located in literature. Hydrogen pick up occurs presumably from atmospheric moisture vide the reaction :

$$H_2O(g) \quad = \quad 2\underline{H} + \underline{O} \qquad \ldots 12.2$$

Therefore the extent of hydrogen pick up would increase with increase in partial pressure of moisture in the atmosphere as well as decrease of $\underline{O}$ in melt.

From the point of view of process control in industry, we want to minimize pick up of gases during tapping and teeming, especially during teeming into mould. Best, of course, is shielding the stream from air by argon or nitrogen. Submerged nozzles have become common in continuous casting of steel. Studies on entrainment mechanism suggest that the primary attention is to be given to protecting the region above the plunge point.

Cost considerations do not always permit adoption of shielding. Then the guideline is that the stream should be continuous (i.e. no breakup) and it should be as smooth as possible with low turbulence. How it can be achieved may be worked out from our understanding of the phenomena involved as discussed in this section.

12.2 INCLUSION MODIFICATION

Chapter 7 has presented fundamentals of deoxidation and clean steel technology. It has already been stated there that inclusions are mostly oxides and sulphides, and sometimes oxysulphides. Inclusions, especially larger ones are generally harmful to properties of steel. However it is not always so. Small inclusion particles inhibit grain growth and also help equiaxed crystal formation with consequent improvements in properties.

Recognizing that, first of all, it is not possible to attain a high degree of cleanness from techno-economic viewpoint and, secondly, some inclusions of small sizes are beneficial, industries now-a-days go for modification of inclusions for some special grades of steel. The principal agent is calcium and occasionally Rare Earth elements (RE) for this purpose. Additions are made in secondary steelmaking ladles. However, benefits from inclusion modification can be obtained only when the liquid steel has been well deoxidized, desulphurized (sulphur far below 0.01%) (8,9,10), and the steel is fairly clean.

12.2.1 Influence of Inclusion on Properties of Steel

Extensive informations are available in literature on this topic. Only a few are referred to here (8,11-14). Properties that are adversely affected are fracture toughness, impact properties, fatigue strength, hot workability, resistance to corrosion. The factors responsible for the above may be classified into:

(a) geometrical factors-size, shape (may be designated as the ratio of major axis to minor axis), size distribution, and total volume fraction of inclusions.
(b) property factors-deformability and modulus of elasticity at various temperatures, coefficient of thermal expansion.

From a fundamental point of view, an inclusion/matrix interface has a mismatch. This causes local stress concentration around it. Application of external forces during working or service can augment it. If local stress becomes high then microcracks i.e. voids, develop. Growth of voids leads to fracture.

The concept of critical inclusion size proposed by Kiessling (11) has already been presented in Sec.7.3. Broadly speaking, it is in the range of 5 to 50 microns. It decreases with increase in yield stress.

The great majority of oxide inclusions belong to the pseudo-ternary system : $AO-SiO_2-B_2O_3$ where A is Ca,Fe(II), Mg and Mn, and B is Al,Cr,Fe(III). The sulphide inclusions are usually MnS or solid solutions of the (Mn,Me) (S,O) type. Me would be typically Fe(II) or Ca.

Very often the inclusion is a **duplex** one, the core consisting of one compound and the outside layer of some other compound. Examples are sequential formation of alumina, galaxite, and manganese alumino-silicate by reoxidation of aluminium-killed steel or coating of CaS on calcium aluminate in Ca-treated aluminium killed steel (9,11,15,16). Division into exogenous and endogenous is also too simplistic. It is well-established that precipitation of oxides/sulphides occurs on both exogeneous and endogenous inclusions in the melt or upon subsequent cooling and freezing of liquid steel in the mould. Inclusions may undergo further reactions as well. The subject of inclusion formation is incomplete unless we consider also the phenomena occurring in mould, which are :

(i) further reactions of elements with oxygen and sulphur during freezing leading to formation of oxides and sulphides,
and (ii) entrapment of non-metallic particles during freezing.

However this is beyond the scope of the present text.

Although the solidification morphology of inclusions is of importance in steel castings, the morphology of inclusions in wrought products is largely controlled by their mechanical behavior during subsequent steel processing, i.e. whether they are hard or soft relative to the steel matrix. Fig.12.4 shows behaviour of some inclusions during rolling of steel (9). The oxides are hard, whereas the sulphides are less hard. $C_{12}A_7$ (12 CaO.7Al_2O_3) particle being hard (i.e. undeformable) and large, gives rise to void during rolling. The stringer, especially MnS stringer, causes anisotropy in mechanical property and is responsible for loss of transverse and through-thickness ductility in plates. Advantage of a duplex inclusion with CaS-MnS coating is obvious from above points of view. It is harder than MnS.

Stresses arise around inclusions as a result of their thermal expansion coefficients, which differ significantly from that of the metal matrix. Metal manufacture involves heating and cooling and hence this aspect is important. For example, alumina and calcium aluminates are stress raisers due to their lower coefficient of thermal expansion as compared to ferritic matrix (12).

In materials where surface properties are important, such as good surface finish, surfaces for coating etc., inclusions have adverse effect. Moreover there is considerable evidence that non-metallic inclusions, particularly sulphides can act as nucleation sites for pitting corrosion (8).

In free-cutting steel, sulphur is deliberately kept high to generate large MnS inclusions which act as chip breakers, and also to provide lubricating film between tool and chip. However silicates and aluminates are harmful because they are hard and act as abrasives contributing to tool wear. In this area also calcium addition seems to be beneficial. Encapsulation of oxides by CaS leads to the same chip breaker action (8,10) at much lower sulphur content (0.1% or less). This gives the additional advantage accruing from better mechanical properties of steel.

12.2.2 Reaction of Calcium

Thermodynamics of reaction of calcium with oxygen and sulphur has been discussed in chapters 7 and 9. Thermodynamics has also provided very valuable guidance in understanding and prediction of formation of various types of inclusion.

Phase diagrams of oxide, sulphide and mixed oxide-sulphide systems have allowed ascertaining of liquid field, and various compounds that are likely to form. Hilty and coworkers (15) used metal-sulphide-oxide type ternary phase diagrams to explain formation of inclusions. However these provide only qualitative understanding.

For quantitative predictions chemical equilibrium calculations have been resorted to (8-10). For example, such calculations indicate that MnS would precipitate as a separate phase only when

$$[W_{Mn}]\ [W_{s}] > 2 \qquad \ldots 12.3$$

For most steels the $\underline{Mn}$ and $\underline{S}$ levels in steel are not high enough for MnS formation in the bulk liquid. However as the steel solidifies, Mn and S are rejected from the solid steel causing an increase in their concentration in remaining liquid, and ultimately condition noted in Eq.12.3 is obtained leading to interdendritic MnS inclusions.

So far as formation of duplex inclusions (i.e. $C_{12}A_7$ with sulphide ring in Fig.12.4) is concerned, analysis of the following type may be made.

$$12\ CaS + 11\ Al_2O_3 = 12\ CaO.7Al_2O_3 + 12\ \underline{S} + 8\ \underline{Al} \qquad \ldots 12.4$$

If CaS and $C_{12}A_7$ are treated as pure, then their activities are 1. Activity of Al_2O_3 is taken as that in $C_{12}A_7$. In that case, from ΔG^o of reaction 12.4 and other thermodynamic data the relationship shown in Fig.12.5 has been constructed. Holappa et al (10) carried out experiments in laboratory and determined inclusion types. Their data points for CA type inclusion matched well with thermodynamic predictions.

When calcium is added to Al-killed steels, it is predicted that first Ca would react with oxygen in liquid steel to form CaO. The resulting CaO would react with Al_2O_3 progressively forming CA_2 first, then CA and $C_{12}A_7$. The last one is liquid. CA is also a liquid above approx. 1610^{o}C. Further addition of Ca would next lead to formation of CaS or even CaS-MnS (in this case activity of CaS is not 1), which will form an envelop. It has also been experimentally confirmed (10).

Alumina clusters have been found to be responsible for nozzle clogged during teeming in continuous casting mould. Formation of liquid $CaO-Al_2O_3$ or $CaO-SiO_2-Al_2O_3$ deoxidation products eliminates this problem. According to Kitamura et al (16) it is not always true that (Ca,Mn)S forms envelop over calcium aluminate. CaS has been found to be dispersed as well. Depending on concentration levels of elements the following 4 types of inclusions were obtained.

A- type : Oxysulphide containing Ca,Al,O and S distributed throughout inclusion

B- type : $CaO-Al_2O_3$ having a ring of CaS around it

C- type : $CaO-Al_2O_3$

D- type : CaS

12.2.3 Reaction of Rare Earths (9,15,17,18)

A brief mention was made in ch.9 on reaction of Rare Earths (RE). Cerium is the most predominant element in Mischmetall or RE silicide which are the commercial forms in which REs are added into melt. It has already been mentioned in ch.9 that CeS is the stablest sulphide, and Ce also forms an oxysulphide under steelmaking conditions.

The stability diagram for Ce-O-S system in liquid iron is shown in Fig.12.6 (17). It shows the stable phase fields at various values of h_s and h_O (i.e. approx. weight pct. O and S dissolved in liquid steel). It may be noted that, under conditions prevalent in secondary steelmaking Ce_2O_3 and Ce_2O_2S are the compounds likely to occur.

RE consists of about 50% Ce, 25% La and the remainder Pr,Nd etc. Hence, % RE is taken as 2x(%Ce). In liquid iron at 1600° C, the following equilibrium relations may be employed for calculations.

for RE_2O_3, $[W_{RE}]^2 [W_O]^3 = 9.4 \times 10^{-18}$ ...12.5

for Ce_2O_2S, $[W_{Ce}]^2 [W_O]^2 [W_s] = 4 \times 10^{-16}$ ...12.6

and for CeS, $[W_{Ce}] [W_s] = 1.2 \times 10^{-4}$ ...12.7

During cooling RE oxysulphides form continuously such that there is a fine dispersion of hand nondeformable inclusions. In order to get desirable results, however, the steel should be very well deoxidized and desulphurized before addition of RE.

Following practical problems have been encountered in connection with RE addition.

(a) Since densities of RE inclusions are similar to that of liquid steel, floating out is more difficult. This may lead to adverse bottom cone segregation in ingots. It has been found that to avoid this as well as to obtain sulphide shape control.

$$[W_{Re}]\,[W_S] < 4 \times 10^{-4} \text{ and } \frac{[W_{Re}]}{[W_S]} > 3 \qquad \ldots 12.8$$

It is clear that these two conditions can be satisfied only if W_S is less than 0.01% .

(b) RE is very reactive. Unlike Ca, it has good solubility in molten steel and does not vaporize. Hence it tends to react with refractory lining, atmospheric air etc. thus producing adverse effects. Hence very good quality basic refractory lining should be used as ladle lining (very low FeO, MnO, and relatively low SiO_2). Also extensive precautions are required to prevent reoxidation of REs by contact with atmosphere and slag.

12.2.4 Concluding Remarks

As is obvious from previous discussions, inclusion modification is capable of bringing improvements in properties so desirable in high performance steels. However it is a challenging task from processing point of view. Molten steel is to be fairly clean and well deoxidized, desulphurized before additions of Ca or RE is made for modification purposes. Amongst the two again, RE treatment calls for more precautions.

Reoxidation by contact with atmosphere in ladle or during teeming is to be prevented. For this, stream protection is a must. It is also not possible to obtain either a clean steel or benefits from inclusion modification without good quality refractory lining for ladle, tundish, nozzles, stoppers and slide gate plates. Therefore the success of secondary steelmaking would not have been possible unless newer and newer refractory materials with better and better corrosion-erosion resistance were also simultaneously developed. This will be briefly dealt with in the next section.

12.3 REFRACTORIES FOR SECONDARY STEELMAKING

Importance of refractories to steelmaking processes is well-known to all steelmakers and needs no elaboration. The success or failure of processes is closely linked with development and/or choice of proper refractories for lining furnaces, ladles etc. Hence it is only proper that a section is devoted to it. However it is to be recognized that the subject is complex. Optimization of refractory practice in a shop is achieved with continuous operating experience, and trial. That is the reason why there is a large body of information in literature on refractories for steelmaking, but most of these deal with shop floor experience and related developmental work detailing successful practices. Since it is neither possible nor desirable within the purview of this course to get into such details, the brief discussions that follow will be restricted to some salient features only. At the outset some general references are being provided (18-22) for convenience of readers.

Up to the decade of 1950, secondary steelmaking did not make much headway. Refractories for ladle lining used to be fire clay with some variations. Scientists and technologists were carrying on development work in connection with primary steelmaking only. Life of lining is principally governed by corrosion-erosion. Corrosion refers to chemical attack. In primary steelmaking, the highly oxidizing slag is the principal corroding agent followed by oxygen dissolved in liquid metal. Erosion refers to spalling and detachment of grains and pieces of refractories caused by abrasion and impact. Corrosion and consequent weakening (i.e. loosening) of refractory surface speeds up erosion. Bath turbulence causes impact. Thermal shock is an additional factor aggravating spalling tendency.

In LD converter, the refractory material is burnt dolomite or magnesite or a mixture of the two in some proportions. Bonding is by tar or pitch. The practice varies from country-to-country. Dolomite is cheaper than magnesite, but tends to wear faster. Again SiO_2 and other impurities are harmful. Pure magnesia,manufactured from sea water, has proved to be superior to natural magnesite but is more costly as well.

The tar or pitch, after firing leaves carbon as residue. This retards slag attack in the following way.

(a) Slag does not wet carbon.
(b) Carbon reduces iron oxide in slag, which is the principal corroding constituent.

Therefore, it is necessary that the surface layer of refractory gets decarburized first for significant slag attack. Such a decarburized layer is very thin (1 mm or less).

Besides chemical composition of refractory lining, its porosity is an important factor in slag corrosion. A porous brick offers more surface area speeding up slag attack. From this point of view graphite is better than tar or pitch since the former is denser than the carbon residue of latter. Moreover graphite is more crystalline than the residue. More crystallinity means less defects and hence more resistance to chemical attack. However, here again the issue of cost is coming into picture. Dense materials are more costly.

Chesters (18) has mentioned that resistance to slag corrosion is a difficult property to measure, and in the area of converter steelmaking simulated tests are preferred. It is nothing but a comparison with some brick taken as standard, whose erosion rate is arbitrarily assigned a value of 1.0. Results of some measurements after Kappmeyer and Hubble (23) may be of interest. Fig.12.7 shows beneficial influence of increasing MgO content of refractory on erosion rate. Fig.12.8 shows the beneficial effect of increasing carbon content in brick.

It had also been long recognized that there are other factors governing liming life of steelmaking vessels, such as :

(a) technique of bonding and brick making

(b) technique of brick laying
(c) vessel design
(d) operating conditions
(e maintenance of lining.

In primary steelmaking, choice and design of refractory lining is governed by lining life and its impact on overall steelmaking cost. However in secondary steelmaking, we are additionally concerned with its effect on steel quality, cost of ladle heating etc. as illustrated by the following discussions.

(a) Chapter 7, sec.7.3 has a table showing the findings of Pickering that products of erosion of refractory contributed most significantly to harmful inclusions of large size. This behaviour pattern has been widely recognized. In section 12.2.4, it has been mentioned that without good quality refractory, not much benefit can be obtained from inclusion modification.

(b) Refractory lining may assist in removal of deoxidation products, if the latter gets chemically bonded on to it. Mention has been made in chapter 7 of the investigations made by Nakanishi et al in this connection. In injection metallurgy, dolomite lining has been found to lead to better desulphurization than magnesite lining (9,10). This may presumably be attributed to presence of CaO in dolomite.

(c) Refractory lining should be stable as well as inert to liquid steel. Otherwise it would tend to introduce undesirable impurities into the metal. Such tendencies are aggravated by use of vacuum and higher temperature, and are specially important for superior quality steel. This issue can be discussed fairly well with the help of knowledge of thermodynamics and shall be taken up again.

(d) Secondary steelmaking and continuous casting cause additional temperature loss of molten steel. Hence higher tapping temperatures (often 1700 to 1750°C for alloy steels) are required. This enhances the tendency for lining wear aggravating the problem further.

(e) From the above point of view, a low thermal conductivity of ladle lining is desirable to prevent heat loss by conduction through wall. Again a low thermal conductivity tends to enhance spalling by thermal shock at the hot face. An interesting development is use of higher percentage of graphite (10% or more) which allows through-and-through continuity in carbon phase thus increasing thermal conductivity. The conductivity again can be made directional by proper technique of brick making and by use of flake graphite (24). In that case heat will flow easily in direction parallel to hot face thus reducing tendency of spalling. On the other hand, thermal conductivity in direction perpendicular to hot face would be low.

(f) Ladles require preheating. The heat requirement can be cut down if heat capacity of the material is less. Large heat capacity also cools the steel more upon pouring and causes more temperature loss.

(g) Porous ceramic plugs are employed for gas purging in ladles. Also attempts are being made now-a-days to pass liquid steel through ceramic filters for removal of foreign particles. In these applications, besides wear-resistance and stability, permeability is an important issue. Permeability can be increased by increasing pore diameter and porosity. But then the tendency of penetration of molten steel and consequent clogging gets aggravated. In-situ sintering of particles and densification is undesirable as it leads to loss of permeability. Okawa et al (25) have discussed some fundamental considerations for development of improved permeable ceramics.

Erosion of lining by phenomena (a) and (c) above is most severe in the case of nozzle, because the liquid metal flows through it at high velocity. This not only affects quality but also teeming rate by progressive enlargement of nozzle diameter with time. Phenomenon (b) may lead to nozzle clogging, the well-known case being that by alumina clusters present in melt.

12.3.1 Thermodynamic Considerations of Refractory Stability and Inertness

Fig.2.1 shows the standard free energies of formation of oxides as function of temperature. This is guide to stabilities of oxides. It shows that, at steelmaking temperatures, CaO is stabler than Al_2O_3, which is again stabler than MgO, and so on. Stability of a pure oxide can be improved further if it is present as a double compound. An example is $MgCr_2O_4$, which forms according to the reaction.

$$MgO + Cr_2O_3 = MgCr_2O_4 \qquad \ldots 12.9$$

Since ΔG° for this reaction is negative, $MgCr_2O_4$ is stabler than MgO. Displacement of free energy curve as a consequence is illustrated in Fig.12.9 (21).

The displacement would be in the reverse direction if the oxide is in contact with the respective element dissolved in liquid steel as illustrated by the curve $\underline{Si}$ - SiO_2 in Fig.12.9. In other words it is easier for SiO_2 to dissociate as follows,

$$SiO_2(s) = \underline{Si} + 2\,\underline{O} \qquad \ldots 12.10$$

as compared to dissociation into pure Si and oxygen.

Thermodynamic considerations tell us that dissociation would occur if

$$[W_{Si}]\,[W_O]^2 \text{ in melt} < [W_{Si}]\,[W_O]^2_{\text{equlm}}$$

i.e. $[W_{Si}]\,[W_O]^2 < K_{Si}$ (i.e. deoxidation constant for Si) (see sec. 7.1)

In the event of such dissociation occurring, the melt shall pick up silicon and oxygen. The pick up may not cause serious composition change for Si, but may do so for oxygen if it is a highly deoxidized melt. SiO_2 may further react with Al,C,Cr etc. dissolved in liquid steel. The possibilities and extent of such reactions may be estimated with the help of data and procedure outlined in sec.7.1 under deoxidation thermodynamics. Broadly speaking, a low oxygen potential in the melt would enhance tendency for such reactions.

Harki et al (26) in a recent study examined the stability of refractory materials against deoxidized steels. Equilibrium calculations were performed. Laboratory investigations were carried out by simulation tests at 200g and 50kg scales. Oxygen sensor was used to monitor changes in dissolved oxygen in melt due to reaction with refractory materials. Fig.12.10 shows calculated equilibrium oxygen content for 4 steel grades and different refractory materials. Laboratory tests also demonstrated importance of thermodynamic stability as well as flow rate of steel.

In connection with vacuum treatment of steel, vapourization phenomena require considerations. The vapour pressures of refractory oxides are quite low and need not cause any worry. However reactions such as :

$$MgO(s) = Mg(g) + \underline{O} \qquad ...12.11$$

$$CaO(s) = Ca(g) + \underline{O} \qquad ...12.12$$

$$MgO(s) + \underline{C} = Mg(g) + CO(g) \qquad ...12.13$$

would be favoured at low pressures and hence may lead to objectionable quantity of oxygen pick up by melt. Similar statement is applicable for sub oxide formation such as :

$$SiO_2(s) + \underline{C} = SiO(g) + CO(g) \qquad ...12.14$$

However it is to be recognized that in a ladle only the refractory below free surface of melt is at low pressure. Way down vacuum conditions do not exist.

It is to be recognized that such problem of reaction is more with alloy steels containing stable oxide formers such as titanium and vanadium.

12.3.2 Refractories for Secondary Steelmaking

With the background informations provided so far a brief mention shall now be made on refractories employed in secondary steelmaking. Fire clay, which was the traditional ladle refractory material, is relatively inexpensive, possesses a low bulk heat capacity, and goes through a nonreversible expansion on heating which helps form tight fitting joints(9). However SiO_2 in fireclay is unstable with respect to aluminium killed steel as well as basic top slag. The refractory materials of present day secondary steelmaking are high alumina

(70-80% Al_2O_3), dolomite, magchrome, tar-bonded MgO, direct-bonded magchrome, Zircon. In Europe, dolomite is most commonly used. One of the reasons is that it contributes to more efficient desulphurization in ladle (9,10). This trend has been picked up in North America as well (19), especially for injection metallurgy. Dolomite seems to give long ladle life.

As compared to fireclay, high alumina and dolomite linings lead to more temperature loss of melt due to their higher bulk heat capacity as compared to fireclay. Dolomite linings if allowed to cool, can pick up water from atmosphere causing faster wear and possible hydrogen pick up by steel(9).

Ritza et al (19) have discussed the recent steel ladle practices at Algoma's No.2 steelmaking shop. They used fireclay up to 1984, then changed over to high alumina. However at present they are using Zircon, which is giving ladle life of almost 100 campaigns (Table 12.1).

Masood et al of Inland Steel (19) tested various refractory materials in the laboratory. Their data are presented in Table 12.2.

In India some refractory manufacturers like ORIND, Tata Refractories Ltd. are making or trying to develop refractories for secondary steelmaking. Bose et al have discussed various refractory types and some of the grades Tata Refractories Ltd. are making (20). According to them, the products are yet to be standardized in the country and, in general, improvements are required especially for VOD, AOD and MRF.

Table 12.1 : Brick Type Comparison (Ref.19, p.92)

BRICK TYPE	PROS	CONS
Fireclay	no preheat, ease of Skull removal, inexpensive, no build up	low life, 35 heats, silica pick up, poor slag protection, 2 bottom changes
High alumina	long life, 80 heats, no chemical pick up, good slag protection	preheat needed, 2 bottom changes, build up, expensive, poor Skull removal
Zircon	long life, 95 heats, ease of Skull removal, no chemical pick up, no build up	fair slag protection, expensive, preheat needed

Ladle lining is a composite one. A common practice is to use high alumina in the bottom (Pitch bonded dolomite are also being employed) and sides with a few courses of magchrome or carbon-bonded magnesia at the slag line. To reduce on weight, expense, and the total heat capacity of the refractory system, a fireclay back -up lining is provided. The lining pattern of VAD/VOD ladles at Alloy Steel Plant, Durgapur (Barua et al, ref.20) is shown in Fig.12.11 as an illustration. Table 12.3 (Bose et al, ref.20) shows the lining for ladle furnaces in some countries. It is to be recognised that design of ladle lining is quite a specialized task. An optimization is called for, which should take into consideration :

(a) process requirements including steel quality
(b) cost and availability
(c) lining life

The design would of course depend on the process we are talking about. Gas stirring leads to faster wear of lining. This will be aggravated by presence of basic top slag. In AOD/VOD vessels, oxygen is also blown raising oxygen content and generating iron oxide at impingement spots. Their contact with refractory poses an additional problem.

Ladle covers are typically lined with high alumina refractory (above 85% Al_2O_3). Zircon, Zirconia and alumina-graphite nozzles are considered as best. Porous plugs are made of high alumina or magnesia. Slide gate plates are typically made of alumina-graphite.

REFERENCES

1. A. McLean and I.D. Sommerville, in. Proc.Int. Symp.on Modern Developments in Steelmaking, ed. A. Chatterjee and B.N. Singh, Jamshedpur (1981), p.739.
2. T. Choh, K. Iwata and M. Inouye, Trans. ISIJ, 23 (1983), 598.
3. Ibid, p.680.
4. J. Kumar and A. Ghosh, Trans. IIM, 30 (1977), 39.
5. J. Szekely, Trans. AIME, 245 (1969), 341.
6. K. Iwata, T. Choh and M. Inouye, Trans. ISIJ, 23 (1983), 218.
7. R.D. Pehlke and J.F. Elliott, Trans. AIME, 227 (1963), 814.
8. A. Nicholson and T. Gladman, Ironmaking and Steelmaking, 13 (1986), 53
9. R.J. Fruehan, Ladle Metallurgy Principles and Practices, ISS-AIME, USA (1985), chs.2,7.
10. LEK Holappa and H.Y.S. Ylonen, Proc. Steelmaking Conference, 69, Washington D.C. (1986), 277.
11. R. Kiessling and N. Lange, Non-metallic Inclusions in Steel, The Metals Soc., London, 1978.
12. D. Brooksbank and K.W. Andrews, JISI, 210 (1972), 246.
13. Iron and Steel Inst., Production and Application of Clean Steels, London, 1972.
14. L.H. Vanvlack, Oxide Inclusions in Steel, Review 220, Int. Metals Rev, The Metals Soc, London, 1977.
15. D.C. Hilty and D.A.R. Kay, in Electric Furnace Steelmaking, ed. C.R. Taylor, ISS-AIME, USA (1985), ch.18.

16. M. Kitamura, T. Soejima, S. Kawasaki and S. Koyama, Proc. 63rd Steelmaking Conf. of ISS-AIME, Washington D.C. (1980), 154.
17. P. Apte, D.N. Ghosh and D.A.R.Kay, Proc. NOH-BOS Conference,AIME, Chicago, 1978.
18. J.H. Chesters, *Refractories for iron-and steelmaking*, The Metals Soc, London (1974).
19. Iron & Steel Soc, *Refractories for modern steelmaking systems*, USA (1987).
20. Proc. National Seminar on Secondary Steelmaking, Tata Steel and Ind. Inst. Metals, Jamshedpur (1989).
21. A. Muan in ref. 15.
22. 69th Steelmaking Proceedings, ISS-AIME, Washington D.C. (1986).
23. K.K. Kappmeyer and D.H. Hubble, in *High temperature oxides*, Part 5-1, Acadedmic Press,London (1970).
24. R.P. Hart et al, p.73, ref. 19; also p. 171 of ref. 22.
25. Okawa et al, p. 237 of ref. 22.
26. J. Harkki, R. Rytila, M. Palander and S. Sundstrom, Scand J. Met, 19 (1990), 116.

Table 12.2 Chemical and physical properties of refractories evaluated

	Refractory						
Chemistry (Wt %)	Resin-Bonded Dolomite	Tar-Bonded Dolomite		Direct Bonded Mag-Chrome	Zircon	70% Alumina	Tar-Bonded Magnesite
		(A)	(B)				
Al_2O_3	0.4	<1	0.4	11.1	3.4	70.0	0.5
SiO_2	0.6	<1.5	0.6	1.8	33.4	26.0	1.0
MgO	41.0	36	41	60.6	-	0.3	95.0
CaO	57.0	61	57	0.7	-	0.25	2.5
ZrO_2	-	-	-	-	61.3	-	-
Fe_2O_3	1.0	<1	1.0	9.2	-	1.3	0.5
Cr_2O_3	-	-	-	16.4	-	-	-
Bulk density (kg/m^3)	2900	2900	2950	3100	3600	2600	3100
Porosity (as shipped) (%)	6	8	8	15.5	19	17	5.1
(ignited) (%)	15.5	16	16	-	-	-	17.0
Modulus of Rupture (kPa) as Shipped	18,620	10,000	-	5,150	-	14,100	9,650
Coked	-	6,895	-		-	-	6,200
Thermal Expansion @ 1200°C (%)	1.4	1.6	1.6	1.3	0.5	0.8	1.7
Thermal conductivity @ 1000°C (W/mK)	2.4	2.4	2.5	2.8	2.4	2.0	4.5
Specific heat @ 1425°C (J/kg.K)	1050	1050	1040	1050	760	1068	1175

Table 12.3 Examples of refractory lining for secondary steelmaking in some countries(ref.20, p.48)

Country Plant	Cap.	Process Route	Bottom	Side Wall	Slag Line	Lining life heats
West Germany ,, Plant-1	110 T	EAF/LF	PB Dol.	PB Dol.	12% Mag-C	45-50
,, Plant-2	60 T	,,	DB Dol	,,	PB Mag.	50-55
,, Plant-3	110 T	,,	Cr.Mag	PB Dol	,,	30-33
,, Plant-4	60 T	,,	PB Dol	PB Dol	RB Mag.	45-50
Great Britain Plant-1	90 T	,,	80% Al_2O_3	DB Dol	,,	28
,, Plant-2	130 T	,,	DB Dol	DB Dol	DB Dol	30
France						
,, Plant-1	30 T	EAF/APC	PB Dol	PB Dol	RB Mag	15
,, Plant-2	105 T	,,	80% Al_2O_3	,,	DB Dol (PI)	30-35
Italy						
,, Plant-1	60 T	EAF/LF	PB Dol	,,	,,	45
,, Plant-2	90 T	,,	Dol.Carbon	,,	Dol.Carbon	45
Sweden	60 T	,,	DB Dol	DB Dol	DB Dol	45
Denmark	120 T	,,	PB Dol	PB Dol	PB Dol	30-35

PB = Pitch bonded, DB= Direct bonded, RB= Resin bonded

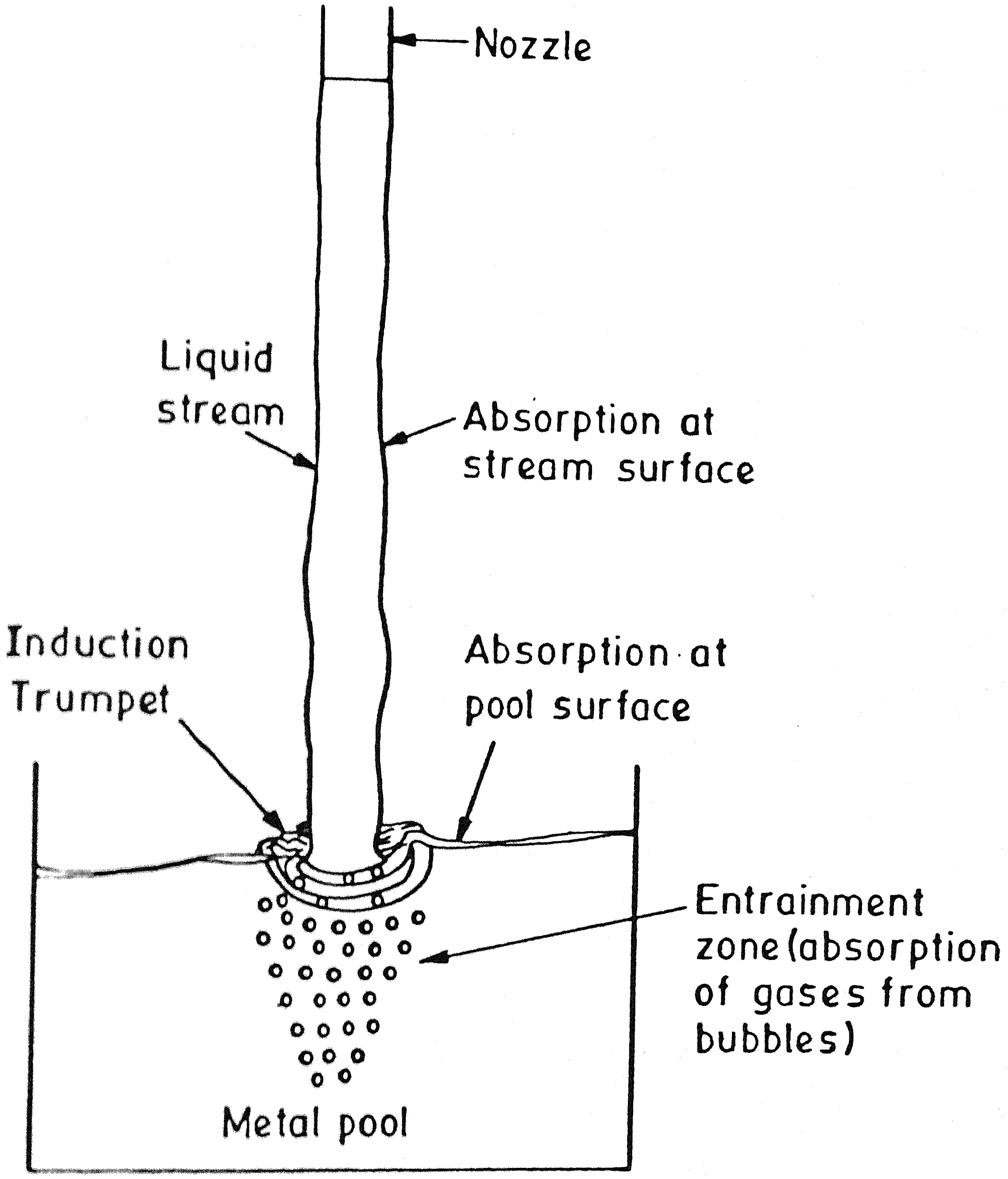
Nozzle
Liquid stream
Absorption at stream surface
Induction Trumpet
Absorption at pool surface
Entrainment zone (absorption of gases from bubbles)
Metal pool

Fig. 12.1 : Mechanism for absorption of air by metal

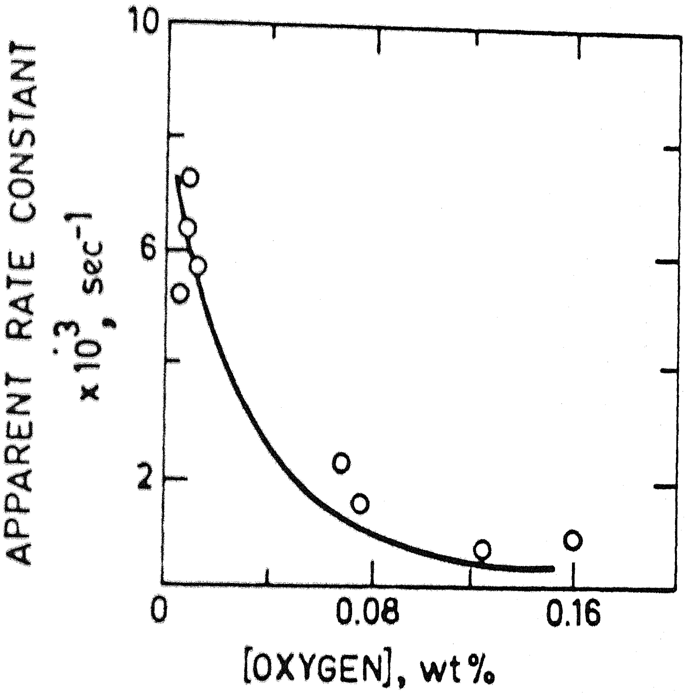

Fig. 12.2 : Influence of oxygen content on rate of absorption of nitrogen by liquid iron

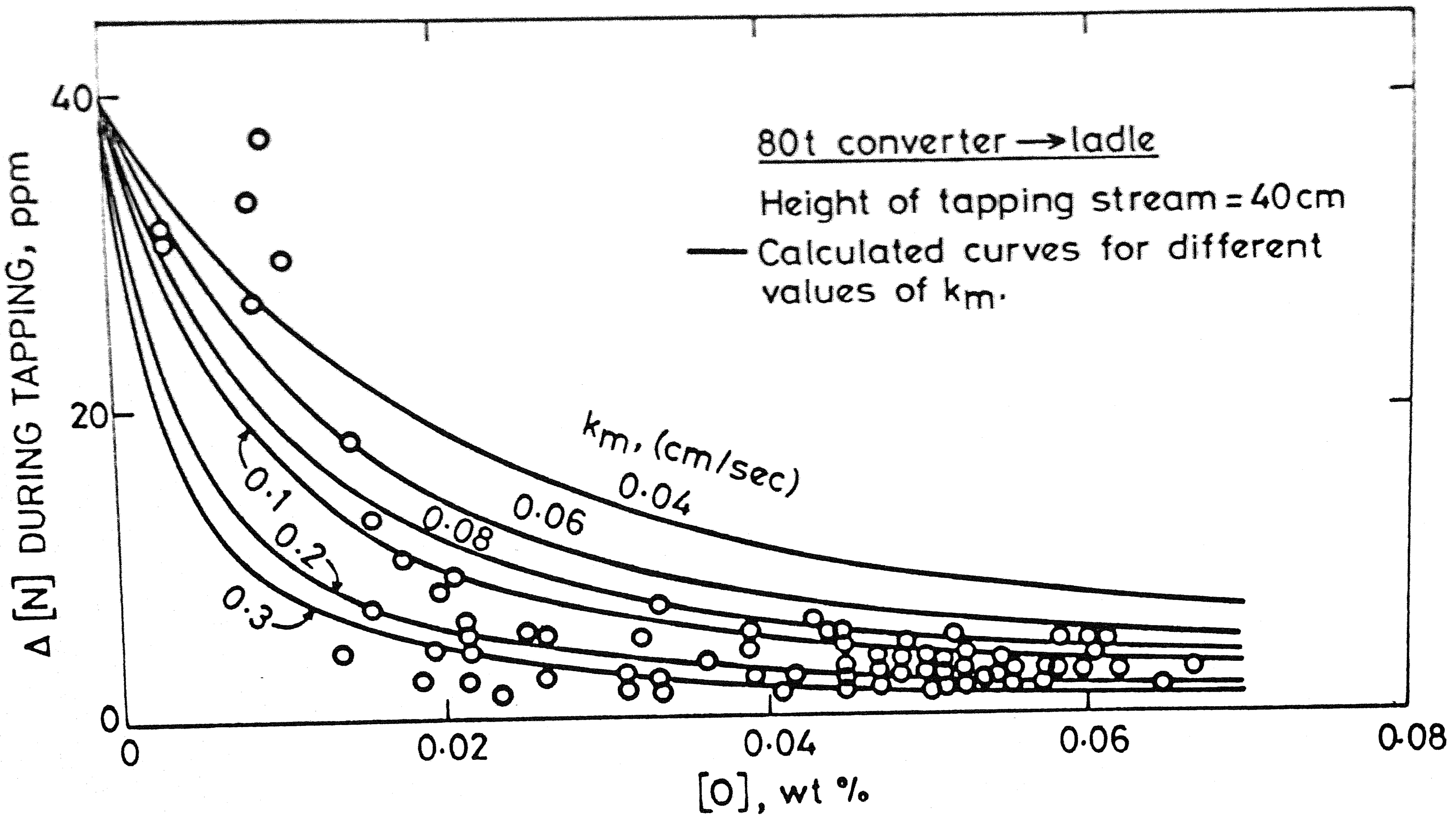

Fig. 12.3 : Variation of nitrogen pick up during converter tapping as function of oxygen in metal

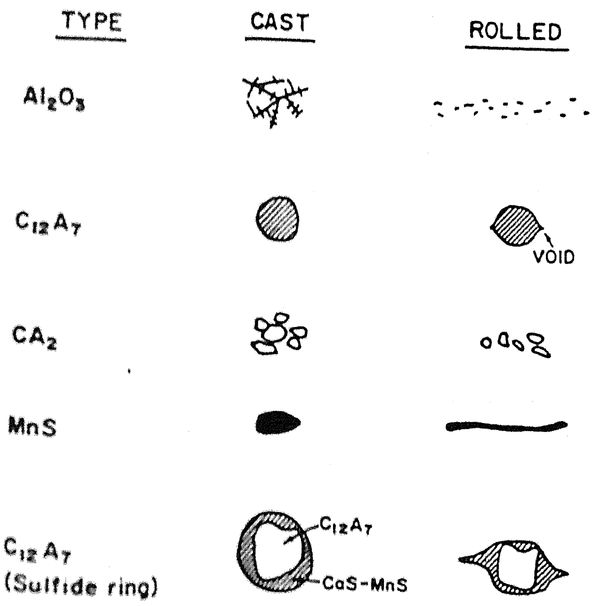
TYPE
CAST
ROLLED
Al_2O_3
$C_{12}A_7$
VOID
CA_2
MnS
$C_{12}A_7$
(Sulfide ring)
$C_{12}A_7$
CaS-MnS

Fig. 12.4 : Schematic diagram of inclusions in Al - killed steels

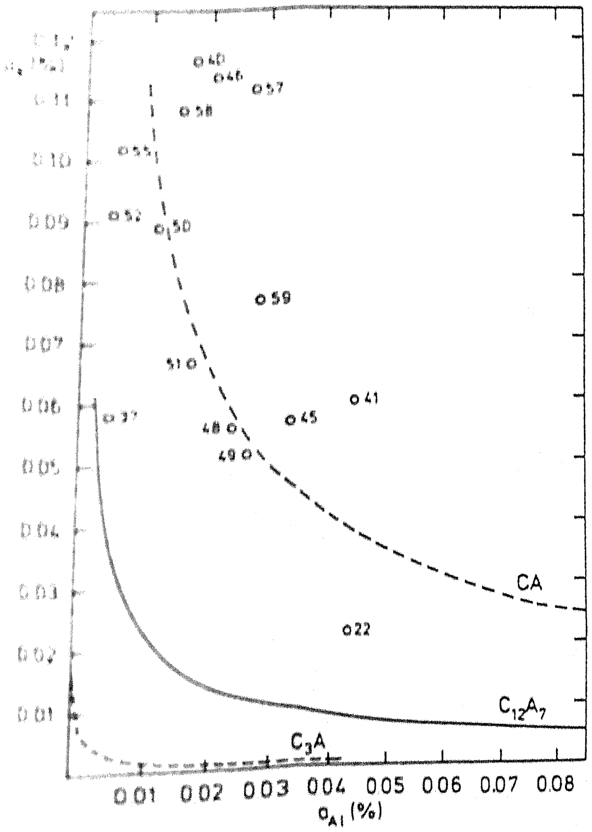

Fig. 12.5 : Calculated equilibria between calcium aluminate slag inclusion s and steel melt (10); T = 1550°C, a_{CaS} = 1

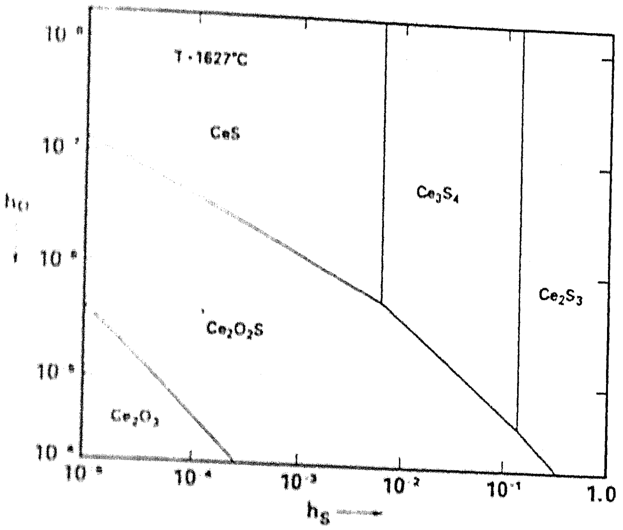

Fig. 12.6 : Ce-O-S inclusion precipitation diagram for liquid steel at 1627°C

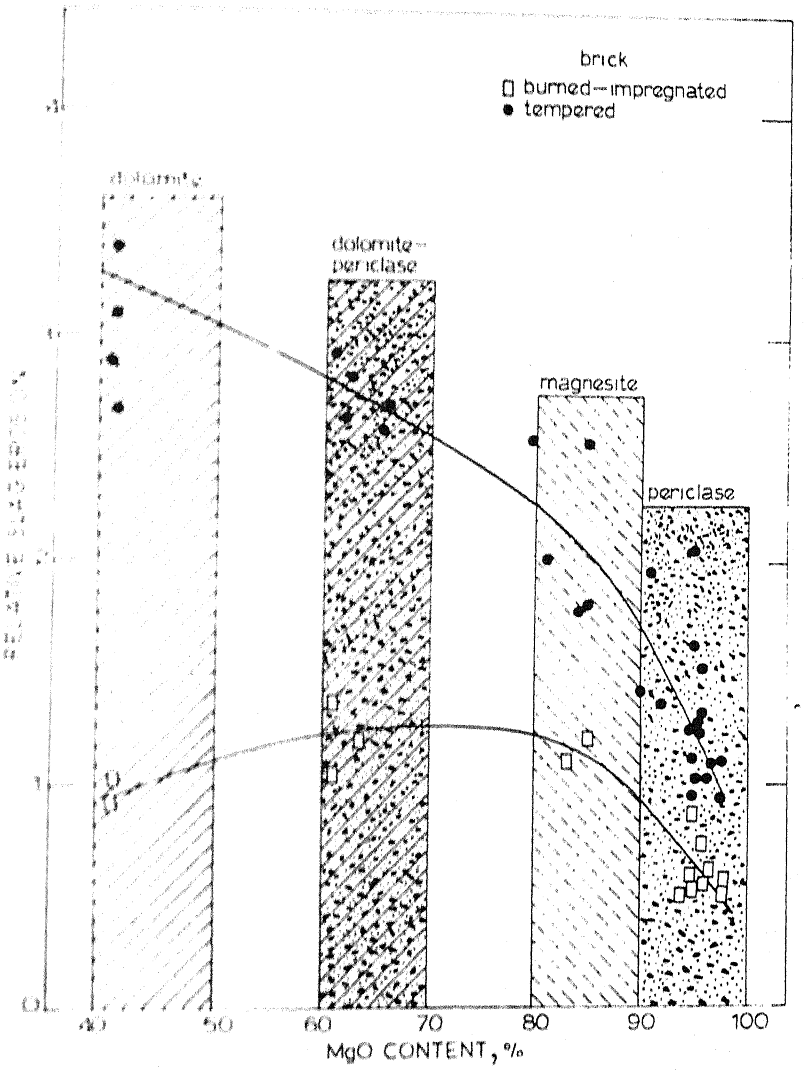

Fig. 12.7 : Relative slag erosion vs. MgO content for LD refractory lining (23)

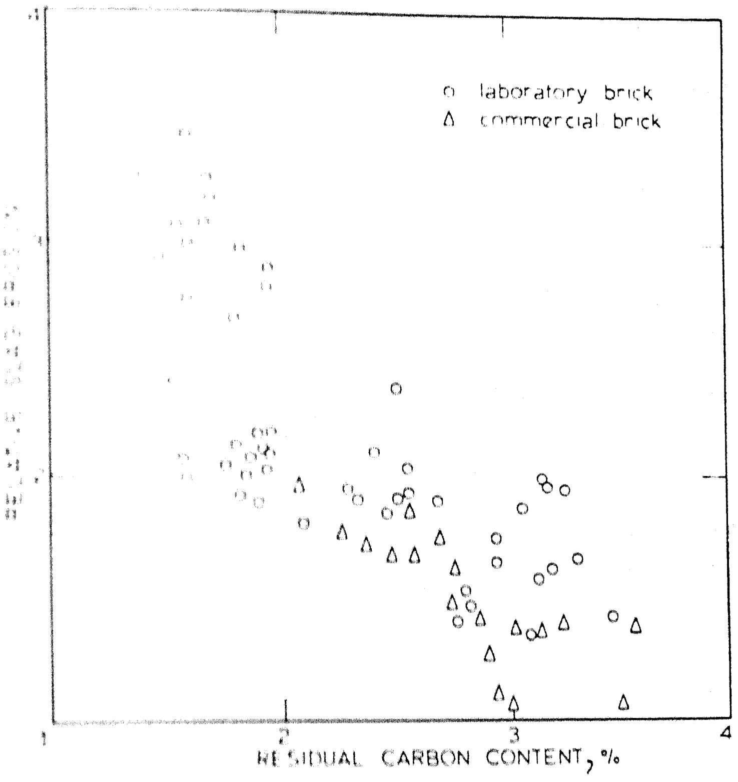

Fig. 12.8 : Relative slag erosion vs. residual carbon content in LD bricks (23)

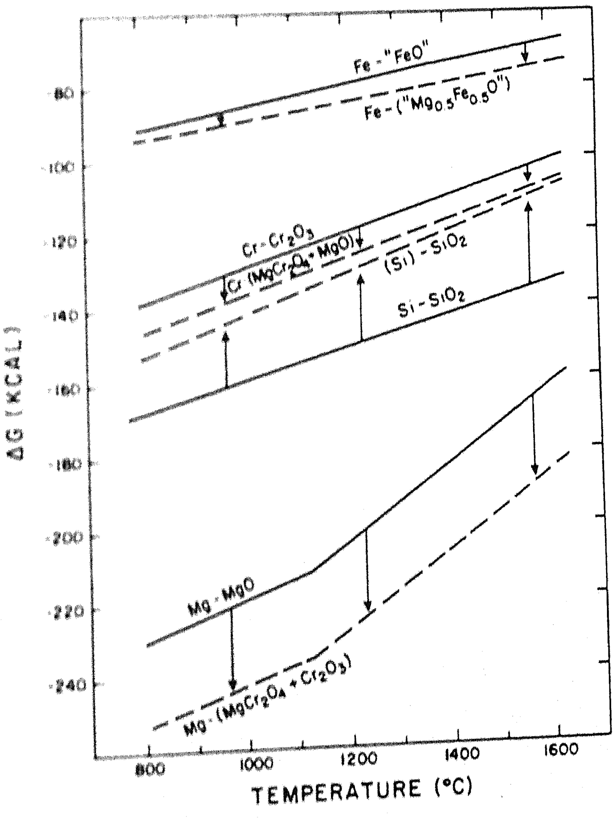

Fig. 12.9 : Displacement of free-energy curves at constant oxygen pressure (1 atm) for some metal - metal oxide systems (21)

Compositions of steels used in equilibrium calculations

	Steel 1	Steel 2	Steel 3	Steel 4
C	0.10	0.35	0.80	0.20
Si	0.40	0.22	0.25	0.40
Mn	1.30	0.70	0.70	1.10
Al	0.030	0.003	0.004	0.030
Cr	–	–	0.15	0.54
Cu	–	–	–	0.34
Ni	–	–	–	0.20

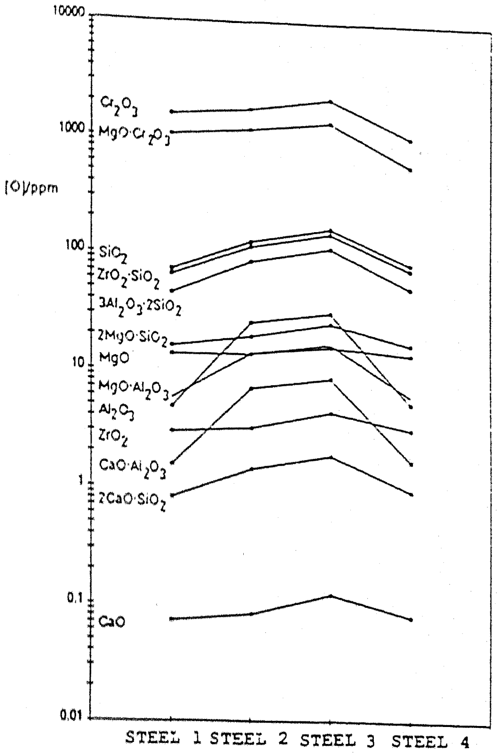

Fig. 12.10 : Dissolved oxygen content in some steel melts at equilibrium with different oxides at 1600°C (26)

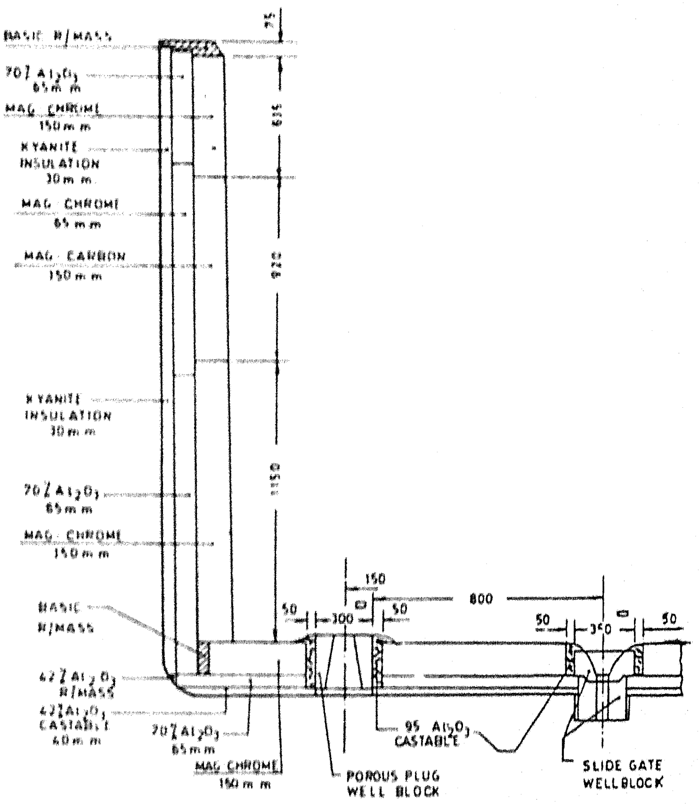
BASIC R/MASS
70% Al_2O_3 65 m m
MAG CHROME 150 m m
KYANITE INSULATION 30 m m
MAG CHROME 65 m m
MAG CARBON 150 m m
KYANITE INSULATION 30 m m
70% Al_2O_3 65 m m
MAG CHROME 150 m m
BASIC R/MASS
42% Al_2O_3 R/MASS
42% Al_2O_3 CASTABLE 40 m m
70% Al_2O_3 65 m m
MAG CHROME 150 m m
75
1150
150
800
50
300
50
50
350
50
95 Al_2O_3 CASTABLE
POROUS PLUG WELL BLOCK
SLIDE GATE WELLBLOCK

Fig. 12.11 : Lining patterns of VAD/VOD ladles at ASP, Durgapur, Barua et al (20)